IODP-ICDP Kolloquium 2006 in Greifswald

Ernst-Moritz-Arndt-Universität

Wi55en lockt.
550 Jahre Universität Greifswald

27. - 29. März 2006

Deutsche
Forschungsgemeinschaft
DFG

IODP-ICDP-Kolloquium 2006

27. - 29. März 2006

im Rahmen des 550-jährigen Jubiläums
der Ernst-Moritz-Arndt-Universität Greifswald

Gemeinsames Kolloquium der DFG-Schwerpunkte

IODP - Integrated Ocean Drilling Program

und

ICDP - International Continental Scientific Drilling Program

27. - 29. März 2006
im Berufsbildungszentrum Greifswald

Institut für Geographie und Geologie
Friedrich-Ludwig-Jahn-Str. 17a
D-17487 Greifswald
Tel. 03834 864560
Email: meschede@uni-greifswald.de

Umgebung Tagungszentrum

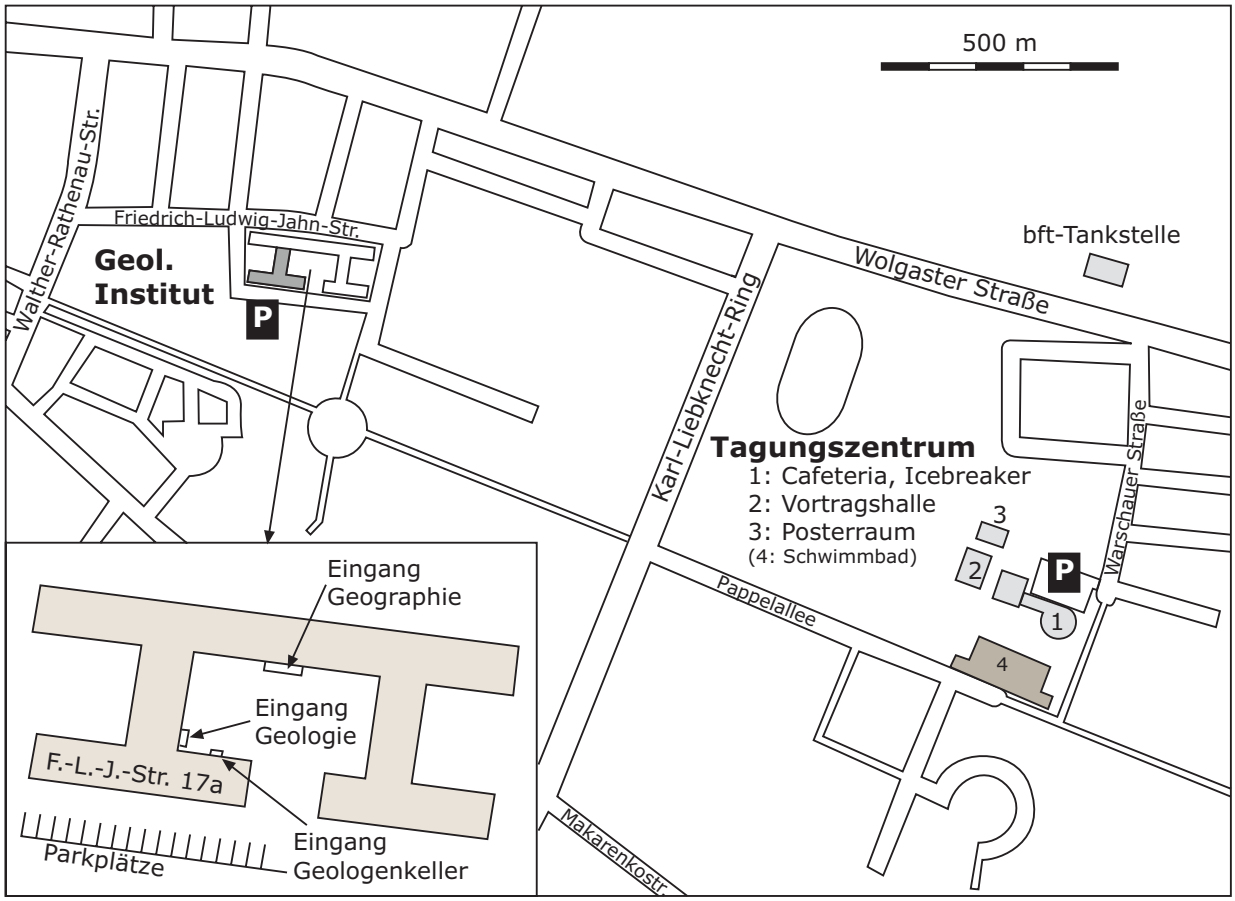

Innenstadtplan

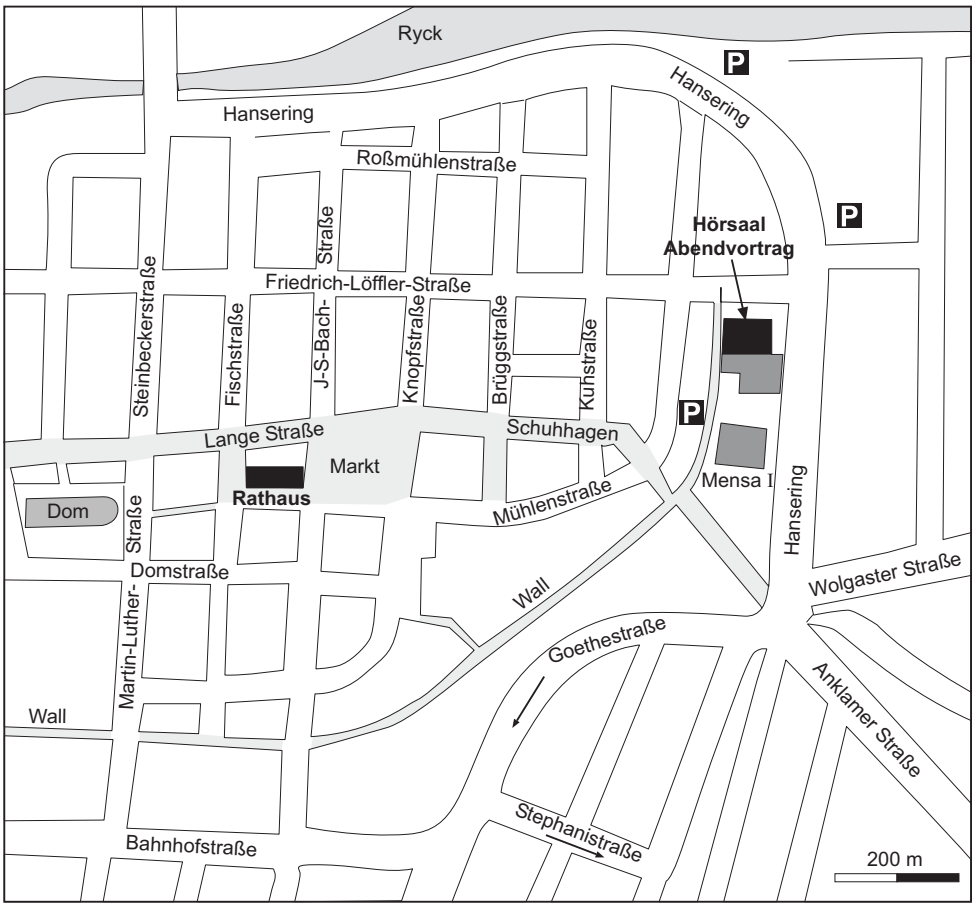

Montag, 27. März 2006

11:00	13:00	**Registrierung**	
13:00	14:00	**Eröffnung** - Oberbürgermeister der Universitäts- und Hansestadt Greifswald, Dr. Arthur König - Prodekan der Mathematisch-Naturwissenschaftlichen Fakultät der Universität Greifswald, Prof. Dr. Reinhard Zölitz-Möller - DFG-Referent Dr. Sören Dürr - Koordinatoren - Gastgeber	
Paläoozeanographie / Paläoklima			Abstract - Seite
14:00	14:20	R. Stein, J. Grützner, J. Hefter, T. Kanamatsu, C. Alvarez-Zarikian and IODP Expedition 306 scientists **IODP Expedition 306: Quaternary and Late Neogene North Atlantic Paleoceanography**	11
14:20	14:40	L. Perez, E. Vinogradova, W. Riss, B. Scharf and A. Schwalb **Paleoclimate and paleoecology of the northern lowland Neotropics, Phase 1: Limnological survey of modern aquatic environments**	95
14:40	15:00	F. Niessen, B. Zolitschka, C. Ohlendorf, F. Anselmetti, D. Ariztegui, M. De Batist, C. Gebhardt, T. Haberzettl, M. Fey and the SALSA team **Seismic investigations of Laguna Potrok Aike, Argentina**	119
15:00	16:00	**Posterpräsentationen** und Kaffeepause	
16:00	16:20	S. Mischke **Opening up a unique high-resolution climate archive of the last 1.3 Ma from the Qaidam Basin, China**	93
16:20	16:40	D.A. Hepp, T. Mörz, J. Thiede and W.-C. Dullo **Cyclic sedimentation processes and diagenetic alteration recorded in a deep-sea sediment drift (Antarctic Peninsula Pacific Margin)**	61
16:40	17:00	A. Holbourn, W. Kuhnt, M. Schulz and H. Erlenkeuser **Impacts of orbital forcing and atmospheric CO2 on Miocene global cooling**	65
17:00	17:20	T. Bickert, M. Butzin, H. Kuhnert, H. Paulsen and T. Westerhold **Subantarctic influence on the mid Miocene initiation of the Benguela upwelling - Evidence from ODP Sites 1085 and 1092 planktonic foraminifer assemblages and stable isotopes**	34
17:20	17:40	T. Westerhold, U. Röhl, G. Wefer, J. Laskar, I. Raffi, J. Bowles, L.J. Lourens and J.C. Zachos **New high-resolution chronology from the first complete late Paleocene - early Eocene marine records from Walvis Ridge: duration of Chron 24r and new constraints on the timing of early Eocene global warming events**	114
17:40	18:00	A. Forster, K. Moriya, S. Schouten, P.A. Wilson und J.S. Sinninghe Damsté **A dual-proxy sea surface temperature record of the Cenomanian/Turonian transition in the tropics (Demerara Rise, ODP Leg 207)**	48
18:00	19:00	Pause	
ab 19:00		**Icebreaker-Party** im Gebäude des BBZ (gegenüber Tagungsgebäude)	

Dienstag, 28. März 2006

Magmatische Petrologie / Metamorphismus			Abstract - Seite
09:00	09:20	J. Koepke, B. Scheibner, Expedition 309, and Expedition 312 Scientific Parties **IODP Expedition 312: Superfast Spreading Rate Crust III**	21
09:20	09:40	J. Geldmacher, K. Hoernle, P. v. d. Bogaard and A. Klügel **Age and geochemistry of Central American forearc basement rocks (DSDP Leg 67 and 84) reveal a complex geodynamic history**	51
09:40	10:00	K. Bräuer, H. Kämpf and G. Strauch **Indications of progressive magmatic activity beneath the Cheb Basin (Central Europe)**	37
10:00	10:20	M. Rosner, W. Bach, H. Paulick and J. Erzinger **Carbonate veins from oceanic core complexes: Trading different stages of sub-seafloor alteration**	99
10:20	10:40	H. Behrens, F. Vetere and F. Holtz **Viscous flow of magmas from Unzen volcano, Japan - implications for magma mixing and ascent**	30
10:40	11:40	H.-J. Brumsack, J. Erbacher und R. Oberhänsli **IODP/ICDP: Struktur und Chancen für Jungwissenschaftler**	
11:40	14:00	**Posterpräsentationen,** Kaffeepause und Mittagspause	
Tiefe Biosphäre			
14:00	14:20	T.G. Ferdelman, K. Mangelsdorf, J. Titschack, A. Kano, T. Williams, the IODP Expedition 307 Scientists and J.P. Henriet **IODP Expedition 307: Drilling Challenger Mound - a cold-water coral structure in the Porcupine Seabight**	13
14:20	14:40	A. Schippers and L.N. Neretin **Development and Application of New Quantitative Molecular Ecological Techniques to Study the Abundance and Activity of Microorganisms in the Marine Deep Subsurface**	101
14:40	15:00	J.S. Lipp, J. Biddle, H.F. Fredricks, M. Elvert, J.E. Brenchley, A. Teske, C.H. House and K.-U. Hinrichs **Novel heterotrophic Archaea dominate deeply buried sulfate-methane transition zones in sediments off Peru**	83
15:00	15:30	**Posterpräsentationen** und Kaffeepause	
Fluide			
15:30	15:50	J. Lippmann-Pipke, S. Niedermann, J. Erzinger, M. Zimmer and T.C. Onstott **Implications for the timing of gas release: crush degassing Experiments (lab), continuous gas monitoring (near-field) and analysis of >1.5 Ma old crustal fluids (regional), Witwatersrand Basin, South Africa**	84
15:50	16:10	W. Kessels, S. Kuhlmann and Xuan Li **Groundwater and Fluid Component Transport in the KTB SE1 and SE2 Fault Zones and a Possible Connection with the Eger Rift Valley**	73
16:10	16:30	C.I. McDermott, M. Lodemann, I. Ghergut, H. Tenzer, M. Sauter and O. Kolditz **A geomechanical facies model to investigate the coupled hydraulic-geomechanical processes at the KTB site**	90
16:30	16:50	Y. Xiao, J. Hoefs, R.L. Romer, A. v. d. Kerkhof and Z. Zhang **Isotope (O-Sr-Nd-Pb) and fluid inclusion distributions in the CCSD main hole**	117

16:50	19:00	**Posterpräsentationen** und Pause
19:00	20:00	**Empfang im Rathaus,** Oberbürgermeister Dr. Arthur König
20:00	21:00	**Öffentlicher Abendvortrag**, im Hörsaal Löfflerstr. 70 Prof. Dr. André Freiwald, Erlangen
ab 21:00		***Geologenkeller*** (im Institut für Geographie und Geologie, Friedr.-Ludw.Jahn-Str. 17A)

Mittwoch, 29. März 2006

Fluide			Abstract - Seite
09:00	09:20	C. Hensen and W. Brückmann **Modes of fluid expulsion and its significance for forearc dewatering - IODP drilling proposal 633 to decipher deep fluid processes at an erosive convergent margin**	60
09:20	09:40	J.H. Behrmann, P.B. Flemings, C. John and IODP Expedition 308 Shipboard Scientific Party **Synopsis of IODP Expedition 308 Results, Gulf of Mexico Hydrogeology**	15
09:40	10:00	M. Heesemann, H. Villinger, H.W. Jannasch, M. Kastner, E.A. Solomon, and Expedition 301T Scientific Party **Long-term temperature measurements in ODP Holes 1253A and 1255A off Costa Rica, ODP Leg 205**	57
10:00	10:30	**Posterpräsentationen** und Kaffeepause	
Seismogene Zone / Impactstrukturen			
10:30	10:50	A. Kopf and NanTroSEIZE Proponents **The Nankai Trough Seismogenic Zone Experiment, a complex drilling proposal within IODP**	77
10:50	11:10	M. Becken, O. Ritter, S. Park, P. Bedrosian, U. Weckmann and M. Weber **The electrical conductivity structure across the San Andreas Fault near the SAFOD site - a regional magnetotelluric study**	28
11:10	11:30	D. Doman, U. Riller and K. Hofmann **Deformation of the central Sudbury Impact Structure, Canada: Evidence for meteorite impact into an active orogen and implications for deep drilling**	41
11:30	11:50	G.S. Gohn, C. Koeberl, K.G. Miller and W.U. Reimold **The 2005 ICDP-USGS Deep Corehole in the Chesapeake Bay Impact Crater**	52
11:50	12:10	A. Deutsch and the German Bosumtwi Team **Lake Bosumtwi Drilling Project - First Results**	39
12:10	13:00	**Posterprämierung und Schlußworte**	
13:00		***Tagungsende***	

Fahrtenbericht IODP Expedition 305: Atlantis Massif, 30˚N (Mittelatlantischer Rücken)

G. Suhr[1,2] und E. Hellebrand[2]
[1]Geologisch-Mineralogisches Institut, Uni Köln, guenter.suhr@uni-koeln.de;
[2]Max Planck Institut Chemie, Mainz, ehelle@mpch-mainz.mpg.de

IODP Leg 305 unternahm die zweite Etappe einer insgesamt viermonatigen Ausfahrt zur Erkundung der ozeanischen Lithosphäre am Mittelatlantischen Rücken (MAR). Die Lokation liegt auf einer topographische Schwelle (Atlantis Massif) nördlich der Atlantis Transform Störung auf 30˚N. Weniger als 1 km westlich der Bohrlokation stehen hochauflösende seismische Refraktionsdaten zur Verfügung. Sie hatten zu der Vermutung Anlaß gegeben, daß frische Mantelgesteine in 500-700 m Tiefe unter dem Meeresboden anstehen und damit problemlos innerhalb der Reichweite der Joides Resolution lagen. Das favorisierte tektonische Modell für das Atlantis Massiv unterstützte diese Annahme: es soll sich dabei um einen Kernkomplex handeln, d.h. um ein durch eine langlebige, asymmetrische Abschiebung tiefgründig exhumiertes Gebiet. Die charakteristisch flache, gefurchte Oberfläche soll die exponierte, ehemals steile, dann aber stark rotierte Störung darstellen. Eine ähnliche Lokation war schon für Leg 118/176 (südwestindischer Rücken, Bohrung 735B) gewählt worden und hatte dort problemlose Bohrbedingungen angetroffen. Voruntersuchungen mittels Dredgen, Tauchfahrzeugen sowie das gesichert in ultramafischen Gesteinen wurzelnde Hydrothermalfeld Lost City 5 km südlich unserer Bohrung wiesen alle auf einen hohen Anteil von Basalt und Peridotit in der Bohrumgebung hin. Allein Gabbro war bei diesen Voruntersuchungen selten gefunden worden.

Nachdem während Leg 304 vergeblich versucht worden war, das Hangende der Abschiebung zu durchteufen, konzentrierte sich Leg 305 (8.1.2005- 2.3.2005) allein auf den Liegendbereich der Störung. Bohrung 1309D startete bei einer Teufe unter dem Meeresboden von 401 m (erbohrt durch Leg 304) und vertiefte das Loch bis 1415.5 m mit einem Kerngewinn von 74%. Entgegen aller Erwartungen waren (für das gesamte Bohrloch) 96% der Gesteine Gabbros, <1% Peridotit und 3% Basalt.

Im Bereich zwischen 400 und 1400 m besteht keine geregelte lithologische Abfolge, welche gesichert einem oder mehreren magmatischen Fraktionierungszyklen zuzuordnen wäre. Oxidgabbros, noritische Gabbros, Olivin Gabbros und Troktolithe, sowie vereinzelt Mikrogabbros, Leucogabbros und Diabase wechseln sich engständig ab. Am markantesten sind zweifellos - in dieser Form bisher vom Ozeanboden unbekannte - sehr frische, olivinreiche Troktolithe (Olivin-Anteil >70%) bei 1100-1200 m Teufe. Troktolithe sind ebenfalls häufig im Niveau um 550 m Teufe. Diese beiden Olivin-reichen Intervalle werden unterlagert von Gabbros mit ungewöhnlich häufigen Oxidgabbro-Anteilen und stellen damit ev. bedeutende magmatische Kontakte dar. Die Oxidgabbros sind hochdifferenzierte Gesteine und oft assoziiert mit Apatit, Titanit und Zirkon. Die olivin-reichen Troktolithe enthalten sehr stark gerundete Olivine und stellen vermutlich recht primitive Kumulate dar. Es kann allerdings noch nicht ausgeschlossen werden, dass es sich dabei um magmatisch stark imprägnierte, reliktische Mantelgesteine (zwischen zwei Intrusionen??) handelt. Erste landgestütze Mikrosondenergebnisse von uns ergeben Mg# im Olivin bis zu 86. Diese Werte liegen immer noch unter denen von Schmelzen, die im Gleichgewicht mit dem Mantel sind (Mg# 90). Nach den Eindrücken an Bord erscheint es, als ob stärker evolvierte Lithologien generell in die primitiveren Gesteine intrudierten. Markant ist weiterhin, daß bis zu mehrere cm-große Klinopyroxene poikilitsch die Plagioklase umschließen, vermutlich sogar resorbieren. Dies weist auf die späte Migration von Schmelze durch ein Kumulusgemenge hin. Damit in Einklang stehen unsere ersten Ergebnisse, welche sehr häufige Zonierungen in den Pyroxenen finden.

Strukturell fällt der geringe Betrag an spröder, plastischer, und magmatischer Deformation auf. Gesteine mit magmatischer Einregelung sind selten, plastische Gefüge treten nur in cm- bis maximal dm-starken Intervallen auf (manchmal an Oxidgabbros gebunden). Ein eventuell signifikanter kataklastischer Bereich liegt bei ~770 Teufe. Unterhalb dieser Zone, die auch bei der Bohrlochvermessung als deutliche Ausbruchzone auffällt, verringert sich die Intensität der Kataklasis, der Veins, von Sulfiden sowie insgesamt der Grad der Alteration. Ein Lithologiewechsel tritt hingegen über die Zone hinweg nicht auf. Der geringe Betrag an Hochtemperaturdeformation legt nahe, daß die Platznahme der Gabbros innerhalb der rheologischen Lithosphäre stattfand.

Bei der Metamorphose/Alteration fällt die generell schwache Entwicklung der amphibolitfaziellen Überprägung auf. Granulitfazielle Gefüge sind lokal entwickelt und oft an plastische Deformation gebunden. Synkinematische, braune Hornblende ist eher selten. Brauner und grüner Amphibol ersetzten lokal statisch die Pyroxene. Im Bereich der Grünschieferfazies wurde die offenbar nur in Gegenwart von Olivin stattfindene Reaktion von Plagioklas zu einer Doppelkorona von Chlorit und Talk/Tremolit häufig beobachtet. Epidotbildung wie auch die Alteration der Pyroxene ist häufig an die höher differenzierten und z.T. mit Kataklasis einhergehenden Differentiate gebunden. Ebenfalls vertreten sind grüne Veins (Amphibol, Chlorit) sowie weiße Veins (zeolithfazielle Phasen) wie natürlich auch die Serpentinbildung aus Olivin. Generell ist die Alteration unterhalb von 800 m aber als gering einzuschätzen.

Paläomagnetische Daten weisen auf vorwiegend negative Magnetisierung mit Inklinationen im Bereich von -30 bis -50˚ hin. Diese Werte sind nicht bedeutend unterschiedlich vom aktuellen lokalen Wert (-50˚). Aufgrund des N-S gerichteten Magnetfeldes sind jedoch auch größere Rotationen um eine N-S Achse mit eher geringen Abweichungen der Inklination verbunden. Dies ist ungünstig, da die wahrscheinlichste Rotation des Atlantis Massifs um eben diese N-S Achse erfolgt ist. Nach ersten Abschätzungen ist eine Rotation der Gabbrosequenz um durchschnittlich 45-50˚ seit Unterschreiten der Curie Temperature möglich - durchaus im Einklang mit dem vermuteten rolling hinge Modell. Bereiche starker Serpentinisierung zeigten abweichend von anderen Lithologien eine positive Inklination. Diskutiert wurde daher, ob die Serpentinisierung erst nach einer Umkehr des Magnetfeldes stattgefunden hat.

An Bord gemessene seismische Geschwindikeiten Vp erreichten, ganz im Gegensatz zu den geophysikalischen Voraussagen, maximale Werte von 6.8 km/s und blieben damit weit unter dem Wert von frischen Mantelgesteinen. Unter etwa 750 m Teufe fielen die durchschnittlichen Geschwindigkeiten von ~ 6 km/s sogar um 10% ab, wobei die Ursache hierfür noch nicht klar ist. Spekuliert wurde über den Einfluß der Entlastung beim Kernziehen auf die Proben, aber eine Korrelation mit der Dichte konnte nicht nachgewiesen werden. Die Dichten liegen bei 2.93 +/- 0.1 g/cm³. Temperaturen an der Basis der Bohrung scheinen 120˚C zu erreichen.

Aufgrund der Voruntersuchungen muß das Bohrergebnis als vollkommen überraschend bewertet werden. Geophysikalische Voraussagen und das Resultat der Dredgefahrten und submarinen Erkunden trafen nicht zu bzw. bestätigten sich nicht. Dies bedeutet entweder eine extreme Kleinräumigkeit der lithologischen Variation oder einen noch mangelnden Einblick in die geologisch-geophysikalischen Zusammenhänge des Aufbaus der ozeanischen Lithosphäre, zumindest bei langsamen Spreizen. Die Tiefbohrung 1309D belegt in jedem Fall die absolute Notwendigkeit eines wissenschaftlichen Bohrprogramms zur Verifikation und Wahrheitsfindung. Die Bohrung 1309D hat allerdings deutliche Zusammenhänge mit den Bohrungen 735B und 1275 (Leg 209, 20˚ N am MAR) erbracht: In allen drei Fällen wurden Bohrungen auf den flachen Rücken von Kernkomplexen abgeteuft. Sie erbrachten vorwiegend Gabbro während die Oberflächenerkundung hohe Anteile an Peridotit erwarten ließ.

Vermutet wird daher, daß unabhängig von der vorherrschenden Lithologie sich Abscherhorizonte in serpentinisiertem und damit rheologisch schwachem Peridotit lokalisieren. Der tatsächliche "Krusten"-Aufbau bei langsamen Spreizen wartet weiter auf Klärung.

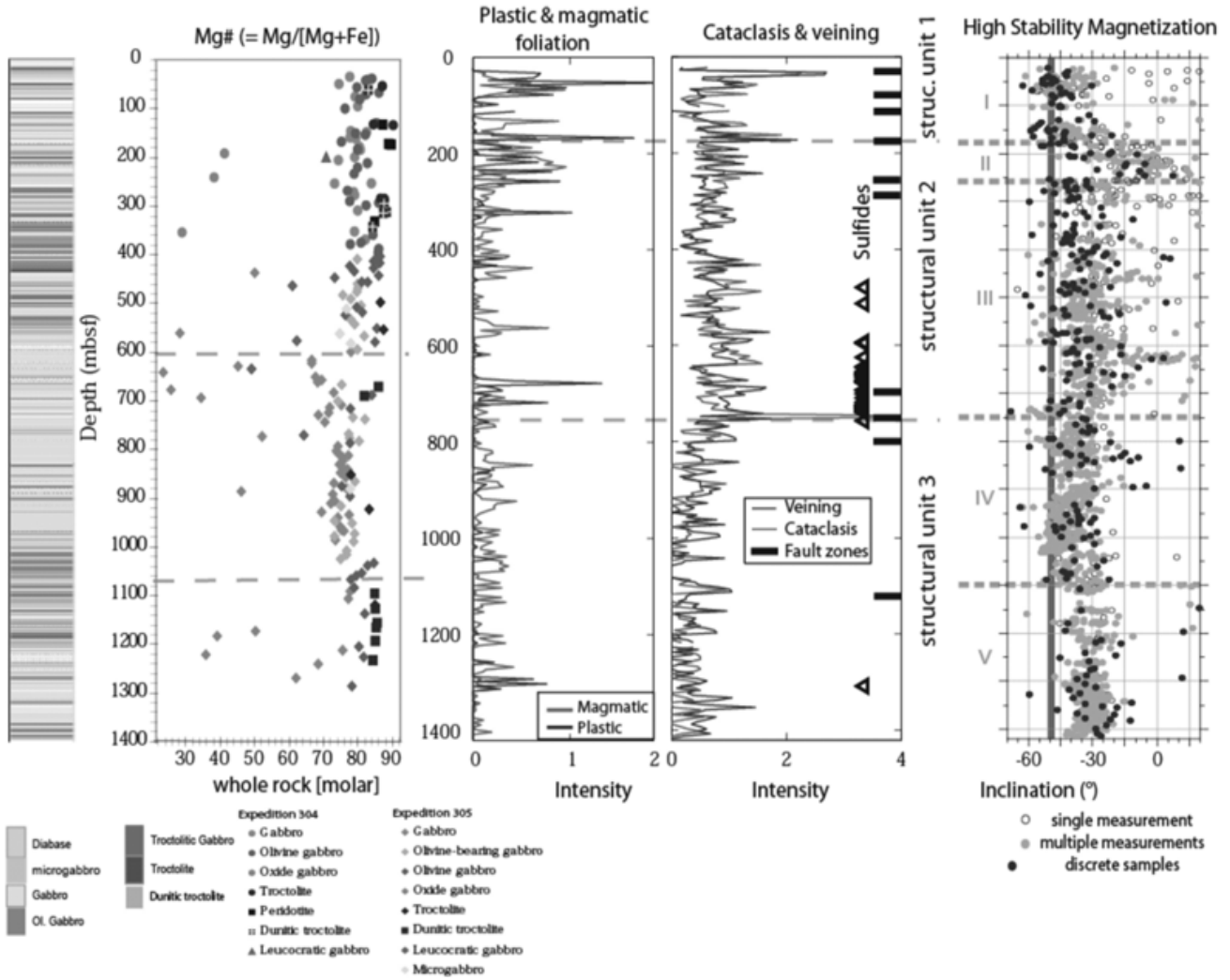

Abb.1 Shipbord Daten der Downhole Variation von Lithologie, Geochemie, Deformation, Vein-Häufigkeit, und Magnetik in Bohrung 1309D

Fahrtenbericht IODP Expedition 306:
Quaternary and Late Neogene North Atlantic Paleoceanography

Stein, R.[1], Grützner, J.[2], Hefter, J.[1], Kanamatsu, T.[3], Alvarez-Zarikian, C.[4], and the IODP Expedition 306 scientists

[1]Alfred Wegener Institute for Polar and Marine Research, Bremerhaven, Germany; [2]Research Center for Ocean Margins (RCOM), Bremen University, Germany; [3]Institute for Research on Earth Evolution, Japan Agency for Marine-Earth Science and Technology, Japan; [4]Integrated Ocean Drilling Program, Texas A&M University, College Station, Texas, USA

Understanding the mechanisms and causes of the abrupt climate change is one of the major challenges in global climate change research today. In this context, the determination of the long-term evolution of millennial-scale variability in surface temperature, ice sheet stability as source for meltwater discharge, and thermohaline circulation can provide clues to the mechanisms responsible for abrupt climate change, which are still poorly understood in detail. Thus, the main goal of IODP Expedition 306 - as of IODP Expedition 303 - was to generate a continuous late Neogene-Quaternary high-resolution chronostratigraphic template for North Atlantic climate proxies. The records will be correlated at sub-Milankovitch scale, and exported to other parts of the globe, using a range of stratigraphic tools including stable isotopes and relative (geomagnetic) paleointensity. (e.g., Channell et al., 2004, 2006; Shipboard Scientific Party, 2005; Expedition Scientists, 2005; Stein et al., 2006).

The JOIDES Resolution left Ponta Delgada (Azores) on March 9, 2005, for Expedition 306. This was the 6th expedition of the Integrated Ocean Drilling Program (IODP) and the second one - after Expedition 303 - primarily devoted to the investigation of North Atlantic climate change over the last few million years. For this specific research program, nine holes were drilled to a depth of several hundred meters below seafloor at three sites in the central North Atlantic between 40˚ and 56˚N in water depth between 2800 and 3400 m (Sites U1312, U1313, and U1314; Figs. 1 and 2). The high-resolution stratigraphic goals require high sedimentation rates (>5 cm/ky) at the chosen sites, as well as complete and undisturbed recovery of the stratigraphic sequences. For the latter purpose, the drilling strategy consisted of Advanced Piston Coring (APC) in multiple holes at each site.

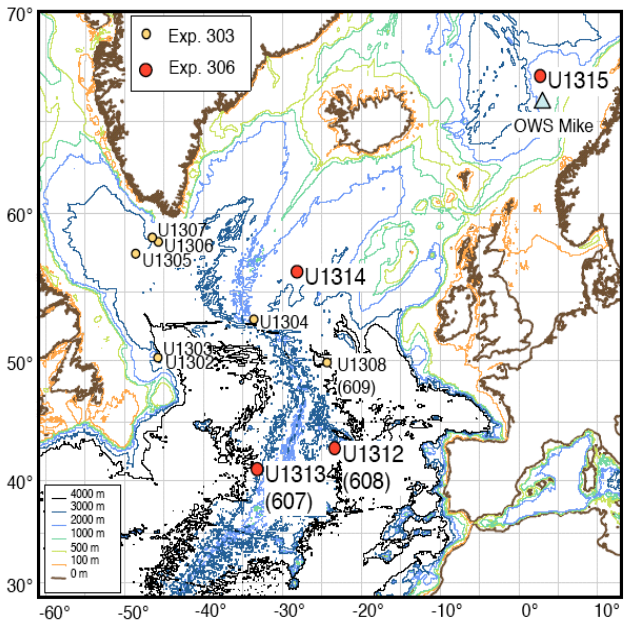

Fig. 1. Locations of Expedition 303 and 306 sites and ocean weather ship station "Mike".

The drilling locations selected for this North Atlantic paleoceanographic study are known, either from Deep Sea Drilling Project (DSDP) Leg 94 (Ruddiman, Kidd, Thomas et al., 1987) or from conventional piston coring, to have the potential for paleomagnetic and isotopic age control and sedimentation rates high enough for high-resolution reconstructions of sea-surface and bottom water characteristics and ice sheet instabilities during late Neogene to Pleistocene times. After having completed the coring activities at the three sites, the JOIDES Resolution steamed towards the north, crossing the Arctic Circle and reaching the Vøring Plateau off Norway on April 15. Here, as the second important objective of Expedition 306, a borehole observatory for measurements of bottom-water temperature and subbottom temperatures for long-term reconstruction of bottom-water temperatures was installed successfully in a newly drilled 180 m deep hole (Site U1315; Fig. 1). After 48 days at sea, JOIDES Resolution arrived in Dublin on April 25, 2005.

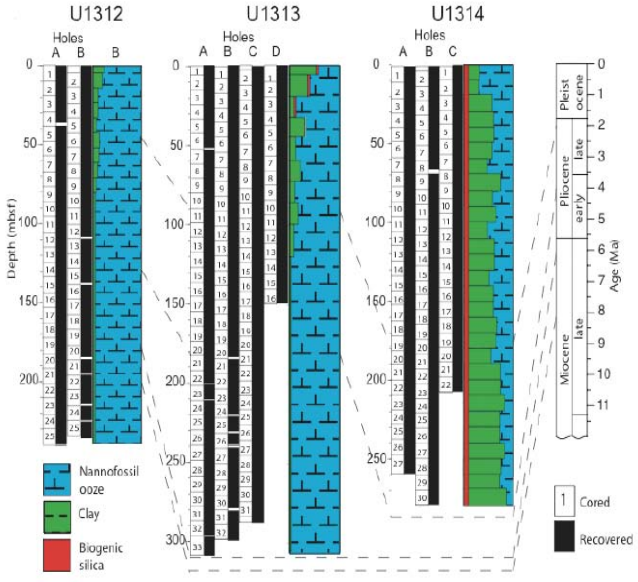

Fig. 2. Main lithology and age of Expedition 306 Sites U1312, U1313, and U1314.

North Atlantic paleoceanography study

For the North Atlantic paleoceanographic study, more than 2.3 km of high-quality sediment cores were recovered at the three sites during Expedition 306 (Expedition Scientists, 2005).

The sedimentary sequence of Site U1312 representing the last ~11 my will allow the study of short- and long-term climate variability and ocean/atmosphere interactions under very different boundary conditions, such as the closure and reopening of Atlantic/Mediterranean connections at the end of the Miocene (6-5 Ma), the closing of the Isthmus of Panama (4.5-3 Ma), and the onset of major Northern Hemisphere Glaciation near 2.7 Ma.

Site U1313 provides a unique and complete Pliocene-Pleistocene sediment section and will allow an optimal reconstruction of the phasing of the temperature records and its relationship to ice-sheet instability and changes in deep-water circulation throughout the last 5 Ma. High sedimentation rates of 13-14 cm/ky will allow a high-resolution study of paleoenvironmental change during the late Messinian.

At Site U1314, a complete Upper Pliocene to Holocene sequence, characterized by high sedimentation rates of 7 to >11 cm/ky, was recovered. Because of its location close to the IRD belt and bathed by NADW, this section will be used to establish a high-resolution (millennial to submillennial) environmental record of sea-surface and bottom water characteristics and a detrital (Heinrich type) stratigraphy for the past ~2.7 my.

All sedimentary sequences were logged for physical and paleomagnetic properties in the well-equipped laboratories onboard JOIDES Resolution. The preliminary shipboard data indicate that the onset of the major Northern Hemisphere Glaciation as well as glacial/interglacial and (sub-) millennial cycles of excellent quality are preserved in these sediments. At Sites U1312 and U1313, the detrital components become much more important and variable in the Upper Pliocene-Pleistocene interval of the sequence (Fig. 2), as indicated by the magnetic susceptibility record as well as the records of carbonate, natural gamma ray (NGR) and lightness (L*) from color reflectance measurements (Expedition Scientists, 2005), probably reflecting increased Northern Hemisphere ice sheet instability. At Site U1313, the lightness (L*) data mimic glacial/interglacial variations in the global benthic oxygen isotope stack of Lisiecki and Raymo (2005) in great detail (Stein et al., 2006).

From the multidisciplinary studies to be performed on these new IODP cores (together with the sites from IODP Expedition 303) during the coming years, new milestones in the understanding of mechanisms and causes of abrupt climate change, one of the major challenges in global climate change research today, are expected to be reached.

Monitoring of bottom-water temperatures in the North Atlantic

Direct long-term observations of bottom-water temperatures (BWT) are sparse. Longer-term BWT records going back beyond time scales of direct measurements, however, can be constructed from subbottom temperature-depth profiles in drill holes because they are continuously influenced by BWT (Chapman and Harris, 1992). The longest homogenous time series of temperature and salinity from the deep ocean over 50 years is available from the ocean weather ship station "Mike" (Gammelsrød et al., 1992), located on Vøring Plateau close to the old Ocean Drilling Program (ODP) Site 642 (Fig. 1). Furthermore, this site is located on the eastern margin of the Norwegian Sea, a climatically sensitive area that records the changing hydrographic character and horizontal exchange of deep water from the Greenland Sea, Arctic Ocean, and Norwegian Sea. As such, BWT histories from this location will yield insight into the complex interplay between these important water masses. This area was revisited by JOIDES Resolution during Expedition 306 to drill a new borehole and install a borehole observatory (Site U1315; Fig. 1). The installed

borehole observatory consists of a circulation obviation retrofit kit (CORK) to seal the borehole from the overlying ocean and instruments to monitor and document both bottom and sub-bottom temperature variations. The instrumentation in Hole U1315 includes two pressure cases and a thermistor string. This configuration allows high-precision temperature measurements as a function of both depth and time. By analysing sub-bottom temperature perturbations we expect to reconstruct for the first time a temperature record of bottom-water during at least the last 100 years, i.e., going back in time far beyond the directly measured temperature records available up to now. This record will contribute significantly to the ongoing discussion about causes and consequences of oceanographic and climatic changes observed in the North Atlantic over the last few decades. For further details see Harris and the IODP Expedition 306 Scientists (2006).

Acknowledgements

This success of Expedition 306 was the result of excellent cooperation between the IODP staff, the Transocean employees, and the Shipboard Science Party.

IODP Expedition 306 Scientists:

T. Kanamatsu (Co-Chief Scientist), R. Stein (Co-Chief Scientist), C. Alvarez-Zarikian (Staff Scientist), E. Aboudeshish, G. Acton, K. Akimoto, I. Bailey, K. Bjørklund, H. Evans, N. Fang, P. Ferretti, J. Gruetzner, Y. Guyodo, K. Hagino, D. Kulhanek, R. Harris, K. Hatakeda, J. Hefter, S. Higgins, S. Judge, F. Nanayama, S. Nielsen, M. Ohno, H. Rashid, F.J. Sierro, A. Voelker, and Q. Zhai.

References

Channell, J.E.T., Sato, T., Kanamatsu, T., Stein, R., Malone, M.J., and the Expedition 303/306 Project Team, 2004. North Atlantic climate. IODP Sci. Prosp., 303/306. http://iodp.tamu.edu/publications/SP/303306SP/303306SP.PDF.

Channell, J.E.T., Sato, T., Kanamatsu, T., Stein, R., Malone, M., Alvarez-Zarikian, C., and IODP Expedition 303/306 Scientists, 2006. IODP Expeditions 303 and 306 monitor Miocene-Quaternary climate in the North Atlantic. Scientific Drilling, in press.

Chapman, D.S., and Harris, R.N., 1993. Repeat temperature measurements in Borehole GC-1, northwestern Utah: towards isolating a climate-change signal in borehole temperature profiles. Geophys. Res. Lett., 18:1891-1894.

Expeditions Scientists, 2005. North Atlantic climate 2. IODP Prel. Rept., 306. doi:10.2204/IODP. PR.306.2005.

Gammelsrød, T., Østerhus, S., and Godøy, Ø., 1992. Decadal variations of ocean climate in the Norwegian Sea at Ocean Station "Mike" (65˚N 2˚E). ICES J. Mar. Sci., 195:68-75.

Harris, R.N. and the IODP Expedition 306 Scientists, 2006. IODP Expedition 306 Installs Borehole Observatory to Reconstruct Bottom Water Temperature Changes Through Time, Norwegian Sea. Scientific Drilling, in press.

Lisiecki, L.E. and Raymo, M.E., 2005. A Pliocene-Pleistocene stack of 57 globally distributed benthic ?18O records. Paleoceanography, 20, PA1003, doi:10.1029/2004PA001071.

Ruddiman, W.F., Kidd, R. B., and Thomas, E., et al., 1987. Init. Repts. DSDP, 94: Washington (U.S. Govt. Printing Office).

Shipboard Scientific Party, 2005. North Atlantic climate: ice sheet-ocean atmosphere interactions on millennial timescales during the late Neogene-Quaternary using a paleointensity-assisted chronology for the North Atlantic. IODP Prel. Rept., 303. http://iodp.tamu.edu/publications/PR/303PR/303PR.PDF.

Stein, R., Kanamatsu, T., Alvarez-Zarikian, C., Channell, J.E.T., and the IODP Expedition 306 scientists, 2006. Late Neogene/Quaternary North Atlantic paleoceanography explored during IODP Expedition 306. EOS, subm.

Fahrtenbericht IODP Expedition 307:
Drilling Challenger Mound - a cold-water coral structure in the Porcupine Seabight

T.G. Ferdelman[1,2], K. Mangelsdorf[1,3], J. Titschack1,[4], A. Kano[5], T. Williams[6], the IODP Expedition 307 Scientists, and J.-P. Henriet[7]

[1]DFG Schwerpunktprogamm: Integrated Ocean Drilling Program (SPP 527); [2]Department of Biogeochemistry, Max-Planck-Institute of Marine Microbiology, Celsiusstr. 1, 28359 Bremen, tferdelm@mpi-bremen.de; [3]GeoForschungsZentrum Potsdam, Dept 4.3, Telegrafenberg B423, 14473 Potsdam, k.mangelsdorf@gfz-potsdam.de; [4]Institute of Palaeontology, Erlangen University, Loewenichstr. 28, 91054 Erlangen, juergen.titschack@pal.uni-erlangen.de; [5]Department of Earth and Planetary Systems Science, Graduate School of Science, Hiroshima University, Kagamiyama 1-3-1, Higashi-hiroshima, 739-8526, Japan, kano@geol.sci.hiroshima-u.ac.jp; [6]Lamont-Doherty Earth Observatory of Columbia University, Borehole Research Group, PO Box 1000, 61 Route 9W, Palisades NY 10964, USA, trevor@ldeo.columbia.edu; [7]Renard Centre of Marine Geology, University of Ghent, Krijgslaan 281, S8, B-9000 Gent, Belgium jeanpierre.henriet@ugent.be

Introduction

Cold-water, coral-covered mounds occur widely along the European continental margin in water depths ranging from 40 - 1000 m, and are particularly abundant in the Porcupine Seabight, southwest of Ireland (Figure 1), where over a thousand mounds exist. At water depths of 600 to 900 meters, the mounds of the Porcupine Seabight form impressive conical bodies several km wide and up to 200 m in height. Whereas several mounds, e.g. Thérèse Mound and Galway Mound, are covered by thriving thickets of cold-water corals (typically Lophelia pertusa and Madrepora oculata), many mound tops and flanks are covered by dead coral rubble or are entirely buried by sediment (De Mol et al., 2002). The widespread discovery of large and numerous coral bearing banks and their association with mounds has generated significant interest as to the composition, origin and development of these structures.

Initiation and growth of these mound structures have been explained by two contrasting hypotheses: (1) oceanographic and paleoenvironmental conditions control mound initiation and growth (external control; Frederiksen et al., 1992), and (2) hydrocarbon seepage initiates microbial-induced carbonate formation and indirectly fuels coral growth (internal control) (Hovland et al., 1998; Henriet et al., 2002). The oceanographic or environmental hypothesis states that the two most important conditions for stimulating mound development are (1) strong, nutrient-rich currents that provide suspended food to the filter-feeding corals, sweeps the polyps clean of detritus, and inhibits sediment burial, and (2) a stable substrate for settlement of coral larvae. The latter hypothesis suggests that hydrocarbon seepage may promote favorable development conditions for deep-sea corals. Elevated dissolved inorganic carbon concentrations derived from the microbial mediated oxidation of methane are conducive to skeletal accretion and for submarine lithification.

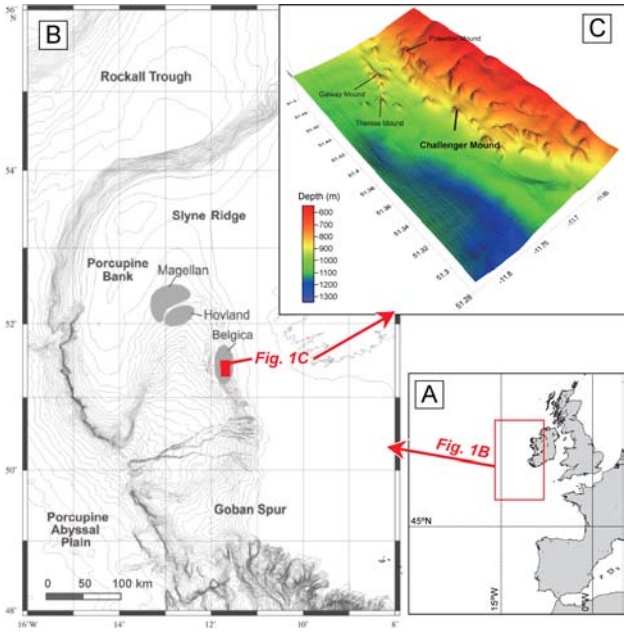

Figure 1: Operations area of IODP Expedition 307 showing A) the location of Porcupine Seabight; B) that the Belgica Mound Province is one of three main mound provinces; and C) multi-beam bathymetry of Belgic mound province on eastern slope of Porcupine Seabight (after Beyer et al. 2003).

Challenger Mound (Figure 1c) is one of thousands of mound structures in Porcupine Seabight and the first to be scientifically cored deeper than 12 meters. It has an elongated shape oriented along a north-northeast to south-southwest axis and lies partially buried under Pleistocene drift sediments. In high-resolution seismic profiles the mounds in the Belgica province appear to root on erosion surfaces (van Rooij et al. 2003). Challenger Mound, unlike the neighboring Thérèse and Galway mounds, has little to

no live coral coverage, and was therefore chosen as the main target for drilling activities. In May 2005, we successfully drilled 3 sites in an off-mound, mound, upper slope transect (Figure 2), within just twelve days of science operations onboard the D/V JOIDES Resolution. The additional sites were chosen to (1) constrain the stratigraphic framework of the slope/mound system, (2) to identify and correlate regional erosion surfaces identified in seismics, and (3) to investigate the hypothesized presence of hydrocarbons as the energy source for mound nucleation and sustained growth in a microbe-dominated environment.

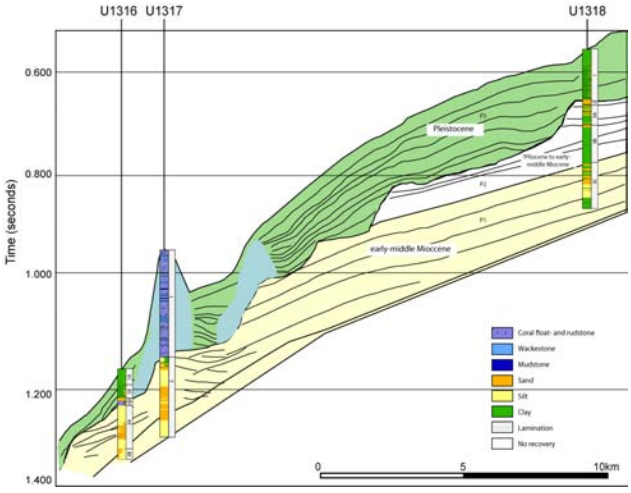

Figure 2: Lithostratigraphy of the three sites projected on the seismic profile of Challenger Mound along a north-northwest to south-southeast transect. Biostratigraphic dates for the 150 m thick mound sequence (blue) are suggest that the mound initiated growth between 1.95 Ma and ended before 0.46 Ma. Note the more recent, siliciclastic Pleistocene sediments that have onlapped and are slowly burying the older Pleistocene mound strata.

Lithostratigraphic Results

Drilling revealed that Challenger Mound (Site U1317) rests on a sharp erosion surface corresponding to the one identified in seismic profiles (Figure 2). This surface cuts across the lower lying Miocene-Pliocene siltstone succession (seismic unit P1). Sediments below this erosion surface consist of glauconitic and silty sandstone drift deposits of middle Miocene age that fine upwards toward more clay-rich intervals. The latter are tentatively interpreted to represent relatively low energy environments during the late Miocene to Pliocene. The Pliocene strata end abruptly in the firmground that is overlain by the Pleistocene mound succession. The first magnetostratigraphic and biostratigraphic results suggest that the hiatus between the two successions spans at least 1.65 million years. While the mound appears to be Pleistocene in age, the mound flanks are draped by comparably younger Pleistocene (< 0.26Ma) silty clay deposits that frequently contain dropstones.

Challenger Mound itself (Site U1317) is dominated by unlithified coral (Lophelia pertusa) bearing float- and rudstones. The muddy matrix of the sediments consists largely of terrigenous clay and calcareous nannofossils. The mound succession shows pronounced recurring cycles on a meter to several meter scale consisting of an alternation of float-, rud- and wackestone. The cycles found in the mound succession are possibly associated with the Pleistocene glacial/interglacial cycles.

Figure 2 shows the first interpretation of the lithostratigraphy and age-model superimposed on the seismic interpretation. Based on this schematic overview, the mound initiated growth on the erosion surface that divides seismic units P2 and P3. The timing of this erosion event is still unclear based on our initial shipboard data, but are tentatively correlated to an Early Pliocene erosion event in the nearby Rockall Basin (DeMol et al., 2002; Van Rooij et al., 2003). Calcareous nannofossil biostratigraphy indicates that deposition of the 150-m thick coral-bearing mound section started after 1.95 Ma and ended before 0.46 Ma. Upper Pleistocene to recent sediments are onlapping and have already buried the older Pleistocene mound strata.

Microbiology and Geochemistry

Significant hydrocarbon seepage is neither evident from the lithostratigraphy, nor from the initial geochemistry and microbiology results. Only low to moderate concentrations of methane or ethane (< 2 mM) were measured in the mound or in the sub-basal mound sediments. At Site U1317 (Challenger Mound), the methane-sulfate transition was detected only in the underlying Miocene silt and sandstones. No carbonate hardgrounds were observed at the mound base to suggest microbial induced carbonate precipitation.

Microbial effects on mound and submound diagenesis are subtle. We detected the methane-sulfate transition only in the deep-lying Micocene silt and sandstones underlying the mound, where methane concentrations and prokaryotic cell abundances increase with increasing depth. In the mound succession, interstitial water profiles of sulfate, alkalinity, Mg, and Sr suggest a tight coupling between carbonate diagenesis and microbial sulfate reduction. Concurrent increases in decreases in dissolved Sr and Mg/Ca ratios, respectively, indicate that dolomite or some other Ca-Mg carbonate mineral (e.g., low Mg calcite, calcian dolomite or dolomite) is precipitating. Decomposition of organic matter by sulfate reduction may be driving this process. At both off-mound sites, periods of rapid sedimentation overlying hiatuses have left distinct signals in the interstitial water chemistry of the predominately Pleistocene sediments that surround and partially bury the carbonate mounds.

Forthcoming Research and Implications

Although coral reefs are commonly associated with shallow-water tropical to subtropical regions, cold-water coral mounds are known from the geological record. Well-known examples include the Danian coral mound communities at Fakse in Denmark (Bernecker and Wiedlich, 2005), the Pleistocene St. Paul's Bay Limestone on the island of Rhodes (Titschack and Freiwald, 2005), and the Plio-Pleistocene deposits on the flanks of the Strait of Messina where probably the sole on-land exposed fossil mound with a comparable faunal association to its recent Atlantic counterparts occurs. We are confident that Expedition 307 will provide insight into the establishment of coral bearing mounds and build-ups in a predominately siliciclastic slope environments. Furthermore, Expedition will also help to place these mounds into the current mound concepts established from the fossil record, find possible fossil analogues, and shed light on their paleoenvironmental interpretation.

References

Bernecker, M. and Wiedlich, O. 2005. Azooxanthellate corals in the Late Maastrictian - Eary Paleocene of the Danish basin: bryozoan and coral mounds in a boreal shelf setting. In, Freiwald, A. and Roberts, M., Cold-water Corals and Ecosystems: New York (Springer-Verlag), 3-25.

Beyer, A., Schenke, H.W., Klenke, M., and Niederjasper, F., 2003. High resolution bathymetry of the eastern slope of the Porcupine Seabight. Mar. Geol., 198: 27-54.

De Mol, B., Van Rensbergen, P., Pillen, S., Van Herreweghe, K., Van Rooij, D., McDonnell, A., Huvenne, V., Ivanov, M., Swennen, R., and Henriet, J.-P., 2002. Large deep-water coral banks in the Porcupine Basin, southwest of Ireland. Mar. Geol., 188(1-2):193-231.

Frederiksen, R., Jensen, A., and Westerberg, H., 1992. the distribution of scleractinian coral Lophelia pertusa around the Faroe Islands and relation to tidal mixing. Sarsia, 77: 157-171.

Henriet, J.-P., De Mol, B., Vanneste, M., Huvenne, V., Van Rooij, D., and the Porcupine-Belgica 97, 98, and 99 Shipboard Parties, 2001. Carbonate mounds and slope failures in the Porcupine Basin: a development model involving fluid venting. In Shannon, P.M., Haughton, P., and Corcoran, D. (Eds.), Petroleum Exploration of Ireland's Offshore Basins. Geol. Soc. Spec. Publ., 188:375-383.

Hovland, M., Mortensen, P. B., Brattegard, T., Strass, P. and Rokengen K., 1998. Ahermatypic coral banks off mid-Norway; evidence for a link with seepage of light hydrocarbons. Palaios, 13:189-200.

Titschack and Freiwald, 2005. Growth, deposition, and facies of Pleistocene bathyal coral communities from Rhodes, Greece. In, Freiwald, A. and Roberts, M., Cold-water Corals and Ecosystems: New York (Springer-Verlag), 61-86.
Van Rooij, D., De Mol, B., Huvenne, V., Ivanov, M., and Henriet, J.-P., 2003. Seismic evidence of current-controlled sedimentation in the Belgica mound province, upper Porcupine slope, SW of Ireland. Mar. Geol., 195(1-4):31-53.

Related Web link: http://iodp.tamu.edu/scienceops/expeditions/exp307.html

Fahrtenbericht IODP Expedition 308:
Synopsis of IODP Expedition 308 Results, Gulf of Mexico Hydrogeology

Jan H. Behrmann[1], Peter B. Flemings[2], Cédric John[3] and IODP Expedition 308 Shipboard Scientific Party[3]
[1]University of Freiburg, Germany, [2]Penn State University, PA, USA, [3]Integrated Ocean Drilling Program, College Station, TX, USA; jan.behrmann@geologie.uni-freiburg.de, Phone: +49-761-2036495

Overview

Integrated Ocean Drilling Program (IODP) Expedition 308 was the first part of a two-component program dedicated to the study of overpressure and fluid flow on the Gulf of Mexico continental slope (Fig. 1). The scientific programme examined how sedimentation, overpressure, fluid flow, and deformation are coupled a passive margin setting. Expedition 308 tested a multidimensional flow model by examining how physical properties, pressure, temperature, and pore fluid compositions vary within low-permeability mudstones that overlie a permeable and overpressured aquifer. A reference location, Brazos-Trinity Basin IV, was drilled and logged at three sites (Sites U1319, U1320 and U1321), and in situ measurements of pressure were performed in where little overpressure was deemed to be present. These measurements were contrasted with experiments performed in a region of very rapid late Pleistocene sedimentation where overpressure was known to be present: the Ursa region of the northern Gulf of Mexico. Drilling there (at Sites U1322, U1323 and U1324) documented severe overpressure. Postcruise studies will illuminate controls on slope stability, seafloor seeps, and large-scale crustal fluid flow.

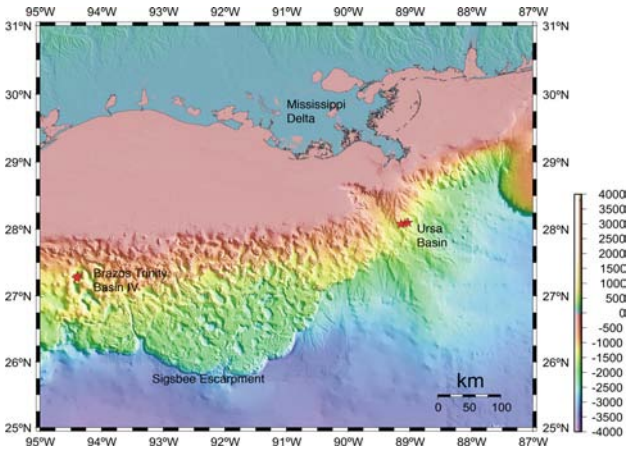

Fig. 1: Bathymetric image of the continental slope of the Gulf of Mexico. Proposed drilling was in the Brazos-Trinity Basin IV and Ursa Basin regions. IODP Sites U1319-U1324 are marked by red asterisks.

Expedition 308 science met many of the objectives proposed in the original IODP Proposal 589-Full3 and provided the foundation to implement long-term in situ monitoring experiments in the aquifer and bounding mudstones in a future expedition designed to meet the full objectives of the mentioned IODP Proposal. An important achievement of Expedition 308 is to have successfully recorded in situ formation pressure and temperature in an overpressured basin. This is the first time that a coherent data set of such measurements has been obtained.

Geological setting of Brazos Trinity IV and Ursa Basins

Brazos-Trinity Basin IV is located 200 km due south of Galveston, Texas (USA) in ~1400 m water depth (Fig. 1). The basin is one of a chain of five basins that are connected by interbasinal highs. It is a classic area for analysis of turbidite depositional environments because it is used as a modern analog to describe the formation of deepwater turbidite deposits. The primary data set used to evaluate the well locations is a high-resolution two-dimensional (2-D) seismic survey shot by Shell Exploration and Production Company to image the turbidite stratigraphy. The three drilled locations are shown on dip seismic Line 3020 (Fig. 2). Site U1320 is located where the turbidite deposits are thickest, whereas Site U1319 is along the southern flank of the basin where turbidite deposits are more condensed. Site U1321 was a pure LWD/MWD (logging while drilling/ measurement while drilling) hole and was not cored. This is the first time in ocean drilling that a hole was exlusively drilled for logging and MWD purposes.

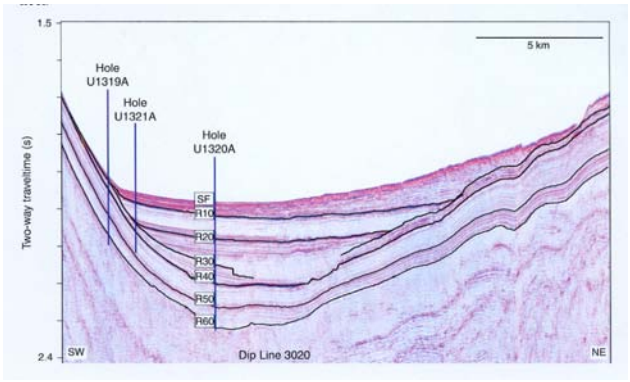

Fig.2: Dip seismic Section 3020, Brazos Trinity Basin IV, showing locations of Sites U1319, U1329 and U1321. R10-R60: regionally mapped seismic reflectors, SF = seafloor.

Ursa Basin is about 150 km due south of New Orleans, Louisiana (USA), and lies in about 1000 m of water. The region is of economic interest because of its prolific oilfields that lie at depths >4000 meters below seafloor (mbsf). We were interested in the sediments from 0 to 1000 mbsf. Four three-dimensional (3-D) seismic data sets are available within Ursa Basin. Fig. 3 shows the line most relevant to the three IODP Sites drilled at Ursa: U1322, U1323 and U1324. The high-resolution surveys were shot by Shell for the purpose of shallow hazards analysis. The sand-dominated Mississippi Canyon Blue Unit (Fig. 3), is a late Pleistocene "ponded fan" deposited in a broad topographic low. The Blue Unit is overlain by a leveed-channel assemblage that is mud dominated. The most spectacular feature is the sand-cored leveed-channel facies pattern of the Ursa Canyon (Fig. 3), overlain by the muddy eastern levee deposits of the Southwest Pass Canyon, and a hemipelagic drape cover. The post-Blue Unit mudstone package has numerous detachment surfaces that record slumping (Fig. 3) to form mass transport deposits.

Geotechnical studies, Brazos Trinity Basin IV

In the three drillholes in Brazos Trinity Basin IV it was learnt that there are discontinuous and continuous downhole changes in physical properties measured on board JOIDES RESOLUTION, especially at Site U1319. Both, basin sediments (down to reflector R40) and pre-basin sediments (below reflector R40) are essentially non-slumped, normally consolidated muds that provide an excellent reference for materials found within the Basin (Site U1320) and at Ursa Basin (Sites U1322 and U1324). Porosity at Site U1319 deceases downhole exponentially from 80% to 50%, while there are marked discontinuities in (vane) peak shear stength below Reflector R50 (Fig. 2).

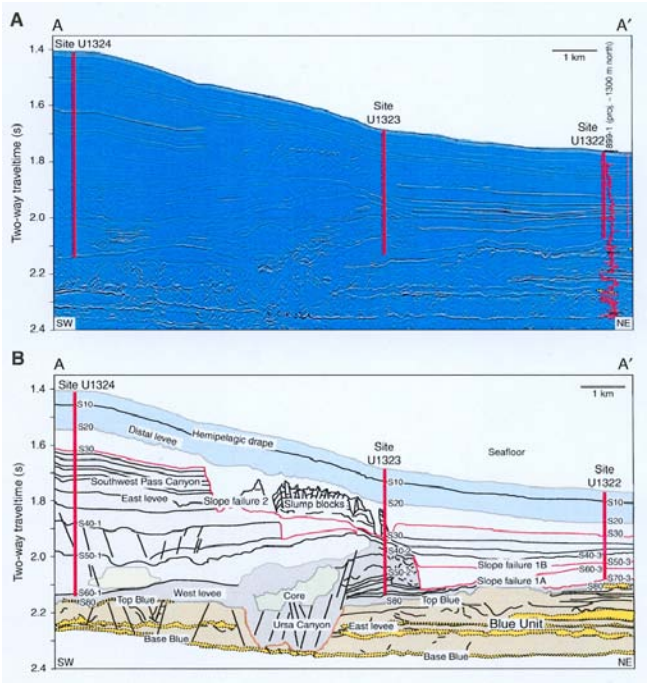

Fig. 3: A. E-W Seismic cross-section of Ursa Basin and Sites U1322-U1324. B. Interpreted cross-section. The sand-prone Blue Unit has been incised by a channel-levee complex and then overlain by a thick and heavily slumped hemipelagic mudstone wedge that thickens to the west (left). Seismic reproduced with permission of Shell Exploration and Production Company.

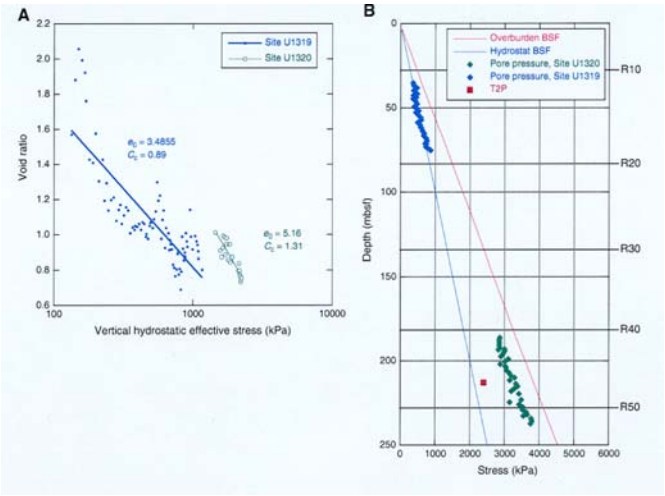

Fig. 4: A. Void ratio (e) versus hydrostatic vertical effective stress (σ'_{vh}) for all sediments below Reflector R40 at Sites U1319 and U1320. The reference void ratio (e0) and compression index (Cc) are derived from a fit of the type e = e0 - Cc ln(σ'_{vh}). B. Pore pressures for Site U1322 and U1324 are derived from parameters derived in A. assuming that trend at Site U1319 is hydrostatically pressured. BSF =below seafloor. From Expedition 308 Scientists (2005).

Site U1320, in comparison with Site U1319, has a section of underconsolidated muds and clays below Reflector R40 (Fig. 2), an effect that was not anticipated, but is easily explained by rapid sediment loading and fluid trapping in the muds of the basin interior. This is shown instructively by Fig. 4, where void ratio (e) is plotted versus hydrostatic vertical effective stress (σ'_{vh}) for all sediments below Reflector R40 at Sites U1319 and U1320, and estimates of ambient overpressures are derived.

Overpressured Sites, Ursa Basin

In the Ursa Basin Expedition 308 tested a flow model by examining how physical properties, pressure temperature, and pore fluid composition vary within low-permeability mudstones that overlie a permeable and overpressured aquifer. Penetrometer measurements, made at two sites, define the spatial variation in pressure and temperature in low permeability mudstones in the shallow sedimentary section. Sites U1322 and U1324 were located ~10 km apart on an E-W transect traversing a clastic sediment prism of Quaternary age, and were drilled to 234 and 608 meters below seafloor, respectively. λ' (fluid overpressure divided by hydrostatic effective stress) is approximately 0.6 in both locations (i.e. the pore pressure lies 60% of the way between hydrostatic and lithostatic). The overpressured section may begin at a shallower depth at Site U1322 (see Fig. 5) than at Site U1324. The temperature gradients are linear, but is 25% greater at Site U1322 than at Site U1324. Thermal conductivities at the two locations are similar (~1.2 vs 1.15 W/m·K), implying a vertical conductive heat flow of ~22 mW/m2 at Site U1324 vs ~30 mW/m2 at Site U1322.

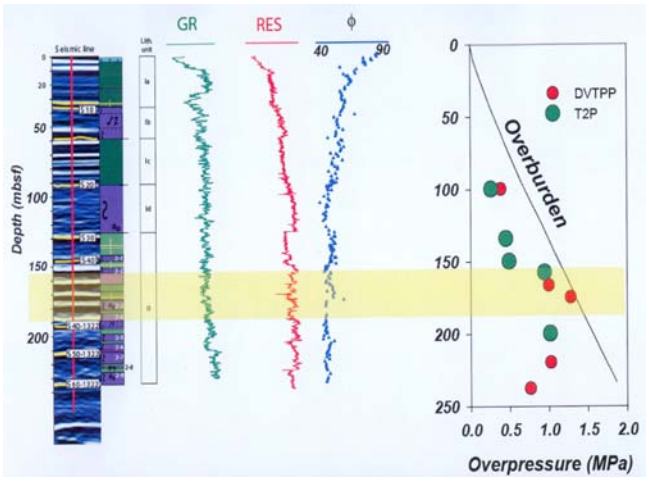

Fig. 5: Seismic strip chart, gamma ray, resistivity and porosity logs, and in situ pressure measurements from the T2P and DVTPP probes for Site U1322.

Sedimentation is considerably faster at Site U1324 than at Site U1322 (10 vs. 3.8 mm/y). The similar overpressure gradients present at both sites in spite of the almost 3-fold difference in sedimentation rate imply a component of lateral flow between them: this flow increases the pressure at Site U1322 relative to a system with only vertical fluid migration. In the Blue Unit, composed of interbedded sheet sands and mudstones and underlying the Ursa mudstones, fluid overpressures generated by rapid loading at Site U1322 may be partially dissipated by efficient lateral fluid migration. This provides an additional explanation for the elevated temperature gradient at Site U1322. Viewed on a basin scale, this pattern of lateral fluid flow may be the prime locator for cold seaps, mud volcanoes, and a trigger for repeated submarine landslides generating major mass transport deposits within the past 50000 years.

Preliminary report of Exp. 308 to be found at:
http://iodp.tamu.edu/publications/PR/308PR/308PR.html

Fahrtenbericht IODP Expedition 309:
Towards a complete in situ section of oceanic crust: Preliminary results from IODP Expedition 309 to Hole 1256D, East Pacific

J. Geldmacher[1] and the Expedition 309 and 312 Shipboard Scientific Parties
[1]Leibniz-Institut für Meereswissenschaften, IFM-GEOMAR, Dienstgebäude Ost, Wischhofstr. 1-3, 24148 Kiel

Sampling of a complete section of in situ oceanic crust is essential for the understanding of crustal formation and the complex interplay between magmatism and seafloor alteration/ metamorphism. However, drilling of an entire section of oceanic

crust is a time-consuming and technically challenging task and therefore has been an unfulfilled goal of Earth scientists since the beginning of scientific ocean drilling. IODP Expedition 309 ("Superfast Spreading Crust II", Christobal 08.07.05 - Balboa 28.08.05) was part of a multi-expedition project to drill a complete section of upper oceanic crust extending through the extrusive lavas, sheeted dikes and eventually into gabbros. Expedition 309 (July-August 2005) successfully deepened ODP Hole 1256D (Wilson et al., 2003) by 503 m to a total depth of 1255.1 meters below seafloor (mbsf) or 1005.1 m below the sedimentary cover (Expedition 309 Scientists, 2005). The average rate of core recovery was 36%, however, at depths below 1200 mbsf core recovery increased to over 70%. The drill site is located on 15 Ma old oceanic lithosphere on the Cocos Plate (6.736˚N, 91.934˚W) that was formed during a period of superfast spreading (~220 mm/yr, ~20 to 11 Ma, Wilson, 1996) on the East Pacific Rise (Fig. 1). This site was chosen based on geophysical models and seismic observations showing an inverse relationship between spreading rate and depth of axial low velocity zones (magma chambers).

Based on Expedition 309 core descriptions (coupled with observations from Leg 206), the upper igneous oceanic crust at Site 1256 is subdivided as follows (Fig. 2): Lava Pond (250-350 mbsf), Inflated Flows (350-534 mbsf), Sheet and Massive Flows (534-1004 mbsf), Transition Zone (1004-1061 mbsf) and Sheeted Intrusives/Dikes (> 1060 mbsf). The first two subdivisions were drilled on Leg 206 and are interpreted to have formed up to several kilometers off-axis (e.g. Teagle et al., 2003).

The Sheet and Massive Flow sequence makes up the largest part of extrusive lavas at Hole 1256D and is formed by sheet flows (up to ~3m thick) and subordinate massive flows (> 3m thick). Individual flows or cooling units can be recognized by grain size variations and chilled margins. Recovered flow contacts are commonly marked by fresh or altered glass or by the presence of volcanic breccia (Figure 2). In contrast to the upper section of the Inflated Flows, no characteristic pillow basalt units have been recovered in the Sheet and Massive Flow section. In general, the flows are non-vesicular, aphyric to sparsely phyric (rarely moderately phyric) and grain size ranges from cryptocrystalline to microcrystalline. Massive, fine-grained lavas, however, become more abundant with depth.

Below ~900 mbsf, sets of subvertical fractures in the recovered rocks attract attention as these features probably indicate nearby diking. Furthermore, the appearance of volcanic breccias increases strikingly downhole. The occurrence of a massive cataclastic unit at 1004 mbsf defines the beginning of the Transition Zone. The cataclastic rock consists of subvertically oriented cryptocrystalline basalt clasts hosted by highly altered, brecciated fine-grained basalt that is crosscut by numerous fine veinelets. The first subvertical intrusive contact recovered during Expedition 309 is also encountered in the Transition Zone at 1018 mbsf.

The upper boundary to the Sheeted Intrusives is defined by the change from sheet flows to massive basalts at ~1060 mbsf. From that level, aphyric massive basalts are the dominant rock type and subvertical chilled dike contacts become increasingly common downhole. The predominance of vertical features such as fractures, chilled margins and intrusive contacts, the rareness of vesicles, and the lack of clear evidence of submarine eruption, suggests that the Sheeted Intrusives represent the beginning of the sheeted dike complex. The difference of massive basalt units of the Sheeted Intrusives compared to massive flows in the upper sequences at Site 1256D is also demonstrated by a significant decrease of their average porosity from 4±1% to 2±1% across the 1060 mbsf boundary. There is also a discrete change in physical properties with significant increase in average thermal conductivity from 1,8 ±0,2 W/m/K to 2,1±0,1 W/m/K and in seismic velocity from 5,4±0,3 km/s to 5,8±0,1 km/s. However, if all these massive units represent subvertical dikes or partly sub-volcanic sills remained unconfirmed.

Preliminary data of trace element concentrations from all recovered basalts are similar to average Mid Ocean Ridge Basalt from the East Pacific Rise. Hole 1256D is only the second drill hole to penetrate the transition from low-temperature alteration to high-temperature hydrothermal alteration in a continuous section of oceanic crust (Teagle et al., 2005). Down to ~964 mbsf, almost to the base of the Sheet and Massive Flow sequence, the lavas show evidence for low-temperature seawater alteration. This alteration style changes from 964 m to 1028 mbsf where pyrite-rich alteration halos and mixed-layered chlorite/smectite start to replace hitherto present pure saponite and celadonite. Below ~1028 mbsf the first characteristic hydrothermal alteration minerals, such as actinolite, prehnite, titanite and epidote are encountered, all are indicative of former subgreenschist to greenshist facies conditions.

Expedition 309 Scientists (2005) A complete in situ section of upper oceanic crust formed at a superfast spreading rate. IODP Preliminary Report, 309. Available from World Wide Web: http://www-iodp.tamu.edu/ publications/PR.html

Teagle D.A.H., Wilson D.S., Acton G.D., and the Leg 206 Shipboard Scientific Party (2003) ODP Leg 206. Upper oceanic crust formed at a superfast spreading rate. Joides Journal 29, No 2, 13-17

Teagle D.A.H., Banerjee N.R., and the Expedition 309 Shipboard Scientific Party (2005) The Hard Yards: Deep basement drilling of an in situ section of oceanic crust formed at a superfast spreading rate. Recent results from IODP Expedition 309 to Hole 1256D, eastern Equatorial Pacific. InterRidge News 14, 8-11

Wilson D.S., Teagle D.A.H., Acton G.D., et al. (2003) Proc. ODP, Initial Reports, 206 (Online). Available from World Wide Web: http://www-odp.tamu.edu/publications/206_IR/206ir.htm

Wilson D.S. (1996) Fastest known spreading on the Miocene Cocos-Pacific plate boundary. Geophys. Res. Lett. 23, 3003-3006

[Figure next page]

Fahrtenbericht IODP Expedition 310:
Tahiti Sea Level Expedition

Thomas Felis and Hildegard Westphal
Universität Bremen

The history of sea level and sea surface temperature variation associated with the last deglaciation is of prime interest to understanding dynamics of large ice sheets and their effects on Earth's eustasy. So far, the only sea level record that encompasses the whole deglaciation is based on offshore drilling of Barbados coral reefs which overlie an active subduction zone, implying that the apparent sea level record may be biased by tectonic movements. The Tahiti Sea Level Expedition (IODP Expedition 310) seeks to establish the course and effects of the last deglaciation in a reef setting which developed in a tectonically inactive area at sites located far away from glaciated regions, in Tahiti (French Polynesia, South Pacific).

The major scientific objectives of IODP Expedition 310 are: To reconstruct the deglaciation sea-level curve for the period 20,000 to 10,000 years BP in order to establish the minimum sea level during the Last Glacial Maximum (LGM), and to assess the validity, the timing and the amplitude of meltwater pulses which are thought to have disturbed the general thermohaline oceanic circulation and, hence, global climate.

To define the sea surface temperature variation for the region over the period 20,000 to 10,000 years BP in order to identify and to establish patterns of short-term paleoclimatic changes such as climate variability associated with the El Niño-Southern Oscillation (ENSO).

To analyse the impact of sea level changes on reef growth, geometry and biological makeup, especially during reef drowning events, in order to improve the modelling of reef development.

IODP Expedition 310 is a Mission Specific Platform Expedition implemented by the European Consortium for Ocean Research Drilling (ECORD) and conducted by the ECORD Science Operator (ESO). The offshore phase of Expedition 310 took place from 6 October to 16 November 2005 in the South Pacific. The onshore phase of Expedition 310 will take place during February to March 2006 at the ODP/IODP Core Repository

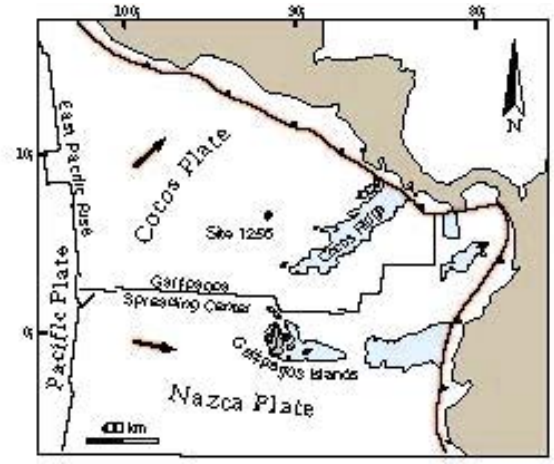

Fig.1:
Present tectonic setting of Site 1256 on the Cocos Plate.

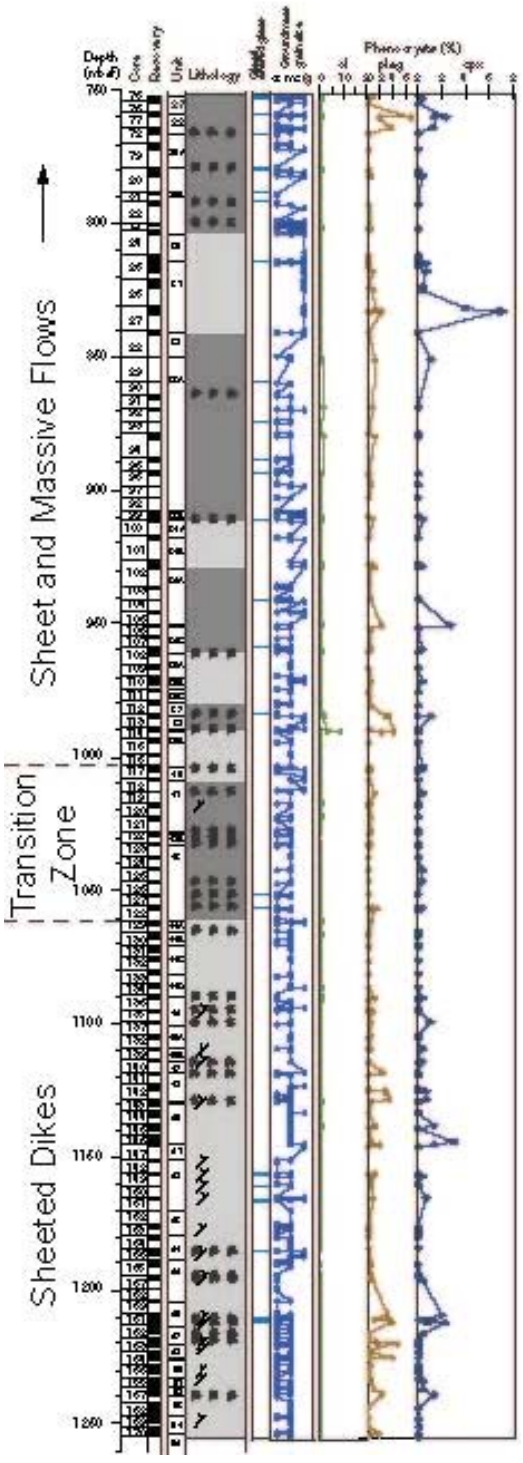

Fig. 2: Simplified igneous stratigraphy of Hole 1256D (section cored during Expedition 309) showing the dominant rock lithologies, petrological parameters and preliminary subdivision (Expedition 309 Scientists, 2005). cx= cryptocrystalline, mc= microcrystalline, fg= fine grained. ol= olivine, plg= plagioclase, cpx= clinopyroxene.

[to Abstract Geldmacher et al.]

at the University of Bremen (Bremen Core Repository, BCR). IODP Expedition 310 will be completed at the end of the Onshore Science Party in Bremen. The departure from Bremen is considered equivalent to disembarking the JOIDES Resolution.

IODP Expedition 310 is one of the most extensive geological research investigations ever undertaken in a coral reef area. The drillship of Expedition 310 was the DP Hunter, a dynamically positioned, 104 m-long ship that has a large moonpool and that mostly is used for diving and ROV work (Figure 1). The drilling contractors were Seacore Ltd. The rig was their R100, the same as that was used in the Arctic for the ACEX Expedition (IODP Expedition 301).

During the offshore phase of IODP Expedition 310 transects were drilled in 3 study areas in water depths ranging from 41 to

117 m, amounting to a total of 37 holes at 22 sites with a maximum penetration of 102.17 m. All transects were very close to the shore (Figure 2). Two transects were immediately outside the barrier reef, and a third extended inside the outer limit of the reef. A total of 1099.83 m was drilled, and the total recovery was 632.12 m. This corresponds to an average recovery of 57.47%. Assuming a cavity porosity of about 20%, recovery reaches almost 80%.

Living reefs are very sensitive ecosystems, and great care was undertaken in order to minimize the impact of drilling on the reefs. Seawater was used as the drilling lubricant, and the dynamic positioning of the vessel restricted the seabed footprint to that of the hole and the baseplate. Furthermore, on location, the drillstring was positioned by colour video camera to avoid live corals. Overall, the offshore drilling in Tahiti did not have any significant impact on the living reef, but will provide a wealth of data on reef development and the oceanographic conditions in which it grew.

An example of the wealth of new information includes time-windows of interannual to decadal climate variability in the South Pacific during the LGM and the last deglaciation, reconstructed from fossil, annually banded reef corals recovered during Expedition 310. Oxygen isotope and Sr/Ca variations in coral skeletons can be used to generate sub-seasonally resolved reconstructions of changes in both temperature and hydrologic balance at the sea surface during time intervals from 21 to 10 kyr ago. Such an approach will provide unique insights into the dynamics of natural modes of atmosphere/ocean variability, such as the El Niño-Southern Oscillation, under boundary conditions different from today. Comparing such coral based reconstructions with state-of-the-art climate model simulations might also help to assess the validity of future greenhouse projections.

Another example is the study of microbial crusts, which are important indicators of varying oceanographic conditions, and are uncommonly abundant in the Tahiti reef succession; a peculiarity that is not fully understood yet. Microbialites and underlying coral heads of the postglacial sequence recovered during Expedition 310 can be studied for geochemical and biogeochemical, and structural and taxonomic trends, complemented by analyses of benthic and planktic foraminifers. Such an approach will provide a comprehensive picture of oceanographic changes with one focus on nutrient levels during the transition from the LGM to present-day sea level. Both approaches address major scientific objectives of the expedition.

References

Camoin, G. F., Iryu, Y., McInroy, D. (2005) Integrated Ocean Drilling Program Expedition 310 Scientific Prospectus, Tahiti Sea Level Expedition, The last deglacial sea level rise in the south Pacific, pp 48.

Evans, D. (2005) Operational aspects of the Tahiti Sea Level Expedition, ECORD Newsletter # 5, 2.

Figure 1. The DP Hunter, the drillship of IODP Tahiti Sea Level Expedition (IODP Expedition 310) offshore Tahiti, South Pacific Ocean, October 2005

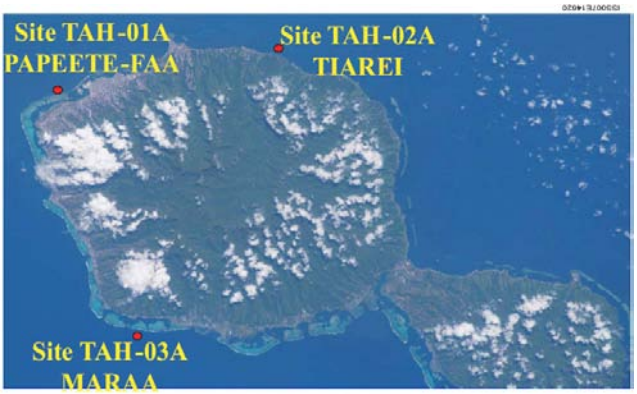

Figure 2. Satellite image showing the location of the 3 study areas of IODP Expedition 310 around the island of Tahiti (South Pacific): PAPEETE-FAA (Prospectus Site TAH-01A), TIAREI (Prospectus Site TAH-02A) and MAARA (Prospectus Site TAH-03A). Note the proximity of the study areas to the barrier reef and the shore, with water depths ranging from 41 to 117 m.

Figure 3. A continuous 3 m core of fossil reef material recovered as a single piece during IODP Expedition 310.

Figure 4. Example of core catcher samples from IODP 310. Core 5C-15CC, 85 mbsl, 26 mbfl. Note lamination.

Fahrtenbericht IODP Expedition 311: Cascadia Margin Gas Hydrates

Heuer, V., Teichert, B.M.A., and Expedition 311 Shipboard Scientific Party

IODP Expedition 311 (September 16 to October 28, 2005) aimed to constrain models for the formation of marine gas hydrate in subduction zone accretionary prisms. The objectives of this expedition were:

- Study the formation of natural gas hydrate in marine sediments.
- Determine the mechanism of development, nature, magnitude, and global distribution of gas hydrate reservoirs.
- Investigate the gas transport mechanism, and migration pathways through sedimentary structures, from site of origin to reservoir.
- Examine the effect of gas hydrate on the physical properties of the enclosing seidments, particularly as it relates to the potential relationship between gas hydrates and slope stability.
- Investigate the microbiology and geochemistry associated with gas hydrate formation and dissociation.

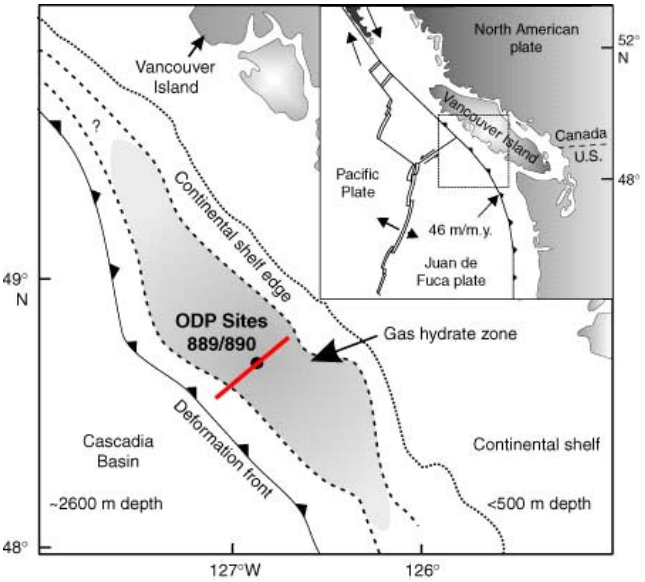

Figure 1: General location of drilling transect near previous ODP Sites 889/890 (Leg 146). A bottom-simulating reflector is present on ~50% of the midcontinental slope (shaded area) from Expedition 311 Scientists (2005).

To meet these objectives, coring and downhole measurements were conducted along a transect of four sites (U1325, U1326, U1327, and U1329) representing different stages in the evolution of gas hydrate across the Northern Cascadia margin (Fig. 1). The earliest occurrence of gas hydrate is found on the westernmost first accretionary ridge (Site U1326) and the final stage in gas hydrate evolution at the Eastern margin where shallower water depths limit the stability of gas hydrate (Site U1329). In addition to the transect, a cold vent with active fluid and gas flow (Site U1328) was visited.

The Cascadia margin off the coast of Oregon and Vancouver Island is a typical subduction zone accretionary prism and represents together with the passive margin setting in the Blake Ridge region off the east coast of North America one of the best studied marine gas hydrate areas (e.g. ODP Legs 146 and 204). Within accretionary prisms, the largest amount of gas hydrate appears to occur in a widespread layer located just above the BSR, but a portion of the upward methane flux follows localized migration conduits and forms concentrated near-seafloor gas hydrate accumulations. Because the latter can dissociate quickly, they are particularly important for the response of marine gas hydrate to global warming. Off Vancouver Island a gas hydrate-related BSR occurs in a 30 km wide band parallel to the coast beneath much of the continental slope. Prior to IODP Expedition 311, gas hydrate was expected to be concentrated in a layer 50-100 m thick, just above the base of the gas hydrate stability field, which is located 200-300 m below seafloor (mbsf), and gas hydrate concentrations were estimated to fill ~30% of pore space (Hyndman et al., 2001; Spence et al., 2000).

To collect the necessary data, IODP Expedition 311 adopted the following approach: (1) At the start of the expedition, logging while drilling/measurement while drilling (LWD/MWD) was carried out first at all five sites (Fig. 2). The obtained data guided subsequent coring and special tool deployments. For further geophysical characterization of the study area, the LWD/MWD program was combined with wireline logging at each site and two vertical seismic profiles were completed at Sites U1327 and U1328. (2) A total of 1217.76 m of sediment core was recovered using the advanced piston corer (APC) and extended core barrel (XCB) systems. Immediately after core retrieval, cold spots indicative for the presence of gas hydrate were localized by infrared imaging (Fig. 2) and visible gas hydrate was sampled

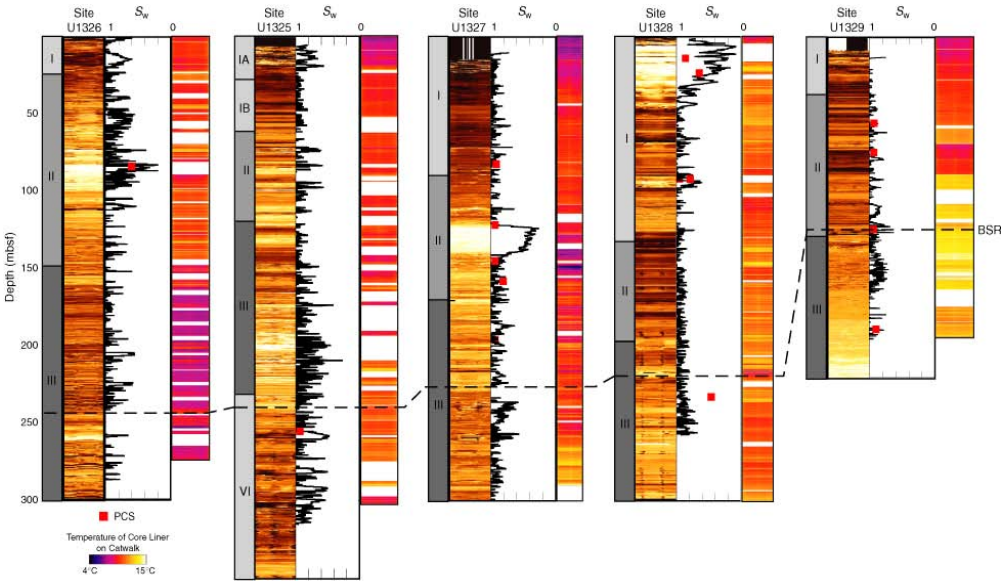

Figure 2: Summary of Expedition 311 results showing from left to right: Lithostratigraphic units, LWD resistivity-at-the-bit (RAB) images, pore water saturations derived from LWD data using Archie's relation (Sw; the mathematical complement of gas hydrate saturation), compressed infrared images of core liner temperature and location of the bottom-simulating reflector (BSR). PCS = pressure core sampler (Expedition 311 Scientists, 2005).

directly. Shipboard analysis of core-derived gas chemistry and interstitial water chlorinities served as further proxies for the occurrence of gas hydrate. (3) Regular APC/XCB coring was interspersed with 24 (16 successful) pressure core sampler runs for onboard degassing experiments and 19 Fugro piston corer/HYACE deployments. In the pressure cores, methane hydrate distribution was determined by non-destructive measurement of physical properties of the cores at in situ pressures. Furthermore, methane hydrate quantities were obtained from degassing experiments and mass balance calculations. In addition, four of the collected pressure cores were stored under in situ pressure for subsequent shore-based studies.

Based on this approach, indirect evidence for the presence of gas hydrate was obtained from increased electrical resistivities and P-wave velocities on downhole logs and low-salinity interstitial water anomalies, numerous infrared cold spots, and decreases in void gas C1/C2 ratios, as well as from gas hydrate-related sedimentological moussy/soupy textures in recovered cores. In addition, gas hydrate was observed directly in the recovered cores, and >30 gas hydrate samples were preserved in liquid nitrogen for shore-based studies. Furthermore, gas hydrate and free gas concentrations derived from degassing experiments with pressure cores agree well with estimates from LWD/MWD data. The combined observations show that gas hydrate often occurs within coarser-grained turbidite sands and silts (Expedition 311 Scientists, 2005).

At the Cascadia margin, the occurrence of gas hydrate appears to be controlled by several key factors, and the concentration of gas hydrate changes significantly as those factors vary in the sediments along the margin. The key controlling factors are (1) local methane solubility linked with pore water salinity, (2) fluid/gas advection rates, and (3) availability of suitable host material (coarse-grained sediments). In the previous model for gas hydrate formation in an accretionary margin (Hyndman et al., 2001; Spence et al., 2000), the highest concentrations of gas hydrate were expected to occur localized near the base of the gas hydrate stability zone above the bottom-simulating reflector (BSR), with concentrations gradually decreasing upward as a result of pervasive fluid advection from overall tectonically driven fluid expulsion. However, the results of Expedition 311 show that this model is too simple and that there are additional overprinting factors. Although evidence for widespread gas hydrate-related BSRs was observed in the data, by far the largest concentrations of gas hydrate were observed at the top of the gas hydrate occurrence zone, at a point where the amount of methane in the pore fluid exceeds the local methane solubility threshold. This was especially observed at Sites U1326 and U1327, where gas hydrate deposits several tens of meters thick occur at a shallow depth of ~100 mbsf with concentrations locally exceeding 80% of the pore volume. Another site of very large gas hydrate concentrations was found at the cold vent Site U1328, where beds of massive gas hydrate occur within the top ~40 mbsf with concentrations exceeding 80% of the pore space as a result of focused fluid/gas migration from underneath (Expedition 311 Scientists, 2005).

Preexpedition models that had predicted the occurrence of a highly concentrated gas hydrate section (50-100 m thick) just above the base of the gas hydrate stability zone do not to take into account the geologic complexity revealed during Expedition 311, in that the occurrence of gas hydrate appears to require the contribution from mixed gas sources, including a potential deep thermogenic gas source. The occurrence of migration conduits and host sands also controls the spatial distribution of gas hydrates on the Cascadia margin (Expedition 311 Scientists, 2005).

References

Expedition 311 Scientists, 2005. Cascadia margin gas hydrates. IODP Prel. Rept., 311. doi:10:2204/iodp.pr.311.2005

Hyndman, R.D., Spence, G.D., Chapman, N.R., Riedel, M., and Edwards, R.N., 2001. Geophysical studies of marine gas hydrate in northern Cascadia. In Paull, C.K., and Dillon, W.P. (Eds.), Natural Gas Hydrates, Occurrence, Distribution and Detection. Geophys. Monogr., 124:273-295.

Spence, G.D., Hyndman, R.D., Chapman, N.R., Riedel, M., Edwards, N., and Yuan, J., 2000. Cascadia margin, northeast Pacific Ocean: hydrate distribution from geophysical investigations. In Max, M.D. (Ed.), Natural Gas Hydrate in Ocean and Permafrost Environments:New York (Kluwer Academic Publisher).

Fahrtenbericht IODP Expedition 312:
Superfast Spreading Rate Crust III

Juergen Koepke, Birgit Scheibner, Expedition 309, and Expedition 312 Scientific Parties

Expedition 312, Superfast Spreading Crust III, started at the 12.11.2005 in Acapulco (Mexico) and ended at 29.12.2005 in Cristobal (Panama). It is the third part of a multi-cruise program to drill a complete section of the upper oceanic crust into the underlying gabbros. Hole 1256D (6.736˚N, 91.934˚W) was initiated during Ocean Drilling Program Leg 206 in the eastern equatorial Pacific in 15 Ma crust that formed at the East Pacific Rise during a period of superfast spreading (~220 mm/y). This site was chosen to exploit the inverse relationship between spreading rate and the depth to axial low-velocity zones, thought to be magma chambers now frozen as gabbros, observed from seismic experiments. During Integrated Ocean Drilling Program (IODP) Expedition 309 in Jul-Aug 2005, Hole 1256D was deepened to a total depth of 1255 meters below seafloor (mbsf). Expedition 312 returned to Hole 1256D and deepened it to 1507 mbsf. The hole now extends through 810 m of extrusive normal mid-ocean-ridge basalt, 345.7 m of sheeted dikes, and 100.5 m into plutonic rocks, completing the first penetration of an intact section of the upper oceanic crust. Gabbros were encountered at 1406.6 mbsf, precisely within the depth range predicted from the extrapolation of multichannel seismic results at modern mid ocean ridges to this superfast spreading rate (Fig. 1).

Expedition 312 continued the drilling at site 1256 by starting at 1255 mbsf within the Sheeted Dikes. Details on the previous drillings at the same site are presented in the cruise report of Expedition 309 (Geldmacher et al., 2006, this volume). In the lower portion of the sheeted dikes, from 1348 - 1407 mbsf, the rocks are highly to completely altered and are locally recrystallized to granoblastic textures, leading to their designation as the Granoblastic Dikes.

At 1406.6 mbsf, Hole 1256D encountered a gabbro dike, marking the end of the sheeted dike complex and the beginning of the 100.5 m thick Plutonic Section, which extends to 1507 mbsf. Intrusive relationships show that the plutonic section is the product of a series of discrete magmatic events. At least two gabbro bodies intruded the sheeted dike sequence, followed some time later by a small cross-cutting basalt intrusion at the base of the drilled section. Gabbroic rocks are highly altered, fine to coarse grained and range from gabbro to oxide gabbro and gabbronorite with some differentiated rocks (quartz diorite and quartz-rich oxide diorite). Fig. 2 shows a summary of the lithological features of the Sheeted Dike Complex and the Plutonic Section in Hole 1256D, cored during Expedition 312.

The Plutonic Section of Hole 1256D includes two medium-grained gabbroic intervals, Gabbro 1 (1407 - 1459 mbsf) and Gabbro 2 (1483 - 1507 mbsf). These gabbroic units are intrusive into the basal dikes of the Sheeted Dike Complex and are probably responsible for the contact metamorphic products observed in the granoblastic dikes. Gabbro 1 and Gabbro 2 are separated by the Dike Screen (1459 - 1483 mbsf), an amphibolite-grade metabasalt interval with a well-developed granoblastic metamorphic texture.

With the exception of a narrow (< 1 meter) quartz-rich oxide diorite dike that is compositionally equivalent to an oceanic Fe-Ti basalt, Gabbro 1 is mineralogically uniform but texturally heterogeneous. Gabbro 1 gabbros are commonly oxide-bearing and oxide abundance decreases erratically downhole. Olivine is present in significant amounts only in the lower two units. Gabbro 2 is characterized by the presence of orthopyroxene and consists

mainly of orthopyroxene-bearing gabbro and gabbronorite. Oxides are present throughout, ranging up to 5% and rarely higher. At the upper margin of Gabbro 2, gabbronorite intrudes and invades the metabasalt of the Dike Screen, isolating and detaching centimeter-sized blocks of metabasalts thus showing complex stoping relations. The base of Gabbro 2 and the drilled section contains a gabbronorite of uncertain origin (intrusive gabbronorite or metamorphosed dike) and is cut by a late dike.

Trace element concentrations of lavas and dikes are within one standard deviation of average EPR MORB, albeit on the relatively trace element depleted side. The gabbro compositions are similar to the overlying dikes and lavas, showing in part effects due to cumulate processes and are evolved compared to primary magmas in equilibrium with mantle olivine.

Hole 1256D shows the transition from low-temperature alteration to high-temperature hydrothermal alteration in a continuous section of oceanic crust. The transition zone marks a change from predominantly low temperature secondary alteration minerals to greenschist hydrothermal assemblages. Actinolite, hornblende, and secondary plagioclase occur within 100-200 meters of the dike transition indicating a very steep thermal gradient in the dikes. The lowermost ~50 m of dikes are strongly recrystallized showing granoblastic textural features. Characteristic are irregularly distributed local granoblastic patches, where the rock is completely recrystallized to secondary plagioclase and equant secondary clinopyroxene, magnetite, ilmenite, and rare orthopyroxene. The mineralogy and textures indicate recrystallization at high temperatures related to underlying gabbros.

Following the completion of drilling Hole 1256D, a complete suite of geophysical wireline logs were performed. Caliper readings from both the triple combo and FMS tool strings show generally good borehole conditions. The borehole deviation measured at 1507.1 mbsf reaches ~5˚. A vertical seismic profile experiment was conducted, and velocities generally follow those of the sonic log and discrete samples. Preliminary analysis of downhole geophysical measurements and images recorded in Hole 1256D show a high degree of variation, reflecting the basement lithologies, and a number of petrophysical intervals can be distinguished that closely match the subdivisions developed from core observations.

References:
Carbotte, S., Mutter, C., Mutter, J., and Ponce-Correa, G., 1997. Geology, 26:455-458.
Geldmacher, J., Expedition 309, and Expedition 312 Scientific Parties, 2006. This volume.
Phipps Morgan, J., and Chen, Y.J., 1993. J. Geophys. Res., 98:6283-6297.
Purdy, G.M., Kong, L.S.L., Christeson, G.L., and Solomon, S.C., 1992. Nature, 355:815-872.

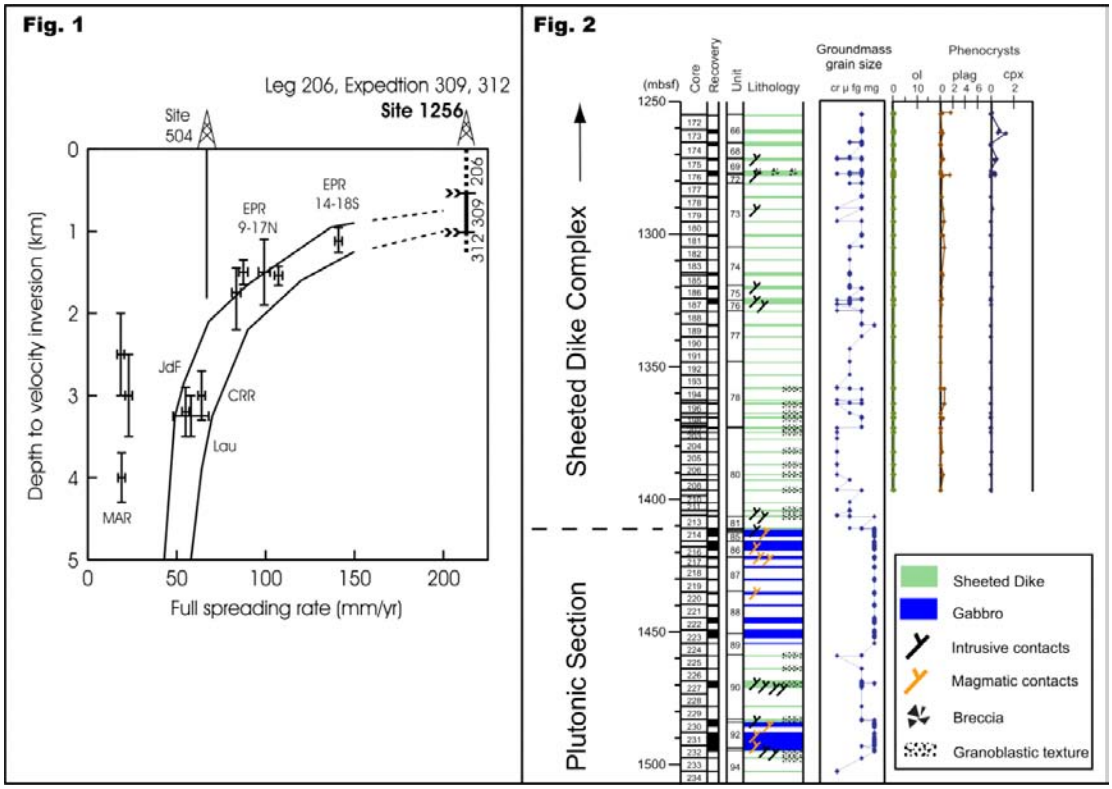

Figure 1. Depth to axial low-velocity zone plotted against spreading rate (modified from Purdy et al., 1992, and Carbotte et al., 1997). Depth versus rate predictions from two models of Phipps Morgan and Chen (1993) are shown, extrapolated subjectively to ~ 200 mm/y (dashed lines). Penetration in Holes 504B and 1256D is shown by vertical lines. For Hole 1256D the depths of the individual drillings are indicated. MAR = Mid-Atlantic Ridge, EPR = East Pacific Rise, JdF = Juan de Fuca Ridge, Lau = Valu Fa Ridge in Lau Basin, CRR = Costa Rica Rift.

Figure 2. Summary of the Sheeted Dike Complex and Plutonic Section stratigraphy in Hole 1256D, cored during Expedition 312. Shown is (from left) a depth scale, core numbers, recovered intervals, unit boundaries, igneous lithology, groundmass grain size, and phenocryst percentage. cr = cryptocrystalline, µ = microcrystalline, fg = fine grained, mg = medium grained. ol = olivine, plag = plagioclase, cpx = clinopyroxene.

IODP

Systematic compositional and susceptibility variations in basaltic dykes of Atlantis Massif, 30˚N Mid-Atlantic Ridge (IODP Leg 304/305)

Michael Abratis[1], B. Ronald Frost[2], Roger Searle[3] and IODP Exp. 304/305 Shipboard Scientific Party
[1]Institute for Geosciences, University of Jena, D-07749 Jena, Germany, michael.abratis@uni-jena.de; [2]University of Wyoming, Laramie, WY 82071, USA; [3]Durham University, Durham, DH1 3LE, UK.

We assume that some of the variation in magnetite content and structure is caused by alteration, since magnetite is consumed by the alteration process of pyroxene to actinolite. Apparently, during alteration, the magnetite in the primary Ti-magnetite grains had been consumed, leaving a skeleton of ilmenite lamellae. On the other hand, magmatic processes like within-dyke differentiation may also produce compositional variations in the dyke profiles. First geochemical analyses indicate that compatible elements such as Mg, Ni, Cr are enriched in the central parts, whereas incompatible elements such as Fe, Ti, Na, Zr are more enriched in the margins of the dykes. In a new interdisciplinary study we aim to evaluate the different contributions of primary (magmatic) processes and secondary (hydrothermal alteration) processes on the observed across-dyke zoning in physical properties.

IODP Expeditions 304 and 305 (Nov. 17, 2004 to March 2, 2005) drilled into the Atlantis Massif, an oceanic core complex which is located at the Mid-Atlantic Ridge at 30˚N, adjacent to the Atlantis Transform Fault. The lithosphere at Atlantis Massif is tectonically thinned and exhumed due to asymmetric extension and denudation along a major detachment fault so that rocks of the lower oceanic crust and the upper mantle are exposed.

During Leg 304/305 we encountered predominantly gabbros of a wide compositional range. Doleritic basalts (Am.: diabase) make up the second-most abundant lithology. These basalts occur as dykes of cm- to m-width and are present throughout the cores U1309B and U1309D, however predominantly in the upper 130 m. The dykes crosscut gabbros and serpentinites, indicating that they intruded the crust during a late evolutionary stage of the oceanic core complex. These late-stage intrusions are thus witness for long-lived magmatic activity at ridge segment ends, which are generally expected to be rather magma-starved.

The basalts are of normal tholeiitic MORB composition and have slightly higher FeO and TiO2 contents than typical MORB glasses from the MAR. Lower CaO, Al2O3 and K2O and higher Na2O contents than in comparable MORB glasses may be due to the pervasive greenschist facies alteration of the rocks. Shipboard measurements of the magnetic susceptibility yielded the highest values for the basalts and conspicuous variation patterns in profiles across the basaltic dykes (see figure): the margins of the dykes tend to have high magnetic susceptibilities, whereas the interiors are not or only slightly magnetic. Good correlations of bulk magnetic susceptibility and non-contact conductivity imply that the same minerals carry each signal, most likely oxides such as magnetite and ilmenite and possibly minor sulphides. Petrographical observations show that euhedral Ti-magnetite crystals are more concentrated towards the margins of the dykes whereas more skeletal crystals predominate in the centre.

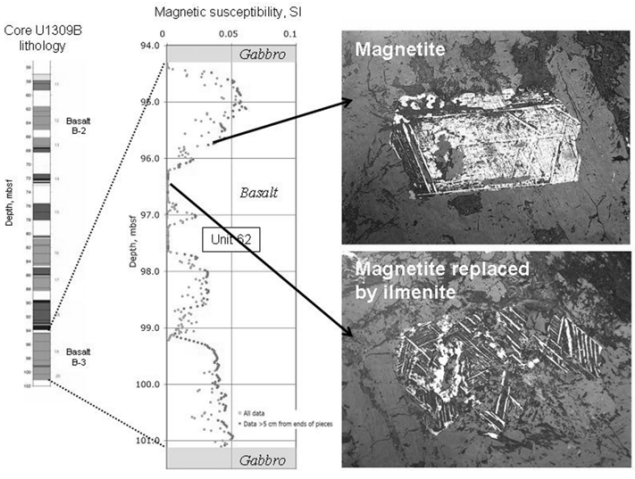

IODP

Novel two-dimensional experiments on drill cores with a new generation of the mobile NMR Halbach scanner

S. Anferova[1], V. Anferov[1], E. Talnishnikh[1], B. Blümich[1], H. Pape[2], A. Hartmann[2], and C. Clauser[2]
[1]Institute of Technical Chemistry and Macromolecular Chemistry, [2] Applied Geophysics, RWTH Aachen University, 52056 Aachen, Germany

In our previous project (BL 231/26-1) we designed, tested and proved that the mobile NMR Halbach scanner can be used as an instrument for fast and non-destructive measurements to determine routinely rock porosity and to estimate the pore size distribution of fresh water saturated drill ODP/IODP cores at the site of recovery. The measurement time is a few seconds, and the drill cores do not need to be dried and cut for investigations. Studies are published in Blümich et al. (2004) and Anferova et al. (2004). Currently we are providing novel two- dimensional (2D) correlation experiments involving diffusion (D), longitudinal (T1), and transverse (T2) relaxation with a new generation of the Halbach scanner on water saturated drill cores. The advantages of the new generation are described. The main objective of our new application (BL 231/31-1) that started on 01.01.2006 is to refine and extend the developed NMR techniques for a more detailed characterization, and to provide experimental data beyond the pore-size distribution function and the NMR porosity. In the first stage of this project special software for 2D experiments was designed:

2D pulse programs for T1-T2 and D-T2 correlation measurements with a mobile NMR Bruker spectrometer; a program written in MatLab for analysis of experimental data and their transformation to matrix form for further processing, 2D inverse Laplace transformation programs from M. Hürlimann and P. Callaghan were tested.

The results of two-dimensional distribution functions F(T1,T2) extracted from measurements on different sandstones are presented and discussed. They are compared with one-dimensional distribution functions measured on the same sandstones. T1/T2 ratios are derived from the two-dimensional distribution function F (T1,T2) and conclusions are made about the molecular mechanism of surface and bulk relaxation. An important practical use of two-dimensional distribution functions is to identify different fluids with distinct T1/T2 ratios inside the rocks (for example water and oil).

B. Blümich et al.. J. Geophys. Eng. 2004, 1, 177-180,
S. Anferova et al, Concepts in Magn. Reson. Part B: Magnetic Resonance Engineering 2004, 23B, 1, 26 - 32.

ICDP

Comparative evaluation of tracing experiments conducted in deep sedimentary and crystalline formations in Germany, 2003-2005

Arbeitsgruppe 'Angewandte Geologie', Universität Göttingen, Goldschmidtstr. 3, 37077 Göttingen, Germany

Tracer methods are generally used, either, to determine residence times or the volume (mobile-domain porosity) of a flow system, or to determine the size of relevant internal surfaces within the system in terms of tracer interactions or processes taking place at these surfaces. The specific area ( ) of the contact surface between fractures and rock matrix, playing an important role in solute and heat transport, is not properly captured by hydraulic and geophysical tests, nor by flow-path tracings in highly dispersive flow fields. A single-well 'push-pull' tracing method that increases the sensitivity of tracer breakthrough curves (BTCs) w. r. to the

contact-surface area parameter was described in our previous contribution (ICDP Colloquium 2004), alongside with its first application in crystalline reservoirs in Germany. The deep-reservoir tracing programme started in 2003 was continued as listed in Table 1.

Tests#3,4 were conducted in the same fracture system around the KTB pilot hole but in different THM states: test#3 in a depleted system, during recovery after a long-term pumping test, test#4 in a relaxing overpressurized system, following massive hydraulic stimulation. The tracer slug for test#5 (flow-path tracing) had to be added during the massive water injection and thus it preceded the tracer slug for test#4 (push-pull type); thereby slug#5 also generates a push-pull signal during the withdrawal phase of test#4, superimposing the push-pull signal from slug#4. To facilitate BTC separation, slug#4 was moderately oversized (relatively to target formation size). Slug#3, of which some 50 % had been left inside the formation before the start of massive injection, was expected to no longer yield detectable signals during tests#4,5. Separation of BTCs stemming from tracer slugs#4,5 was based on closed-form approximations for early (#5) and mid-late (#4) times; push-pull signals from slug#5, of which only an incipient ascending phase can be captured by free outflow at the injection hole, characterize a much larger formation volume and they become increasingly univoque as the tailings from slug#4 gradually vanish. Let the idea of test#5 be explained in some more detail here: the massive hydraulic stimulation conducted at the pilot KTB hole, with about 84×10^3 m^3 of cold freshwater injected between mid 2004 and mid 2005, has provided the opportunity for probing a solute transport connection between the two seismic reflectors intersected by the main, 9-km deep KTB hole (of which only the upper is intersected by the pilot, 4-km deep KTB hole), given the prospect of a long-term fluid abstraction to start at the main hole by mid 2007. To appreciate the chance of a pilot-hole injected tracer reappearing at the main hole in due course and to assist in dimensioning tracer slug#5 (added before the last 16×10^3 m^3 of injected freshwater), a number of transport scenarios were simulated within a simplified 2D model of reflector zone projections, using transport parameter estimations from the first push-pull test (#3) at this site, and assuming an average fracture porosity of 5×10^{-5} (as estimated by McDermott and Kolditz 2004 from hydraulic testing at the pilot hole). Tracer quantities in slug#5 were limited by legal/environmental considerations; as a consequence, if the effective fracture porosity nf of the assumed transport connection exceeds 2×10^{-4} (as had been estimated by Kessels et al. 2004 from hydraulic testing at the main hole), tracer concentrations at the extraction hole may stay below detection limits for the whole duration of the planned pumping test - to be noted, fracture porosity nf is not a scaling parameter of the complete transport problem, not even for a conservative tracer (a N × higher n_f is not compensated just by injecting the N-fold tracer quantity). The withdrawal signal of a long-term 'push-pull' hypothetically and involuntarily performed in terms of drilling fluids formerly added at the main hole (curve 'S' on the figure) could further be used to characterize fracture surfaces around the main hole (not the flow connection between the two boreholes), but it might also negatively interfere with the analytics of purportedly injected fluorescent tracers.

All tracers used can be regarded as approximately thermally-stable for the respective test duration, except for test#5, in which thermal decay may lead to considerable tracer loss.

In the practice of deep-reservoir tracing, there are physical and financial limitations to test design and duration. Insufficient flushing volumes can render BTC peak regions unusable for fracture characterization, and insufficient outflow volumes (durations) can make characteristic 'mid-late' BTC slopes difficult to recognize.

Table 1 Overview of AGG tracer experiments, 2003–2005 ('SW' abbreviates 'single-well')

#	site and borehole identification	location and characteristics	type of test; space scale	target information (derived value)
1	"Lindau" underground facility for fractured rock testing, borehole N8	Black Forest, shallow granite formation (crystalline rock), hydrothermally altered, highly-permeable fault zone	SW, push-pull; < 20 m^3	contact-surface area or fracture density σ (>100 m^{2}m^{-3})
2	Urach Spa, borehole Urach-3 (pilot geothermal project)	Swabian Alb, crystalline basement, 4.4 km deep (< ~170° C), 'hot-dry-rock' type, low permeability, several fracture systems in 3 – 4 km depth	SW, push-pull; < 1 500 m^3	σ (3 – 10 m^{2}m^{-3})
3	KTB, pilot borehole, before hydraulic stimulation	NE Bavaria, crystalline basement, 4 km depth (~120° C), localized fracture system, good permeability	SW, push-pull; < 1 000 m^3	σ before hydraulic stimulation (10 – 30 m^{2}m^{-3})
4	KTB, pilot borehole, after massive hydraulic stimulation	*ibid.*, 4 km depth (cooling to ~50° C estimated), enhanced permeability, fracture network structure may be changed by coupled THM processes	SW, push-pull; < 10 000 m^3 (within larger-scale fault sys.)	σ after massive hydraulic stimulation (increased)
5	KTB, pilot borehole and main borehole, during and after *ibid.*	*ibid.*, suspected transport connection between fracture systems in 5 and 7 km depth (~210° C), within complex fault system	monopole-to-monopole (broken dipole), flow-path tracing; >10^5 m^3	transport-effective porosity, σ, fault system structure
6	Horstberg, borehole Z1 (using inner and outer casing as '2 boreholes in 1')	Lower Saxony, sedimentary basin, 2 sandstone horizons in ~3.6 and ~3.8 km depth (~150° C), connected by hydrofrac (created by massive injection just before adding tracer)	SW, monopole (divergent), flow-path tracing; > 10^4 m^3	transport properties of hydrofrac, σ (10$^{3.4}$ m^{2}m^{-3}), flow-capacity distribution (cf. plot)

#	drawbacks with test design, and failures in test execution ($V_{B,in,out}$ denote the borehole, the injected, and the extracted volumes)	models and methods used
1	packer failure, borehole not properly flushed (despite $V_{in} / V_B \sim 5$, and despite having adjusted the density of injected solution to match formation fluid density; $V_{out} / V_{in} \sim 10$ still insufficient)	advection – dispersion in parallel-plate multiple-fracture system (1D), matrix diffusion (1D), equilibrium or first-order kinetic sorption at fracture surfaces and within rock matrix, mid-late BTC approximations; flow–capacity distribution from flow-path tracings, 'transfer–storage' distribution from push-pull tests; parameters assumed as known: – fracture porosities (except for #5,6), – matrix porosities, – tracer diffusion coefficients (calculated from matrix porosities, formation temperatures and corresponding fluid viscosities, discarding salinity influences)
2	$V_{in} / V_B \sim 1.5$; $V_{out} / V_{in} \sim 3.2$; bulk signal from at least 2 different fracture systems; at least one tracer did not fully dissolve before injection (tracer mass actually entering target system remains unknown → BTCs cannot be normalized, and BTCs' height difference cannot be interpreted)	
3	$V_{in} / V_B \sim 2.6$; $V_{out} / V_{in} \sim 2.4$ (both rather low)	
4	$V_{in} / V_B \sim 2.6$ (rather low); $V_{out} / V_{in} \sim 4.2$ (almost ok)	
5	test design imposed by project financing schedule: first divergent flow from pilot hole, next >1 year resting, then convergent flow to main hole → unnecessarily high dilution of tracers in the formation (requiring injection of large tracer quantities, which prohibits the use of 'chemically inert' tracers like HTO), and long in-situ residence times (→ increased risk of tracer loss by thermal decay); V_{in} / V_B was large enough, but V_{out} / V_{in} is likely to be insufficient	
6	$V_{in} / V_B \sim 14$ sufficient, but $V_{out} / V_{in} \sim 2.8$; divergent flow field → low tracer recovery; extreme salinity of formation fluid raises detection limits and reduces detection accuracy for all tracers (including HTO)	

Table 1

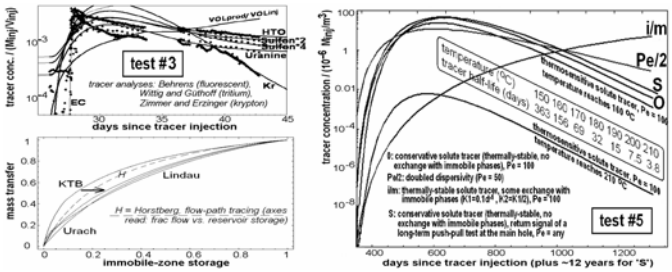

Test#3: tracer BTCs with transformed (mid-late equivalent) model fit. Test#5: tracer fate and BTC expectation spectrum at the KTB main hole as of 2007. Transfer-storage distributions: derived from all tests except #5 (arrow indicates change in KTB reservoir structure after massive stimulation).

Determining from tracer BTCs presupposes reliable knowledge of tracer properties. A qualitative interpretation of BTC differences, beyond the amount accountable for by different diffusion coefficients, may rely on structure-activity considerations, before tracer thermostability and sorption are quantified in the laboratory. A field push-pull test can partly substitute the required laboratory investigations if at least one assuredly 'reference' tracer is injected alongside with the tracers

whose physico-chemical behaviour is less secured.

Table 2 Tracers used, and their estimated recoveries (using uncorrected outflow data)

#	actual fluid production (approximate field records)	BTC extrapolation used in computing FC diagrams	tracers used, and estimated recovery values (actual, extrapolated)	
1	free outflow: 1500 L in 3 h (stopped)	17 h (assuming exponential decrease of outflow rate)	Uranine	(3.8 % , 7 %)
			NDS	(4.9 % , 9.1 %)
			Naphthionate	(3.1 % , 5.5 %)
			Lithium	(3.4 % , 6.1 %)
			Bromide	(4.3 % , 8.2 %)
2	free outflow (regulated): 438 m^3 in 5 d (stopped)	100 d (assuming exponential decrease of outflow rate)	Uranine	(53 % , 72 %)
			NDS	(60 % , 82 %)
			freshwater tracers	(no data as yet)
3	forced outflow (pumping): 300 m^3 in 16 d (stopped)	100 d (assuming constant pumping rate)	Uranine	(38 % , 51 %)
			NDS	(54 % , 85 %)
			PTS-Behrens	(54 % , 89 %)
			HTO	(50 % , 86 %)
4	free outflow: 520 m^3 in 6 d (ongoing)	100 d (assuming exponential decrease of outflow rate)	Uranine	(28 % , 30 %)
			NDS	(36 % , 44 %)
			HTO	(24 % , 32 %)
5	(shut-in phase till 2007, then forced outflow, about 22×10^2 m^3 planned)	up to 10^4 d might be necessary; *recovery estimations pertain to push-pull signals induced by slug#5 at its injection hole*	Uranine	(<0.5 % to date)
			NDS	(<0.5 % to date)
			freshwater tracers	(no data as yet)
6	free outflow: 3600 m^3 in 10 d (stopped)	100 d (assuming exponential decrease of outflow rate)	Uranine	(6.4 % , 8 %)
			NDS	(10 % , 12.4 %)
			HTO	(7.4 % , 10.3 %)

Acknowledgements: Field work in tests#2,3,4 was led by M. Lodemann (AGG). The tests would not have been possible without the expert technical skills of M. Kühr, K. Bohn (GFZ Potsdam) and S. Fischer (AGG). Financial support from the German Research Foundation (DFG), from the Stadtwerke Bad Urach, the Geo-Zentrum Hannover and the GFZ Potsdam is gratefully acknowledged. Expert tracer knowledge provided by H. Behrens and T. Licha (AGG) was essential to all tests. J. Erzinger (GFZ Potsdam), H.-J. Kümpel, W. Kessels (GGA-Institute), S. Shapiro (FU Berlin), I. Stober (Geol. Survey Freiburg) supported the work through valuable initiatives, questions and comments.
Verantwortlich für Fehler in Text, Tab. u. Abb.: I. Ghergut, Geo-Zentrum, Goldschmidtstr. 3, 37077 Göttingen (ighergu@gwdg.de)

IODP
Porosity and Permeability from mobile NMR core scanning

J. Arnold[1], C. Clauser[1], R. Pechnig[1], S. Anferova[2], B. Blümich[2]
[1]Institute of Applied Geophysics; [2]Institute of Technical and Macromolecular Chemistry; [1,2]RWTH Aachen University, D-52056 Aachen, Germany; e-mail: J.Arnold@geophysik.rwth-aachen.de

1. Objectives: This project is focused on the calibration of a mobile NMR core-scanner for porosity determination and the estimation of permeability within the ODP/IODP.

2. Instrumentation: The HALBACH core-scanner, used for transverse relaxation (T2) measurements, encloses the sample in a large cylindrical volume resulting in a nearly homogeneous magnetic field. Besides the application in the laboratory, the tool is suitable to travel with it right to the drilling platform because of its small size and low weight (Anferova et al., 2004).

3. Porosity determination: We studied different drill cores, as limestone, basalt, sandstone, shale and clay with varying values of porosity, pore size and magnetic susceptibility. In water-saturated cores, the number of spins in the fluid within the sensitive volume of the sensor is proportional to the sample porosity. Porosity can be calculated from NMR measurements by normalizing the echo amplitudes measured on water-saturated cores to the amplitude measured on pure water, equivalent to a porosity of 100 %. The porosity values obtained from NMR measurements were compared to porosities determined with a helium gas pycnometer. The correlation coefficient R^2 for both measurements $R^2 = 0.89$ (Fig. 1). Because of the large sensitive volume of the HALBACH core-scanner and its high signal-to-noise-ratio porosity values down to 2 % could be determined.

4. Permeability prediction: T2-measurements can be used to predict permeability prediction because the T2 relaxation time is proportional to the pore size rpore according to (Coates et al., 1999): $r_{pore} = 2\, T_2\, \rho$ in µm (1)
where δ is surface relaxivity given in µm/s. The surface relaxivity is a measure of how quickly protons lose orientation or phase coherence due to magnetic interactions at the fluid-solid interface.

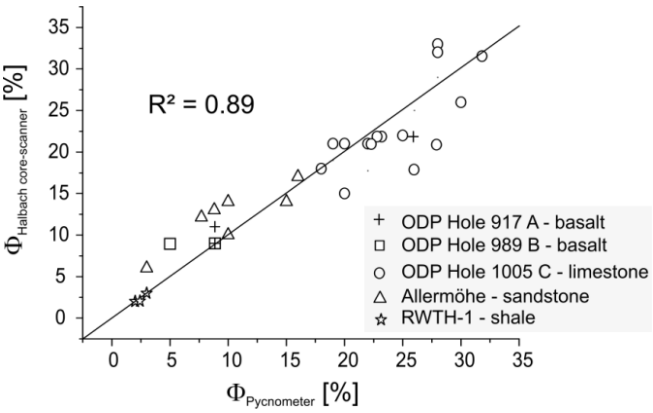

Figure 1. Correlation of porosities Φ determined with the HALBACH core-scanner and a gas pycnometer.

It is dominated by paramagnetic ions in grain surfaces (Kleinberg et al., 1994). Kenyon et al. (1988) showed that the following equation provides a good permeability prediction (k_{NMR}) for sandstones:

$k_{NMR} = a\, T_{2gm}^2 \Phi^4$, (2)

where T_{2gm} is the geometric mean value of the T_2 distribution, and the constant a depends on the surface relaxivity and is determined empirically. Usually, for sandstones a = 4 mD/(ms)² (Morris et al., 1996) (mD = millidarcy; 1 darcy = 9.87 × 10-12 m²). We measured the T_2-distribution at various positions along a limestone core (ODP Leg 166, Hole 1105C) with low magnetic susceptibility values (~10×10^{-5} SI). Porosities of the limestone section range from 26 % - 32 %. For the calibration of a, we measured gas permeability kGas on the corresponding core plugs. A good match between k_{NMR} and k_{Gas} was found for a = 0.7 (Table 1).
Additionally, we compared the distribution curves from T_2 measurements and from mercury injection performed on different positions along the limestone core. The pore radius rpore were converted to the T2 values according to equation (1). An optimum match between the two data sets, i.e. the maxima of both frequency distributions coincide, was found for ρ = 18 µm/s on average (Figure 2).

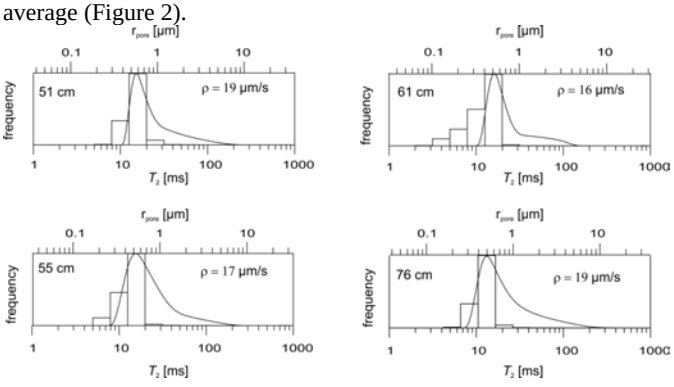

Figure 2. Distributions of pore sizes rpore (bar charts) and NMR relaxation times T2 (black curves). At various positions along a limestone core (ODP Leg 166, Hole 1005C, 34R, 1W, 48 - 80 cm).

Alternatively we determined permeability from an equation modified after Pape et al. (1999):

$k_{Max} = (R_{Max}^2)/(8F)$, (3)

where R_{Max} is the pore radius corresponding to the maximum of the pore size distribution and F is the formation factor. F is a purely geometric parameter, describing how the porous medium obstructs transport processes. This quantity is obtained from electrical resistivity measurements. Measurements on our limestone core yield values from 19 till 26. Permeabilities for our limestone core calculated from equation (3) agree well with those determined by the NMR method (Table 1).

position [cm]	K_{Gas} [mD]	k_{NMR} [mD]	k_{Max} [mD]
51	3.86	3.24	1.32
55	1.62	1.55	1.43
61	1.93	2.74	1.80
76	2.15	1.90	1.49

Table 1. Permeabilities determined with different methods at various positions along a limestone core (ODP Leg 166, Hole 1005C, 34R, 1W, 48 - 80 cm): kAir (gas permeability), kNMR (equation 2) and kMax (equation 3).

Further studies were performed on silty clay samples recovered during Leg 204. Figure 3 compares the T2 and pore size distribution measured on one core (204,1244E,2H,2W,5-25cm). The magnetic susceptibility value of the clay is about 33×10-5 SI. For a surface relaxivity of = 21 µm/s, the pore size distribution from mercury injection data coincides with the NMR T2 distribution. The permeability of the clay core was calculated using the NMR method. Because of instability of the clay the a-value could not be calibrated. However, surface relaxivity values for the limestone core and the clay are similar (Figures 2 and 3). Hence, we inserted the same a-value in equation (2) and obtained a clay permeability of 0.11 mD.

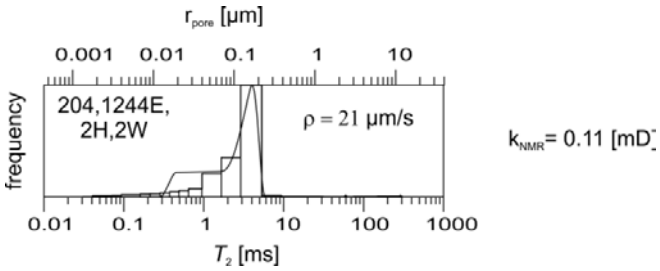

Figure 3: Distribution of pore sizes rpor (bar charts) from mercury injection and NMR relaxation times T2 measured on a clay core (204,1244E,2H,2W,5-25cm). For the given surface relaxivity , the pore size distribution from mercury injection plots on top of the NMR T2-distribution. Permeability determined by the NMR method is given (right).

5. Outlook: In the current period of the project we will further interpret NMR measurements on different rock types with respect to permeability. We will perform additional petrophysical studies on transport properties of rocks, such as permeability, pore size distribution from mercury injection, specific surface and electrical resistivity measurements to obtain formation factor and tortuosity. This will provide new and significant data on permeability to ODP/IODP.

Acknowledgement: This study is financed by the Deutsche Forschungsgemeinschaft (DFG) within the framework of ODP/IODP under grant CL 121/16-2.

References

Anferova, S.; Anferov, V.; Rata, D.G.; Blümich, B; Arnold, J.; Clauser, C; Blümler, P. & Raich, H. A. 2004. Mobile NMR Device for Measurements of Porosity and Pore Size Distributions of Drilled Core Samples, Magnetic Resonance Engineering, 23B(1), 26-32.

Coates, G.R., Xiao, L. & Prammer, M.G., (1999): NMR Logging - Principles and Applications. Halliburton Energy Services, Houston.

Kenyon, W.E., Day, P.I., Straley, C. & Willemsen, J.F. 1988. SPE Formation Evaluation, 3 (622).

Kleinberg, R.L., Kenyon, W.E. & Mitra, P.P. 1994. Mechanism of NMR relaxation of fluids in rock, J. Magn. Reson., Ser. A, 108, 206-214.

Morris, C.E., Deutsch, P., Freedman, R., McKeon, D. & Kleinberg, R.L. 1996. Operating guide for the combinable magnetic resonance tool, Log Anal., 37 (6), 53-60.

Pape, H.; Clauser, C. & Iffland, J. 1999. Permeability prediction based on fractal pore-space geometry. Geophysics, 64 (5), 1447-1460.

IODP

Hydrothermal alteration in young oceanic crust at Juan de Fuca Ridge - Evidence from downhole logging data

A. Bartetzko (Research Center Ocean Margins, University of Bremen, Leobener Strasse, 28359 Bremen, Germany. Phone 0421-218 65809, Fax 0421-218 65810. E-mail: bartetzko@uni-bremen.de)

Integrated Ocean Drilling (IODP) Expedition 301 drilled at the eastern flank of Juan de Fuca Ridge to study the nature of fluid pathways in the oceanic crust. Thick sediment successions delivered from the continental margin lap onto the crust and thermally and hydrologically isolate the basement at young crustal age (Figure 1). Therefore, this region is particularly suitable to study the processes of fluid circulation through the oceanic basement. The region was target of several previous research expeditions; Ocean Drilling Program Leg 168 drilled a transect of 11 holes along the eastern flank of the ridge (Davis et al., 1997). Expedition 301 drilled four holes in total at a location where basement age is ~ 3.5 m.y. Two holes, one shallow (U1301A) and one deep (U1301B) drilled the basaltic basement and two holes (U1301C and D) were drilled to sample sediments. The two basement holes U 1301A and B were equipped with CORKs (Circulation Obviation Retrofit Kit) for long term monitoring of pressure and temperature and for biogeochemical fluid sampling. The deep basement Hole U1301B drilled 265 m of sediments and 318 m of volcanic basement with an average core recovery of 30 % in the basement. Hole U1301B is one of the few successful deep oceanic basement drillings with coring and downhole logging in the history of ocean drilling. Downhole measurements were carried out in the open basement section and included measurements of electrical resistivity, natural radioactivity, density, and neutron porosity.

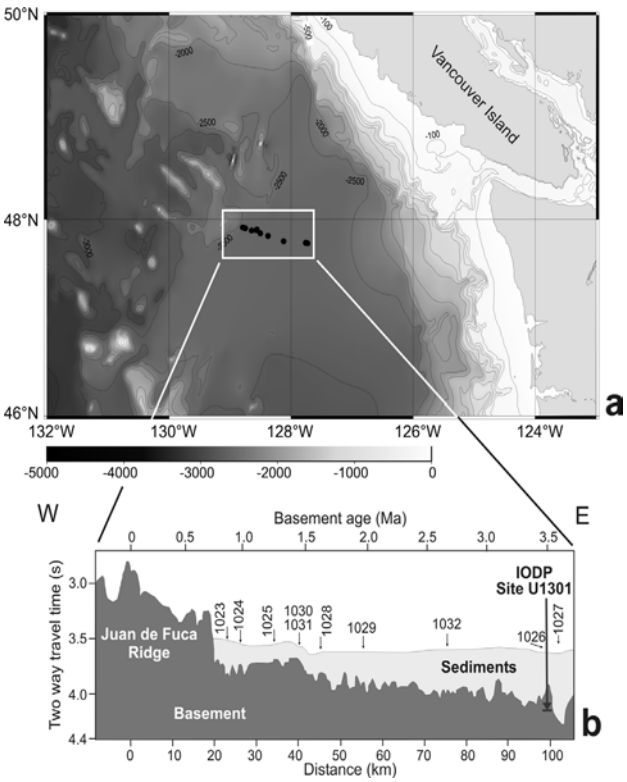

Figure1: (a) Location of ODP Leg 168 and IODP Expedition 301 drill sites; (b) schematic profile through the eastern flank of the Juan de Fuca Ridge and location of Leg 168 and Expedition 301 drill sites (modified after Davis et al., 1997).

In this project, geophysical downhole measurements and physical properties measured on core samples from the basement interval of Hole U1301B are used to (1) identify possible fluid pathways in the basement and their relation to volcanic

architecture, and (2) to investigate the influence of hydrothermal alteration on the physical properties of the oceanic crust. In addition, whole-round core samples from the sediment cover will be used to (3) analyze the hydraulic properties of the turbidite and hemipelagic sequences. In the following, interpretation of downhole logging data will be presented.

Downhole logs from Hole 1301B are strongly affect by borehole enlargements in the upper 100 m of the basement. This particularly concerns the density and neutron porosity logs (Figure 2). Due to the bad borehole conditions in the upper part of the borehole, no borehole images (electical or acoustic) of reliable data quality for are available and the interpretation is restricted to the standard wireline logs. In the core lithostratigraphy of Hole 1301B, the dominant rock type is pillow basalt, with some intercalations of massive basalts and breccias. Three intervals of massive basalts observed in the cores can be identified using downhole logging data. They show slightly higher density and resistivity values than the adjacent pillow basalts. However, differences in in-situ physical properties between pillow basalt units and massive basalts are only minor in this hole. Based on the succession of pillow basalts and massive basalts, three major lithostratigraphic sequences may be distinguished: (a) an upper pillow basalt sequence from the bottom of the casing at 350 mbsf (meters below sea floor) down to 420 mbsf, (b) a middle sequence with massive lava flows and pillow basalts between 420 and 465 mbsf, and (c) a lower pillow basalt sequence down to the bottom of the hole (Figure 2). Borehole conditions indicate strong fracturing and/or brecciation in the upper 100 m of the open basement and the three sequences show significant differences in fracturing that most likely reflect differences in porosity and also in permeability. The upper pillow basalt sequence is therefore interpreted to have a higher permeability than the lower pillow basalt sequence. Thus, the massive basalts of the middle sequence may act as a hydrologic barrier between the pillow basalt sequences.

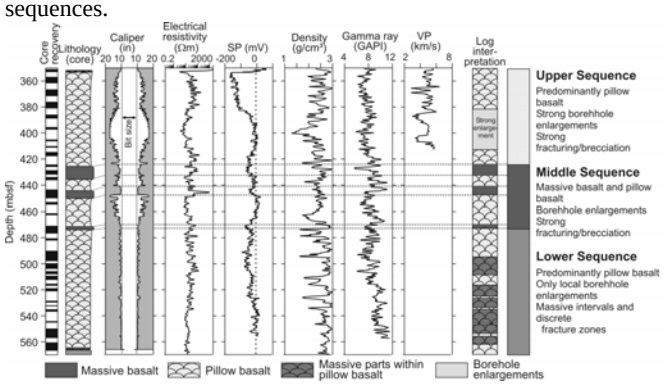

Figure 2: Composite log of Hole U1301B. The left panels show the core recovery and lithostratigraphy (from Fisher et al. 2005), the middle panels give a selection of downhole logs and the right panels show the results of the interpretation of downhole logging data. Dashed horizontal lines mark massive basalt horizons. SP = Spontaneous potential.

Differences in physical properties between the lava morphologies (pillow basalt and massive basalt) are insignificant in Hole U1301B and in-situ properties of the lava morphologies overlap (Figure 3). However, differences in physical properties between lava morpholgies are known from other boreholes into oceanic crust. Variations for example in electrical resistivity, density, and natural radioactivity reflect differences in fracturing and alteration between the lava morphologies. Compared to massive basalts, pillow basalts are usually characterized by lower electrical resisitvity and density and higher total gamma ray values (e.g. Bartetzko et al., 2001). Total gamma ray reflects changes in potassium content that is enriched in secondary minerals during low-temperature seafloor alteration (e.g. Alt, 1995). Hence, in-situ physical properties of the oceanic crust not only reflect differences in lava morphology but also mirror the sealing of fractures and voids with secondary minerals during aging of the crust (e.g. Bartetzko, 2005). Aging of the crust results in a higher variability of in-situ physical properties. Hole U1301B drilled very young oceanic crust of only 3.5 m.y. compared to other holes into older crust (e.g. Holes 504B - Costa Rica Rift, 6 m.y.; 418A - Bermuda Rise, 110 m.y.). Young crustal age and a less intense alteration in Hole U1301B are a possible explanation for the similarity in physical properties of massive basalts and pillow basalts in this hole.

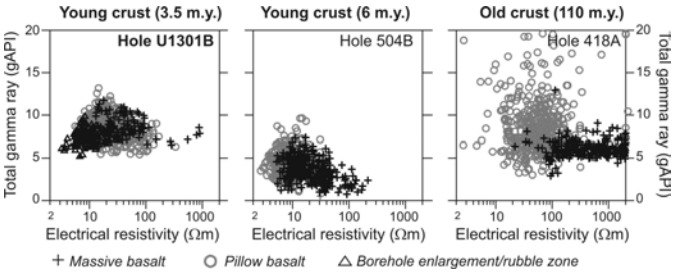

Figure 3: Downhole log responses of electrical resistivity and total gamma ray for pillow basalts and massive basalts from Hole U1301B in comparison to another borehole into young oceanic crust (Hole 504B, Costa Rica Rift, depth interval 290 - 587 mbsf) and one hole into old crust (Hole 418A, Bermuda Rise). Lava morphologies for Hole 504B and 418A are from Bartetzko (1999).

References

Alt, J.C. 1995. Subseafloor processes in Mid-Ocean Ridge hydrothermal systems. In: Humphries, S.E., Zierenberg, R.A., Mullineaux, L.S., and Thomson, R.E. (Eds.). Seafloor Hydrothermal Systems - Physical, Chemical, Biological, and Geological Interactions. AGU, Geophysical Monogragh. 91: 85-114..

Bartetzko, A. (1999) Aufbau und Entstehung ozeanischer Kruste an mittelozeanischen Rücken - Eine Interpretation von Bohrlochmessungen. Diss. RWTH Aachen,. 132 Seiten.

Bartetzko, A., Pezard, P., Goldberg, D., Sun, Y.-F., and Becker, K. (2001). Volcanic stratigraphy of DSDP/ODP Hole 395A: An interpretation using well-logging data. Mar. Geophys. Res. 22: 111-127.

Bartetzko, A. (2005). The effect of hydrothermal ridge flank alteration on the in situ physical properties of oceanic crust. Journal of Geophysical Research. Vol. 110, B06203, doi: 10.1029/2004JB003223.

Davis, E.E., Fisher, A.T., Firth, J.V. et al. 1997. Proc. ODP Init. Repts. 168: College Station, TX (Ocean Drilling Program)

Fisher, A.T., Urabe, T., Klaus, A. et la. 2005. Juan de Fuca Hydrogeology, Proceedings of the IODP, Volume 301, Expedition reports.

IODP

Cultured deep-biosphere bacteria from Equatorial Pacific Ocean and Peru Margin sediments: Physiological and phylogenetic diversity

Anja Batzke[1], Bert Engelen[1], Henrik Sass[2] and Heribert Cypionka[1]

[1]Institut für Chemie und Biologie des Meeres, Universität Oldenburg, Carl-von-Ossietzky-Str. 9-11, D-26111 Oldenburg, Germany. www.icbm.de/pmbio; [2]School of Earth, Ocean and Planetary Sciences, Cardiff University, Main Building, Park Place, Cardiff, CF10 3YE, Wales, UK.

The first ODP leg dedicated to microbiology, ODP Leg 201, was a milestone for deep-biosphere research (D'Hondt et al. 2004, Schippers et al. 2005). During this expedition, sediment cores of up to 40 million-year-old sediments in the Eastern Equatorial Pacific and the Peru Margin were taken from the sea bottom down to 420 meters below the seafloor. The sampled sediments ranged in temperature from 1˚ to 25˚C, and underlay water columns between 150 and 5100 meter depth (D'Hondt et al., 2003 Init Rep.).

The aim of our research was the quantification, cultivation and characterization of indigenous and relevant microorganisms by means of microbiological and molecular biological methods. Several cultivation assays were inoculated with contamination-checked anoxic slurries in media containing different substrate combinations, all at low concentration. These culture media were designed for a broad spectrum of physiological groups. Finally, 162 pure cultures were isolated that could be grouped into 19

different phylotypes based on 16S rRNA gene analysis. The culture collection obtained in our study comprises a larger variety of bacteria from marine subsurface sediments than any previous study. The main part of our cultivation results was published in Science (D´Hondt et al. 2004) and was commented in the same issue by De Long (2004).

The isolates belonged to the Alpha-, Gamma- and Deltaproteobacteria, the Firmicutes, Actinobacteria, and Bacteroidetes. Comparison of strains with the same phylotypes by enterobacterial repetitive intergenic consensus (ERIC-PCR) analysis revealed the presence of several subgroups that did not correlate with medium, sediment depth or sampling site. The genera most frequently found were Bacillus (68 isolates) and Rhizobium (40 isolates). Close relatives of the Rhizobium species have also been recently isolated from Mediterranean subseafloor sediments (Süß et al 2004). We did not isolate any Archaea, although this group could be detected with molecular techniques (A. Schippers, A. Teske and F. Inagaki, personal communications). Most strikingly, one isolate from the open-ocean Site 1225 shared only 86 % 16S rRNA sequence similarity to species within the Bacteroidetes and therefore represents a so far unknown genus. The physiological characterisation of this slowly growing strain is still in progress and will be used for the description of a new genus. The majority of the isolates - although obtained from anoxic environments and isolated under strictly anoxic conditions - turned out to be facultativly aerobic. Physiologically, the isolates were characterized as generalists, able to utilize a broad variety of electron donors with either oxygen, nitrate and in some cases manganese oxides as electron acceptors. The diversity inferred from physiological tests was even higher than that on the phylogenetic or genomic level. The results of the diversity study were submitted to be published in a special issue of Geomicrobiological Journal (Batzke et al. 2006).

In summary, the outcome of the contamination tests, the isolation of close relatives of already known subsurface bacteria, the repeated finding of the same phylotype from different sites and the level of diversity present in the culture collection strongly suggest that indigenous deep-biosphere bacteria have been isolated.

References:

Batzke A, Engelen B, Sass H, Cypionka H (2006) Phylogenetic and physiological diversity of cultured deep-biosphere bacteria from Equatorial Pacific Ocean and Peru Margin sediments. Geomicrobiol. J. (submitted)

D´Hondt SL, Jørgensen BB, Miller DJ, Aiello IW, Bekins B, Blake R, Cragg, BA, Cypionka H, Dickens GR, Ferdelman T, Ford K, Gettemy GL, Guèrin G, Hinrichs K-U, Holm N, House C, Inagaki F, Meister P, Mitterer RM, Naehr T, Niitsuma S, Parkes RJ, Schippers A, Skilbeck CG, Smith DC, Spivack AJ, Teske A, Wiegel J (2003) Controls on microbial communities in deeply buried sediments, Eastern Equatorial Pacific and Peru Margin, Sites 1225-1231. Proc ODP, Init Repts, 201 [Online]. http://www-odp.tamu.edu/publications/201_IR/201ir.htm.

D'Hondt SL, Jørgensen BB, Miller DJ, Batzke A, Blake R, Cragg BA, Cypionka H, Dickens GR, Ferdelman T, Hinrichs KU, Holm NG, Mitterer R, Spivack A, Wang G, Bekins B, Engelen B, Ford K, Gettemy G, Rutherford SD, Sass H, Skilbeck CG, Aiello IW, Guèrin G, House C, Inagaki F, Meister P, Naehr T, Niitsuma S, Parkes RJ, Schippers A, Smith DC, Teske A, Wiegel J, Padilla CN, Acosta JLS (2004) Distributions of microbial activities in deep subseafloor sediments. Science 306:2216-2221

De Long (2005) Microbial life breathes deep. Science 306:2198-2200

Schippers A, Neretin LN, Kallmeyer J, Ferdelman TG, Cragg BA, Parkes RJ, Jørgensen BB (2005) Prokaryotic cells of the deep sub-seafloor biosphere identified as living bacteria. Nature 433: 861-864

Süß J, Engelen B, Cypionka H, Sass H (2004) Quantitative analysis of bacterial communities from Mediterranean sapropels based on cultivation-dependent methods. FEMS Microbiol Ecol 51:109-121

ICDP

The electrical conductivity structure across the San Andreas Fault near the SAFOD site - a regional magnetotelluric study

Becken, M., Ritter, O., Park, S., Bedrosian, P., Weckmann, U., and Weber, M.

With the magnetotelluric (MT) project DeepRoot, we aim to image the electrical conductivity distribution of the deep structures (brittle-ductile transition zone and the ductile roots) of the San Andreas Fault (SAF) zone at Parkfield, CA. The experiment addresses the dynamics of interplate transform faulting and contributes to the site characterization of the San Andreas Fault Observatory At Depth (SAFOD) - a major Earth Science initiative to study the in-situ physical and chemical conditions of the San Andreas interplate transform fault (Hickman et al., 2004). The project DeepRoot is part of the ICDP.

Previous MT studies of Unsworth et al. (2004) played an important role to pin-point the location of the SAFOD site. The electrical conductivity models from these studies suggested the presence of fluids, causative for the so-called fault zone conductor (FZC), in regions with abundant seismicity and thereby provided complementary information to the seismic velocity structure and other geophysical site characterization studies. As fluids seem to be intimately linked to the brittle deformation processes within active fault zones, the FZC was interpreted in terms of over-pressured fluids, which in turn prevent the fault from rupturing. However, previous MT models were limited to a few kilometres in depth due to short profile lengths.

In spring 2005, we acquired a huge volume of new magnetotelluric (MT) array and profile data in the vicinity of the SAFOD site. Overall, we recorded at 45 combined long-period / broad-band stations distributed in an area of 50 square km in the vicinity of the SAFOD site and an additional 41 broad-band stations coincident with a 50 km long seismic reflection/refraction profile (Hole et al., 2004; Ryberg et al., 2004). The profile data were used to derive a two-dimensional (2D) electrical conductivity model down to a depth of more than 25 km. The array data will give us the unprecedented opportunity to develop a three-dimensional (3D) electrical conductivity model in the surrounding of the SAFOD (see Figure 1).

Data analysis and 2D modeling results of the new profile data together with existing data from the previous experiments reveal the conductivity structure of the crust from the top to the bottom. They also recover the previous local MT model, which can now be looked at in a regional context. The new MT models - in conjunction with local seismicity, seismic velocity tomography, seismic reflection profiles and surface magnetic anomaly maps - image the major units of the heterogeneous upper crust with the sedimentary sequences, the Franciscan subduction complex and terranes of Salinian granite. We find a remarkable agreement between the upper crustal conductivity distribution and other geophysical models as well as known geological structures.

The regional conductivity model clearly shows that the seismically active zone along the SAF zone is bent around the north-eastern edge of an isolated, large granitic body (Salinian Granite). An upper wedge of the Granite was drilled by the SAFOD main hole; its lateral extensions were previously modeled from surface magnetic anomaly maps. The conductivity model traces the granite down to a depth of 8 kilometers and thereby suggests a lithological contrast in the vicinity of or directly at the plane of seismicity.

Modeled conductivities in the brittle portion of the SAF are not high enough for a significantly increased fluid volume and, associated with that, enhanced porosity of fractured rocks within the fault zone. This means that either there is no significant increase in the bulk porosity or there is only a narrow zone of increased porosity - too narrow to be resolved with magnetotelluric measurements. Borehole measurements in the SAFOD main hole yield a fluid pressure contrast across the fault zone which indicates that the SAF is a barrier for horizontal fluid-flow. Mud-gas studies from Wiersberg and Erzinger (2005) and water sample analyses from Thordsen et al. (2005), in turn, yield low mantle gas contents on either side of the fault, contrasting higher mantle gas contents in shallower wells (the Varian-Phillips well and middle-mountain oil well, located 1km-1.5km east of the SAF; see Kennedy et al., 1997), which may suggest that the SAF does not provide a vertical fluid and gas

migration path from the mantle to the brittle crust. If the SAF is largely impermeable within the upper crust, then the amount of fluids would not be significantly increased in the vicinity of the fault.

However, we do resolve a broad zone of enhanced conductivity, located two to five kilometers east of the active SAF. This zone provides a linkage between the surface conductors, in particular the FZC topping the seismic region, and the lower crust. It also provides an apparent link of the Coast Range Fault (15 km to the east) and the SAF at depth. The middle and lower crust (>10 km) below the SAF zone is generally conductive (<20 ohm-m) in a ~20 km wide zone. A clear transition zone from brittle to ductile deformation which may be expected at a depth of ~15 km cannot be deduced from our conductivity model. There are, however, indications for a localized conducting anomaly in the lower crust, which seems to coincide with the lower bound of the observed seismicity.

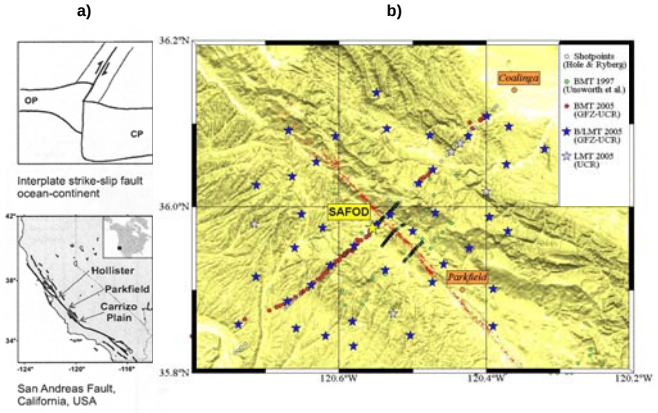

Fig. 1. a) The SAF separates the oceanic Pacific Plate from the continental North American Plate. MT data were previously acquired at different segments of the SAF near Carrizo Plain, Parkfield and Hollister. Limited by short profile lengths, these studies concentrated mostly on structures of the brittle crust. **b)** MT sites in the Parkfield area. New broad-band sites (BMT) are shown as red dots; new combined broad-band/long-period sites (B/LMT) are indicated by blue stars. Existing BMT data from *Unsworth et al.* (2000) are shown as green dots. The seismicity along the San Andreas Fault zone is depicted with red dots.

It is not entirely clear, if the high mantle gas content in the shallow wells east of the SAF requires a migration path from the mantle to the surface, as the mantle gas may also originate from earlier magmatic activity. However, it is possible that the deep-reaching zone of anomalously high conductivities east of the active SAF images a migration path for fluids. High conductivities could indicate increased fluid volumes, which must be inter-connected to increase permeability (and conductivity). In this respect, the conductivity image could indicate that a pathway for the mantle gas found in the shallow crust may be provided by the 2km-5km wide zone east of the SAF but not by the active SAF itself.

References:

Hickman, S., Zoback, M. D., Ellsworth, W., 2004. Introduction to special section: Preparing for the San Andreas Fault Observatory at Depth, Geophys. Res. Lett. (31), 1-4.

Hole, J. A., Ryberg, T., Sharma, A. K. and Fuis, G. S., 2004. Seismic velocity structure from a refraction - reflection survey across the San Andreas Fault at SAFOD. AGU 2004 Fall Meeting, San Francisco.

Kennedy, B. M., Kharaka, Y. K., Evans, W. C., Ellwood, A., DePaolo, D. J., Thordsen, J., Ambats, G. and Mariner, R. H., 1997. Mantle fluids in the San Andreas Fault System, California. Science (278), 1278-1281.

Ryberg, T., Hole, J. A. and Fuis, G.S., 2004. Controlled Source P and S Wave Tomography at SAFOD, AGU 2004 Fall Meeting, San Francisco.

Thordsen, J. J., Evans, W. C., Kharaka, Y. K., Kennedy, B. M. and van Soest, M., 2005. Chemical and Isotopic Composition of Water gases from the SAFOD wells: Implications to the dynamics of the San Andreas Fault at Parkfield, California. AGU 2005 Fall Meeting, San Francisco.

Unsworth, M. J., Bedrosian, P., 2004. Electrical resistivity structure at the SAFOD site from magnetotelluric exploration. Geophys. Res. Lett. (31) 1-4.

Wiersberg, T. and Erzinger, J., 2005: Real-Time Fluid and Gas Monitoring during Drilling of the SAFOD Main Hole in Parkfield, CA. AGU 2004 Fall Meeting, San Francisco.

IODP

Black shale sedimentation in the tropical Atlantic during the upper Cretaceous Oceanic Anoxic Event 3 (OAE 3) - Land-Ocean interaction and oceanic response at the Suriname Margin (ODP Leg 207)

Beckmann, B.[1], Schouten S.[2], Sinninghe Damsté, J.S.[2], Wagner, T.[3], Hofmann, P.[1]
[1]University of Cologne, Institute for Geology and Mineralogy, Zülpicher Str. 49a, 50674 Köln, Germany (bbeckman@uni-koeln.de); [2]Dept. of Marine Biogeochemistry and Toxicology, Royal NIOZ, PO Box 59, 1790 AB Den Burg, Texel, The Netherlands; [3]School of Civil Engineering and Geosciences, University of Newcastle, Newcastle upon Tyne, NE1 7RU, United Kingdom.

Oceanic anoxic events (OAEs) provide deep insights in the functioning of rapid climate change and land-ocean interaction in an extreme warm mode of the Earth system. Despite their fundamental role in late Mesozoic climate evolution, underlying causes and effects of these events, especially regarding the influence of orbital forcing on the Cretaceous atmosphere-continent-ocean system, are still poorly constrained. This project anticipates developing integrated, orbital-scale climate records of the Coniacian-Santonian OAE 3 for the western tropical Atlantic (ODP Leg 207, Demerara Rise) of terrigenous matter supply, organic matter production and burial, sea-surface temperature (SST), and the development of photic zone euxinia (PZE) and bottom-water anoxia. We therefore applied a combination of elemental (LECO and XRF), pyrolytic (Rock Eval pyrolysis) and biomarker analyses (composition of organic matter and TEX86-derived SSTs) on samples from the upper Turonian to early Santonian interval.

Previous studies and newly recovered sections from Demerara Rise document thick organic matter-rich intervals covering the OAE 2 and 3 bundled in sediment cycles that were tentatively linked to Milankovitch cycles (Erbacher et al., 2003). The investigated section at Site 1261 is characterised by a clearly recognizable cyclicity, which is best documented in the carbonate record. The prominent cycle pattern is locally disrupted by intervals displaying unusually high carbonate contents, low TOC values, and a high density. Differences in the faunal assemblage (Bornemann, pers. comm.), erosive basal contacts, and internal grading identify these intervals as turbidites. To provide realistic estimates, turbidites were removed from the section and a turbidite-free adjusted depth record was generated before application of cycle analysis. Consistent with the biostratigraphic framework, cycle analysis supports that the CaCO3 pattern is mainly linked to orbital variations of the short eccentricity frequency; higher frequencies appear to be less dominant.

Bulk organic geochemical analysis focussed on biozone CC14, which displays the best-developed cycle pattern. Results from Rock Eval pyrolysis suggest the dominance of lipid-rich marine derived organic matter, preliminary results from biomarker analysis are in favour of generally elevated nutrient levels throughout the investigated interval. Enrichment of redox-sensitive elements such as Ni and Zn indicate generally low oxic conditions. The Ni/Al and Zn/Al ratios and TOC content show overall synchronous cycle pattern suggesting that anoxia at the sea floor had an additional control on organic matter preservation. Isorenieratane derivates, indicative for photic zone euxinia, were only detected at trace level in samples from the lowermost 9m of the study section. For these intervals we infer that anoxic deep waters at least temporarily invaded the photic zone. However, it comes as a surprise that these highly specific biomarkers are absent in the middle and upper part of investigated sections, contrasting results from the conjugate eastern tropical Atlantic where PZE markers were encountered throughout the late Coniacian/early Santonian (Wagner et al., 2004). To further evaluate the dynamics of the upwelling system along the South American continental margin we intend to extend the record of redox-sensitive elements to biozone CC13 and to improve the resolution of the data set for PZE marker in the future.

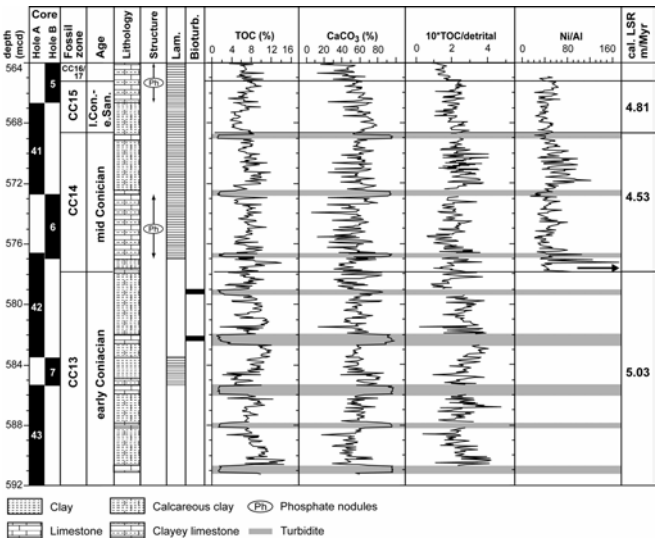

Figure 1: Lithology, biostratigraphy, TOC and carbonate content, TOC/detrital and Ni/Al records of the early Coniacian to early Santonian at ODP Site 1261. Fossil zone according to Bornemann (pers. comm.), age, lithology, structure, lamination, and bioturbation based on Shipboard data (Shipboard Scientific Party, 2004). Cal. LSR = linear sedimentation rate calculated on turbidite-free record.

First TEX86-derived sea-surface temperatures for ODP Leg 207 vary between 33.8 and 35.2˚C at Site 1261 and 34.0 and 36.2˚C at Site 1259 in the investigated interval. These TEX86-SST data are well within the range of SSTs calculated from ?18O of planktic foraminifers (Bornemann, pers.comm.), showing that biozones CC13-15 are characterised by a low degree of SST variability. The foram-based SST, however, detect a distinct cold spell in CC12, which is tentatively assumed to correspond to the global upper Turonian cooling event (e.g., Clarke and Jenkyns, 1999; Wiese and Voigt, 2002, Voigt et al., 2004). Up to now, magnitude and transition times of the observed cold spell remain to be addressed. TEX86-derived SSTs to our knowledge provide the best method to circumvent the problem of influence of temperature and salinity on foraminiferal oxygen isotope data, thus we intend to analyse selected samples for TEX86-derived SSTs to investigate the upper Turonian cooling event in more detail.

References:

Clarke, L.J., Jekyns, H.C., 1999. New oxygen-isotope evidence for long-term Cretaceous climate change in the Southern Hemisphere. Geology, v. 27, p. 699-702.

Erbacher, J., Mosher, D.C., Malone, M.J., et al., 2004. Demerara Rise: Equatorial Cretaceous and Paleogene Paleoceanographic Transect, Western Atlantic. Proceedings of the Ocean Drilling Program, Initial Reports, v. 207.

Shipboard Scientific Party, 2004. Visual Core Description Site 1261. In: Erbacher, J., Mosher, D.C., Malone, M.J., et al. Proceedings of the Ocean Drilling Program, Initial Reports, College Station, v. 207.

Voigt, S., Gale, A.S., Flögel, S., 2004. Midlatitude shelf seas in the Cenomanian-Turonian greenhouse world: Temperature evolution and North Atlantic circulation. Paleoceanography, v. 19, doi: 10.1029/2004PA001015.

Wagner, T., Sinninghe Damsté, J.S., Hofmann, P., Beckmann, B., 2004. Euxinia and primary production in upper Cretaceous eastern equatorial Atlantic surface waters fostered orbitally driven formation of marine black shales. Paleoceanography, v. 19, doi: 10.1029/2003PA000898.

Wiese, F., Voigt, S., 2002. Late Turonian (VCetaceous) climate cooling in Europe: faunal response and possible causes. Geobios, v. 35, p. 65-77.

ICDP

Viscous flow of magmas from Unzen volcano, Japan - implications for magma mixing and ascent

H. Behrens, F. Vetere, and F. Holtz

Institut für Mineralogie, Uni Hannover, Callinstr. 3, 30167 Hannover, e-mail: h.behrens@mineralogie.uni-hannover.de

Introduction: The rheological behavior of magmas of the Unzen volcano in Japan (compositions: rhyodacite to andesite) is determined at conditions relevant to the local geological situation. Effects of pressure, water content, redox state of iron and degree of crystallization on rheological properties of the magma are of special importance. At present the influence of these parameters on viscosity of rhyodacitic to andesitic melts can not be modeled due to a lack of reliable experimental data. Our project is designed to yield background information which helps to interpret observations during the drilling project at Unzen volcano in Japan. Rheological properties of magmas must be known for understanding and for modeling the ascent and the evolution of the magmas. The rheology of a magma is controlled by the melt viscosity at least when the crystal content of the magma is low. In our project we investigate systematically the viscosity as a function of temperature, pressure and various compositional-related parameters. Not only the bulk composition of the melt is important but also dissolved volatiles (i.e., water), the redox state of iron and degree of crystallization of the melt. The chemical parameters may be correlated and, therefore, combined effects of the parameters must be taken into consideration.

Experimental study: The first part of this thesis focuses on the investigation of a synthetic andesite analog in which iron was replaced by adequate proportions of Al, Ca and Mg. The study of the viscosity of Fe-free melts simplifies the experimental procedures (e.g. no crystallization due to Fe-Ti oxides). The viscosity of a Fe-free andesite was measured in the low viscosity range (101 - 106 Pa·s) using the falling sphere(s) method and in the high viscosity range (108 - 1013 Pa·s) using parallel-plate viscometry. The sinking velocity of Pt and Pd spheres, and in one case of a corundum sphere, was used to measure the melt viscosity. Using this procedure, a model was created for the prediction of viscosity as a function of water content and temperature.

In a second step, the viscosity of an iron-bearing melt with composition similar to Unzen andesite was determined experimentally with the same techniques and devices as used for the Fe-free andesite. Particular attention was given to the influence of oxidation state of iron in the melts on the viscosity. Based on our knowledge of the effect of water and temperature on viscosity of Fe-free melts and on the effects of the redox state of iron, a new model was derived to describe the viscosity ? (in Pa·s) as a

$$\log \eta = -5.72 + \frac{8530.8}{(T-59.8)} + \frac{1845.1}{(T-650.6)} * \exp\left[\frac{196.1}{\left(\frac{Fe^{2+}}{Fe_{tot}} * T\right)}\right] * \exp\left(-452.5 * \frac{w}{T}\right)$$

function of temperature T (in K) and water content w (in wt%) and $Fe2+/Fe_{tot}$ ratio:

The application of the viscosity data to Unzen volcanic system shows that the viscosities of the rhyolite and andesite melts from the two end-member magmas are nearly identical prior and during mixing (Fig. 1). This enables an efficient magma mixing and may explain the homogeneous composition of the groundmass observed in Unzen volcanic rocks.

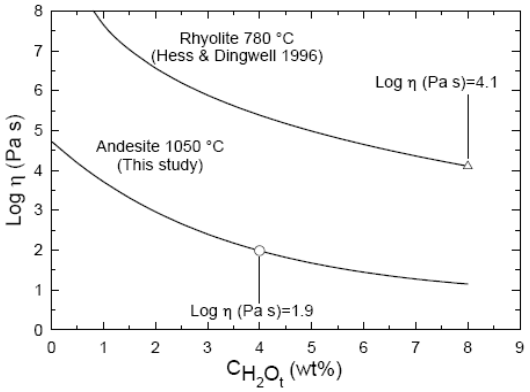

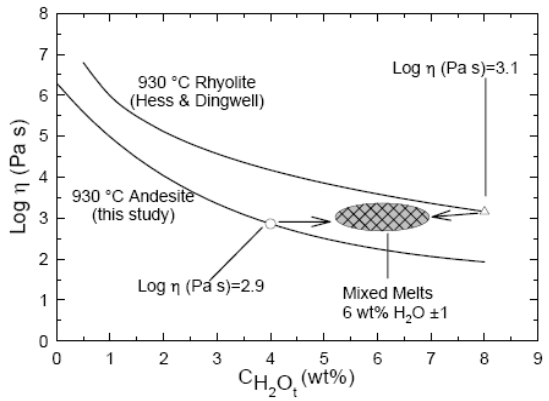

Fig 1. Viscosity of rhyolitic and andesitic melts at conditions prior to eruption of the Unzen volcano. The figure on top (a) shows the initial viscosity of the melt in the magma chamber (rhyolite) and in the ascending melt (andesite). This situation favors mingling of the magmas. The figure on bottom (b) illustrates the situation after thermal equilibrium. Similarity of viscosity observed in this case favors magma mixing.

The third part of this work focuses on the viscosity of crystal-bearing andesite. The viscosity was studied in the high (109.5-1012 Pa·s) and low viscosity range (103-103.5 Pa·s). Creep data were carried out at room pressure and in the temperature range 779 -1028 K using hydrous sample containing between 0.8 and 3.8 wt% H2Otot. The samples were treated at high pressure (crystallization experiments) and contained approximately 21 - 38 vol% crystals. Falling sphere experiments were performed in IHPV at 300 MPa and temperature between 1373 and 1523 K in samples containing 0.52, 2.98 and 4.02 wt% H2Otot. Zircon crystals, which are only little soluble in andesitic melt at high temperature, were added to fix the desired crystals/melt ratio. The results show that, in both the high- and low-viscosity ranges, viscosity is higher than predicted by the Einstein-Roscoe equation, which is commonly used to predict the viscosity of magmas. The viscosity can be up to one log unit higher than that predicted by the Einstein-Roscoe equation for mixtures composed of 20 vol% crystals and melts containing 4.02 wt% H2O.

In the final part of our study we want to investigate rheological properties of samples recovered from the conduit drilling at Unzen volcano. Such samples are available from the last visit of Holtz and Botcharnikov at the Unzen 2004 workshop in Shimabara, Japan. A major problem in these studies, however, is the strong hydrothermal alteration of the volcanic rocks in the last decade.

Application of experimental results to the Unzen Drilling Project Several evidences are given that mixing of an almost aphyric andesitic magma to a phenocryst-rich rhyodacitic magma has initiated the 1991 eruption of the Unzen volcano (Holtz et al. 2004; Sato et al. 2004). Temperature of the injected andesitic magma is estimated to be near 1050˚C and water content near 4 wt%. The temperature of the magma in the chamber has been much lower (760-780˚C) and the water content of the residual rhyolitic melt is inferred to be about 8 wt%. Using our viscosity data we can investigate how efficient mixing of the two magmas is. Directly after injection the viscosity of the hot andesitic melt is about two orders of magnitude lower than that of the cold rhyolitic melt. Hence, both magmas will mingle each other. However, heat transfer is fast compared to magma mingling and mixing and both magmas will approximate in temperature. Finally, when the temperatures of the interpenetrated magmas are the same, the andesitic melt with 4 wt% H2O will have a similar viscosity as the rhyolitic melt with 8 wt%. Then mixing of both magmas will be very efficient. This explains the absence of indications for mingling in the dacitic rocks produced by the eruption. The results of the viscosity studies are used to model the evolution of Unzen magmas prior to eruptions.

Publications in the project:
Vetere F., Behrens H., Holtz F. and Neuville D.R. (2005) Viscosity of andesitic melts - new experimental data and a revised calculation model. Chem. Geol. (in press).
Vetere F., Behrens H., Schuessler J.A., Holtz F., Misiti V. and Borchers L. (2006) Viscosity of andesite melts - implication for magma mixing prior to Unzen 1991-1995 eruption. J. Volc. Geotherm. Res. (Unzen special issue) (submitted).

ICDP

Aktive seismische Überwachung von Änderungen des Reflexionsverhaltens injektionsinduzierter Druckänderungen in der SE2 Scherzone des Kristallin der KTB

Beilecke, T., Bram, K., Buske, S.

Das Ziel des Projektes ist die Bestimmung von Änderungen der Reflexionsamplituden der SE2-Scherzone im Kristallin als Folge von in ihr durch eine Bohrung gezielt hervorgerufenen hydraulischen Druckerhöhungen im Verlauf eines Jahres. Theoretische Betrachtungen sagen die mögliche Detektion einer Reflektivitätsänderung unter bestimmten Bedingungen voraus. Dabei liegt das so genannte ‚worst-case scenario' für eine einfache Modellannahme bei ca. 15% Amplitudenänderung (Kaselow, 2004).

Die Feldarbeiten fanden zwischen Mai 2004 und November 2005 statt. Somit ist der Druckaufbau in der Störzone bis zu seinem Maximum und nach Abschalten der Pumpen ein halbes Jahr der Abklingphase seismisch erfaßt worden.

Kern der Meßgeometrie war ein fest in ca. 70 cm Tiefe installiertes, 5-armiges Geophon-Array mit 90 m Durchmesser, bestehend aus 24 3K-Geophonen. Die Signalquelle des aktiven Experiments war der Vertikal-Minivibrator des GGA-Instituts, Hannover. Die Sweepdauer betrug 30 s linear über den Frequenzbereich 30 bis 120 Hz mit 27 kN Peak Force. Die zwei Anregungspunkte befanden sich in ca. 300 - 500 m Entfernung nördlich und nordöstlich des Arrays. Das Signal wurde während eines Meßzyklusses 32-mal wiederholt, einzeln mit jedem Geophonkanal gemessen und unkorreliert aufgezeichnet, um ein Maximum an nachträglicher Datenbearbeitung zu gewährleisten. Die asymmetrisch-sternförmige Anordnung der Geophone ermöglicht zudem eine räumlich eindeutige Filterung der Signale.

Zentrale Parameter des Experiments sind sowohl die Wiederholbarkeit des Quellsignals als auch die Stabilität der Signale auf der Empfängerseite. Für die Qualitätskontrolle auf der Quellseite waren einzelne 3K-Geophone ca. 15 m von der Vibratorbodenplatte entfernt in ca. 50 cm Tiefe über den gesamten Meßzeitraum fest im Boden installiert. Vier Beschleunigungsmesser waren auf der Vibratoreinheit verschraubt. Es zeigt sich, dass die Standardabweichung an dem 3K-Geophon innerhalb eines Meßzyklusses bei unter 10% liegt (Bild 1 links). Die alleinige Bestimmung der Standardabweichung aus den Signalen der Beschleunigungsmesser birgt Unsicherheit und weicht uneinheitlich von den Werten des 3K-Geophons ab. Die Bestimmung der Standardabweichung aus den Signalen des Referenzgeophons über den einjährigen Zeitraum der Injektion ist andererseits ebenfalls schlecht bestimmbar, da der Vibrator nicht fest installiert war (Bild 1 rechts). Ergebnis: Selbst wenn die Standardabweichung im gesamten Zeitraum bei nur etwas über 10% liegt, ist dieser Wert nur knapp unterhalb der Größenordnung der zu erwartenden Amplitudenänderungen der SE2 Reflexionen im oben genannten ‚worst-case scenario'.

Das 3K-Referenzgeophon in der KTB Hauptbohrung (KTB-HB) in Höhe des Zielhorizonts wäre für eine Qualitätskontrolle entsprechend der Projektplanung besser zu gebrauchen gewesen, kann diese Aufgabe aber nicht erfüllen, weil es durch Systemausfälle, starke Störsignale und durch Versatz innerhalb der Bohrung im Verlauf des Meßzeitraums beeinträchtigt war.

Auf der Empfängerseite liegt die Standardabweichung der Rohdaten eines Meßzyklusses für die schwachen Reflexionen aus

dem Bereich des SE2 in der Größenordnung von 70% (Bild 2 rechts). Hier wirkt sich der Noise der Umgebung im Verhältnis stärker als an der Quelle aus. Durch selektives Stapeln bzw. durch den Einsatz des so genannten ‚Diversity Stack' kann dieser Wert verbessert werden. Insbesondere können hierdurch Störsignale von Fahrzeugen unterdrückt werden. Es ist allerdings schwierig die Verbesserung durch den Diversity Stack zu quantifizieren. Schwerpunkt der weiteren Auswertung muß deshalb vor allem die Verbesserung der Signalfilterung sein. Ohne eine solche Maßnahme werden die Fehlerbalken weiterhin sehr wahrscheinlich über den zu erwartenden druckinduzierten Amplitudenänderungen liegen.

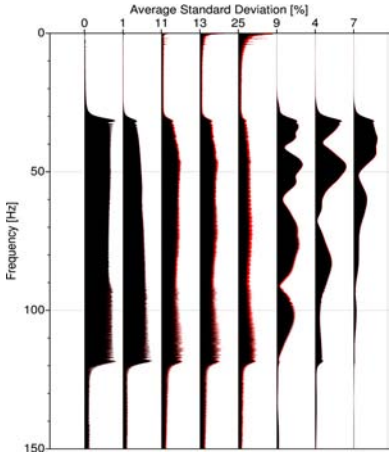

Bild 1a: Durchschnittliches Amplitudenspektrum verschiedener Sensoren in der Nähe der Vibratorquelle (schwarz) und addierte Standardabweichung in rot. Die Spuren zeigen von links nach rechts den Signal-Sweep (hier fehlerbehaftet), den Beschleunigungsmesser auf der Vibratormasse, 3 Beschleunigungsmesser auf der Bodenplatte von innen nach außen und Nord, Ost und Z-Komponente eines Geophons ca. 15 m vom Vibrator entfernt. Input jeder dargestellten Spur sind 32 Sweeps eines Meßzykluses am Vibratorpunkt 1. Die Nummern über den Spuren repräsentieren die durchschnittliche Standardabweichung entlang der Frequenzachse.

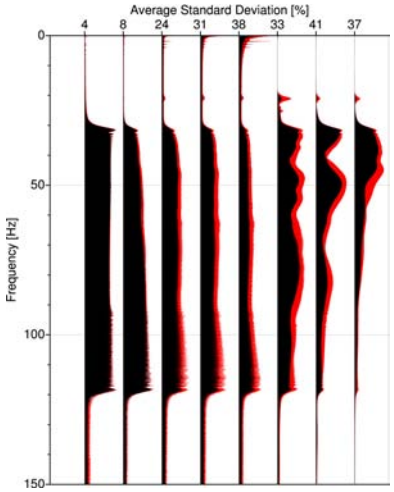

Bild 1b: Wie Bild 1a aber für alle der 416 Sweeps am Vibratorpunkt 1 zwischen dem 1. Juni 2004 und dem 29. April 2005

Interessant ist, dass sich beim Vergleich zweier Messzyklen an einem Tag kaum Unterschiede im P-Wellenersteinsatz zeigen aber Differenzen in der Coda der Oberflächenwellen. Inwieweit dieses auf tageszeitabhängige Bodenveränderungen hindeutet, die auch Auswirkungen auf die Abstrahlcharakteristik der Signalquelle gehabt haben könnten, muss noch geklärt werden. Es gibt zudem aufgrund von Polarisationsanalysen Hinweise, daß die Wellenausbreitung in der Kruste nicht exakt der erwarteten entspricht. Somit könnten die von den seismischen Signalen erfassten Störzonenbereiche andere als die erwarteten sein und möglicherweise weniger Druckeinfluss aufweisen, als erhofft. Die kurzen Reflektorelemente der kristallinen Strukturen in den seismischen Sektionen an der KTB erschweren die Korrelation mit älteren, nur wenige zehner Meter entfernter Referenzdaten des INSTRUCT'93 Experiments.

Es sollen im letzten Zeitraum der Auswertung außerdem die praktischen Konsequenzen neuerer, detaillierter Fluiddruckmodellierungen (Gräsle, 2005) als Kontrapunkt zu den ursprünglichen Abschätzungen der Reflexionsamplitudenänderungen betrachtet werden.

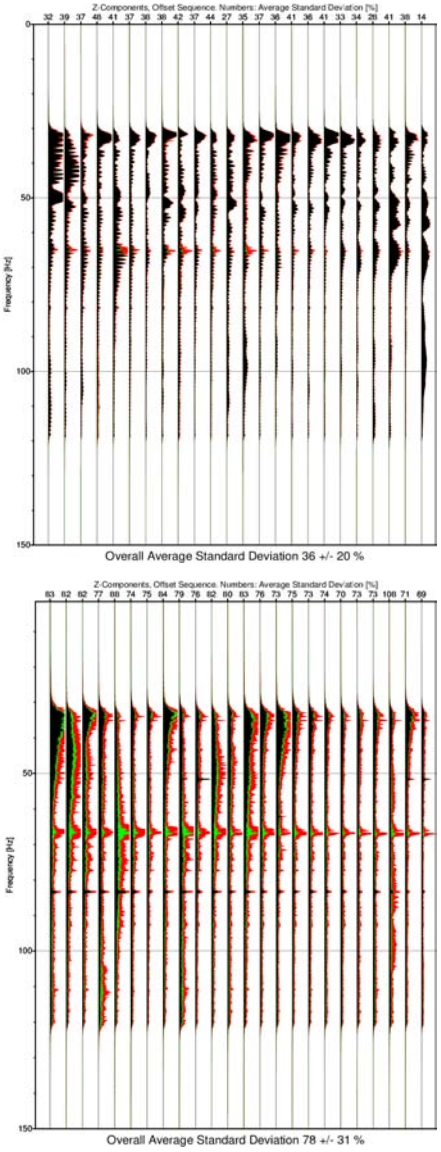

Bild 2 oben: Diversity Stack des Amplitudenspektrums der Vertikalkomponenten des Geophon-Arrays (schwarz). Die Durchschnittswerte sind grün dargestellt und die Standardabweichung addiert in rot. Eingangswerte für jede Spur sind wie bei Bild 1 links 32 Messungen eines Meßzykluses am Vibratorpunkt 1. In diesem Fall ist die gesamte Spurlänge für die Berechnung der Spektren herangezogen worden.
Unten: Berechnungen wie Bild 2 oben, wobei die Spektren aber nur für das hintere Wellenfeld ohne die starken Ersteinsätze berechnet wurde.

Danksagung
Das Projekt wird von der Deutschen Forschungsgemeinschaft (DFG) unter den Kennzeichen BR 606/7-1 und BR 606/7-2 gefördert.

Bibliographie

Gräsle, W., Kessels, W., Kümpel, H.-J., & Li, X. akzeptiert 2005. Hydraulic observations from a one year fluid production test in the 4000 m deep KTB pilot borehole. Geofluids.

Kaselow, A. 2004. The Stress Sensitivity Approach: Theory and Application. Dissertation, Freie Universität Berlin.

IODP

Reconstruction of the geomagnetic field strength over the past 300.000 years derived from 10Be data of ODP-drift sediments from the Northwest and South Atlantic Ocean

Bernsdorff, F.[1], Christl, M.[1,2], Schulze, B.[1], Wenderoth, P.[1], Lippold, J.[1], Böhm, E.[1], Mangini, A.[1], Kubik, P.[2]

[1]Heidelberger Akademie der Wissenschaften, Im Neuenheimer Feld 229, 69120 Heidelberg, Germany; [2]Institute of Particle Physics, ETH Hoenggerberg, CH-8093 Zurich, Switzerland; Email: Frank.Bernsdorff@iup.uni-heidelberg.de

The cosmogenic nuclide 10Be is mainly produced in the lower stratosphere by interaction of galactic cosmic rays with oxygen and nitrogen atoms, and its production is known to be anti-correlated with the solar- and/or geomagnetic field strength. After a short atmospheric residence time of about 1 year ^{10}Be is deposited onto land, ice sheets and (mainly) the ocean surface. Therefore it should be possible to extract a record of geomagnetic paleointensity (GPI) from depositional profiles of these radionuclides in marine, terrestrial and ice core archives.

In this project we are investigating two deep sea sediment cores from the Northwest and South Atlantic Ocean (ODP-Site 1063 and ODP-Site 1089) for highly resolved 10Be profiles. The application of a special correction procedure ($^{230}Th_{xs}$-method, and box model calculations) allows to quantify the transport of ^{10}Be in the ocean, extracting the global ^{10}Be-production from marine records. Based on these profiles, a marine ^{10}Be stratigraphy will be developed that can be compared to ^{10}Be records from Greenland (GRIP, GISP II) and Antarctic (EPICA) ice cores. In particular, enhanced global ^{10}Be production during geomagnetic events (Lachamp, Blake, Jamaica) can be used as global time marker for the synchronization of marine and ice core chronologies.

Results from ODP site 1089: The global ^{10}Be-production rate was extracted from Site 1089 covering the past 300 kyr. To correct for marine transport processes, first $^{230}Th_{ex}$-normalization was applied to correct for sediment redistribution. Then, simple box model calculations were used to quantify the lateral transport of ^{230}Th and ^{10}Be in the South Atlantic. Our results show strong evidence that the transport corrected flux of ^{10}Be at Site 1089 reflects global ^{10}Be-production on a multi centennial to millennial timescale and therefore is inversely related to the geomagnetic dipole strength over the past 300 kyr.

To document the global character of the ^{10}Be-record from Site 1089 over the whole 300 kyr range it is compared to four paleointensity and ^{10}Be-records, respectively (Figure 1).

In the first panel Site 1089 ^{10}Be-flux (blue line) is plotted together with the PI-record from the same site [Stoner et al., 2003] (black line) and the globally stacked SINT 800 record [Guyodo and Valet, 1999] (red line). For comparison with paleointensity records a logarithmic scale type is used to account for the higher sensitivity of ^{10}Be-production to low dipole field strengths. Over the whole 305 kyr a good correlation of the ^{10}Be-flux to the PI-records is observed. During MIS 1 - 2 and during MIS 7 - 8 (Marine Isotope Stages are indicated by the numbers in Figure 1) Site 1089 ^{10}Be-flux corresponds better to the SINT 800 than to Site 1089 PI probably indicating local overprints in the Site 1089 PI-record. Both, SINT 800 and Site 1089 ^{10}Be-record are plotted on their own chronology, so that small adjustments of the age models probably improve the observed correlation.

The second panel which shows the transport corrected ^{10}Be-flux in two different ocean basins (Site 1089 vs. Equatorial Pacific Ocean) with two different sedimentarry regimes indicates that these records represent global variations of ^{10}Be production.

Results from ODP site 1063: The comparison of the $^{230}Th_{ex}$-normalized ^{10}Be-flux at Site 1063 with the NAPIS-75 paleointensity record (Figure 2) and other cosmogenic records (^{10}Be-fluxes from GISP/GRIP, atmospheric Δ^{14}C) reveals a reasonable interhemispheric correlation further emphasizing the idea of using ^{10}Be as a global matching-tool and as a proxy for

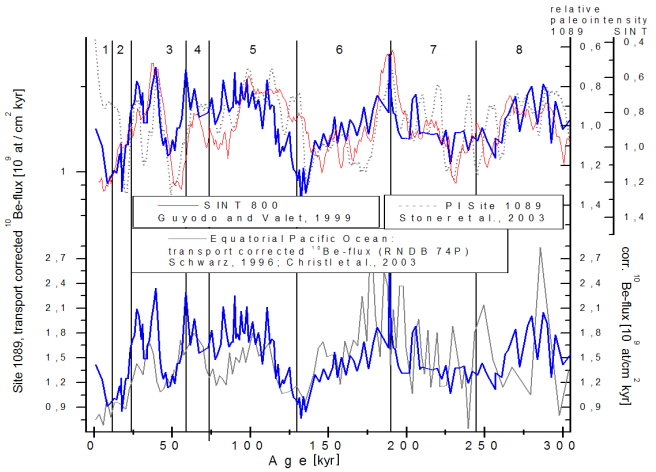

Figure 1: Comparison of the 10Be-flux of Site 1089 to PI and SINT800-records.

geomagnetic paleointensity [Schulze, 2006]. Figure 3 shows that, over the past 100 kyr, the 230Thex-normalized 10Be-flux at Site 1063 correlates reasonably well with Site 1089. Nevertheless, compared to the absolute values of 10Be-deposition at Site 1089 and also regarding to the recent value of the global 10Be-production rate (Monaghan et al., 1986), 10Be-deposition at Site 1063 is constantly increased by a factor of about 1.4.

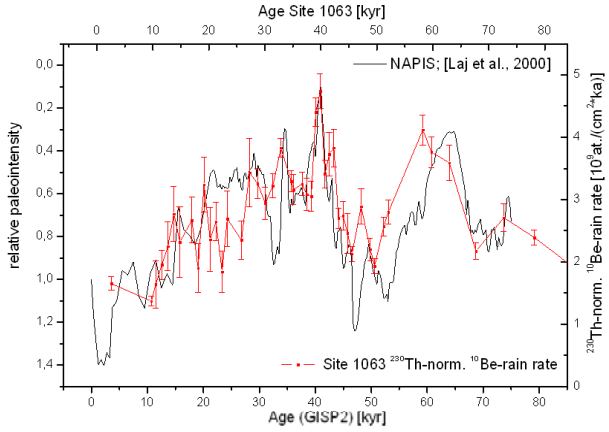

Figure 2: The red curve shows the 230Thex-normalized ^{10}Be-flux (10Be-rain rate) at ODP Site 1063 over the past 100 kyr. It is compared to the $^{230}Th_{ex}$-normalized 10Be-flux at ODP Site 1089 (blue curve; red and blue curve plotted on the left scale). Plotting the ^{10}Be-record of Site 1063 on a compressed scale (factor 1,4; grey curve), the very good correlation of both records is obvious.

This might indicate that lateral transport of dissolved ^{230}Th and ^{10}Be (i.e. the effect of boundary scavenging) significantly influenced the deposition of these at Site 1063. Consequently, the $^{230}Th_{ex}$-normalized ^{10}Be-flux at Site 1063 has to be corrected for oceanic transport effects by model calculations. Therefore, an existing two-box model was applied to the 10Be-flux data [Christl, 2003]. As the constraining input values describing water mass circulation are yet to be determined by measurement of the ^{231}Pa/^{230}Th-ratio, these are only preliminary calculations.

Conclusions: Our results convincingly show that ^{10}Be in deep sea sediments can be used as a proxy for geomagnetic paleo-intensity. Our results, futhermore, demonstrate the global significance of the transport corrected ^{10}Be-record from Site 1089.

However, it is still an open question if ocean circulation (e.g. the strength of the North Atlantic Overturning circulation) has a

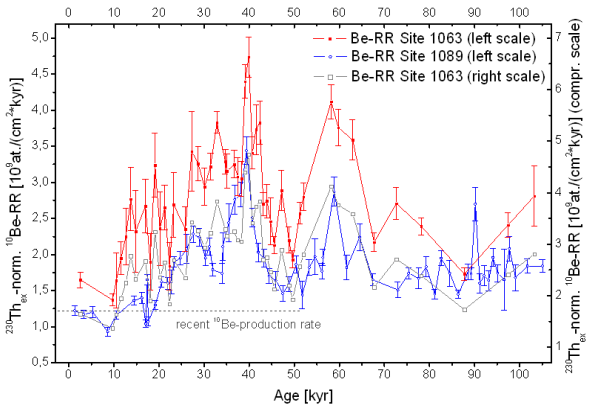

Figure 3: 230Thex-normalized 10Be-flux at Site 1063 (red curve) compared to the NAPIS-75 paleointensity stack [Laj et al., 2000] (black curve).

significant impact on the deposition of 230Th and 10Be at Site 1063. Measurements of the 231Pa/230Th-ratio at Site 1063 will help to solve this question.

Literature:

Christl M., Strobl C., and Mangini A. (2003) Beryllium-10 in deep-sea sediments: a tracer for the Earth's magnetic field intensity during the last 200,000 years. Quaternary Science Reviews 22(5-7), 725-739.

Guyodo Y, Valet J-P. (1999). Global changes in intensity of the Earth's magnetic field during the past 800 kyr. Nature, 399:249-252.

Laj C., Kissel C., Mazaud A., Channel J. E. T., and Beer J. (2000) North Atlantic paleointensity stack since 75 ka (NAPIS-75) and the duration of the Laschamp event. Phil. Trans. R. Soc. Lond., 358 (A), 1009-1025.

Monaghan M. C., Krishnaswami S., and Turekian K. K. (1986) The global-average production rate of 10Be. Earth and Planetary Science Letters 76(3-4), 279-287.

Schulze B., (2006). Hochaufgelöste Rekonstruktion der 10Be-Produktionsrate aus Tiefseesedimentkernen des Bermuda Rise über die letzten 70.000 Jahre. Diplomarbeit, Universität Heidelberg.

IODP

Subantarctic influence on the mid Miocene initiation of the Benguela upwelling - evidence from ODP Sites 1085 and 1092 planktonic foraminifer assemblages and stable isotopes

T. Bickert , M. Butzin, H. Kuhnert, H. Paulsen, T. Westerhold
MARUM, Universitaet Bremen, 28334 Bremen / bickert@ uni-bremen.de

We present middle to late Miocene stable isotope and foraminiferal assemblage data of Ocean Drilling Program (ODP) Sites 1085 from the continental margin off southwest Africa and 1092 from the subantarctic South Atlantic. The studied interval (14-7 Ma) covers the middle Miocene cooling at 14 Ma and the initiation of the Benguela upwelling system at around 11.5 Ma. The middle Miocene Antarctic glaciation, represented by the globally recorded $\delta^{18}O$ increase events Mi-3 and Mi-4, comes along with a distinct stratification of the upper SE Atlantic water column. However, sustained oceanic upwelling in the Benguela region starts as late as 11.5 Ma, reflected by the development of high productivity foraminifer faunas containing *G. bulloides*, and by distinctly increasing mixed-layer to thermocline $\delta^{13}C$ gradients. The first occurrence of *N. pachyderma* (s) in the Benguela region at 11.5 Ma as well as the deep water cooling at Site 1085 at the same time indicates the growing influence of subantarctic water masses on the Benguela upwelling. This observation is in line with the hypothesis of Sarmiento et al. (2004) that nutrient advection by subantarctic water masses plays an important role for high productivity in the upwelling region of the southeast Atlantic. Two pulses of Indian Ocean-derived foraminifer species *Globorotalia menardii* at 11.3 and 10.7 Ma may indicate an enhanced spatial variability of the South Atlantic oceanic fronts associated with the establishment of the Benguela upwelling. The assumed leakage of potentially nutrient rich Indian Ocean water via the Agulhas current, that is indicated by the occurence of this species in the southeast Atlantic offers an alternative source for enhanced nutrient content responsible for the initiation of Benguela upwelling. Modeling experiments will help to better constrain the factors and feedback mechanisms associated with the middle to late Miocene evolution of South Atlantic Ocean circulation and productivity.

IODP

A paleotemperature record of the Cretaceous Thermal Maximum (ODP Leg 207, tropical western Atlantic)

André Bornemann[1,2] and Richard D. Norris[1]
[1]Scripps Institution of Oceanography, La Jolla, CA 92093-0244, USA; [2]Institut für Geologie, Mineralogie & Geophysik, Ruhr-Universität Bochum, D-44780 Bochum
E-mail: andre.bornemann@rub.de

Paleoclimate records have shown that global sea surface temperatures (SSTs) reach a peak in the latest Cenomanian to Santonian. The detailed structure of this Cretaceous Thermal Maximum (KTM) is not well known, nor have we a clear understanding of the causal factors behind this temperature peak. Until recently, there were few sedimentary successions known that had continuous records through this interval and well preserved foraminifera or other proxies that could be employed to reconstruct the temperature history. The cause of global warmth has also been controversial with most authors invoking elevated pCO2 (up to 3000-5000 ppmv) as a means of reaching tropical temperatures several degrees higher than the modern and subpolar temperatures that are perhaps as much as 20˚C above modern values. The source of this greenhouse gas is unclear because the KTM follows the peak of volcanic outgassing and seafloor production by at least 20 myrs (Wilson et al., 2002).

New multispecies C/O isotope data from tropical planktic foraminifera present a first highly resolved picture of the history of the KTM. Our data are derived from ODP Sites 1259 and 1261 (Demerara Rise, ~4˚N paleolatitude) in the tropical western Atlantic. Planktic foraminifera from Turonian to Santonian sediments show a glassy appearance, hollow chambers and primary surface ornamentation. This state of preservation allows for a detailed geochemical investigation in order to reconstruct SSTs. We analyzed ten different species of planktic foraminifera. The scatter of data is fairly consistent through the sequence at around 0.5‰ for 18O and 0.5-0.8‰ in $\delta^{13}C$. The range of $\delta^{18}O$ values is -4.2 to -4.95‰ through the Turonian and this period is followed by a steady drift to ratios of -3.6 to -4.4‰ in the Coniacian/ Santonian. There is little distinct stratification of different species, although Whiteinella baltica and Heterohelix globulosa typically yield more negative $\delta^{18}O$ than the other species of Hedbergella, Whiteinella, Dicarinella, Archaeoglobigerina and Marginotruncana. $\delta^{13}C$ data show a trend toward ratios of 1.5 to 2‰ in the mid Turonian to ~0.2 to 1‰ in the late Turonian followed by a gradual increase to ~1 to 2‰ in the Santonian.

Calculation of past SSTs from these data requires several assumptions. For the $\delta^{18}O$ (δw) of Cretaceous seawater we assume conservatively an "ice free" w of -1‰ (SMOW) and a more realistic δw of -0.25‰. The latter considers variations in $\delta^{18}O$ of seawater with latitude. Our most negative Turonian $\delta^{18}O$ ratio (-4.95‰) corresponds to calculated SSTs of ~34 to 38˚C for conservative and more realistic assumptions of w. If we assume a latitudinal change in w (as almost certainly has always existed) our isotopic data for all foraminifera species suggest a range of upper ocean temperatures from 34˚C to 36˚C in the Turonian (excluding the most negative $\delta^{18}O$ measurements) and to ~31˚C to 34˚C in the Santonian. These temperatures can be adjusted toward colder values by about 1˚C if we assume that Cretaceous seawater was about 0.25‰ more negative than today owing to uptake of ^{18}O in basalt weathering, likely an important process in an era of high sea floor spreading (Wallmann, 2001). Conversely, an adjustment of 2-3˚C toward warmer temperatures is justified if we consider

the probable effects of increased pCO2 on oceanic pH (Zeebe, 2001). Independent from the latter two corrections the estimated SSTs for the KTM are considerably higher than the modern tropical oceanic maximum of about 28-29˚C.

References:
Wallmann, K. (2001): Geochim. Cosmochim. Acta 65, 2469-2485.
Wilson, P. A., Norris, R. D. & Cooper, M. J. (2002): Geology 30, 607-610.
Zeebe, R. E. (2001): Palaeogeogr. Palaeoclimatol. Palaeoecol. 170, 49-57.

ICDP

Pre-eruptive conditions prior to and after magma mixing at Unzen volcano: constraints from high pressure experimental investigations

Botcharnikov R.E.[1], Holtz F.[1], Behrens H.[1], and Sato H.[2]
[1]Institut für Mineralogie, Universität Hannover, Callinstr. 3, 30167 Hannover, r.botcharnikov@mineralogie.uni-hannover.de; [2]Dept. of Earth and Planetary Science, Kobe University, Kobe 657-8501 Japan

The 1991-1995 eruption of Unzen volcano is initiated by a mixing event (as observed in many eruptive systems) between a low-temperature phenocryst-rich dacitic magma and a high temperature andesitic magma. Thus, understanding pre-eruptive conditions requires determination of pre-mixing (in the two end-member magmas) and post-mixing conditions, and modeling of the processes occurring during magma mixing and ascent.

Here we report new constraints on the pre-mixing magmas, especially on the high- temperature end-member, (including volatile contents, melt and phenocryst compositions) and on processes occurring in magma chamber prior to eruption. These constraints are obtained from high pressure - high temperature experimental investigations on phase relations and volatile solubilities in silicate melts and from natural samples obtained from lava dome (including andesitic enclaves) and from the ICDP-drilling. The experiments on magma mixing and a compilation of natural data and experimental results are used to understand the evolution of high-temperature magma prior to and during the eruption and the role of mixing processes in magma forcing and ascent.

Natural samples: (a) Core samples from conduit drilling. The successful drilling of Unzen conduit in 2004 provided unique samples of magma stored at 1300 m depth in magmatic conduit for about 10 years after the eruption was ceased (Nakada et al., 2005; Goto et al., 2005). The maximum temperature of conduit rocks is estimated to be about 180-200˚C (Nakada et al. 2005; Suto et al., 2005). The significant temperature decrease in less than 10 years after the eruption is supposed to be due to intensive hydrothermal circulation around magma conduits and small cross-section of conduit dikes (up to 40 meters thick; Nakada et al., 2005). Another important feature of rocks sampled from the conduit zone is a strong hydrothermal alteration of mafic minerals, in particular hornblende, and devitrification of groundmass. The bulk chemical composition of conduit magma is very similar to the composition of dome lava (last lava spine at the top of Unzen). However, there is a significant difference in texture of groundmass in these two types of rocks: The conduit lava has fine-grained matrix groundmass and the size of microlites in the groundmass is much smaller than in the dome lava. This may result from different storage conditions of Unzen magma after the eruption.

(b) Mafic (andesitic) enclaves. Mafic enclaves in the erupted Unzen dacite rocks represent the droplets or small batches of high-temperature andesitic magma quenched inside low-temperature rhyolitic magma during magma mixing. The compositions of the homogenized (pre-heated at 1100˚C, 200 MPa, fO_2 < NNO) melt inclusions trapped in Pl microphenocrysts (40-200 ?m) show variations of SiO_2 content in a range of 64-70 wt% while the variations of concentrations of all major elements in melt inclusions have systematic trends with SiO_2. The composition of host Pl varies from #An=50 to 70. The measured concentrations of volatiles in andesitic melt inclusions reach values up to 600 ppm dissolved S and up to 500 ppm dissolved Cl. A significant difference between concentrations of dissolved S and Cl in melt inclusions in Pl of mafic enclaves and concentrations of S (< 50 ppm) and Cl (500-1100 ppm) in melt inclusions in phenocrysts of the dacitic magma clearly indicates the two distinct sources for S and Cl in the 1991-95 eruption of Unzen volcano. Sulfur degassing was generated by a release of fluids from the high-temperature andesitic magma whereas Cl was degassed from the low-temperature rhyolitic magma.

High-T,P experiments and comparison with natural data. The stability fields (in terms of temperature and water activity) of natural Pl and coexisting melts from the melt inclusions were estimated from data of phase equilibria experiments performed with a synthetic andesite at T=950-1050˚C, P=200 MPa, log fO_2=NNO-1 - NNO, and water activity of about 0.2-1. The temperatures and H2O melt concentrations, calculated using the compositions of coexisting Pl and melt inclusions, provided an estimation of the conditions of andesitic magma evolution within the mafic enclaves during mixing event prior to the eruption. The Pl-melt inclusion pairs show a maximum temperature of ~1020˚C for a melt containing about 2 wt% H_2O and a minimum temperature of ~910˚C for a melt with ~4 wt% dissolved H_2O. The estimated evolution trend of andesitic magma within the mafic enclaves is shown in Fig.1.

Fig. 1. Phase relations in the synthetic Unzen andesite at 200 MPa and logfO_2 ≤ NNO. Ol = olivine, Pl = plagioclase, Opx = orthopyroxene, Cpx = cliniopyroxene, Ilm = ilmenite, Mt = magnetite,
Hb = hornblende. Numbers are #An. The fields represent: (1) stability field of Pl with An=50-70; (2) stability field of experimental glasses corresponding in composition to the natural glasses of mafic enclaves; (3) stability field of coexisting Hb and Pl in natural enclaves based on the calculations after Holland and Blundy (1994); (4) evolutionary trend of melts trapped in Pl microphenocrysts estimated according to the compositions of Pl-melt inclusion pairs from mafic enclaves.

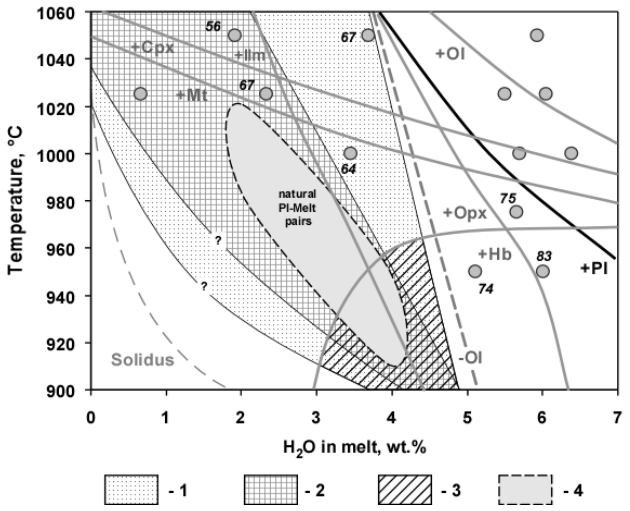

It must be noted that the andesitic magma evolution recorded by trapped melt inclusions in Pl microphenocrysts represents only a part of magma differentiation which is limited to the conditions of Pl crystallization.

According to the phase diagram obtained at 200 MPa (Fig.1), the observed natural mineral assemblage of mafic enclaves, i.e., Opx, Cpx, Pl, Hb and oxides, can be reproduced experimentally only at relatively low temperatures (< 980˚C), which correspond to post-mixing conditions. The estimated temperature of andesitic magma prior to mixing is about 1050˚C and the estimated water content is ca. 4 wt% (Holtz et al., 2005). At 200 MPa, 1050˚C and such a water content, the andesite magma would be at or close to liquidus conditions. The results also imply that olivine could crystallize as liquidus phase and that this mineral brake down (peritectic reaction) during further interaction with cold

rhyodacitic magma. Temperature decrease with ongoing magma mixing processes causes the crystallization of hornblende. Since pressure has a positive effect on the stability of Cpx and Hb, additional series of experiments at 300 and 400 MPa are necessary to better constrain the processes and conditions during mixing in the mafic enclaves (crystallization, temperatures determined from natural mineral pairs).

Magma mixing: an experimental approach. Mixing processes between two magmas of rhyolitic and andesitic composition were studied experimentally at 300 MPa, 1000˚C, and log $fO_2 \leq$ NNO+3. The mixing experiments were done with the conventional diffusion-couple technique (e.g., Watson, 1994) using the following pairs: hydrous andesite (5 wt% H2O) - hydrous rhyolite (6 wt% H_2O), dry andesite - hydrous rhyolite (6 wt% H_2O) and hydrous andesite (5 wt% H_2O) - dry rhyolite. To avoid gravitational instability, the cylinder of andesite glass was always placed at the bottom of the capsules and the rhyolite glass at the top. For all melts the amount of water in the starting glasses was lower than the H_2O-saturation value at 300 MPa. The results of experiments with the three combinations of glasses indicate that the mixing process between the two magmas with significant contrast in composition like andesite and rhyolite is controlled by diffusion, crystal growth/dissolution and convection. The presence of water in the system has a strong control on the crystal growth/dissolution and favors convection of the melts and magma mingling processes. Petrological and experimental constraints indicate that Unzen magmas were volatile-rich prior to mixing providing prerequisite conditions for effective magma hybridization. The extent of hybridization at a given temperature can be quantified by time-dependent experiments. In addition, although mixing at the scale of the magma chamber is controlled by convections processes, the data are useful to understand local exchanges between highly solidified andesitic enclaves and rhyodacitic melt. The investigation of the chemistry and texture of enclaves, compared with the experimental results, is useful to estimate the residence time and/or temperature of enclaves in magma chamber before the eruption.

Additional set of experimental and natural data is needed to better reconstruct the mixing processes in the magma chamber of Unzen and to model the evolution of magma after mixing and during magma ascent. In particular, the decompression-induced crystallization and degassing processes should be investigated experimentally providing insights on magma eruption history.

References:
Goto Y. et al. (2005) Unzen Workshop 2005, Shimabara, Japan. O-9.
Holland, T. J. B., Blundy, J. (1994) Contrib. Miner. Petrol. 116, 433-447.
Holtz F. et al. (2005) Journal of Petrology, 46, 319-337.
Nakada, S and Motomura, Y (1999) Journal of Volcanology and Geothermal Research 89, 173-196.
Nakada S. et al. (2005) Unzen Workshop 2005, Shimabara, Japan. O-8.
Suto Y. et al. (2005) Unzen Workshop 2005, Shimabara, Japan. O-6.

IODP

The late-stage evolution of oceanic gabbros - Combined experimental and in-situ isotope study on gabbros of the ODP Legs 118/176 drilled at the Southwest Indian Ridge

Botcharnikov R.E., Koepke J., and Horn I.
Institut für Mineralogie der Universität Hannover, Callinstr. 3, 30167 Hannover, r.botcharnikov@mineralogie.uni-hannover.de

Gabbroic rocks from Hole 735B at the Southwest Indian Ridge (SWIR; Legs 118 and 176), represent the longest continuous section of oceanic lower crust ever drilled by ODP (Ocean Drilling Program). About 25% of the core is strongly influenced by late-stage magmatic processes leading to Fe-rich (ferrogabbros) and Si-rich (plagiogranites) compositions as end-members. For a comprehensive understanding of the late magmatic processes occurring in the deep oceanic crust, we present here a new approach, by combining experimental and analytical investigations of natural gabbros from the ~ 1500 m long section drilled at SWIR. In three experimental subprojects we attempt to clarify (1) the phase relations and phase compositions in a typical late-stage magmatic system. Due to the lack of relevant experimental data, it is at present not possible to understand the late magmatic crystallization processes proceeding in the deep crust of SWIR or of other slow-spreading ridge systems. Thus, we perform a phase equilibria study in a typical late-stage system at 200 MPa with special focus on the role of water, oxygen fugacity, and sulphur. The comparison of the experimental phases with those of the natural gabbros from Hole 735B will help to constrain the extensive parameters of the conditions at the end of MORB differentiation in the deep oceanic crust. (2) whether liquid immiscibility is an important late-stage magmatic process. This subproject addresses the important question, whether liquid immiscibility does occur in natural hydrous tholeiitic systems under crustal pressure or not, and if yes, under what physical and compositional conditions. In the case of an experimental verification of liquid immiscibility, we attempt to investigate the distribution of selected element between the two liquids, in order to obtain partitioning data which are well-suited for an application to the natural rocks of the SWIR core. (3) how percolating late-stage melts influence the just solidified normal gabbro. A considerable part of the deep oceanic crust at SWIR was modified by a permeable flow of late Fe-rich melts through the just solidified gabbro pile, causing both reactions with the primocrysts by dissolution-precipitation and changes of the primocryst composition by diffusion. Our goal is an experimental simulation of these processes, by performing percolation experiments using a synthetic late-stage melt and a natural "pure" cumulate gabbro from Hole 735B under physical conditions prevailing in the deep oceanic crust. The experimental results will show which magmatic processes proceeded as a consequence of late-stage melt percolation at the end of differentiation (e.g., the precipitation of interstitial amphibole). Moreover, the evaluation of the experimental data will lead to the determination of realistic rates of reaction and/or diffusion enabling the quantification of the time scales on late-stage melt percolation ongoing in the deep oceanic crust.

Since it has been recently discussed whether late-stage magmatic processes can also be the result of hydrothermal circulation in the deep oceanic crust at very high (magmatic) temperatures, we use in-situ Sr isotope analyses of selected late-stage phases in the 735B gabbros in order to clarify the nature of these fluids, i.e., whether they are pure magmatic or seawater-influenced. Provided that the fluids show a general imprint of seawater, these results may help to establish new cooling models of the deep oceanic crust considering the additional cooling effect of hydrothermal circulation at very high temperatures.

IODP

Organic petrography on Cenozoic sediments from Hole 302 (Lomonosov Ridge): a classical approach for estimations of organic carbon fluxes

B. Boucsein, Alfred-Wegener-Institut für Polar- und Meeresforschung, Forschungsstelle Potsdam, Ruediger Stein, AWI Bremerhaven

The organic matter (OM) content in marine sediments depends on several environmental factors such as terrigenous supply of OM (fluviatil and wind driven) and, therefore, geology, vegetation and proximity of the source area (hinterland) and, primary productivity of marine and aquatic phytoplankton in the surface water layers and its preservation. Additionally, sediment transport by ocean bottom currents, turbidities or sea-ice affects the OM accumulation. Studies of the sedimentary OM facilitate reconstructions of the depositional settings and factors controlling the accumulation and preservation of the OM.

Organic petrographical analysis (maceral analysis, vitrinite reflectance) reveals quantitative data about the terrigenous and

marine (aquatic) organic matter contents in marine sediments. Additionally, helpful information about the biological sources of the OM can be obtained. Although petrological studies were performed successfully in different climatically regions of the Earth for paleoenvironmental reconstructions (e.g., Stein 1991; Littke and Sachsenhofer 1994; Littke et al. 1998; Wagner 1999) until now, for the Arctic Ocean only little information about the petrographical inventory of the sedimentary OM exists.

In this study, new organic petrological results will be presented for sediments from different time slices in the central part of the Arctic Ocean (Hole 302, Lomonosov Ridge) for a reconstruction of the depositional settings. Samples were chosen from: a) surface sediment samples from the vicinity of the ACEX cores, b) Quaternary sediments, c) the Azolla event (Middle Eocene), d) the Palaeocene/Eocene Thermal Maximum (PETM) and d) the Campanian.

By using the petrographical characteristics obtained by maceral analysis and vitrinite reflectance measurements different marine deposits can be recognized: For example, the particulate OM in the recent surface sediments and Quaternary sediments (core 302-4C) is dominated by terrigenous macerals (>90%) including huminite/vitrinite, inertinite and generally detritus of this macerals. Marine OM (lamalginite, dinoflagellate cysts) is absent in these sediments or occurs only in small amounts (<1%). The TOC content (<1%) and HI values (<90) are quite low. The dominance of allochthonous terrigenous macerals, the absence of significant amounts of marine OM and, rounded and weathered vitrinite particles indicate OM sedimentation in an open marine environment. The small amounts of marine OM can be explained by the more or less permanent ice cover of the Central Arctic Ocean which impede primary production. Additionally, most of the labile organic compounds are remineralised in the oxic water column, resulting in a poor preservation in the sediments.

In contrast, in the sediments from the PETM we found the highest amounts of marine/aquatic OM (lamalginite, dinoflagellate cysts) and bituminite (60-80%), correlating with an increase in the HI values. An input of recycled (geological older) vitrinite is documented in the vitrinite reflectance histograms (polymodale distribution), while inertinite is absent. High amounts of small pyrite framboids (Ø: 5µm) and well preserved marine/aquatic algae material indicate anoxic conditions. The organic petrographical characteristics of these sediments may be interpreted as an aquatic/marine depositional setting with enhanced primary productivity of phytoplankton (and good preservation) probably in a shallow (neritic) anoxic environment.

Based on these first preliminary results we will now focusing on more detailed analyses of the time slices listed above.

Literature:

Stein, R. (1991): Accumulation of organic carbon in marine sediments. Lecture Notes in Earth Sciences. Heidelberg (Springer), 34, 217 p.

Littke, R. & Sachsenhofer, R.F. (1994): Organic petrology of deep sea sediments: a compilation of results from the Ocean Drilling Program and the Deep Sea Drilling Project. Energy and Fuels, 8, 1498-1512.

Littke, R., Lückge, A. & Wilkes, H. (1998): Organic matter in neogene sediments of the southern canary channel, canary islands (sites 955 and 956). In: Weaver, P.P.E., Schmincke, H.-U., Firth, J.V. & Duffield, W. (Eds.) Proceedings of the Ocean Drilling Program, Scientific Results, Vol. 157, 361-372.

Wagner, T. (1999): Petrology of organic matter in modern and Late Quaternary deposits of the Equatorial Atlantic. Climatic and oceanographic links. Int. J. Coal Geol., 39 (1), 155-184.

ICDP

Indications of progressive magmatic activity beneath the Cheb Basin (central Europe)

Karin Bräuer[1], Horst Kämpf[2], Gerhard Strauch[1]

1UFZ Centre for Environmental Research Leipzig-Halle, Department of Hydrogeology, Theodor-Lieser-Str. 4, D-06120 Halle, Germany; 2GFZ GeoForschungsZentrum Potsdam, Section Organic Geochemistry, Telegrafenberg, D-14473 Potsdam, Germany

In 2005 we started a pre-ICDP research project in NW Bohemia (Czech Republic). The region is part of the European Cenozoic rift system and is characterised by Quaternary volcanism, CO_2-rich mineral springs and mofettes that are supplied by fluids (CO_2, He) derived from the earth's mantle, and the occurrence of swarm earthquakes. For studying driving forces of the geodynamic of the Eger Rift including magmatic/fluid and earthquake activities an optimal location for a deep drilling site must be found. Based on our experience in investigations of the gas and isotope composition of free gas from numerous CO_2-rich mineral spring and mofettes in the Vogtland and NW Bohemia we are convinced of supporting this goal.

From north to south along the Mariánské Lázně fault two degassing centres may be distinguished: the Cheb Basin and the surroundings of Mariánské Lázně. Both degassing centres are characterised by high gas fluxes, $\delta^{13}C\text{-}CO_2$ between -2 and -4‰ and high upper mantle derived helium portions. Our investigations have shown a marked increase of the $^3He/^4He$ ratios in CO2-rich fluids from the degassing centre Cheb Basin between 1992 and 2003, resulting in values which are among the highest ones measured in continental Europe (up to 6.2). In contrast to that the 3He/4He ratios of the degassing locations of the Mariánské Lázně degassing centre showed little variation in the same time span (Bräuer et al., 2005). Known from xenolithe studies worldwide, the He isotope signature of the continental lithospheric mantle is marked by a lower $^3He/^4He$ ratio ($\approx 6.3 \pm 0.4$ Ra) than MORB ($\approx$ 8 Ra) due to higher U and Th concentrations in the sub-continental mantle. Consequently, at the free gas of degassing locations of the Cheb basin 3He/4He ratios were found that cover the range of the sub-continental mantle. Such high helium isotope ratios have been found at the free gas of mineral springs or mofettes neither of the Eifel area nor of French Massif Central, two areas in the European Cenozoic rift system with a comparable geodynamic situation.

We repeated the sampling of several locations of the Cheb Basin and from the degassing centre Mariánské Lázně in 2005. The results demonstrate that the $^3He/^4He$ ratios in the Cheb Basin are still higher than ten years ago. A further clear increase of $^3He/^4He$ ratios were found at Hartoušov and Dolni Častkov, two mofettes near the Bublák mofette where the highest values were measured up to now.

The different behaviour of the $^3He/^4He$ characteristic of the degassing centre Cheb Basin and that of Mariánské Lázně seems to be connected with different strong periods of seismicity by which both areas can be distinguished. The Cheb Basin is closed to the epicentral area of Nový Kostel that is known for the occurrence of swarm earthquakes with magnitudes up to ML = 4.6, whereas the seismicity in the surrounding of Mariánské Lázn? is weak. The up-to-date $^3He/^4He$ data of Bublák and other locations of the Cheb Basin indicate that the presently active magmatic process beneath the Cheb Basin is not finished up to now. The observed phenomenon as a whole (increasing $^3He/^4He$ ratios connected with swarm earthquake seismicity) may be an indication of future unrest in a presently inactive volcanic region.

The results of our investigations should contribute to find an optimal ICDP location.

Bräuer, K., H. Kämpf, S. Niedermann, and G. Strauch (2005), Evidence for ascending upper mantle-derived melt beneath the Cheb basin, central Europe, Geophysical Research Letters 32, L08303, doi:10.1029/2004GL022205.

ICDP

Active and passive seismic imaging of the San-Andreas-Fault-System

Buske, S. and Shapiro, S.A.

Department of Geophysics, Institute for Geological Sciences, Free University Berlin, Malteserstr. 74-100, 12249 Berlin, Germany, buske@geophysik.fu-berlin.de

The San-Andreas-Fault Observatory at Depth (SAFOD) is part of the EarthScope project and provides unique active and passive seismic data measured downhole directly at the San-Andreas-Fault zone. A combined investigation using these active and passive seismic data is the topic of this proposal. It aims at answering basic questions about the physical and chemical

processes that control deformation and seismic emissions at an active plate-boundary related fault system. We propose the processing and interpretation of different data sets using recently developed techniques.

First, we want to apply 3D Fresnel-Volume-Migration (FVM) to the SAFOD2003 data set as well as to two 3D-VSP data sets (one VSP data set has been already acquired in 2002, the second is planned for 2006). The basic idea of FVM is to restrict the imaging procedure to the physical relevant part of the subsurface within the final step of transforming the seismic data from time to depth. This technique is an extension of the widely used method of Kirchhoff prestack depth migration. Compared with the latter it increases image quality significantly. FVM has been developed and successfully applied to multi-component seismic data within the framework of engineering seismology. We have further developed and already applied it to a small part of the SAFOD2003 data set. The results are encouraging and we propose to apply it to the complete data set as well as to the mentioned two VSP data sets.

Second, we want to apply a new location algorithm (which is based on a migration technique similar to FVM) to passive seismic data recorded at the San-Andreas-Fault system. Recently, a recording network was deployed in the SAFOD main hole. This network consists of 80 three-component receivers and recorded about 80 seismic events from the 28th April 2005 till 11th May 2005. The advantage of a migration technique to locate seismic events is that time consuming manual picking of arrival times is not required. We want to locate these and also further detected events using our new location algorithm. In addition we want to use the obtained hypocenters and treat them as pseudo-active single shot experiments. Possible reflections from the nearby fault system will then be imaged using the FVM technique mentioned above.

The FVM and the location technique use the same velocity model. This enables a direct comparison of the obtained seismic images of the San-Andreas-Fault zone. A combination and interpretation of these images can provide new important information on the structure of the fault, both on a large scale as well as the small scale. Such an improved structural image provides a better basis for the joint interpretation with other geophysical signatures (seismic velocity, electrical resistivity, etc.) and a more profound characterization of the subsurface in the vicinity of the San-Andreas-Fault system.

IODP

Water mass properties and circulation in the Cape Basin (ODP Site 1089) on Glacial/Interglacial timescale - a multiproxy approach

Christl, M. [1,2], Lippold, J.[1], Bernsdorff, F.[1], and Mangini, A.[1]
[1]Heidelberger Akademie der Wissenschaften, Im Neuenheimer Feld 229, 69120 Heidelberg, Germany; [2]Institute of Particle Physics, ETH Hoenggerberg, CH-8093 Zurich, Switzerland
Email: mchristl@phys.ethz.ch

In this study highly resolved profiles of Th/U-isotopes and major element concentrations from ODP Leg 177, Site 1089 are presented covering the past 310 kyr. The ^{230}Th-profiling technique is applied to calculate vertical mass accumulation rates and rain rates of calcium carbonate that reflects variable carbonate dissolution at ODP Site 1089. The deposition of authigenic uranium and the Mn/Fe-ratio are used to reconstruct redox conditions over the past 310 kyr. A combination of these tracers allows the reconstruction of bottom water properties in the abyssal Cape Basin on glacial/interglacial timescale. Our results suggest that glacial carbonate preservation in the abyssal Cape Basin was caused by well-ventilated water masses probably stemming from the Antarctic region. The combination of our data with mineralogical proxies from Site 1089 [1] reveals a "see-saw" effect between surface/deep and bottom water circulation in the Cape Basin during interglacials, while no close relation is observed during glacial times. This suggests that the observed link between surface/deep and bottom water circulation in the Cape Basin was provided by a variable stability of Thermohaline Circulation (THC) on glacial/interglacial timescale. Furthermore, our results suggest that during glacial times deep and bottom water formation in the Southern Ocean was independent from THC-strength producing most dense and non-corrosive bottom waters filling the abyssal Cape Basin.

[1] Kuhn G. and Diekmann B. (2002) Late Quaternary variability of ocean circulation in the southeastern South Atlantic inferred from the terrigenous sediment record of a drift deposit in the southern Cape Basin (ODP Site 1089). Palaeogeography Palaeoclimatology Palaeoecology 182, 287-33.

ICDP

Viscous flow of magmas from Unzen volcano, Japan - Preliminary results

Cordonnier B., Hess, K.-U., Lavallee, Y., Dingwell, D.B.
All at: Ludwig-Maximilians-Universität, Earth and Environmental Science, 80333 Munich, Germany

The lack in understanding the flow behaviour of ascending highly viscous conduit magmas is a major drawback in forecasting explosive volcanic eruptions. Thanks to the very recent development of a unique high-load, high-temperature deformation apparatus it is now, for the first time, possible to determine the effective non-Newtonian viscosity of rhyolitic multi-phase magmas at strain rates actually occurring prior to and during volcanic eruptions.

This device is ideal for volcanological studies, experimental conditions corresponding closely to the volcanic processes: temperature (25-1300˚C), stress (0 up to 500 MPa), strain rates (10-6-10-2 s), and total strain (0- 100%). Even if the apparatus still has to be optimised, we can already present some preliminary results.

This opportunity comes at a time where, for the first time, core from conduit sections from Unzen are available. Taken together, the new technique and the new sample availability provide a unique opportunity to advance the rheological understanding of Unzen.

These new data will offer a new opportunity in modelling of biphasic fluid silicate melt. Moreover, this model provides an essential tool for the construction of ascent and emplacement models for erupting conduit magmas at Unzen. Such models have important implications for the interpretation of (a) shallow volcanic earthquakes (e.g. low frequency events) and their potential use as indicators for near-future volcanic eruptions, (b) self-sealing mechanisms of the Unzen conduit.

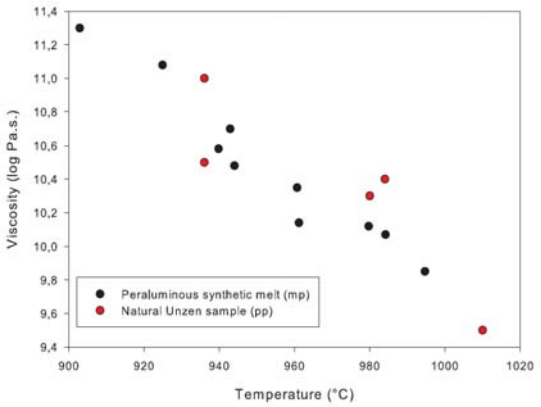

Fig.1 : Comparaison between one phase peraluminous melt vs. Unzen multiphase sample below 20 MPa

ICDP

Seismische STRATIGRAPHIE im nördlichen Bereich des Tatvan Beckens Zur Bestimmung potentieller ICDP-Lokationen Am Van See, Türkei

F. Demirel-Schlüter[1], S. Krastel[1], E. Demirbag[2], C. Imren[2], M. Toker[2,3], F. Niessen[4]
[1]Fachbereich Geowissenschaften, Universität Bremen; [2]Abteilung für Geophysik, ITÜ, Istanbul, Türkei; [3]Institut für Geologie, YYÜ, Van, Türkei; [4]Alfred-Wegener-Institut, Bremerhaven, (fdemirel@uni-bremen.de; skrastel@uni-bremen.de)

In den ersten zwei Juni Wochen im Jahr 2004 wurden auf dem Van See, Türkei (der viertgrößte Endsee der Welt) reflexionsseismische Messungen durchgeführt. Hauptziel der Messungen war die Bestimmung potentieller ICDP-Lokationen und die Untersuchung der Entstehung des Sees. Insgesamt wurden 50 Profile mit einer Gesamtlänge von ca. 850km mit einem hochauflösenden seismischen Mehrkanal-System und einem GeoChirp-System aufgezeichnet. Die seismischen Profildaten bilden eine wichtige Basis für den ICDP Workshop-Antrag 'Lake Van Drilling - PALEOVAN'. Der Workshop findet im Juni 2006 in Van statt. Aufgrund seiner Lage in der Ost-Türkei und des Vorkommens jährlich geschichteter Seesedimente stellt der Van See einen besonders geeigneten Ort für die Rekonstruktion der quartären Klimaentwicklung im Nahen Osten dar. Ein weiteres Ziel der Untersuchungen ist die Analyse der Paläo-Seismizität in dieser tektonisch aktiven Region.

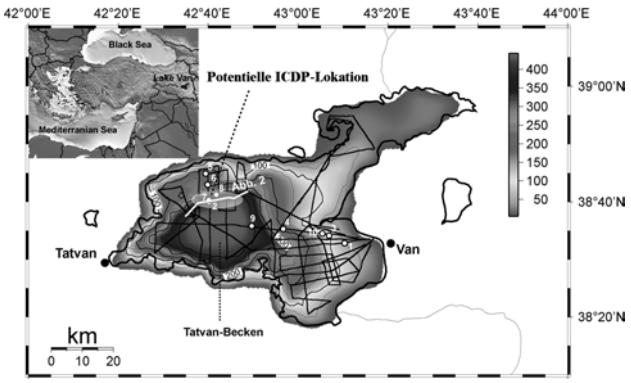

Abb. 1: Übersichtsplan der Messprofile am Van See. Die schwarzen Linien zeigen die Lage der seismischen Profile. Die weißen Punkte kennzeichnen die Lokationen der Sedimentkerne (siehe Abstract von LITT et. al). Die transparente Ellipse zeigt das Gebiet potentieller ICDP-Lokationen.

Während der seismischen Messungen konnte im nördlichen Teil des Tatvan Beckens ein Sedimentrücken und ein Nebenbecken identifiziert werden. Aufgrund ihrer besonderen Charakteristik (Lage, Sedimentation, usw.) stellte dieser Bereich eine potentielle ICDP-Lokation dar; daher wurde in diesem Gebiet ein dichtes Profilnetz aufgezeichnet (Abb.1). Das Nebenbecken wird von dem Tatvan Becken durch einen Sedimentrücken abgegrenzt. Das Nebenbecken weist im Gegensatz zum Tatvan Becken ungestörte Sedimente auf und stellt damit eine viel versprechende Lokation für einen ICDP-Vorschlag dar. Als eine weitere wichtige ICDP-Lokation wird aufgrund kondensierter Sedimentlagen der Sedimentrücken betrachtet, der im Holozän um ca. 30% reduzierte Sedimentationsraten im Vergleich zum Tatvan Becken aufweist. Das Profil GeoB 04-023 (Abb. 2) läuft entlang des Sedimentrückens in O-W Richtung. Dort wurde im Sommer 2004 der 942cm lange Sedimentkern VAN04-2 entnommen. Aufgrund der Erhebung des Rückens im Vergleich zum umliegenden Seeboden wurden im Kern keine Turbidite und Schüttungs-Sedimente gefunden.

Die seismischen Daten auf dem Profil GeoB 04-023 (Abb. 2a) zeigen, dass unter den ungestörten Sedimentlagen eine progradierende Sequenz liegt. Wir vermuten, dass diese Sequenz unmittelbar nach Aufbau des Lava-Damms abgelagert worden ist, der den Wasserabfluss aus dem See bis heute blockiert und somit die initiale Phase des Van-Sees als Terminalsee repräsentiert. Oberhalb dieser Sequenz finden wir keine seismischen Hinweise auf ein Trockenfallen des Sees. Die gut geschichteten Sedimentlagen oberhalb der progradierenden Sequenz interpretieren wir daher als kontinuierliche lakustrine Ablagerungen. Die Mächtigkeit der lakustrinen Ablagerungen von 120m bei durchschnittlichen Sedimentationsraten von <75cm/1000J. (siehe unten) weist darauf hin, dass der See deutlich älter als die bisher postulierten 100.000 Jahre ist.

In den GeoChirp-Daten des Profils GeoB 04-023 (Abb. 2b) können zwei Reflektoren in einer Tiefe von ca. 1.5m und ca. 6m deutlich identifiziert werden. Sie lassen sich mit den magnetischen Suszeptibilitätswerten des Sedimentkerns VAN04-2 sehr gut korrelieren (Abb.2c). Die datierten Aschenlagen (Litt, persönliche Mitteilung) können im ganzen Tatvan Becken verfolgt und damit als Markerhorizonte benutzt werden. Die zwei Reflektoren befinden sich im Tatvan Becken in einer Tiefe von ca. 2.5m und ca. 9m. Aus dem Alter der Aschenlagen ergibt sich für das Holozän eine durchschnittliche Sedimentationsrate von 75cm /1000J. im Tatvan Becken. Die Markerhorizonte können ohne Problem zwischen den verschiedenen Stationen verfolgt werden.

Charakteristische Strukturen der Hänge und des Schelfs sind Delta-Vorschüttungen, große Gebiete, die durch eine Abfolge U- und V-förmigen Depressionen charakterisiert sind, sowie eine große Anzahl von Ablagerungs- und Erosions-Diskordanzen, welche die abwechslungsreiche Entwicklungs-Geschichte des Van Sees widerspiegeln. Im Ostteil des Sees liegen drei übereinander abgelagerte Deltaformationen, die vor den Mündungsgebieten der Flüsse erosiv zerschnitten sind und somit niedrigere Seestände anzeigen.

→ [Abb. 2 nächste Seite]

ICDP

Lake Bosumtwi impact crater drilling project Assessment of shock metamorphism in core LB-8A (nature vs. experiments)

Alex Deutsch[1] and Falko Langenhorst[2]
[1]Inst. f. Planetologie, WWU Münster; D-48149 Münster, Germany. deutsca@uni-muenster.de; [2]Inst. f. Geowissenschaften, FSU Jena, D-07749 Jena, Germany

Petrographic shock barometry is an indispensable tool to constrain cratering mechanics. Decay of shock pressure in the crater center is of specific interest as rapid uplift, followed by collapse in the late stage of cratering cause large-scale mass movements. Impact lithologies in the central uplift include breccias (with/without melt) and shocked/unshocked target materials. In the 5 km-long Vorotilovo core, cental uplift of the Puchezh-Katunki structure [1], rocks are shocked at P in excess to 45 GPa. Shock levels of 35-40 GPa have been reported from the uplift of other structures; commonly shock attenuation is rather regular both downwards and in radial directions. At ambient °T, quartz is totally converted to diaplectic glass in crystalline rocks at shock pressures above ~35 GPa [2].

Core BCDP-8A in the central uplift of the L. Bosumtwi crater - shock metamorphism: The carbonaceous meta-greywackes, and shales to slates display a wide variety of shock features in carbonate minerals and tecto-silikates, yet a systematic pressure decrease is lacking as well as melt lithologies. Just very few clasts of diaplectic qtz have been found so far, yet in general, the material is shocked at only 26 GPa [3].

Numerical modeling (Fig. 1, [4]) predicts (i) presence of up to 200 m melt lithologies topping the uplift, and (ii) shock pressures in excess of 40 GPa in the highest levels of the central uplift. (i) Melt lithologies seem to be nearly absent in the breccias occurring in the uppermost 20 to 30 m of core BCDP-8A, and, (ii) shock levels of 26 GPa are surprisingly low, much less than expected. These strange features can be interpreted either, by a specific

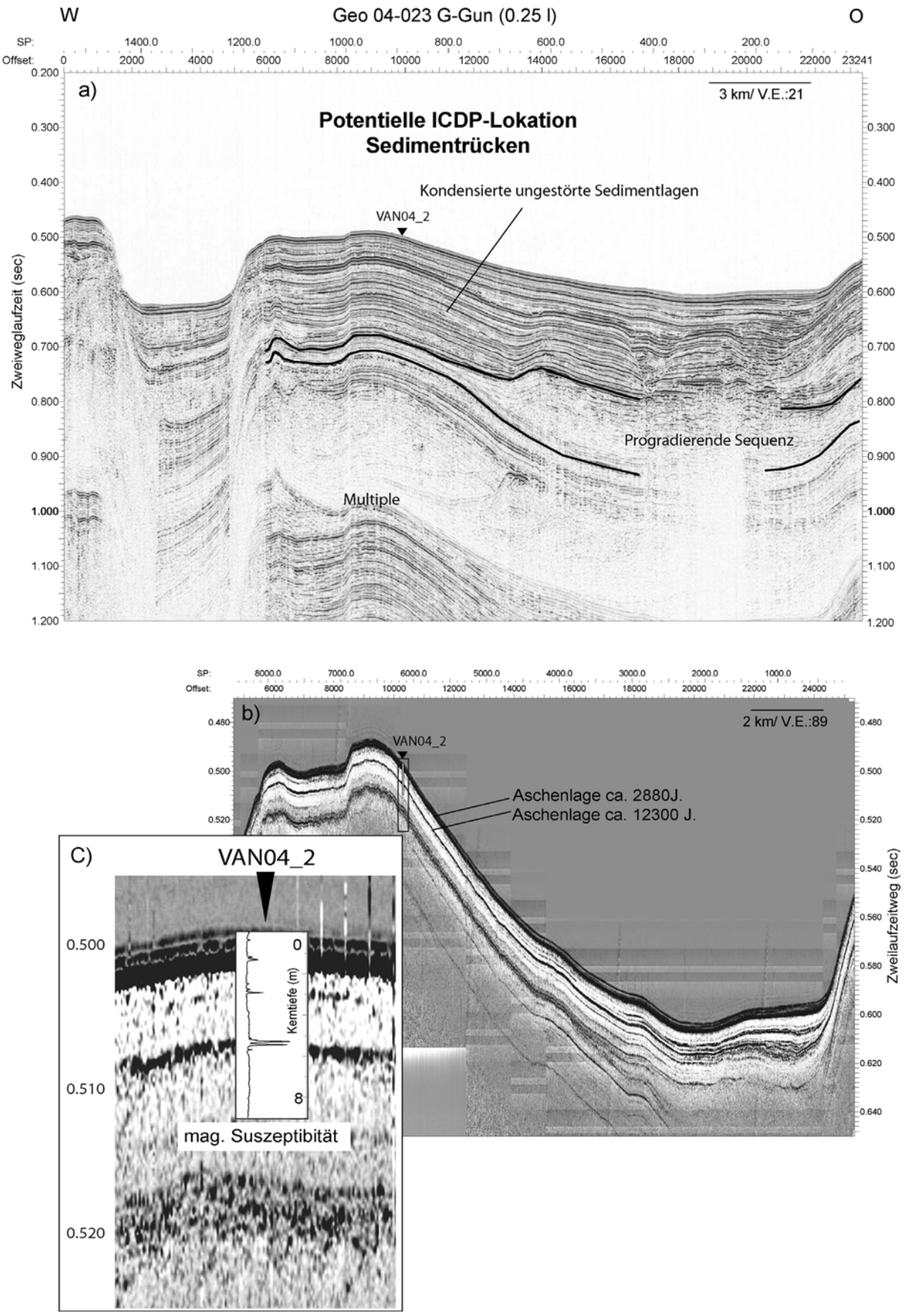

Abb. 2: CMP-Stapelung (a) und ein Teil des GeoChirp (b) Profils GeoB 04-023 sowie deren Korrelation mit den magnetischen Suszeptibilitätswerten des Sedimentkerns VAN04-2 (c). Das Alter für die Aschenlagen und die Suszeptibilitätswerte stammen von Litt (persönliche Mitteilung).
(zu Abtract Demirel-Schlüter et al.)

shock behavior of the soft, porous and fluid-rich meta-sediments or, by specific parameters of the cratering event (e.g., obliquity of the impact).

Shock experiments were carried out with a conventional setup [2] at 34 and 39.5 GPa, using sample disks of carbonaceous greywackes similar in composition to the Bosumtwi rocks. At both shock pressures, most of the qtz is transformed to diaplectic crystals. The overall picture compares well with the generally accepted shock barometry [2]. It is evident that the shock behavior of carbonaceous greywackes is not completely different to that one of experimentally shocked singly crystal quartz or quartz-rich meta-sandstones [2].

Outlook: Suevites collected outside the rim of Bosumtwi crater contain diaplectic crystals, coesite, as well as true melt glasses., whereas, lithologies in core BCDP-8A seem to lack highly shocked material. A specific shock behavior of the soft target material is rather unlikely the reason for the surprisingly low shock levels recorded in the uplift. This unexpected feature may be caused by a rather oblique impact (and calls for re-fined numerical modeling!).

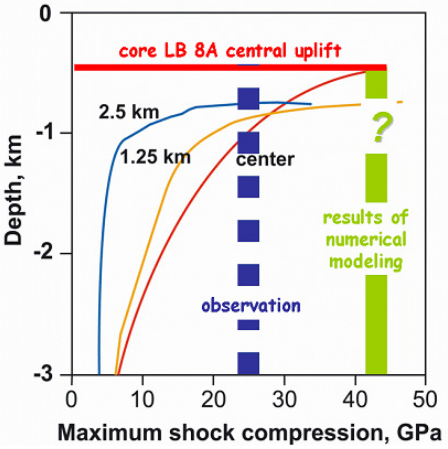

Figure 1. Depth vs. shock pressure graph for three modeled locations [4] at Bosumtwi: crater center (red), 1.25 (yellow), and 2.5 km (blue) off the center. The green line corresponds to the modeled shock pressure for BCDP-8A, the blue one to the pressure actually recorded in the rocks; from [5].

References
[1] Masaitis V.L. & Pevzner L.A. (eds.) Deep Drilling in the Puchezh-Katunki Impact Structure. VSEGEI Press, 1999, 392 pp.
[2] Langenhorst F. & Deutsch A. (1998) Mineralogy of Astroblemes - Terrestrial Impact Craters. In A.S. Marfunin (ed.), pp 95-119, Springer.
[3] Deutsch A. et al. (2006) Lunar Planet. Sci. Conf. XXXVII, Abstr. #1292.
[4] Artemieva N. et al. (2004) Geochem. Geophys. Geosyst. 5.
[5] Deutsch A. (2006) Lunar Planet. Sci. Conf. XXXVII, Abstr. #1327.
We acknowledge support by DFG grants De 401/19 and LA 830/7

IODP
Middle and late Miocene global carbon isotopes shifts and marine biological productivity

Liselotte Diester-Haass, l.haass@mx.uni-saarland.de
Katharina Billups, kbillups@udel.edu

The Miocene contains two major global carbon isotope shifts: a negative shift during the late Miocene (~8-6 Ma) and a positive shift during the mid-Miocene (16-14 Ma). We aim at deciphering possible changes in marine biological export productivity during these shifts by calculating paleoproductivity in gC/cm²*ky from benthic foraminiferal numbers and accumulation rates at a number of sites spanning the world ocean. Our previous work has illustrated that the onset of the late Miocene negative ? 13C shift, which has been attributed to enhanced erosion of terrestrial biomass and expansion of C4 plants, is also accompanied by an increase in marine export productivity from lower than present day values up to 2-3 times modern values at six sites (982, 1088, 721, 846, 1146, 1172; Diester-Haass et al, 2005; Diester-Haass et al., submitted). The Mid-Miocene "Monterey Event", on the other hand, has been attributed to sequestration of organic material in circum-Pacific basins (Vincent and Berger, 1985) or wide spread deposition of brown coal and drowning of carbonate platforms (Föllmi et al., 2005). For this particular time interval, our initial results from Site 608 (Atlantic Ocean) reveal relatively constant paleoproductivity values similar to modern ones (about 10 gC/cm²*ky) until 16.5 Ma, after which time paleoproductivity begins to increase until the end of our record at 11 Ma. Superimposed on the trend of generally increasing productivity, there are a number of productivity minima spaced roughly 0.5 million years apart. The long term trend in the paleoproductivity finds some similarities in the global composite benthic foraminiferal $\delta^{13}C$ record as both proxies show an overall increase until ~14 Ma. Thereafter, however, paleoproductivity continues to increase while $\delta^{13}C$ values decrease marking the end of the Monterey excursion. Stable isotope analyses from these same intervals will show to what extend the smaller scale fluctuations in paleoproductivity can be related to changes in the $\delta^{13}C$ of the oceanic reservoir or regional water masses.

Diester-Haass, L., Billups, K., Emeis, K-C., 2005, Paleoceanography, vol.20,PA4001, doi:10.1029/2005PA001139
Diester-Haass, L., Billups, K., Emeis, K-C., 2005 submitted. Paleoceanography.
Vincent, E. and Berger, W., 1985, In: The carbon cycle and atmospheric CO2: Natural variations Archaen to present, edited by Sunquist, E.T. and Broecker, W.S., Am.Geophys. Union Monogr.
Föllmi, K.B. et al., 2005, Geol.Soc.Am.Bull., 117/5, 589-619.

IODP
Late Miocene carbon isotope records and marine biological productivity: was there a (dusty) link?

Liselotte Diester-Haass, l.haass@mx.-uni-saarland.de
Katharina Billups, kbillups@udel.edu
Kay C. Emeis, emeis@geowiss.uni-hamburg.de

We examine the temporal relationship between the late Miocene carbon isotope shift (~7.6-6.6 Ma) and marine productivity at four sites from the Indian and Pacific Oceans (Ocean Drilling Program Sites 721, 1146, 1172, and 846). We use a multi-proxy approach based on benthic foraminiferal accumulation rates, elemental ratios, and dissolution indices, and compare them to benthic foraminiferal $\delta^{13}C$ values measured on the same samples. Although some of these sites have been targeted previously in studies of either the late Miocene/early Pliocene 'biogenic bloom' (Sites 721 and 846), or the late Miocene carbon isotope shift (Site 1172), our records are the first to establish paired proxy records of both parameters allowing a direct assessment of a potential link. Our results indicate that at all sites, productivity increased during the $\delta^{13}C$ shift; at three sites (721, 1146 and 846) productivity increased at the beginning of the shift. Productivity maxima, however, did not occur at the same time and are not related to $\delta^{13}C$ values. The Site 846 paleoproductivity record is similar to temporal patterns in the Site 848 eolian flux reconstructions of Hovan [1995]. Both records display, for example, maxima at ~ 7.4 Ma, 6.4 Ma, 5.6 Ma, and 4.8 Ma. These observations lead us to consider that there might be a link between late Miocene continental aridity, marine productivity, and the foraminiferal $\delta^{13}C$ shift.

ICDP
Deformation of the central Sudbury Impact Structure, Canada: Evidence for meteorite impact into an active orogen and implications for deep drilling

Daniel Doman[1], Ulrich Riller[1] and Kai Hofmann[2]
[1]Humboldt-Universität zu Berlin, Museum für Naturkunde, Institut für Mineralogie, Invalidenstrasse 43, D-10115 Berlin; daniel.doman@museum.hu-berlin.de; [2]Freie Universität Berlin, Institut für Geologische Wissenschaften, Malteserstrasse 74-100, D-12249 Berlin

The 1.85 Ga Sudbury Igneous Complex (SIC) in central Ontario is now widely considered to be the erosional remnant of a deformed paleo-horizontal impact melt sheet, about 2.5 km in thickness. Deformed impact melt breccias of the Onaping Formation and post-impact metasedimentary rocks overlie the layered SIC, which in turn rests on shocked Archean basement and Paleoproterozoic metasedimentary cover rocks. The main mass of

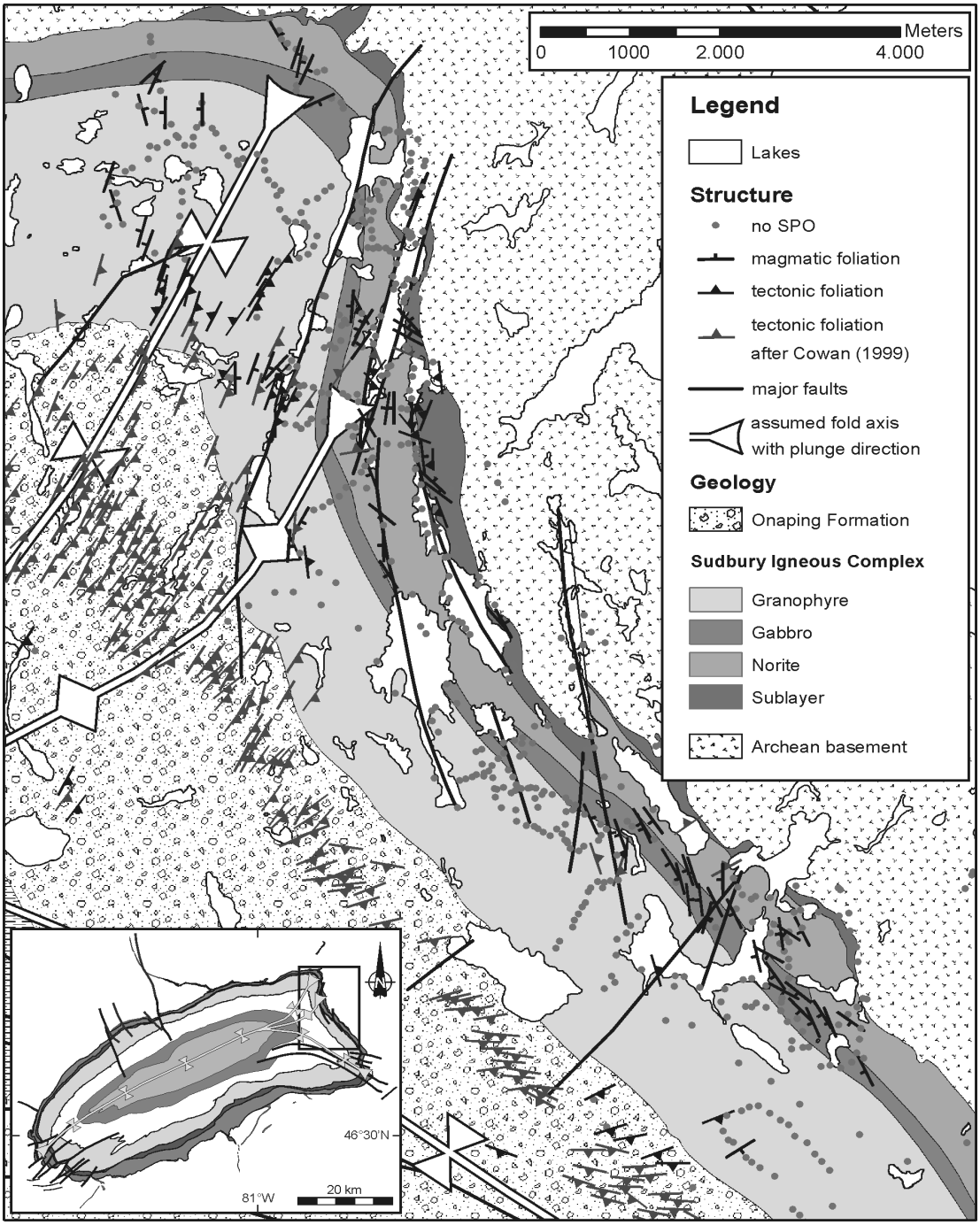

Figure 1. Structural map of the East Range SIC and the overlying Onaping Formation showing the orientations of magmatic and metamorphic mineral foliations and large-scale structures. Dots delineate stations devoid of any shape-preferred orientation (SPO) of minerals in the SIC.

the SIC consists from top to bottom of the granophyre, quartz-gabbro and norite layers. Previous workers considered non-cylindrical folding and NW-directed reverse faulting as the main structural processes that formed the asymmetric, syn-formal geometry of the SIC, well apparent in map view and seismic section. Structural studies support this model in the southern part of the impact structure where greenschist-facies metamorphic tectonites of the South Range Shear Zone (SRSZ) accomplished structural uplift of the southern SIC by NW-directed reverse shearing. However, little evidence for pervasive, mesoscopic ductile strain has been reported from the weakly metamorphosed eastern part of the SIC, the East Range (Fig. 1), which is characterised by steep basal dips and maximal curvature in plan view. The objective of this study, conducted in the framework of ICDP, is to assess the structural inventory of the East Range in terms of post-emplacement deformation mechanisms, specifically the relationships between magmatic, metamorphic and brittle structures. Conclusions are based on published and newly acquired structural data and are discussed in the context of the regional structural setting.

The intermediate quartz-gabbro and lower norite layers of the southern East Range SIC (Fig. 1) are dominated by planar mineral shape fabrics made up of euhedral plagioclase and pyroxene (Fig. 1a). Collectively, these mineral phases form cumulates (Fig. 2b), whereby interstitial quartz is largely devoid of intracrystalline deformation. Magmatic foliation of the cumulates is concordant to SIC contacts and large-scale discontinuities in this area but are rarely observed in the northern portion of the East Range (Fig. 1).

Here, metamorphic foliations and S-C fabrics are developed sporadically at, and concordant to, N-S striking brittle discontinuities. A weak metamorphic foliation defined by chlorite, which replaces magmatic minerals, is developed toward the top of the granophyre layer of the NE-lobe that connects the SIC's North and East Ranges via a 105˚ arc. This metamorphic foliation grades into a shape-preferred orientation of primary, i.e., magmatic mafic minerals, observed in the lower granophyre and its underlying layers of the SIC. Moreover, mineral fabrics observed in the NE-lobe SIC are concordant to metamorphic foliations developed in the overlying Onaping Formation (Fig. 1). Both foliation types strike parallel to the NE-lobe's acute bisectrix and, thus, display an axial-planar geometry typical for fabrics formed in the core of buckle folds.

Brittle discontinuities observed in the eastern SIC and its host rocks range from centimetre-scale shear fractures to kilometre-scale fault zones. Large-scale faults strike N-S and cut the NE-lobe's eastern limb causing variable magnitudes of strike separation of SIC contacts. Centimetre- to metre-scale, brittle faults (Fig. 2d) and chlorite-filled brittle-ductile shear zones cause distinct offsets of markers (Fig. 2c) and are pervasive in the eastern SIC. Microstructures from first-order fault-zones formed at, and below, greenschist-facies metamorphic conditions.

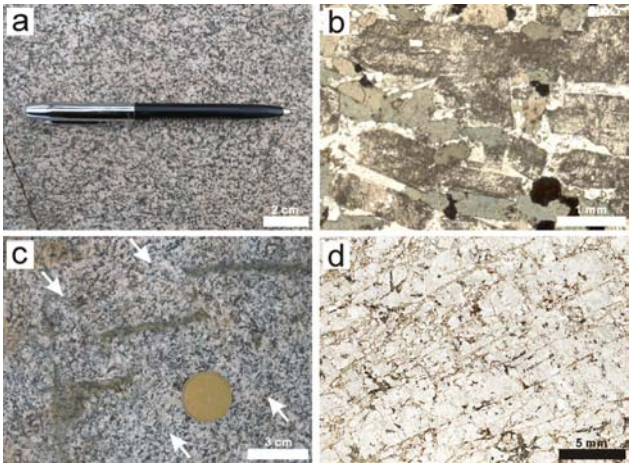

Figure 2. Mesoscopic and microscopic structures from the East Range SIC. (a) Magmatic foliation defined by cumulate plagioclase (white) and pyroxene (dark). (b) Euhedral plagioclase (grey) and pyroxene (green) in thin section (plain-polarised light). (c) Small-scale, brittle discontinuities (between arrows) displacing epidote- and chlorite-filled vein. (d) Pervasive brittle discontinuities in cataclastically deformed SIC as it is seen in thin section (un-polarised light).

The concordance of magmatic and metamorphic mineral shape fabrics in the NE-lobe indicates progressive deformation of the SIC during its cooling from the magmatic state to lower greenschist-facies metamorphic conditions. Interestingly, maximum principal paleo-stress directions inferred from the inversion of fault-slip data collected in the Onaping Formation are orthogonal to metamorphic foliation surfaces at the same localities. This points to a similar deformation regime in the Onaping Formation during ductile and brittle deformation. The observed concordance of magmatic, metamorphic and brittle fabrics is explained best by a single progressive deformation event that was active while the SIC cooled and solidified. The lack of pervasive ductile deformation fabrics in the East Range SIC can be explained by cooling of the impact melt sheet that was rapid (within 100-500 ka) with respect to natural tectonic strain rates. Collectively, the structural observations, in particular evidence for syn-magmatic deformation of the SIC, suggest that it was emplaced and subsequently deformed during ongoing orogenic deformation.
With respect to drilling into the central Sudbury Impact Structure, it is important to note that the geometry of mineral fabrics in the study area is compatible with large-scale, non-cylindrical folding, as has been suggested previously. However, the lack of mesoscopic ductile strain but pervasive presence of discontinuities on all scales in the eastern SIC indicates that shape change of the SIC in this area was accomplished mainly by discontinuous deformation. In the western part of the central impact structure discontinuous deformation may have accomplished bulk NW-SE shortening by reverse shearing within the SRSZ, leading to large strike separations of SIC contacts. By contrast, the eastern SIC may have accommodated such shortening by brittle-ductile, non-cylindrical folding at the eastern terminus of the SRSZ (Fig.1). Thus, one of the previous objectives of drilling, i.e., to test whether the SIC was affected either by folding or by thrusting, is no longer relevant; in fact, both deformation mechanisms contributed to shortening of the SIC, but at different portions of the central Sudbury Impact Structure.

IODP

Influence of fluids from the ocean crust on growth and activity of deep-biosphere populations (IODP Leg 301)

Bert Engelen, Katja Ziegelmüller, Falko Mathes, Lars Wolf and Heribert Cypionka
Institut für Chemie und Biologie des Meeres, Universität Oldenburg, Carl-von-Ossietzky-Str. 9-11, D-26111 Oldenburg, Germany. www.icbm.de/pmbio

The sampling site at the Juan de Fuca Ridge is characterized by a diffusive fluid flow from the underlying basalt to the sediment column, which results in an "upside down" electron acceptor series (Fisher et al. 2005). These electron acceptors were supposed to fuel the deep biosphere (De Long, 2004). The influx of oxidized compounds at Site 1301 is much higher than in other marine sediments. This offers the possibility to study highly active microbial communities within the deep biosphere. Interesting aspects also arise from the temperature gradient of 2 to 65˚C within the sediment column. There are layers with comparable geochemical characteristics, but different temperatures. This allows to study the specific influence of different temperature regimes on community composition and activities.

High quality samples from the entire sediment column of IODP Site 1301 were obtained during IODP Leg 301 by advanced piston coring (APC). The samples were almost free of contamination as indicated by contamination tests using a perfluorocarbon tracer (PFT). Subsamples were subjected to enrichments in dilution series, molecular biological investigations and microbial activity measurements.

Enrichments of indigenous microorganisms were obtained from all subsamples. Approximately 1% of the directly counted cells was cultivated from some sediment layers. The enrichments are currently beeing analyzed for their composition by molecular biological screening and will be used for the isolation of indigenous microorganisms. A strong increase of phosphatase activities towards the sediment-basement interphase indicates the presence of a highly active microbial community near the bedrock. Our preliminary results support the hypothesis that hydrothermal fluids serve as a driving force for the deep biosphere. Our work will mediate between the first molecular investigations at the sampling site by Cowen et al. (2003) and a long-term growth experiment that was started during IODP Leg 301.

Cowen JP, Giovannoni SJ, Kenig F, Johnson HP, Butterfield D, Rappé MS, Hutnak M, Lam P (2003) Fluids from aging ocean crust that support microbial life. Science, 299:120-123.
De Long (2005) Microbial life breathes deep. Science 306:2198-2200
Fisher, A.T., Urabe, T., Klaus, A., and the Expedition 301 Scientists (2005) Juan de Fuca Hydrogeology. Proc. IODP, Vol. 301
(http://iodp.tamu.edu/publications/exp301/301toc.htm)

ICDP

Low temperature magnetometry of the ilmenite-hematite solid solution (LA 1164/5)

Ralf Engelmann[1], Agnes Kontny[2], Dominique Lattard[1], Thomas Frederichs[3]
[1]Mineralogisches Institut, Universität Heidelberg, INF 236, D-69120 Heidelberg;
[2]Geologisch-Paläontologisches Institut, Universität Heidelberg, INF 234, D-69120

Heidelberg; [3]Fachbereich Geowissenschaften, Universität Bremen, Postfach 330440, D-28334 Bremen

The Hawaiian Scientific Drilling Project (HSDP) provides an excellent opportunity to study the evolution of rock magnetism in relation to the growth history and magmatic evolution of a shield volcano. The main magnetic carriers in Hawaiian basalts are the Fe-Ti oxide minerals titanomagnetite (magnetite-ulvöspinel solid solution, Tmt) and ilmenite-hematite (Ilm_{ss}). Low-temperature magnetometry of these minerals becomes increasingly important, especially for the identification of complex Fe-Ti oxide assemblages in rocks where conventional mineralogical methods fail (e.g. Lagroix et al. 2004). Especially the characterisation of the Ilmss with magnetic methods is currently a matter of great interest to several working groups (e.g. in Cambridge, UK, Trondheim, Norway, Minneapolis, USA etc.). But the interpretation of the initial susceptibility and the saturation isothermal remanent magnetisation (SIRM) as function of temperature in the range 5-280 K for these minerals are still under debate. An example for low-temperature magnetometry of submarine basalts from the HSDP drill core is given in Fig. 1a and b. The aim of the present study is a re-evaluation of low-temperature magnetic behaviour of Ilm_{ss}, which is relevant for compositions with $X_{Ilm} > 0.7$.

Recent studies have clarified some of the chemical and structural factors that control the magnetic properties in this rhombohedral solid solution series (e.g. Harrison and Becker 2001; Robinson et al. 2004). The present knowledge on the low-temperature magnetic behaviour essentially stems from studies by Ishikawa and co-workers (Ishikawa et al. 1985, Arai et al. 1985a, b, and Senftle et al. 1975). The ilmenite end member shows antiferromagnetic behaviour at temperatures beneath the Néel temperature of 56 K (Senftle et al. 1975). On the basis of low-temperature magnetic measurements on two discrete compositions (X_{Ilm} = 0.9 and 0.79) within the ilmenite solid solution, Ishikawa et al. (1985) concluded that the antiferromagnetic ordering also extends to lower X_{Ilm} with a cluster-type spin glass behaviour at temperatures below the remanence decay in this compositional range. The spin glass behaviour transforms into a superparamagnetic behaviour at a sharp maximum in the χ-T curve, at 38 K. Superparamagnetism was deduced from hysteresis curves. Figure 2a shows the magnetic phase relations at high X_{Ilm} proposed by Ishikawa et al. (1985), whereby the dashed lines represent magnetic phase transitions that are not well established. There is a need for a re-examination of these transitions to better understand natural occurrences.

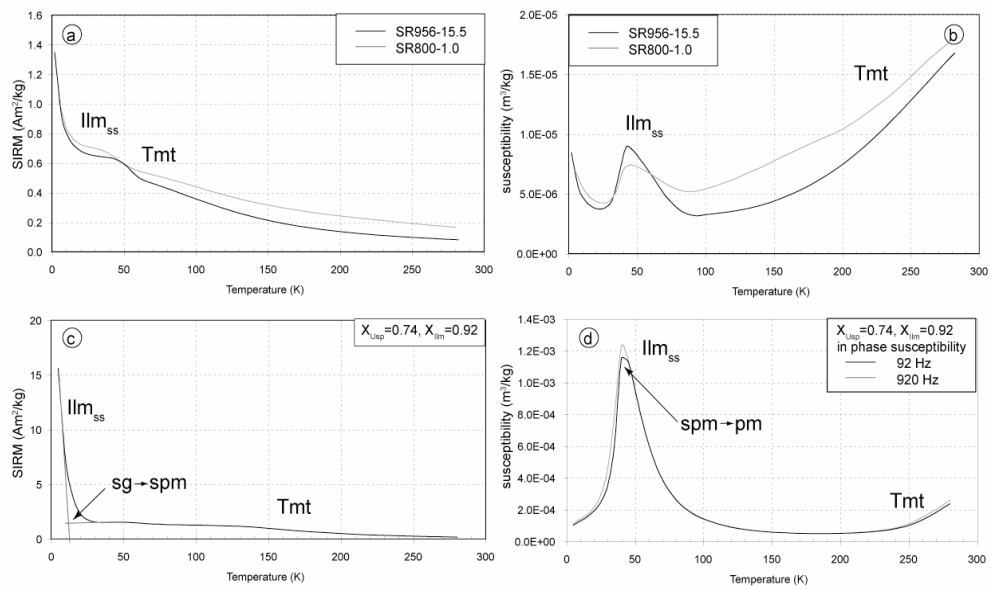

Fig. 1 Temperature dependent SIRM and AC in-phase susceptibility between 2 and 280 K for basaltic rocks of the HSDP-2 drill core (SR956-15-5: basalt intrusion, XIlm = 0.9, and SR800-1.0: pillow basalt; a and b) and comparable synthetic Tmt+Ilmss assemblages (c and d). Strong decrease in the SIRM-T curve is interpreted as transition from spin glass (sg) to superparamagnetic (spm) behaviour, peak in (d) marks the superparamagnetic to paramagnetic (pm) transition, used as TN (afm ==> pm) or TC (fm ==> pm). For further explanation see text.

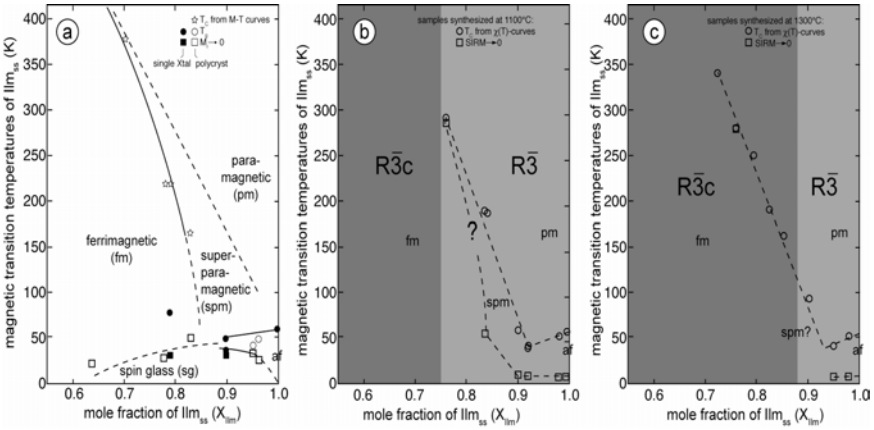

Fig. 2: Comparsion of the magnetic phase diagram after Ishikawa et al. (1985) (a) with our data from the 1100˚C (b) and 1300˚C synthesis (c). The dashed lines in (a) represent magnetic phase transition, which are not well established. MR-T curves, ?-T curves, and hysteresis loops were used by Ishikawa et al. to define the magnetic phase transitions. The magnetic phase transition shown in (b) and (c) (dashed lines) were determined using SIRM and ?-T curves. Dark grey area shows the stability field of R-3c structure, light grey area the stability field of R-3 structure of Ilmss (after Harrison & Becker 2001).

Our magnetic measurements were performed on Ilmss-Tmt assemblages synthesised under subsolidus conditios in the Fe-Ti-O system. All syntheses were performed from homogenised mixtures of TiO_2 and Fe_2O_3 that were pressed to pellets and fired in high-temperature vertical quench furnaces. The oxygen fugacity was controlled using CO/CO_2 gas mixtures. The experiments lasted >24 h at 1300˚C, up to 160 h at 1100˚C and were terminated by drop quenching into water, resulting in very fast cooling of the run products. All run products were carefully characterized using optical microscopy, X-ray powder diffraction, BSE images from a scanning electron microscope (SEM) and chemical analyses with the electron microprobe (EMP). All run products consist of polycrystalline, roughly equigranular aggregates, with grain size around 10-50 μm.

Very low-temperature saturation isothermal remanence (SIRM) measurements were performed from 5 to 300 K with a Quantum Design (MPMS XL-7) SQUID magnetometer. Samples were cooled in zero field to 5 K, given a saturation magnetization in a field of 5 T, and then measured in zero field at 2, 5 or 10 K intervals up to 300 K (Fig. 1c). The temperature dependence of the in-phase AC susceptibility (Fig. 1d) was measured in a static field of 4 Oe in the same temperature interval using frequencies of 9.2 and 920 Hz.

Figure 2b and c show the results of our MPMS measurements for Ilm_{ss} in equilibrium with Tmt at 1100˚C and 1300˚C, respectively. Because there are some discrepancies between the magnetic phase relations of Ilmss with $X_{Ilm} > 0.7$ given by Ishikawa et al. (1985) and our results, we shortly describe the magnetic transition temperatures we used in our study. From SIRM-T curves (Fig. 1c) we defined the remanence loss temperature by using the tangent intersection method as transition from spin glass (or antiferromagnetic) to superparamagnetic behaviour. Superparamagnetism is derived from the strong increase in susceptibility in the ?-T curves, which coincides with the remanence loss temperature, and from the frequency-dependence of χ at the peak (Fig. 1d). The peak temperature in the χ-T curves is used for Néel or Curie temperature determination.

We have estimated the Néel temperature for end member ilmenite (1100 ˚C) at 60 K, which is 4 K above the temperature given by Senftle et al. (1975). The Néel temperature, decreases for $X_{Ilm} = 1.00$ to 0.92 from 60 to 40 K. These temperatures are similar for the 1100 and 1300˚C synthesis but are slightly lower compared to those proposed by Ishikawa et al. (1985; see Fig. 2). The temperatures, which define the spin glass to superparamagnetic transition, are distinctly lower in our study and therefore the spin glass field is much smaller in Fig. 2b and c compared to Fig. 2a. From XIlm = 0.93 to 0.76, the Curie temperature increases from 40 to 285 K, which gives higher TCs as proposed by Ishikawa et al. (1985). The T_{Cs} of the 1100 and 1300˚C synthesis lie on a line, which is intermediate to the ones defined by Ishikawa et al. (1985) between the ferrimagnetic to superparamagnetic (their T_{Cs}) and their suggested superparamagnetic to paramagnetic behaviour (Fig. 2a). Comparing Fig. 2 b and c with our 1100 and 1300˚C synthesis, the superparamagnetic behaviour may be related to the temperature-dependent R-3 (ordered ilmenite structure) to R-3c (disordered hematite structure) phase transition. If this is true the superparamagnetic field for the 1300˚C synthesis should be distinctly smaller. To verify this assumption, we have to complete our measurements in the range $0.78 < X_{Ilm} < 0.95$.

Comparing the Tmt and Ilmss-bearing submarine HSDP basalt samples with the synthetic samples, a good agreement for Ilm_{ss} with similar X_{Ilm} was observed (Fig. 1). Therefore our work clearly contributes to a better understanding of the characterisation of Ilmss using magnetic methods.

References

Arai, M., Ishikawa, Y., Saito, N. Takei, (1985a): A new oxide spin glass system of the (1-x)FeTiO3-xFe2O3. III. Neutron scattering studies of a cluster type spin glass of 90FeTiO3-10Fe2O3. Journal of the Physical Society of Japan, 54(2), 781-794.

Arai, M., Ishikawa, Y., Takei, (1985b): A new oxide spin glass system of the (1-x)FeTiO3-xFe2O3. IV. Neutron scattering studies on a reentrant spin glass of 76FeTiO3-21Fe2O3. Journal of the Physical Society of Japan, 54(6), 2279-2286.

Harrison, R.J. & Becker, U. (2001): Magnetic ordering in solid solutions. In: Geiger, C.A: Solid solutions in silicate and oxide systems. EMU Notes in Mineralogy, vol. 3, Eötvös University press, Budapest 349-383.

Ishikawa, Y., N. Saito, M. Arai, Y. Watanabe, H. Takei (1985): A new oxide spin glass system of (1-x)FeTiO3 - xFe2O3. I. Magnetic properties. Journal of the Physical Society of Japan, 54, 312-325.

Lagroix, F., S. K. Banerjee, M. J. Jackson (2004): Magnetic properties of the Old Crow tephra: Identification of a complex iron titanium oxide mineralogy, Journal of Geophysical Research, 109, B01104, doi: 10.1029/2003JB002678.

Robinson, P., Harrison, R.J., McEnroe, S.A., Hargraves, R.B. (2004): Nature and origin of lamellar magnetism in the hematite-ilmenite series. American Mineralogist, 89, 725-747.

Senftle, F.E., Thorpe, A.N., Briggs, C., Alexander, C., Minkin, J., Griscom, D.L. (1975): The Néel transition and magnetic properties of terrestrial, synthetic, and lunar ilmenites. Earth and Planetary Science Letters, 26, 377-386.

ICDP

KTB - Two Massive Hydraulic Tests in 4 km Deep Pilot Hole Completed

Jörg Erzinger[1], Hans-Joachim Kümpel[2], Serge A. Shapiro[3] & KTB-VB Science Team

[1]GFZ Potsdam; [2]GGA-Institut, Hannover; [3]Freie Universität Berlin

Two massive hydraulic tests at Germany's super deep drill site KTB have focused on transport processes of energy and fluids in crystalline crust. The experiments have further exploited the scientific potential of the 4.0 km deep pilot hole (VB) and the 9.1 km deep main hole (HB). A research target of particular interest of the recent tests was a major fault system known as SE2 seismic reflector. It is intersected by the boreholes at roughly 4.0 km depth. The KTB site allows studying hydraulic parameters of such a structure under in-situ conditions on the kilometre scale and e.g., to verify the mechanical stability of the crust if submitted to elevated pore pressure. The fault system SE2 is hydraulically accessible through the open hole part of KTB-VB i.e., from 3.85 to 4.0 km depth.

The 1st experiment was a massive pump test in KTB-VB with production of 22.300 m^3 of saline formation fluids (Fig. 1). Seismic activity, recorded both at the surface and in KTB-HB at depths down to 3.9 km, was absent during the pumping. The 2nd experiment was a massive fluid injection test in KTB-VB. It started in June 2004, following a 12 months period of recovery from the pump test, and ended in April 2005. Over 10 months, 84.600 m^3 of fresh water (20 times more than an injection test in KTB-HB in summer 2000) were injected at rate 200 l/min, on average. Pressure build-up in KTB-VB during injection was surprisingly low and varied between 95 and 120 bar (well head). The SE2 fault system that must have stored most of the water appears to have a bulk permeability of about 2×10^{-15} m^2.

Fluid level observations in KTB-HB have shown a weak hydraulic contact to KTB-VB (Fig. 2): The height of the fluid level in KTB-HB steadily rose from nearly 40 m below surface, at the beginning of the test, up to the surface in Oct. 2004. Prior to the recent hydraulic tests, i.e. in mid 2002, the well level was close to the surface, too. Induced seismicity started in Sept. 2004 only, i.e., with a delay of about three months with respect to the beginning of the injection. Up to the end of the test, ca. 3000 seismic events were recorded by the borehole seismometer in KTB-HB, and 200 events by surface stations (Fig. 3). When compared with short-duration, less massive injection tests in KTB-HB in 1994 and 2000, the newly induced seismic activity was rather low. Yet, in 1994 and 2000, water was injected into rock formations aside of major fault systems. Seismicity started almost instantaneously then. The delay in the onset of the seismic activity in 2004 is believed to be due to incomplete pore pressure recovery from the previous pump test when the injection began. Further investigations of the 2nd experiment included repeated large scale DC measurements, high resolution tilt-monitoring to control the surface deformation field, and repeated active seismic reflection measurements to find out whether the forced hydraulic 'inflation'

of the fault zone can be imaged from the surface.
Although detailed interpretation work is still ongoing, three major conclusions are:

- The fault system SE2 probed at depth 4 km is a virtually open hydraulic system.
- Bulk permeability of the fault system is surprisingly high.
- Massive pumping at that depth has mechanically stabilized the crust

Some recent publications are listed below. Future use of the KTB boreholes for scientific or other purposes is presently open.

Acknowledgements: This research was funded by the DFG and by GFZ Potsdam. The experiments were enabled by the Operational Support Group of ICDP. We are particularly grateful to on-site staff Miel Kühr and Karl Bohn for excellent and continuous support.

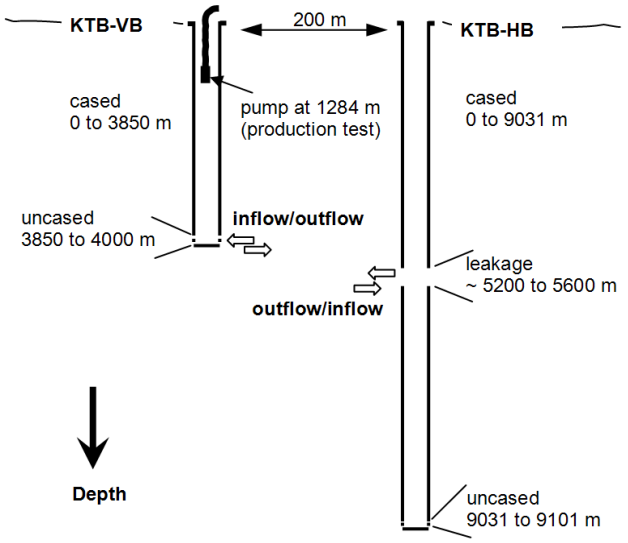

Figure 1: Sketch of the two KTB boreholes, KTB-VB and KTB-HB, showing sections that are in hy-draulic contact to the cry-stalline rock (not to scale). During the test in 2002/-03, the pump in KTB-VB has produced 22 300 m³ of formation fluid. Pressure sensors were operated in KTB-VB (below pump) and KTB-HB, seismome-ters at the surface and in KTB-HB. During the test in 2004/05, 84 600 m³ of fresh water were injected in KTB-VB, with inflow and outflow directions opposite to the pump test.

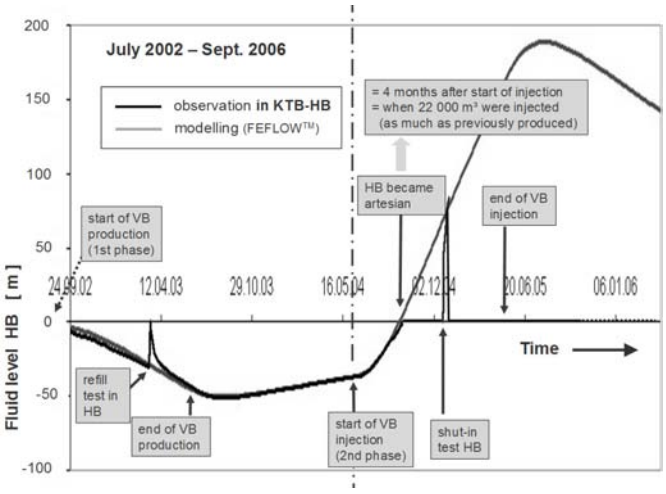

Figure 2: Fluid level change in KTB-HB as observed and simulated (FEFLOWTM, by Kessels, Kuhlmann, Li) from start of pumping to beyond end of injection test. Except for the refill test in KTB-HB in March 2003, the fluid level is responding to the hydraulic forcing in KTB-VB.

[Figure 3 next page]

Literature

Gräsle, W., Kessels, W., Kümpel, H.-J., Li, Xuan, 2006: Hydraulic observations from a one year fluid production test in the 4000 m deep KTB pilot borehole. - Geofluids, 6, 8-23.

Jahr, T., Letz, H., Jentzsch, G., 2006: Monitoring fluid induced deformation of the earth's crust: A large scale experiment at the KTB location/Germany. - J. Geodyn., 41(1-3):190-197.

McDermott, C.I., Lodemann, M., Ghergut, I., Tenzer, H., Sauter, M., Kolditz, O., 2006: Investigation of coupled hydraulic-geomechanical processes at the KTB site: pressure-dependent characteristics of a long-term pump test and elastic interpretation using a geomechanical facies model. - Geofluids, 6, 67-81.

Shapiro, S.A., Kummerow, J., Dinske, C., Asch, G., Rothert, E., Erzinger, J., Kümpel, H.-J., Kind, R., 2006: Fluid induced seismicity guided by a continental fault - Injection experiment of 2004/2005 at the German deep drilling site (KTB). - Geophys. Res. Lett., 33, L01309, doi: 10.1029/2005GL024659.

IODP

Mid-Pleistocene nutrient supply in low-latitude Namibian and Peruvian upwelling systems

Johan Etourneau[1], Thomas Blanz[1], Philippe Martinez[2] & Ralph R. Schneider[1]
[1]Institut für Geowissenschaften, Christian Albrecht Universität, Ludwig-Meyn-Str.10, 24118 Kiel, BRD [2]Département de Géologie et Océanographie, UMR CNRS 5805 EPOC, Université Bordeaux I, Avenue des facultés, 33405 Talence, France

The Mid Pleistocene climate transition (MPT) from 1.1 to 0.6 Ma BP is characterized by a gradual growth in global ice volume and a shift in the dominant orbital periodicity associated with the onset of 100 kyr glacial-interglacial periodicity. We examine MPT sediment cores from ODP Sites 1082 and 1237, located off Namibia and Peru, respectively, to reconstruct changes in low-latitude upwelling and nutrient conditions for this period. Alkenone unsaturation ratios are used as a proxy for sea surface temperatures while the $\delta^{15}N$ signal of bulk organic matter serves as nutrient proxy for both systems. Both parameters are also compared to total organic carbon mass accumulation rates (C_{org} MAR), a common bulk parameter for paleoproductivity changes. For both upwelling systems, the SST records are quite similar. In the time interval considered (1.3 to 0.4 Ma BP) warmest SST occurred during the onset of the MPT at about 1.15 Ma BP, corresponding to the interglacial Marine Isotopic Stage (MIS) 35. Then, a gradual cooling by about 4 ˚C towards the very cold MIS 22 around 0.9 Ma BP took place in the Benguela and Humboldt current systems. Pronounced warm-cold swings typical for the glacial-interglacial periods of the late Pleistocene commenced at about 0.7 Ma BP, while coldest temperatures were reached in MIS 12. In contrast, the $\delta^{15}N$ and C_{org} MAR records are quite different between the Peruvian and Namibian upwelling systems. The Site 1082 off Namibia is characterized by generally very low $\delta^{15}N$ values ranging between 3 and 5 ‰. Therefore, the Namibian $\delta^{15}N$ values during the MPT are very similar to those found in Southern Ocean sediments for the last Glacial. This suggests that the northern Benguela system was continuously supplied by southern-mode source waters independent of Mid-Pleistocene climate change (SST) and strong variance in marine productivity as revealed by C_{org} MAR changes. At Site 1237 off Peru the $\delta^{15}N$ signal shows a much greater variability compared to Namibia. Site 1237 $\delta^{15}N$ values range between 3 and 8 ‰ with lowest values corresponding to periods with step-like increases in paleoproductivity off Peru at about 1.25, 0.8, and 0.4 Ma BP. Interestingly, the latter is opposite to the continuous decline in paleoproductivity off northern Namibia since 1.1 Ma BP. The strong contrast between very high and low $\delta^{15}N$ values at Site 1237 probably suggests that the nutrient supply to the Peruvian upwelling system was alternating between a tropical component of low-oxygen water masses exposed to strong denitrification and characterized by high $\delta^{15}N$ values of supplied nitrogen, typical for local subsurface water masses in the equatorial undercurrent, and a northward propagating well-oxygenated Southern Ocean water mass characterized by low $\delta^{15}N$ values. The temporal variations in Site 1237 $\delta^{15}N$ and SST records together indicate that such a cold water supply with a Southern Ocean nitrogen isotope signature

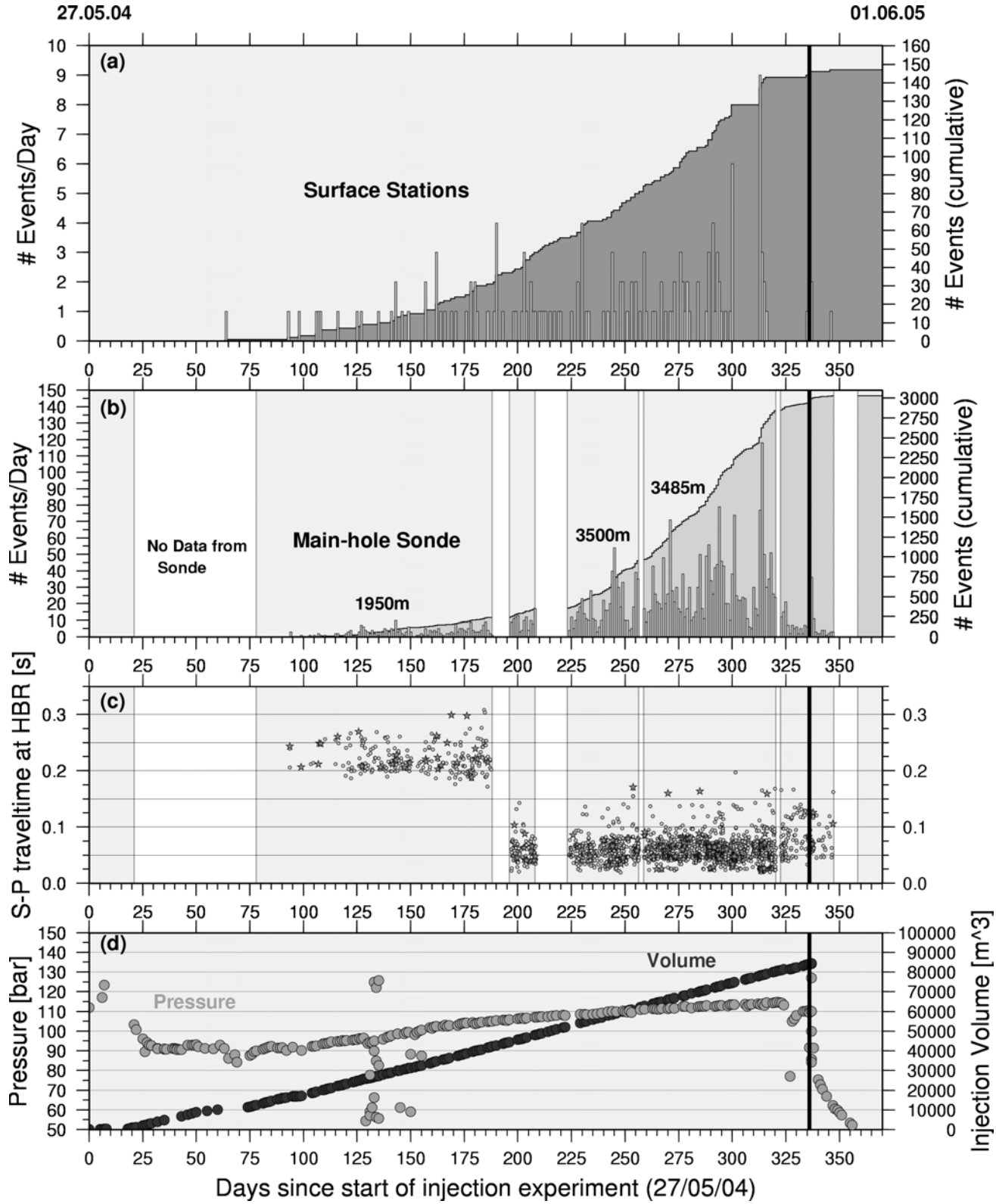

Figure 3: Micro-seismicity recorded by local seismic array and geophone in KTB-HB with time history of injected fluid volume and KTB-VB well-head pressure (by. J. Kummerow).

occurred in the eastern tropical Pacific mainly during MIS 22 and 12. This may further indicate a very strong reduction in tropical ocean denitrification levels when global climate run into its two most extreme Mid-Pleistocene glaciations.

IODP

Experiments on the effect of H2O and fO2 on the phase relations in a primitive basaltic system

S.T. Feig[1], J. Koepke[1], J.E. Snow[2,3]
[1]Institute of Mineralogy, University of Hannover, Callinstr. 3, 30167 Hannover, Germany; [2]Max-Planck-Institute of Chemistry, Postfach 3060, 55020 Mainz, Germany; [3]Department of Geosciences, University of Houston, Houston, TX 77204-5007 USA; (present address), S.Feig@Mineralogie.Uni-Hannover.de

We present crystallization experiments on a basaltic composition from the Southwest Indian Ridge (SWIR) with the aim of determining the effect of water and oxygen fugacity on the phase relations. Both parameters affect significantly the stabilities and compositions of the phases in the system. The comparison of the experimental results with natural oceanic gabbros from Leg 176 from SWIR, the longest section in the deep oceanic crust ever drilled by ODP, will help to constrain magmatic processes occurring in the oceanic crust.

A fused microgabbro, from the drill core of Leg 176 (Hole 735B), showing characteristics of a crystallized melt was used as starting material. The experiments were performed in an internally heated pressure vessel, specially designed for high-temperature basic systems. The vessel is equipped with a hydrogen membrane for controlling the oxygen fugacity and with a rapid-quench system to prevent the formation of quench-crystals [1]. At temperatures < 1050˚C gold, and at higher temperatures $Au_{80}Pd_{20}$ was used as capsule material. At reducing conditions (QFM+2 and QFM), $Au_{80}Pd_{20}$ capsules pre-saturated with iron were used. No significant iron loss into the capsule material was observed.
The effect of water on the phase equilibria was investigated from nominally dry to water-saturated conditions in the temperature range 940 to 1220˚C. Depending on the water activity, the oxygen fugacity varied from QFM+1 to QFM+4. In these experiments we also varied the total pressure, since the depth of MORB differentiation may vary considerably (Fig. 1a, b, c). Low pressures < 100 MPa are expected in typical axial magma chambers from fast-spreading ridges below the sheeted-dike sequence. Medium pressures (100-200 MPa) are relevant for the deep crust, the Moho-transition zone, and the sub-Moho mantle, while relatively high pressure (500 MPa) must be considered for the intrusion of gabbroic plutons into the mantle beneath slow-spreading ridges.

The addition of water to the dry system shifts the solidus to lower temperatures by more than 250˚C and increases the amount of melt drastically. For instance, at 1100˚C and 200 MPa, the melt fraction increases from 12.5 % at a water content of 1.6 wt% to 96.3 % at a water content of 5 wt% in the melt.

Besides the general lowering of the mineral saturation curves, water affects the slope of the stability curves of individual minerals. That means that water influences the crystallization sequence. For example at 200 MPa, clinopyroxene crystallizes before plagioclase at high water activities, while at low water activities plagioclase crystallizes first (Fig. 1b). The amount of water in the melt is controlled by the water activity and by the pressure. At higher pressures, the effect on the phase stabilities is enhanced (Fig. 1a, b, c).

Water also influences significantly the composition of the occurring phases. For example, the anorthite content of plagioclase increases drastically with water. Current models which predict the plagioclase composition from the composition of the melt [e.g., 2] cannot reproduce the observed trend.

Finally, water influences the element partitioning between the occurring phases. For example the partitioning coefficient for CaO between olivine and melt is affected. When compared to results in dry systems [3],

$$\ln D^{*ol-melt}_{CaO}$$

in our hydrous system is systematically lower for a given forsterite content of olivine.

We have compared the experimental results with evolution trends calculated by the thermodynamic models "MELTS" and "Comagmat", which are often used to determine phase relations and compositions. For clarity, we have focused on the main phases in basaltic systems: Olivine, orthopyroxene, plagioclase and clinopyroxene (Fig. 2). Due to the lack of a sufficient number of experiments in hydrous mafic systems neither model can predict the experimental phase relations with adequate accuracy.
The oxygen fugacity of some of the nominally dry experiments, applied in the experiments focusing on the effect of water, correspond to the upper level of redox conditions known from nature (QFM+1). To determine the effect of oxygen fugacity on the phase relations, and to investigated the whole range in oxygen fugacity determined for mid-ocean ridge processes (QFM-2 to QFM+1; [e.g., 4]) two sets of experiments under reducing conditions were conducted (Fig. 3), the first set at QFM+2 (QFM+2 to -1, depending on the water activity), the second set at QFM (QFM+0 to -3, depending on the water activity).

The oxygen fugacity controls the Fe^{2+}/Fe^{3+} ratio and thus influences the composition and stability of all iron bearing phases (compare Fig. 3a-c). For example, the stability of magnetite, occurring only at relatively oxidizing conditions, is affected. As well as water, oxygen fugacity influences the crystallization sequence. While at "oxidizing" conditions a chromium-rich spinel crystallizes as liquidus phase, olivine is the liquidus phase under "reducing" conditions (Fig. 3). Finally, the composition of iron bearing phases is affected. For example, the Fo-content of olivine is strongly influenced by the redox-conditions.

The experimental results combined with the analyses of minerals of natural rocks from SWIR will be used to constrain the prevailing conditions occurring during differentiation (especially aH_2O and fO_2). The dataset of this study can also be used to calibrate thermodynamic models for hydrous basaltic systems.

[1] Berndt et al. (2002): Am Mineral 87:1717-1726
[2] Panjasawatwong et al. (1995): Contrib Mineral Petrol 118:420-432
[3] Libourel (1999): Contrib Mineral Petrol 136:63-80
[4] Bezos and Humler (2005): Geochim Cosmochim Acta 69:711-725

[Figures 1 - 3 next page]

IODP

A dual-proxy sea surface temperature record of the Cenomanian/Turonian transition in the tropics (Demerara Rise, ODP Leg 207)

Forster, A.[1], Moriya, K.[2], Schouten, S.[1], Wilson, P. A.[2] & Sinninghe Damsté, J. S.[1]
[1]Royal Netherlands Institute for Sea Research (NIOZ), Department of Marine Biogeochemistry and Toxicology, P.O. Box 59, 1790 AB Den Burg, Texel, The Netherlands (forster@nioz.nl); [2]National Oceanography Centre Southampton, School of Ocean and Earth Science, University of Southampton, European Way, Southampton SO14 3ZH, UK

The mid-Cretaceous represents a time in Earth history characterized by extreme global warmth. Records of paleo-sea surface temperatures (SSTs) from the mid-Cretaceous oceans are considered to be important for the understanding of greenhouse climate conditions and related processes of climate change. The peak-temperatures of the Cretaceous "greenhouse" were reached shortly after the Cenomanian/Turonian (C/T) Oceanic Anoxic Event (OAE-2). In comparison to other Cretaceous OAEs, OAE-2 is prominent with regard to the quantity of organic carbon (OC) deposited in black shales in different marine settings world wide. OAE-2 is marked by a strong biotic crisis and a globally observed positive carbon-isotope excursion that is thought to be caused by the massive perturbation of the carbon-cycle linked to the OC-burial spanning the C/T-boundary interval (CTBI).

Here we present a detailed tropical SST-record across the C/T-transition from Ocean Drilling Project (ODP) Leg 207 Site

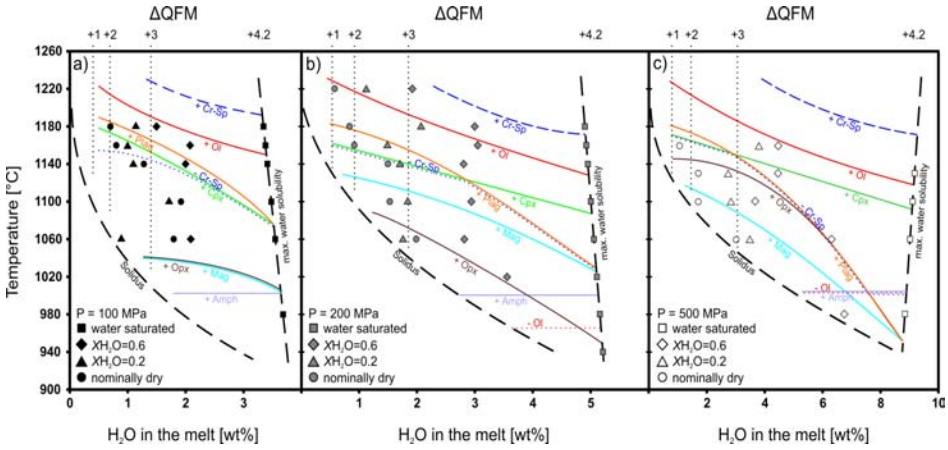

Fig. 1a-c: Phase relations for a hydrous basaltic system for 100 (a), 200 (b) and 500 (c) MPa. The amount of water was determined with the "by-difference" method. Depending on the water activity, the oxygen fugacity varies between QFM+1 and QFM+4.2. The symbols represent the experimentally investigated conditions. The phase boundaries correspond to the appearance (+) and disappearance (-, dotted) of phases. Abbreviations: Ol - olivine; Cr-sp - chromium-rich spinel; Cpx - clinopyroxene; Opx - orthopyroxene; Plag - plagioclase; Mag - magnetite; Amph - amphibole.

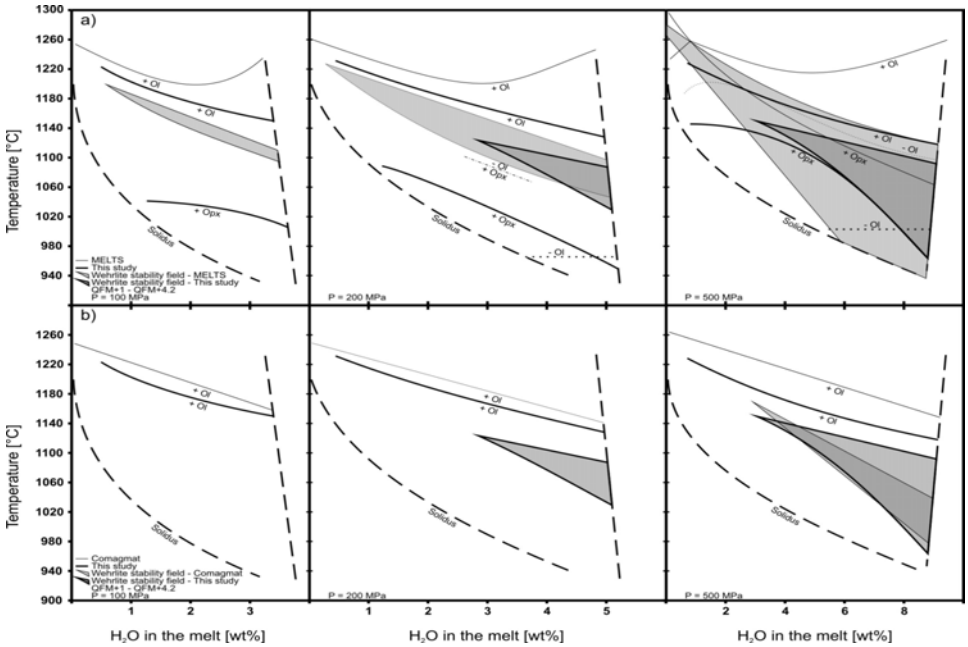

Fig. 2: Shown are the phase relations of our system compared with two of the most commonly used models - MELTS (a) and Comagmat (b). The thin lines are calculated phase boundaries, the thick lines correspond to our observations. The stability fields of plagioclase and clinopyroxene are combined and shown as "wehrlite stability field".

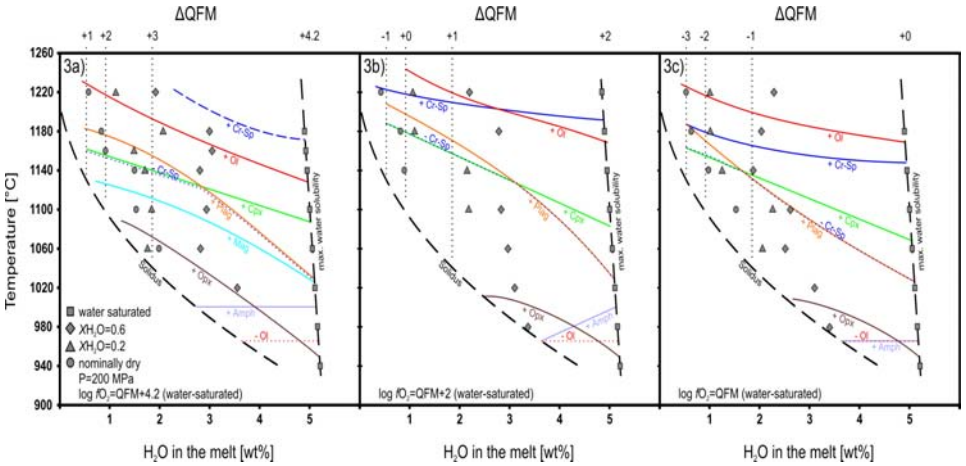

Fig. 3: Phase relations in a primitive basaltic system at QFM+4.2 (a), QFM+2 (b) and QFM (c) at 200 MPa. Within a phase diagram, the oxygen fugacity varies about 3 log units depending on the water activity. The symbols represent the experimentally investigated conditions. The phase boundaries correspond to the appearance (+) and disappearance (-, dotted) of phases. Abbreviations: Ol - olivine; Cr-sp - chromium-rich spinel; Cpx - clinopyroxene; Opx - orthopyroxene; Plag - plagioclase; Mag - magnetite; Amph - amphibole.

1260 by employing the TetraEther indeX of 86 carbon atoms (TEX_{86}), a novel organic SST-proxy, in combination with stable oxygen isotope paleo-thermometry on planktic foraminifera. Leg 207 recovered 30-95 m thick intervals of mid-Albian to Santonian organic matter rich black shales from sites 1257-1261 located on the north-western tip of the Demerara Rise, a submarine plateau off-shore Suriname and French Guyana (western equatorial Atlantic). We investigated 20 m of partially highly carbonaceous C/T-black shales at Site 1260. The CTBI is evident from a positive $\delta^{13}C_{org}$-excursion with a 6.6‰ magnitude and an increase in the average total organic carbon content (8-11%). Because age-indicative fossils are widely absent within this interval, the stratigraphic range of the CTBI is defined here by the isotopic excursion. Excellently well preserved specimens of the foraminiferan species Hedbergella delrioensis and Heterohelix moremani were used to reconstruct Cenomanian to Turonian SSTs. Deteriorated preservation of the carbonate phase and paucity of planktic foraminifera precluded oxygen isotope-paleothermometry throughout the CTBI itself. Thus, here but also in stratigraphically adjacent intervals, we employed the TEX_{86} SST-proxy.

On a long-term perspective, the dual-proxy SST-record from Site 1260 shows that the CTBI falls into a broad thermal maximum near 35-36˚C. This observation is consistent with paleotemperature-records from other regions located outside the tropics, corroborating that the C/T-transition represents the warmest Cretaceous time-interval. In agreement with studies arguing for warm and not cold mid-Cretaceous tropics, reconstructed SSTs were permanently exceeding 30˚C during this interval at Site 1260. Generally, a good match of TEX_{86}-SSTs with $\delta^{18}O$-paleothermometry is observed. Our high resolution TEX_{86} SST-record through the CTBI shows that the onset of the event coincided with a rapid rise by ~2-3˚C in tropical SSTs, which were already much warmer than today (≥33˚C). The initial warming is followed by a strong SST-decline by ~4˚C to even lower than pre-OAE temperatures likely caused by the excessive carbon burial. Then, SSTs stepwise rise to 35-36˚C again and persist into the early Turonian. These findings give new insights into trigger- and feedback processes of OAEs and to those related to climate changes under greenhouse conditions.

IODP

Paleo- and Rock Magnetic Investigation of Brazos Trinity #4 and Ursa Basin, Gulf of Mexico - IODP Expedition 308

C. Franke[1,2], Y. Fu[2], D. Heslop[2], T. von Dobeneck[2], P.B. Flemings[3], J. Behrmann[4], C. John[5], and the Expedition 308 Shipboard Scientific Party
[1]Paleomagnetic Lab. 'Fort Hoofddijk', Utrecht University, The Netherlands; [2]Department of Geosciences, University of Bremen, Germany; [3]Department of Geosciences, Pennsylvania State University, University Park PA, USA; [4]Geologisches Institut, Albert-Ludwigs-Universität Freiburg, Germany; [5]Integrated Ocean Drilling Program, College Station, TX, USA

During IODP Expeditions 308 ('Overpressure and Fluid Flow Processes in the Deepwater Gulf of Mexico: Slope Stability, Seeps and Shallow Water Flow') four late Quaternary sediment series were recovered in the Brazos-Trinity #4 minibasin (Sites U1319 and U1320) and in the Ursa region (Sites U1322 and U1324) of the northern Gulf of Mexico to test multidimensional flow models and deformation processes in passive margin settings.

To understand the time frame of such above mentioned processes, we will refine the preliminary bio- and magneto-stratigraphic Brazos-Trinity age model developed on the ship and link it to the Ursa drill sites using rock magnetic, physical property and color data for cyclostratigraphic correlation. Shipboard measurements of the natural remanent magnetization (NRM) and low-field magnetic susceptibility of the mainly muddy sediments allowed the establishment of a preliminary age model. It concurs reasonably well with shipboard micropaleontologic data. In the combined age model the younger parts of the Brazos-Trinity #4 minibasin drill sites seem to represent MIS 1 to 5 with strongly varying sedimentation rates. A change in the overall sedimentation process, and therefore in accumulation rate, could be found for the older part of the drilled Brazos-Trinity #4 drill sites, which is presumably coupled to a dramatic sea level change at the termination of MIS 6 (~120 ka).

So far, further shorebased NRM analysis was performed in particular on discrete samples of Site U1319 to compare the results to the shipboard measurements. A higher number of alternating field (AF) demagnetization steps allowed a better definition of the NRM components. A vertical drilling induced overprint was generally removed after the 20 mT AF-demagnetization step. The stable characteristic magnetic component therefore could be determined between fields from 20 to 60 mT. Between 60 and 100 mT, the demagnetization curve shows 'curling up' behaviour and a sudden change in direction. This is a typical effect of gyroremanent magnetization carried by an authigenic greigite (Fe4S4) phase. We also use laboratory induced rock magnetic proxies such as anhysteretic remanent magnetization (ARM) and isothermal remanent magentization (IRM) to describe variations in continental input (iron oxides), the stage of early diagenetic alteration (iron sulfides), changes in the magnetic mineral inventory and its grain size distribution. Magnetite grains usually a few µm across and clusters of very fine grained greigite particles with grains sizes of < 500nm have been identified by pilot rock magnetic and scanning electron microscopy (SEM) studies. The element composition of the single particles was identified and (semi-)quantified using element dispersive spectroscopy (EDS). In a new follow-on project, we plan to combine available and new rock magnetic and geochemical data to examine low-permeability mudstones overlying overpressured aquifers to track fluid flow pathways and precipitation horizons related to changes in the sedimentary milieu.

IODP

Evidence for warm saline bottom waters in the Cretaceous tropical Atlantic Ocean

Oliver Friedrich[1], Jochen Erbacher[1], Kazuyoshi Moriya[2], Paul A. Wilson[2]
[1]Bundesanstalt für Geowissenschaften und Rohstoffe, Stilleweg 2, 30655 Hannover, Germany; [2]National Oceanography Centre Southampton, University of Southampton, School of Ocean & Earth Science, European Way, Southampton SO14 3ZH UK; (emails: oliver.friedrich@bgr.de / j.erbacher@bgr.de / paw1@soc.soton.ac.uk / kazu@soc.soton.ac.uk)

A new bottom-water $\delta^{18}O$ long-term record of glassy benthic foraminifera of Ocean Drilling Program (ODP) Leg 207 at Demerara Rise (tropical Atlantic Ocean) provides the first tropical long-term paleotemperature record for middle Cenomanian to Turonian bottom-waters. The extremely well-preserved benthic foraminiferal tests and continuous sedimentation at Demerara Rise serve the unique opportunity to decipher paleoceanographic variations before and during the most prominent Oceanic Anoxic Event (OAE) of the Cretaceous. Our data suggest that bottom water temperatures at Demerara Rise were between 20-25˚C and therefore extremely warm throughout the Cenomanian and Turonian. Maximum bottom-water temperatures are recorded below the Mid-Cenomanian Event and during Oceanic Anoxic Event 2 (OAE 2) with temperatures up to 29˚C. During the Late Cenomanian benthic foraminifera document an unexpected and significant increase of the $\delta^{18}O$ values, which is not paralleled by planktic foraminiferal oxygen isotopes. This increase is proposed to reflect a change of the bottom water salinity. An according saline bottom-water mass is interpreted to derive from tropical epicontinental seas of the northern South American continent and is believed to even contribute to intermediate and/or deep waters in the Central Atlantic. At the base of OAE 2, benthic foraminiferal oxygen isotopes decrease, reflecting either a dramatic warming and/or a reduce of the salinity of bottom water, which is paralleled by a moderate increase of sea-surface temperatures. The resulting decreased $\delta^{18}O$ gradients point to a weakening of the thermohaline stratification during the OAE 2 probably contributing to the formation of black shales extremely rich in organic carbon (up to 29%).

IODP

Cenomanian/Turonian (OAE 2) benthic foraminiferal faunas of the Demerara Rise depth transect (ODP Leg 207)

Oliver Friedrich[1], Jochen Erbacher[1], Jörg Mutterlose[2]
[1]Bundesanstalt für Geowissenschaften und Rohstoffe, Stilleweg 2, 30655 Hannover, Germany; [2]Institut für Geologie, Mineralogie und Geophysik, Ruhr-Universität Bochum, Universitätsstrasse 150, 44801 Bochum, Germany ; (emails: oliver.friedrich@bgr.de / j.erbacher@bgr.de / joerg.mutterlose@rub.de)

This study is based on Cenomanian to early Turonian sediments of Ocean Drilling Program (ODP) Sites 1258, 1259, 1260, and 1261 from Demerara Rise (Leg 207, western tropical Atlantic, off Suriname) that are oriented along a paleo-depth transect. Studied sediments include the Cenomanian/Turonian Boundary Event (CTBE) or Oceanic Anoxic Event 2 (OAE 2) and consist of laminated black shales with TOC values between 5 and 10% below and above OAE 2 and up to 29% within the OAE 2 interval. Benthic foraminiferal assemblages in this eutrophic environment are generally characterized by low diversities and strong fluctuations of abundances, indicating oxygen depleted and high organic matter fluxes. Dominant taxa at all sites are *Bolivina anambra*, *Gavelinella dakotensis*, *Tappanina sp.*, *Praebulimina prolixa*, and *Neobulimina albertensis*. Based on the stable carbon isotope excursion paralleling OAE 2 we subdivided the studied successions into three intervals: (1) the interval below the OAE 2; (2) the carbon isotope excursion reflecting the OAE 2; and (3) the interval above the OAE 2. In the bathymetrically shallower Sites 1260 and 1261 benthic foraminiferal faunas indicate anoxic to sometimes slightly dysoxic bottom-waters conditions below the OAE 2. The bathymetrically deepest Site 1258, in contrast, reflects more oxygenated bottom waters with an almost continuous occurrence of benthic foraminifera. It is therefore suggested that the shallower sites were located amidst the oxygen minimum zone (OMZ), whereas the sediments of Site 1258 were deposited below the OMZ. During OAE 2 anoxic conditions prevail at the shallower sites. At Site 1258 benthic foraminifera indicate severe dysoxic but not anoxic conditions. This pattern is proposed to reflect a strengthening of the OMZ possibly related to increasing primary production during OAE 2. A short-termed repopulation event of benthic foraminifera located in the lower third of the OAE 2 was observed at all sites, reflecting a brief bottom-water oxygenation event within the OAE 2. This event parallels a surface-water cooling and is probably equivalent to the "Plenus Cool Event" in Europe and the "benthic zone" in the Western Interior. The benthic foraminifera of a ~0.5 Ma interval following the OAE 2 still indicate oxygen depletion of bottom waters. Subsequently, however, a strong increase in benthic foraminiferal abundance and diversity reflects a better oxygenation of the bottom-water masses, probably related to a weakening of the OMZ.

ICDP

Sedimentary fill of unique 3.6 Mio years old Arctic Lake El'gygytgyn (NE Siberia)

A.C. Gebhardt[1], F. Niessen[1], C. Kopsch[2], M. Melles3, O. Juschus[3], G. Schwamborn[2], J. Brigham-Grette[4], M. Nolan[5]
[1]AWI Bremerhaven, Columbusstraße, 27568 Bremerhaven, Germany; [2]AWI Potsdam, Telegrafenberg A43, 14473 Potsdam, Germany; [3]Institute for Geophysics and Geology, University of Leipzig, Talstraße 35, 04103 Leipzig, Germany; [4]Department of Geosciences, University of Massachusetts, Amherst, MA 01003, USA; [5]Water and Environmental Research Center, University of Alaska Fairbanks, Alaska 99775-5860, USA

The El'gygytgyn crater (diameter 18 km) located in the remote Anadyr Mountains in Central Chukotka, NE Siberia, was formed by a meteorite impact about 3.6 Mio years ago and is now one of the world's best preserved impact craters of its size. The crater has never been glaciated since its formation and, therefore, its lacustrine fill provides up to 3.6 Mio years of Arctic paleoclimate history. The crater lake has a diameter of about 12 km and is bowl-shaped with a maximum depth of about 170 m. It is fed by 50 inlets and drained by a single outlet in the southern part. The crater rim forms the outer margin of the lake's catchment.

In a first step towards continental deep drilling, a seismic refraction and reflection pre-site survey was carried out during expeditions in 2000 and 2003. The seismic data in combination with the echosounder (3.5 kHz) data allowed a first study on the characteristics of the lacustrine sediments (Niessen et al., in press) and on the crater geometry (Gebhardt et al., in press) (Fig. 1).

Debris flows are prominent features in the 3.5 kHz profiles, and debris flows with several meters in thickness can even be observed in the reflection seismic sections. Debris flows seem to occur cyclically in distinct levels of the lacustrine sediments. Within these levels, several debris flows can be observed in different regions of the lake, mainly in proximal areas. The lake and its sediments are highly sensitive to changes in insolation and atmospheric conditions, thus it is likely that the occurrence of debris flows is closely correlated with paleoclimate changes. Thawing of permafrost soil during warmer periods most probably led to thicker active layers and hang instabilities in the catchment and, subsequently, to enhanced mass movements such as lacustrine debris flows. However, little is known about land-lake interactions at the Lake El'gygytgyn so far, and it is not yet clear whether these debris flows are in fact robustly correlated to warmer periods.

Within the "DFG Schwerpunktprogramm ICDP", a three-dimensional model of the lacustrine sediments will be developed based on seismic reflection and high-resolution 3.5 kHz profiles. This model will be the first three-dimensional record from the impact crater lake compared to punctual information from cores and to two-dimensional seismic sections. It will allow us to better understand sedimentary effects due to paleoclimate changes. Furthermore, a detailed correlation between the future ICDP cores will be possible by mapping reflectors between the drillsites.

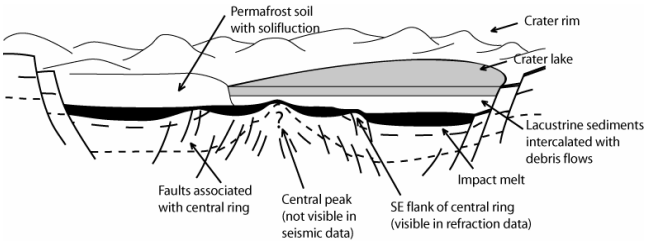

Fig. 1: General geometry of the El'gygytgyn crater and its lake.

IODP

Age and geochemistry of Central American forearc basement rocks (DSDP Leg 67 and 84) reveal a complex geodynamic history

J. Geldmacher, K. Hoernle, P. v. d. Bogaard, Leibniz-Institut für Meereswissenschaften (IFM-GEOMAR), 24148 Kiel, A. Klügel, FB Geowissenschaften, Universität Bremen, 28334 Bremen

The continental shelf outboard of Central America forms a wide shelf with an unusually broad forearc basin (Fig. 1). Geophysical investigations imply that the entire forearc basement is composed of ophiolitic rocks similar to exposed terranes of the widespread Caribbean Large Igneous Province (CLIP). Various geodynamic models have been suggested for the origin of the CLIP including its formation above the Galápagos starting plume head at ca. 83-95 Ma (e.g. Hauff et al., 2000a; b; Kerr et al., 1997). Recent studies, however, show that CLIP volcanism extends as far back as 139 Ma [Hoernle et al., 2004] thus lasting for at least 70 Myr, and therefore placing the plume head model into question. It is therefore possible that the CLIP (and other Large Igneous Provinces?) represent amalgamations of multiple smaller oceanic plateaus formed over long time periods. To address this question, we are investigating the origin of the voluminous Central America forearc basement, in order to determine if the igneous forearc rocks represent old Pacific ocean crust, former arc volcanism (either in situ or accreted), and/or accreted intraplate volcanic

rocks possibly related to the CLIP?

During DSDP Leg 67 and 84 the forearc basement was drilled off the coast of Guatemala and various igneous rocks were recovered below upper Cretaceous slope sediments. Basement rocks from four sites of Leg 84 (567, 566, 569, 570) and one site of Leg 67 (494A) consist of mafic and ultramafic rocks including basalts, dolerites, gabbros and serpentinized peridotites (Bourgois et al., 1985). Several rocks show metamorphic overprints up to the amphibolite facies. In this study we present $^{40}Ar/^{39}Ar$ laser age and geochemical data (including major- and trace elements and Sr, Nd, Pb and Hf isotope ratios) of the drilled basement rocks.

The new data reveal that the igneous forearc basement can't be considered as a monolithic block but is highly heterogeneous even at a single drill site (e.g. Hole 567A). Additionally, the recovered rocks show various states of alteration and metamorphic overprint. However, the mafic (basaltic to gabbroic) rocks can be subdivided into two groups: 1) a geochemically strongly depleted group comprising all samples from Site 494 and samples from the upper part of the basement at Site 567 (~385-440 m sub-bottom), and 2) a geochemically enriched group formed by samples of the lower basement (below 440 m sub-bottom) at Site 567.

Rocks of the depleted group have tholeiitic to basaltic andesitic compositions and display a strong depletion in incompatible elements with $(La/Sm)_N$= 0.19-0.59 and $(La/Yb)_N$= 0.12-0.41 (index N= normalized to primitive mantle). On the other hand, all samples of this group have distinct enrichments of fluid-mobile elements such as Rb, Ba, U, K, and (to a lesser extent) Pb and Sr (Fig. 2). In contrast, alkali basaltic to hawaiitic rocks of the enriched group exhibit enriched incompatible element signatures with (La/Sm)N= 1.63-2.11 and $(La/Yb)_N$= 3.63-4.46 and marked depletions in K, Pb and the heavy rare earth elements similar to signatures of Ocean Island Basalt (OIB). Consistent with the trace element division, both groups form two separated fields in Sr, Nd, Pb, and Hf isotopic space (e.g. Fig. 3 a,b) with the enriched group also having distinctly more enriched isotope ratios (e.g. high $^{206}Pb/^{204}Pb_{in}$=19.42-20.34 and $^{207}Pb/^{204}Pb_{in}$=15.65-15.70 but low $^{143}Nd/^{144}Nd_{in}$=0.51273-0.51285) and the depleted group showing isotopically depleted compositions (low $^{206}Pb/^{204}Pb_{in}$=17.93-18.48 and $^{207}Pb/^{204}Pb_{in}$=15.49-15.53 but elevated $^{143}Nd/^{144}Nd_{in}$= 0.51296-0.51309). Preliminary results of step-heating 40Ar/39Ar age determinations of mineral separates range from ~100-143 Ma for the depleted group and 104-219 Ma for the enriched group.

Compared to the Galápagos and CLIP isotope compositions (when age corrected to an average value of 125 Ma), the enriched group exhibits distinctly more enriched isotopic compositions (Fig. 3). Since CLIP samples generally plot within the extensive Galápagos field (corrected to a same age as the CLIP samples), it is questionable whether the enriched OIB-type Guatemala forearc samples are related to the CLIP or were derived from the Galápagos plume, unless the plume had more radiogenic Pb (a more HIMU-type composition) in the past. Trace element and isotopic compositions, however, are consistent with their origin by intraplate magmatism generally affiliated with geochemically enriched mantle plumes. This interpretation is also supported by tectono-magmatic discrimination diagrams using fluid-immobile (and therefore alteration-resistant) elements such as V and Ti (Fig. 4).

Although the isotopic and immobile trace element compositions of the depleted group rocks are similar to Pacific N-MORB, the marked enrichments in fluid-mobile (LILE) relative to fluid immobile (HFSE and REE) elements are characteristic of island arc volcanic rocks (IAV). Although the strong alteration may have affected the contents of the mobile elements (sometimes producing an apparent Nb+Ta depletion), the high (Th/Nb)N ratios (both being fluid immobile elements) support an IAV origin, since MORB rocks have (Th/Nb)N ratios <1 (Fig. 2). An island arc origin is also consistent with the low V/Ti ratios of the depleted group plotting mainly in the arc-tholeiitic field in Fig. 4.

In conclusion, the enriched group exhibits clear OIB or intraplate-type geochemical compositions and represents either a hitherto unsampled component (with highly radiogenic Pb) of the early Galápagos plume or, more likely, accreted intraplate seamounts/ocean islands of central Pacific origin. The depleted group can be interpreted as a submerged upper Cretaceous island arc, accreted to the Chortis Block subduction zone. Rocks of similar age and geochemistry to both groups are exposed on the Santa Elena Peninsula in Costa Rica (Figs. 3, 4).

Hauff F, Hoernle K.A, Bogaard Pvd., Alvarado G.E., Garbe-Schönberg D. (2000a) Age and Geochemistry of Basaltic Complexes in Western Costa Rica: Contributions to the Geotectonic Evolution of Central America. Geochemistry Geophysics Geosystems 1, paper # 1999GC000020

Hauff F., Hoernle K.A., Tilton G., Graham D., Kerr A..C (2000b): Large volume recycling of oceanic lithosphere: Geochemical Evidence from the Caribbean Large Igneous Province. Earth Planet Sci. Lett. 174, 247-263

Kerr A.C., Marriner G.F., Tarney J., Nivia A., Saundrs A.D, Thirwall M.F., Sinton C.F. (1997) Cretaceous Basaltic Terranes in Western Colombia: Elemental, Chronological and Sr-Nd Isotopic Constraints on Petrogenesis, J. Petrol., 38, 677-702

Hoernle K, Hauff F, Bogaard Pvd (2004) 70 Myr history (139-69 Ma) for the Caribbean large igneous province. Geology 32, 697-700

Bourgois J., Desmet A., Tournon J., Auboin J. (1985) Mafic and ultramafic rocks of leg 84: petrology and mineralogy. In: von Huene R., Auboin J. eds., Init. Rets. DSDP 84, Washington, D.C., US Government Printing Office, 633-642

Shervais J.W. (1982) Ti-V plots and the petrogenesis of modern ophiolitic lavas. Earth Plant. Sci. Lett, 59,101-118

[Figures 1 - 4 next page]

ICDP

The 2005 ICDP-USGS DEEP COREHOLE In the Chesapeake bay impact crater

G.S. Gohn[1], C. Koeberl[2], K.G. Miller[3], W.U. Reimold[4]
[1]U.S. Geological Survey, Reston, VA 20192, USA, [2]Univ. Vienna, Dept. of Geol. Sci., A-1090 Vienna, Austria, [3]Rutgers Univ., Dept. Geol. Sci., Piscataway, NJ 08854, USA, [4] Museum f. Naturkunde (Mineralogie), Humboldt Universität, D-10115 Berlin, Germany, uwe.reimold@museum.hu-berlin.de.

The late Eocene Chesapeake Bay (CB) impact crater is among the largest (presumed 80 km diameter) and best preserved of the known impact structures on Earth. In 2004, a multidisciplinary, international drilling project for this crater was accepted by ICDP. Its location on a passive continental margin has prevented tectonic or orogenic distortion, and its original location on a relatively deep continental shelf allowed marine deposition to resume immediately following the impact, thereby preventing subsequent erosion. CB is the source of the North American tektite strewn field. The upper part of the breccia section inside the crater was derived from resurge currents and impact-generated tsunami waves. The breccia body contains a substantial volume of impact-related brine; the crater underlies a densely populated urban corridor, whose two million citizens are still affected by crater-related phenomena, such as freshwater availability. This project also presented an opportunity for deep biosphere research. Relatively good core recovery allows to study the following stratigraphy: 0-444 m - post-impact sediments; 444-1096 m - sediment-clast breccia and sediment megablocks; 1096-1371 m - granitic megablock(s); 1371-1393 m - sediment and lithic blocks; 1393-ca. 1550 m - suevite and lithic breccia; ca. 1550-1766 m - schist and pegmatite ± few breccia veins.

The cored post-impact section (125 to 444 m) consists of fine-grained, siliciclastic continental-shelf sediments involving: 1) two possible sequences in the upper Miocene Eastover Formation (ca. 6.7-6.9 Ma); 2) one upper Miocene St. Marys Formation sequence, 3) ~4 middle Miocene Calvert Formation sequences; 4) several very thin lower Miocene-Oligocene sequences; and 5) a very thick upper Eocene Chickahominy Formation. The section in the Eyreville corehole is very similar to that in the nearby Kiptopeke corehole, although the upper Eocene section is more expanded at Eyreville.

Matrix-supported sediment-clast breccia constitutes the uppermost part of the impactite section. This breccia overlies thick

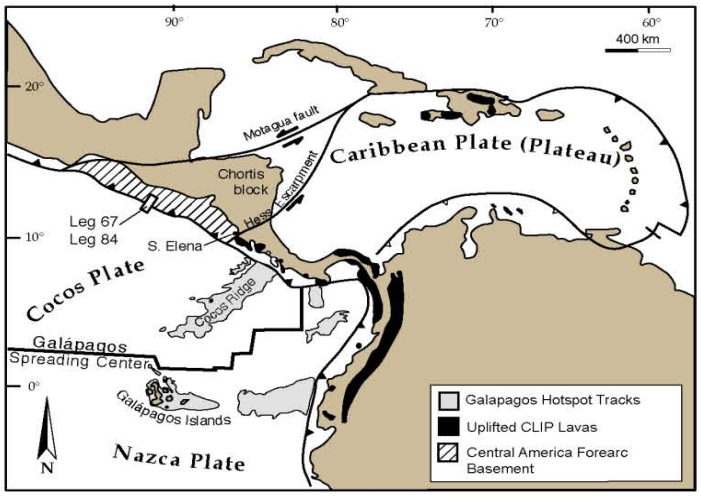

Fig. 1: Tectonic setting of the Central American forearc basement and the Caribbean Large Igneous Province showing location of DSDP Legs 67 and 84.

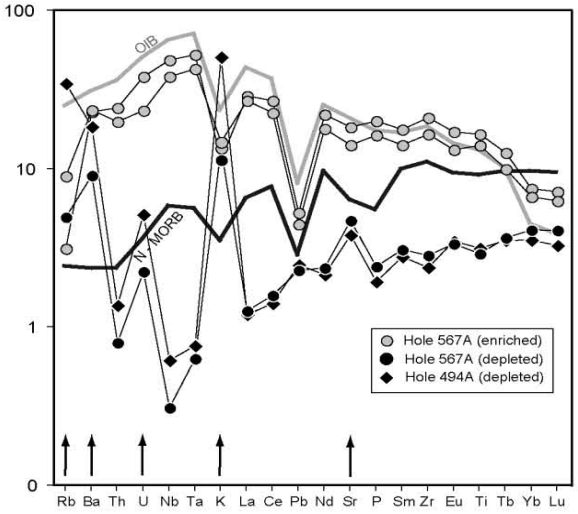

Fig. 2: Multi-element diagram (normalized after Hofmann, 1988) of representative mafic samples of enriched and depleted Central American forearc samples.
N-MORB (black line) and typical HIMU-OIB from St. Helena (gray line) are shown for comparison. The depleted group exhibits characteristic enrichments of fluid mobile elements (black arrows).

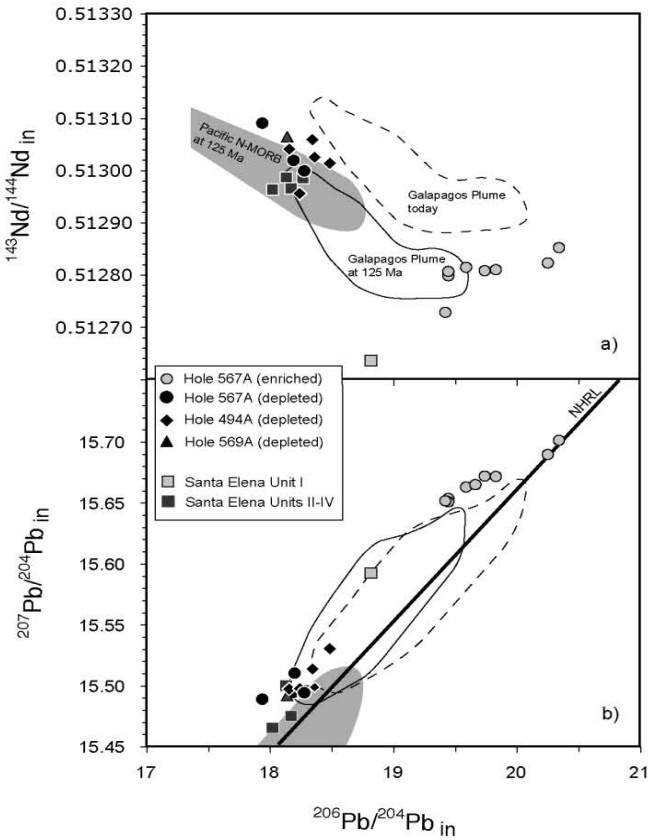

Fig. 3: Initial Pb and Nd isotope ratios of the drilled Central American forearc samples in comparison with the on-shore Santa Elena complex and the Galapagos plume (including CLIP). S. Elena data from Hauff et al. (2000).

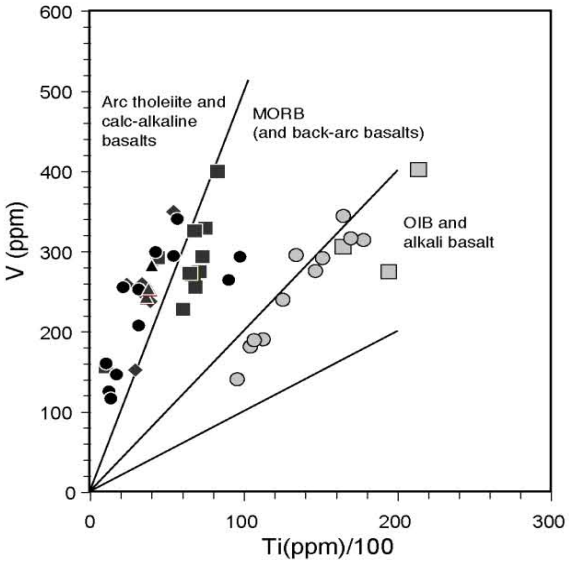

Fig. 4: Ti-V tectonomagmatic discrimination diagram after Shervais (1982). Symbols and S. Elena data source as in Fig. 3.

sections of Cretaceous sands and clays probably representing slumped megablocks. An unexpected 275-m-thick section of granitoid rock underlies the sediment megablocks. The suevitic breccias are cohesive, lithified, and contain variably angular clasts of probable impact-melt rock, and fragments of cataclastically deformed metamorphic and igneous target rocks, in an apparently unsorted matrix of similar but finer grained material (Table 1). Lithic breccias are polymict and resemble the suevite except for a lack of evident impact-melt clasts.

Mica schists and associated pegmatites constitute the lowest unit encountered in the corehole and provide ample scope for regional geological investigations. The pegmatites become increasingly abundant downsection. The schists are fine- to coarse-grained, well foliated, and consist mainly of white mica and (or) graphite, quartz, and plagioclase in varied amounts. Gneissic quartz-feldspar interlayers occur locally. The pegmatite consists mainly of very coarse to coarse-grained feldspars, quartz, and smaller amounts of muscovite. The schists and pegmatite are commonly brecciated, internally faulted, and fractured, and a few suevitic or lithic breccia veins are present in the upper part of this section.

Core samples will be distributed to the Project's Science Team members in March 2006 for detailed investigations.

Acknowledgements: Funding for the CB deep corehole was provided by ICDP, USGS, and the NASA Science Mission Directorate. DOSECC, Inc., managed the drilling operations, and Major Drilling America, Inc. did the core drilling. We thank the Buyrn family for permission to use Eyreville Farm as a drilling site and for their interest in the project, and wish to thank the many scientists, technicians, and students who supported the project.

IODP

First results from high resolution physical and chemical core logging at IODP Site U1314 (Gardar Drift): Age model and millennial-scale sedimentation history for the Middle Pleistocene

Jens Grützner[1], Sean M. Higgins[2], Gerold Wefer[1,3] and the IODP Expedition 306 scientists

[1]Bremen University, Geosciences Department, Bremen, Germany, (jgruetzn@uni-bremen.de); [2]Lamont-Doherty Earth Observatory of Columbia University, Borehole Research Group, Palisades, New York, USA; [3]DFG Research Center Ocean Margins, Bremen, Germany

Following Expedition 303 (October-November 2004), IODP Expedition 306 (March-April, 2005) was the second cruise of the North Atlantic paleoceanography study, which aims to generate a late Neogene-Quaternary chronostratigraphic template for North Atlantic climate proxies, allowing their correlation at a sub-Milankovitch scale and their export to other parts of the globe by using a paleointensity-assisted chronology (PAC). The primary drilling locations selected for the North Atlantic paleoceanography study were known, either from previous Ocean Drilling Program (ODP)/Deep Sea Drilling Project (DSDP) drilling or from conventional piston cores.

A major objective of our new research project is to measure element intensities (e.g. Al, Si, K, Ca, Ti, Fe, Sr, Ba) on selected 303/306 drillsites to derive cm-resolution records of terrigenous and biogenic sediment composition. Combined with detailed age models these records will characterize prominent millennial scale climate cycles of the last glacial period known as Dansgaard/ Oeschger and Heinrich events and help to study their possible occurrence in time intervals prior to 100 ka BP. Here we present first results from Site U1314 that was drilled during Expedition 306 on the southern Gardar Drift in a water depth of 2800 m. The completely recovered Upper Pliocene to Holocene sedimentary sequence will allow a high resolution monitoring of North Atlantic DeepWater (NADW) variability during the last ~2.7 My. Furthermore the site lies close enough to the IRD belt to record the Heinrich-type detrital layers that indicate ice sheet instability.

The sediments at Site U1314 consist of an alternation of predominantly nannofossil oozes and terrigenous silty clays. These changes in lithology are reflected in prominent short-wavelength amplitude variations of the sediment physical properties. The physical property records from Site U1314 exhibit a high similarity with equivalent data from Site 983 (ODP Leg 162, northern Gardar Drift) for which an oxygen isotope based stratigraphy is already available. Thus correlating colour and magnetic susceptibility variations from both sites allowed us to derive an age model for the last 2 My at Site U1314. We also present new X-ray fluorescence (XRF) records of element intensities obtained with a non-destructive XRF core scanner for the time interval 400 - 900 ky. Given the average sedimentation rate of 7.6 cm/ky for this time interval the 1 cm resolution XRF records allow us to explore millennial scale changes in terrigenous provenance and biogenic productivity during the Mid-Pleistocene Transition (MPT).

IODP

Investigation of current conditions and sediment transport pattern along the Antarctic Peninsula using a numerical ocean circulation model

Petra Günnewig1, Katrin Huhn1 & Gabriele Uenzelmann-Neben2

1Research Center Ocean Margins, Leobener Str., D-28359 Bremen; 2Alfred-Wegener-Institute für Polar- und Marine Research, Columbusstrasse, D-27568 Bremerhaven

During the last decade, higher latitudes, particularly the Antarctic continental margin, were main target areas to investigate climate shifts and global ocean circulation over long-time periods. In such a way during several cruises a unique data base, including numerous multi channel reflection seismic profiles, bathymetric maps, shallow gravity measurements, and in particular core data from ODP Leg 178, was collected along the Antarctic Peninsula. These data monitored a number of asymmetric sediment mounds on the continental slope which were interpreted as sedimentary drifts. These drifts serve as an excellent achieve for the geological environment and current conditions during their formation.

In particular, Drift 7 is the best monitored sedimentary mound in this area. Detailed information about spatial extension, internal structures, sedimentary sequences, and grain size distribution exist. These data enable on one hand the identification of sediment sources, the reconstruction of sediment transport pathways and transport mechanisms, as well as current velocities. On the other hand, different theories about controlling parameters for the evolution of drifts could be developed such as: Is an initial topography necessary for the formation of such a sedimentary structure?

Therefore, numerical oceanic circulation models enable extensive parameter sensitivity studies combining multidisciplinary datasets as model input parameters to test different hypotheses. Thus, we are using the Regional Ocean Model System (ROMS) - an academic hydrostatic ocean circulation model, based on the finite difference method to investigate the environmental situation and current conditions during the evolution of Drift 7. Major aim of this project is the reconstruction of depositional and re-depositional processes from observed sediment structure of Drift 7. Therefore, ROMS included a complex sediment transport module to compute particle transport within the water column as well as sediment suspended in the benthic boundary layer at the seafloor using an advection equation for sediment suspended.

For the first series of experiments, we developed a 3d model to obtain qualitative information about ocean currents and sediment distribution under recent conditions along the Antarctic Peninsula, Bellingshausen Sea. The study area is situated between 84˚S - 72˚S and 70˚W - 65˚W. We use a realistic topography with a resolution of 5˚ and a horizontal grid width of 14 km whereas the water column is vertically subdivided into 20 depth levels. We calculate the current field and sediment distribution during a time interval of one year. This simulations supply first information about sediment transport pathways, where should major sediment

sources be expected, what ocean currents must exist to accumulate drift bodies and changed the ocean currents over the last centuries?

However, next step will be the simulation of past situations to keep e.g. sea level changes, temperature variations, as well as wind, wave and tidal effects into account. Furthermore, we develop coevally a simplified 3d slope model to analyse (a) which initial topography is necessary to accumulate sediment drift and (b) how long must be an episode of current activity to generate the drift.

IODP

A transport-reaction model of the hydrological systems of the Costa Rica subduction zone

Matthias Haeckel
Leibniz Institute for Marine Sciences, Wischhofstrasse 1-3, D-24148 Kiel, Germany

ODP Legs 170 and 205 have identified systems of lateral fluid flow at the Costa Rica convergent margin: (i) an aquifer of cold seawater in the oceanic crust, (ii) flow of deep-sourced fluids along conduits parallel to the décollement, and (iii) vertical dewatering of compacted underthrust sediments. Numerical transport-reaction models were developed to quantify the processes of these hydrological systems. The results suggest that the lateral fluid flow in the Costa Rica subduction zone is transient, i.e. not a steady state process.

Model runs reveal that the oceanic porewater composition has been dominated by advective or diffusive connection to the lateral flow of cold seawater in the basement for the past 240 ka to 1 Ma, respectively. Comparing the numerical results of this study with other hydrothermal calculations also suggests that most of this water is subducted and only a small fraction is migrating upwards into the overlying sediments.

High-resolution propane gas data have been collected in the prism sediments at ODP Site 1254 showing a combination of upward advection (in the order of 0.4 cm/a) due to compaction of the subducting oceanic sediments as well as lateral fluid flow with thermogenic origin. Numerical analysis shows that the lateral dewatering in the prism sediments is dominated by episodic events: the conduit at ~220 mbsf has been active for about 2000 a, while fluids have permeated the décollement zone (~360 mbsf) for nearly 4000 a. However, shorter fluid pulses caused by seismic activity do not seem to have much impact.

Finally, the downward progressing AMO reaction front, which developed between methane-rich prism sediments and sulfate-rich oceanic sediments, was analysed. The numerical simulations show that about 15 kg C/m2 are oxidized within 17 ka of subduction (1.5 km arcward of the deformation front), probably partially provided by methane hydrates in the prism wedge.

IODP

The Cenomanian-Turonian succession of ODP Leg 207: biostratigraphy and palaeoecology

Petros Hardas & Jörg Mutterlose
Ruhr-Universität Bochum, Universitätsstr. 150, 44801, Bochum, Germany. E-Mail: petros.hardas@rub.de

Black shales are a characteristic feature of the marine sediments of the mid-Cretaceous. Our understanding of the origin of mid-Cretaceous organic carbon-rich sediments is mainly derived from deep sea environments and epicontinental seas. Organic-rich sediments are restricted here to the distinctive horizons of the Ocean Anoxic Events (OAEs). During ODP Leg 207 (Sites 1257-1261) at the Demerara Rise (Suriname margin, western Atlantic) an extensive and continuous black shale succession covering the late Albian - late Santonian interval was recovered.

We are studying the Cenomanian and Turonian of four Sites (1258, 1259, 1260, and 1261) based on calcareous nannofossils. The main goals of this project are 1) to establish a high resolution biostratigraphic framework for the mid-Cretaceous of the equatorial Atlantic, 2) to understand the palaeobiogeography of equatorial nannofossils and their ecological implications, and 3) to view and interpret the black shale formation in the light of calcareous nannofossil productivity.

At Site 1260 the presence of the species *Corollithion kennedyi* in the lowermost sample, indicates that the studied interval begins in the early Cenomanian (biozone UC1). It reaches the middle Turonian (biozone UC9, defined by the first occurrence (FO) of *Litraphidites septenarius* (Fig.1). At Site 1258 the interval studied so far covers the late Cenomanian to middle Turonian.

We have observed a total of fourteen bioevents, seven of them occurring in the Cenomanian-Turonian boundary interval (CTBI). This interval is characterized by the Ocean Anoxic Event 2 (OAE2), which is marked by the deposition of organic-rich sediments in many sections worldwide and a significant positive stable carbon isotope excursion. We have studied the biostratigraphy of this interval with a resolution of approx. 1 sample/15cm at Sites 1258, 1259, 1260, and 1261. We have observed the following bioevents: the first occurrences (FOs) of *Cylindralithus biarcus, Quadrum intermedium, Quadrum gartneri, Eprolithus octopetalus* and *Eprolithus eptapetalus* and the last occurrences (LOs) of *Corollithion kennedyi* and *Axopodorhabdus albianus*. We have plotted these bioevents against the $\delta^{13}C_{org}$-excursion, which allows us a supra-regional correlation with other locations worldwide. The FO of Q. gartneri lies stratigraphically below that in other published sections, thus it cannot be used as a supplementary datum level for the Cenomanian-Turonian boundary at the Demerara Rise, as it has been proposed for other sections.

Considering the palaeoecology, the lower Cenomanian is characterized by high absolute abundances and low diversity of calcareous nannofossils. The eutrophic species Biscutum constans shows high relative abundances (Fig.1). These observations are indicative of enhanced productivity and r-mode selection. This trend lasts until the upper part of the lower Cenomanian, where the sea surface water became less productive, as shown by the decrease of B. constans and the increase of the oligotrophic species *Watznaueria barnesae* and *Watznaueria fossacincta* (Fig.1).

In the middle Cenomanian Event (MCE) a significant turnover of the nannofossil assemblages occurs. The warm-surface water species *Rhagodiscus asper* declines while the cool surface water species *Eprolithus floralis* increases significantly (Fig.1). We interpret this as a cooling event that occurred during the MCE. Other species, with uncertain palaeoecological affinities, show shifts in the MCE: *Watznaueria biporta* and *Eiffellithus turriseiffelii* become more common while *Gartnerago segmentatum* has its FO and becomes an important component of the nannofossil association after this event (Fig.1). Since these species correlate positive to E. floralis (Pearson coefficients: 0.582, 0.468, 0.503, respectively) we suggest that they also prefer cooler surface waters. R. asper does not recover after the MCE and remains very rare. We therefore suggest, that it cannot be used as a temperature proxy after this event. *Tranolithus orionatus*, which has been described as a cool surface water species, shows a general increase after the MCE but it has no correlation with E. floralis (Pearson coefficient: 0.108). The taxa *Crucibiscutum hayi* and *Repagulum parvidentatum*, also interpreted as cool water taxa, are very rare or absent in our samples and cannot be used.

The palaeoecological analysis of the CTBI at Sites 1258 and 1260 shows that *E. floralis*, *W. biporta*, and *G. segmentatum* decrease during this interval, which we interpret as a warming signal. *T. orionatus* does not show any obvious trend below or during the CTBI but is generally rare. *E. turriseiffelii* does not decrease as we would expect, though this can be caused by the poor nannofossil preservation in parts of this interval, since this species is resistant to dissolution. We have also observed a clear productivity-signal during the $\delta^{13}C_{org}$-excursion of the CTBI: the

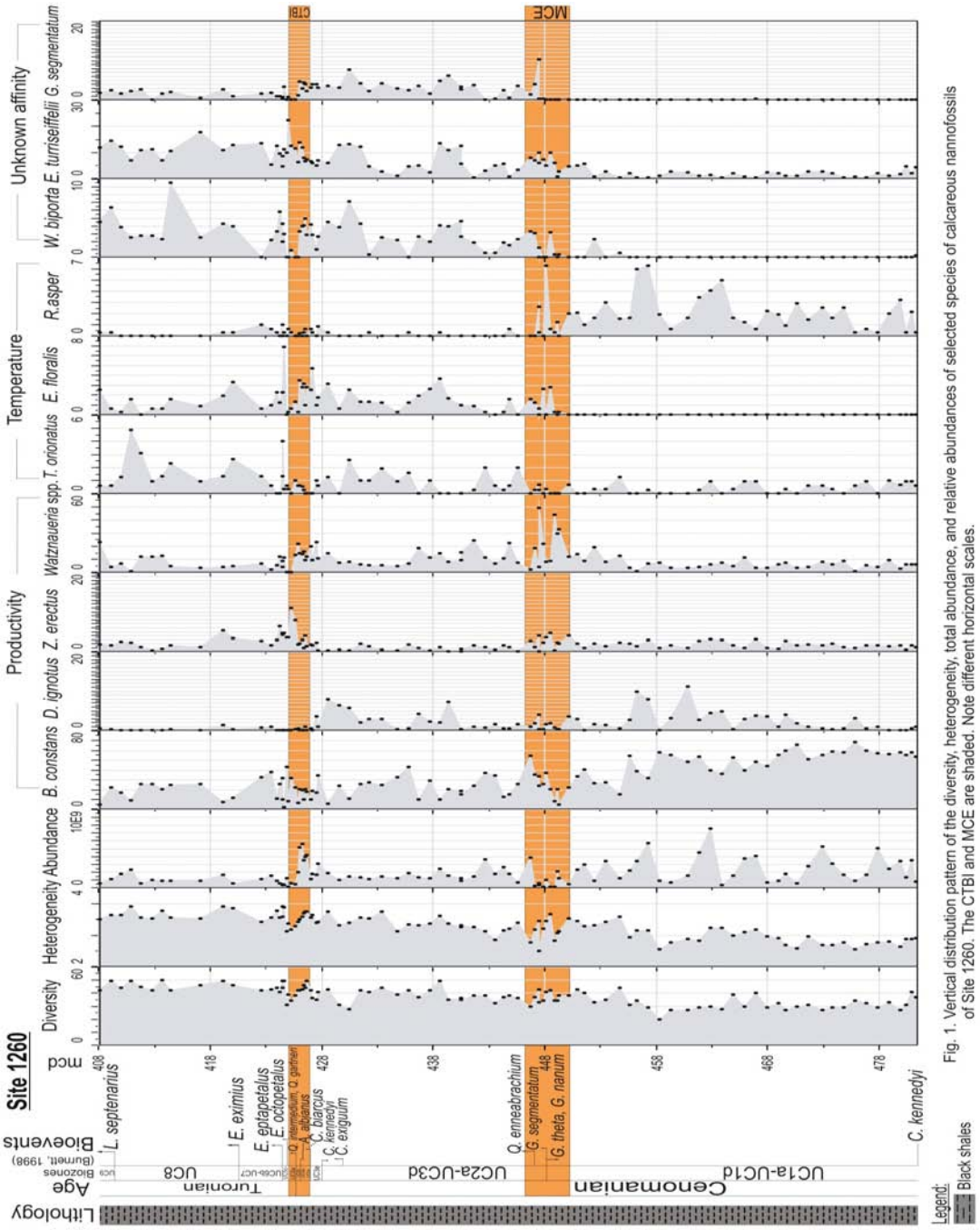

Fig. 1. Vertical distribution pattern of the diversity, heterogeneity, total abundance, and relative abundances of selected species of calcareous nannofossils of Site 1260. The CTBI and MCE are shaded. Note different horizontal scales.

eutrophic species Z. erectus - which is believed to response in higher nutrient levels than B. constans - shows an abrupt increase, while *Watznaueria* spp. strongly decreases. Additionally, in the beginning of the $\delta^{13}C_{org}$-excursion the total abundance of nannofossils increases while the diversity decreases, indicating an r-mode selection during this interval. This shows that the OAE2 was coupled with an enhanced productivity on the Demerara Rise.

IODP

Cyclic changes of paleoproductivity between 20 and 50 kyr BP at ODP Site 1233 in the SE-Pacific

Dierk Hebbeln[1], Jerome Kaiser[2] und Frank Lamy[2]
[1]MARUM - Zentrum für Marine Umweltwissenschaften, Universität Bremen; [2]GeoForschungszentrum Potsdam; dhebbeln@marum.de

The SE-Pacific and especially the Peru-Chile or Humboldt Current belongs to the most productive regions in the world ocean. Its southern part along the Chilean coast is characterised by intense coastal upwelling resulting in exceptionally high productivity. But interestingly, the highest productivity is not observed in this coastal upwelling region, but further to the south (>38˚S). It is assumed that the very high productivity there is based on the advection of macronutrients by the Antarctic Circumpolar Current (ACC) bringing typical high nutrient-low chlorophyll (HNLC) waters towards the South American continent. Upon reaching the continental slope and shelf, these HNLC waters mix with coastal waters rich e.g. in iron, an important micronutrient typically missing in such HNLC waters. The combination of these two nutrient pools enables an extremely high productivity, which can be seen in satellite images as well as in sediment data.

ODP Site 1233 is located at 41˚S at the Chilean continental slope right within this highly productive region unaffected by coastal upwelling. Due to very strong precipitation onshore, the input of terrigenous material is very high resulting in a fast sedimentation. The ~135 m long core covers ~70 kyrs and is marked by sedimentation rates mainly ranging between 100 and 200 cm/kyr.

Basic proxies for the estimation of past productivity are the

contents of organic carbon, carbonate and biogenic opal. In addition, the C/N-ratios serve as a rough indicator about the source of the organic matter preserved within the sediments. Close sample spacing allows for a temporal resolution of <100 years per sample. Focusing on the period between 20 and 50 kyr BP, the organic carbon contents range from 0.6 to 2.1 wt.-%, whereas the carbonate contents vary between 0 and 8 wt.-% and the biogenic opal contents between 6 and 10 wt.-%, respectively. The apparently rather low contents of the biogenic compounds for such a high productivity region are due to the very high flux of terrigenous matter diluting the flux of the productivity indicators. With C/N-ratios mainly between 6 and 9, it is assumed that almost all the organic matter in the sediment is of marine origin and, thus, reflecting the local surface ocean productivity.

Between 20 and 50 kyr BP, organic carbon and carbonate contents co-vary and show a distinct millennial-scale variability. As these data are only contents, they might reflect changes in the dilution of the biogenic material by changing terrigenous sediment input. However, looking at the rain ratio, i.e. the ratio between organic carbon and carbonate carbon, is becomes obvious that also the composition of the biogenic flux reveals the same distinct variability. Interestingly, those intervals marked by high organic carbon and carbonate contents, show low rain ratios. Thus, for the time being, the data are somewhat contradicting, as the high organic carbon and carbonate contents as well as high rain ratios would point to enhanced productivities. The calculation of the accumulation rates of the biogenic compounds will help to solve this problem. Nevertheless, the distinct variability in the data points to a strong forcing mechanism behind it. Over the same period, the rather low resolution biogenic opal data show only very little variability.

Comparing the organic carbon and carbonate contents with the alkenone-based sea surface temperature (SST) reconstruction from the same site, shows that high percentages of the biogenic compounds generally correlate with higher SSTs. Thus, millennial-scale SST changes in the order of 2˚C had a pronounced effect on the paleoproductivity off Chile resulting in cyclic variations with individual cycles lasting between 2 and 4 kyr.

IODP

Long-term temperature measurements in ODP Holes 1253A and 1255A off Costa Rica, ODP Leg 205

Martin Heesemann[1], Heinrich Villinger[1], Hans W. Jannasch[2], Miriam Kastner[3], Evan A. Solomon[3], and Expedition 301T Scientific Party
[1]Universität Bremen, Department of Geosciences, Klagenfurter Straße, 28359 Bremen, Germany; [2]Monterey Bay Aquarium Research Institute, 7700 Sandholdt Road, Moss Landing, CA; [3]Scripps Institution of Oceanography, University of California, San Diego, La Jolla, CA; Corresponding author: heesema@uni-bremen.de

During Ocean Drilling Program (ODP) Leg 205 in September and October 2002, Circulation Obviation Retro?t Kit (CORK)-II observatories were installed in ODP Holes 1253A and 1255A across the Middle America Trench off the Nicoya Peninsula, Costa Rica, in order to study ?uid ?ow across the margin and its implications for the seismogenic zone and subduction factory. Hole 1253A is located on the incoming plate 0.2 km seaward from the deformation front, whereas Hole 1255, which penetrates the décollement, is located 0.4 km arcward of the deformation front. The CORK-II observatories include instruments that were designed to sample fluids and measure ?ow rates, temperatures, and pressures. Fluid sampling is performed by OsmoSamplers that were configured to operate continuously for up to 2 years and incorporate autonomous high-precision miniaturized temperature loggers (MTLs) (Figure 1).

Sixteen months following the CORK-II installation, eight Alvin submersible dives were conducted to recover and replace the OsmoSamplers containing the MTLs. During these dives the pressure data were successfully downloaded from the CORK heads, whereas recovering and replacing the OsmoSamplers failed. Fortunately, the JOIDES Resolution returned during Integrated Ocean Drilling Program (IODP) Expedition 301T in August-September 2004, and succeeded in recovering most of the OsmoSamplers and replacing them with new ones, before valuable data and water samples were lost. All of the three MTLs, recovered along with the OsmoSamplers, were retrieved fully functional, and provided high-resolution temperature records. These records cover a time span of almost 2 years and were sampled at an interval of 17 min. Stable temperatures measured over periods of several months around April 2003, and August 2004 (Figure 2B) demonstrate the high quality of the temperature data recorded by the MTLs. No significant instrument drift can be seen, and the noise level does not exceed the loggers' resolution.

Besides the long-term equilibration trends, caused by drilling induced thermal disturbances, several smaller events are documented in the temperature data. These events, most likely caused by hydrologic processes, are also present in the pressure data recorded by CORK-IIs (Figure 2), and in the fluid samples and flow meter information provided by the OsmoSamplers.

Presented data show that the MTLs are practicable, reliable, and, at the same time, affordable instruments to measure high-resolution downhole temperatures, even over long periods of time. The MTL temperature records can supplement the CORK-II pressure measurements and the data gained from the OsmoSampler fluid samples, in order to understand hydrologic processes of the studied subduction zone.

This research was supported by the German Science Foundation (DFG) grants Vi133/4-1, Vi133/4-2, and Vi133/4-3, and by the U.S. National Science Foundation (NSF) grant OCE 0118478. ODP is sponsored by the U.S. NSF and participating countries under management of Joint Oceanographic Institutions (JOI), Inc.

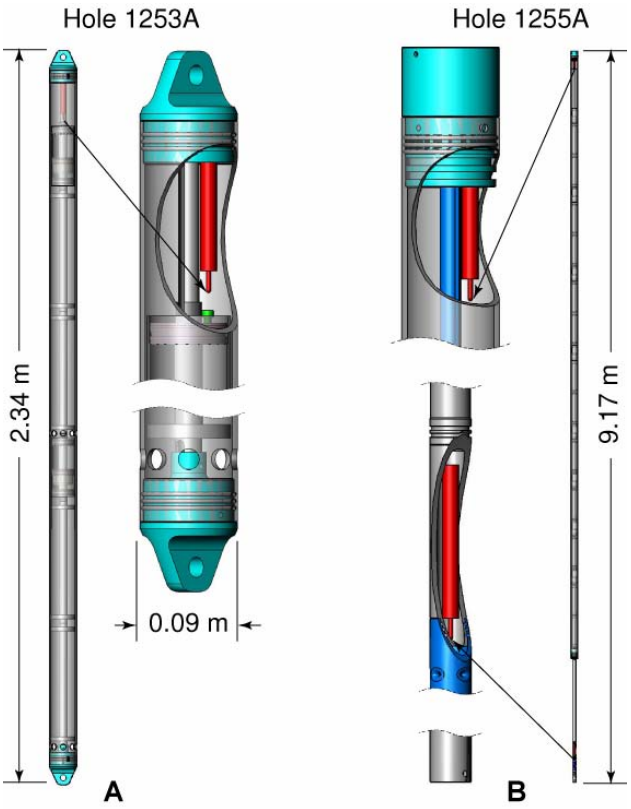

Figure 1: Construction sketches of the OsmoSamplers installed in Hole 1253A (A) and Hole 1255A (B). Hole 1253A contains two identical OsmoSamplers with miniaturized temperature loggers (MTLs) placed in the upper end caps. The OsmoSampler installed in Hole 1255A contains a MTL in the upper end cap and in the probe that samples the décollement zone.

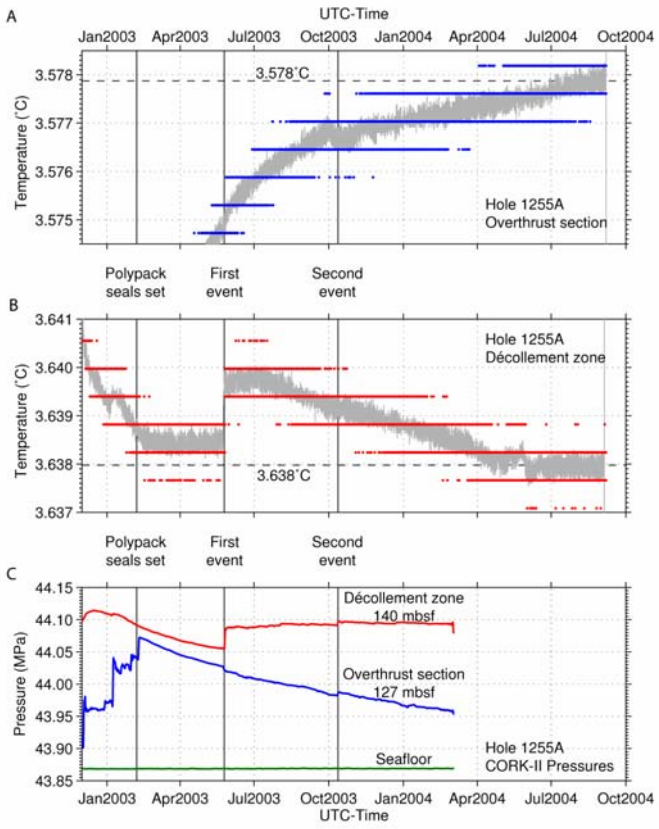

Figure 2: Small scale temperature variations (A, B) and pressure events (C) in Hole 1255A. Most events can be correlated across all data-sets. For example, (1) the setting of the polypack seals, which caused an increase of pressure in the overthrust section and a stabilization of décollement temperatures; (2) the first event," characterized by a sudden increase of pressure as well as temperature in the décollement zone; and (3) the much smaller pressure changes of the "second event" that are hardly seen in either temperature record. At the present time, no pressure data has been downloaded from the CORK-IIs for April-July 2004, when temperatures in the décollement zone start to stabilize after an interim increase during May 2004.

IODP

Testing and Deployment of the New APC3 Tool to Determine In-situ Temperatures While Piston Coring

Martin Heesemann[1], Heinrich Villinger[1], Andrew T. Fisher[2], Anne M. Tréhu[3], and Steffen Witte[4]

[1]Universität Bremen, Department of Geosciences, Klagenfurter Straße, 28359 Bremen, Germany; [2]Department of Earth Sciences, University of California, Santa Cruz, CA; [3]College of Oceanic and Atmospheric Sciences, Oregon State University, Corvallis, OR; [4]ANTARES Datensysteme GmbH, Rudolf-Diesel-Straße 6-8, 28816 Stuhr, Germany; Corresponding author: heesema@uni-bremen.de

During IODP Expedition 311, the third generation advanced hydraulic piston corer temperature (APC3) tool, a new downhole tool to determine in-situ formation temperatures while piston coring, was successfully tested and deployed for the first time. Its development, by a joint German and U. S. team led by H. Villinger and A. Fisher in cooperation with Fa. Antares, was partly driven by the need to replace the APCT tools, which were lost or damaged during many successful deployments. Additionally, many of todays scientific problems require instruments with greater stability, accuracy, measurement frequency, and robustness than available in the past.

Like the earlier generation APC-T tools, the APC3 tool fits in an annular cavity in the APC cutting shoe (Figure 1). Tool electronics are arranged on a cylindrical frame, and sensor and registration prongs extend close to the end and outside edge of the cutting shoe. During standard APC deployment (Figure 2), the drill string is used as a hydraulic accumulator to drive the coring shoe in front of the core barrel 9.5 m into the formation at the bottom of the borehole, well beyond the thermal influence of drilling operations. Following penetration, the core barrel is decoupled from the drill string and the APC3 is left stationary for ~10 minutes. This allows partial equilibration of the formation around the coring shoe and the APC3, including incomplete decay of the thermal disturbance associated with frictional heating during penetration. The coring shoe and core barrel are extracted from the formation and returned to the deck, where communication with the APC3 tool can be established and data are extracted for analysis.

During all 9 deployments the APC3 proved to be very robust, reliable, and user-friendly regarding its mechanics, electronics, and operation software. Therefore, the test deployments provided not only information to evaluate the performance of the tool, but also temperature data that was particularly important for achieving the objectives of the Expedition. Moreover, it could be demonstrated that the APC3 is capable of measuring temperatures with a resolution and an absolute accuracy (depending on careful calibration) of ~1 mK at a sampling interval of 1 s. Compared to the previous generation APCT, it was possible to increase the resolution as well as the absolute accuracy of the tool by at least one order in magnitude.

This research was supported by the German Science Foundation (DFG) grants Vi 133/9-1 and Vi 133/9-2, by the U.S. National Science Foundation (NSF) grant OCE-0326699 to UCSC (ATF) and by JOI/IODP (AMT).

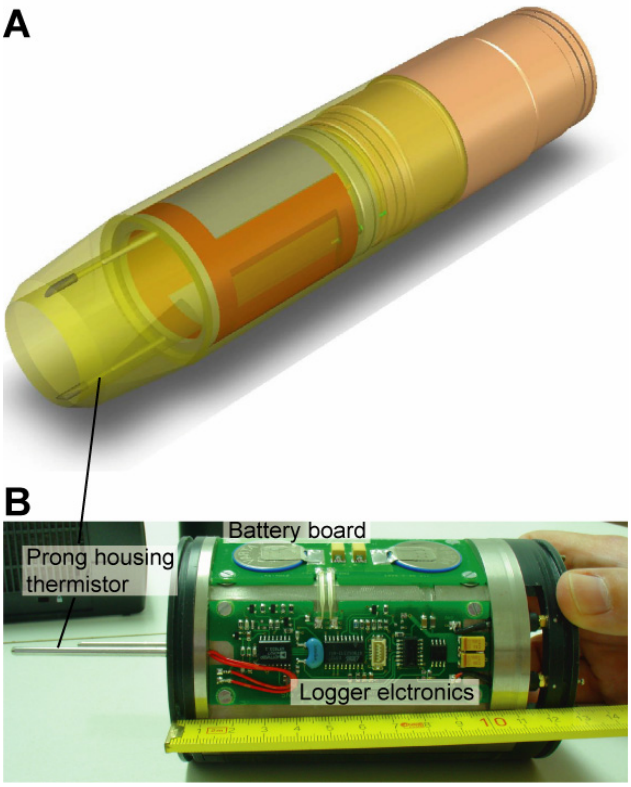

Figure 1: A. Mechanical design of the APC cutting shoe. B. APC3 electronics mounted on a cylindrical frame that fits the annular cavity of the cutting shoe.

Figure 2 [next page]: A. Complete temperature record of a typical APC3 deployment. Firstly, the APC3 is powered on in the lab (1) and lowered down (2) the water column inside the drill string. Then the tool stops (3) at the mudline, to establish a reference temperature for comparison with other downhole temperature. Since temperature variations during this stop are in the order of 0.1˚C (B), this comparison does not replace a proper calibration of all tools, but it can help to reveal major intertool calibration problems. After the stop above mudline, the APC3 is lowered down the hole and briefly stopped at the bit near the bottom of the hole (4), before the coring shoe (5) penetrates the formation in ~5 s (C). While the cutting shoe is held in the formation, the temperature peak, caused by frictional heating, (6) decays slowly, and measured temperatures approach the undisturbed formation temperature. When the decay is interrupted after 6-10 min by the tool extraction, the measured temperature has not reached thermal equilibrium with the surrounding formation, however, the remaining decay rated has decreased to ~1 mK/s (D). Following the (7) extraction of the APC3 from the

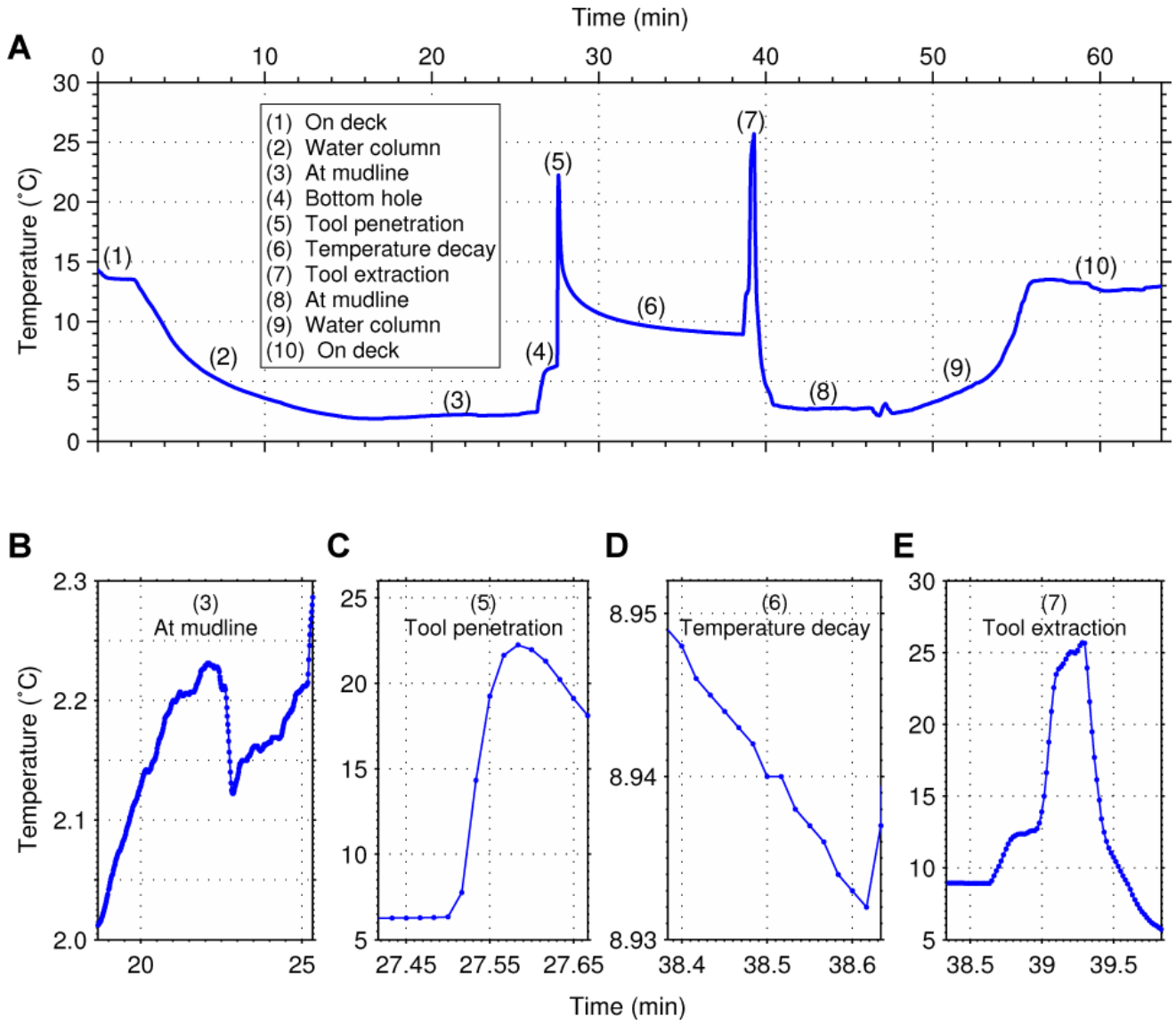

formation, which also causes frictional heating (E), the tool is once again stopped (8) at the mudline, before it is carried up through the (9) water column and recovered on deck (10). Note, that the details of some important stages of the deployment (B-E) are shown at differing time and temperature scales.

ICDP

The 2005 World Stress Map database release

Oliver Heidbach, John Reinecker, Mark Tingay, Birgit Müller, Blanka Sperner
Geophysical Institute, University of Karlsruhe, Germany; Heidelberg Academy of Sciences and Humanities, Germany

Knowledge of the stress state in the Earth's crust is a key issue for understanding geodynamic processes as well as for practical applications in seismic hazard assessment or stability considerations of underground openings such as mines, tunnels, wells, sites of waste disposal. Since 1986, the World Stress Map (WSM) project is a collaborative project between academia, industry and governmental organisations that aims to build a comprehensive global database of contemporary tectonic stress information in order to understand the state and sources of stress in the Earth's crust. Since 1995 the WSM is a research project of the Heidelberg Academy of Sciences and Humanities located at the Geophysical Institute of Karlsruhe University in Germany. Updates of the first release of the WSM database in 1992 have been made available in 1997, 2000, 2003, 2004, and the latest in December 2005. The total number of stress datasets has increased from ~7300 in 1992 to almost 16,000 in the 2005 WSM database release. Much of this newly added data has been obtained in regions where data was previously sparse or absent, such as in Eastern Europe, Australia and SE Asia. Furthermore, large amounts of new data have been collected in regions with significant datasets, such as sedimentary basins, providing new insights from regional to local scale stress fields.

The present-day stress orientation is estimated primarily from earthquake focal mechanism solutions, borehole breakouts and drilling-induced fractures (from borehole image or multiarm caliper log data), in-situ stress measurements (overcoring, hydraulic fracturing) and geological indicators (fault slip, volcanic vent alignment). The stress indicators differ in rock volume involved, depth and measurement technique. The stress information of the different types represent various crustal rock volumes and depth intervals. The minimum information for each stress dataset in the WSM is the azimuth of the maximum horizontal stress (SH), quality of the SH azimuth, the type of stress indicator, the locality in geographical coordinates, the depth of the measurement, the tectonic stress regime, and the reference for the data.

The success of the WSM is based on making information from different stress indicators comparable following a standardized quality-ranking scheme for all stress indicators, which is internationally accepted as the global reference and guarantees

reliability and global comparability of the stress data. All information in the WSM database is public and compiled in a standardized format and are provided electronically in three different formats on the website (http://www.world-stress-map.org): ASCII (wsm2005csv.zip), Excel spreadsheet (wsm2005xls.zip) and dBase (wsm2005dbf.zip). Via the website, software tools to interpret and display the stress data in terms of stress maps are provided. The web based database interface CASMO (Create A Stress Map Online) allows for custom building of individual stress maps. Alternatively the software CASMI (Create A Stress Map Interactively) a program for UNIX/LINUX operating systems is downloadable from the website, it provides additional display features.

For the forthcoming 2006 release we focus on three issues: (1) refined quality assessment for focal mechanism solutions, borehole breakouts and hydro fractures. (2) Continuation of the 2005 initiative to improve WSM for the petroleum industry needs (3) investigation of data from broadband stations and inclusion of the first test data which are available for the southern Africa rift system.

ICDP

First Geothermal Measurements in the ICDP Chesapeake borehole (Eyreville, Virginia)

P. Heidinger[1], H. Wilhelm[1], H. Burkhardt[2], J. Safanda[3]
[1]Geophysical Institute, University of Karlsruhe; [2]Institute of Applied Geosciences, Section Applied Geophysics, Technical University of Berlin; [3]Geophysical Institute, Czech Academy of Sciences, Prague

The Chesapeake Bay impact structure is a late Eocene complex crater which was excavated ~35 Ma ago by a comet or asteroid in a continental shelf environment on the Atlantic margin of Virginia. It is the largest impact crater in the USA and the seventh largest on Earth. It has an average diameter of ~85 km around its centre near Cape Charles. The ICDP drill hole is situated on the central uplift of the crater.

Drilling of the hole Eyre-B started on September 12, 2005 and ended on December 4, 2005 at 1766.3 m depth. After the mud circulation had stopped, first temperature measurements were recorded from the bottom of the hole upwards by the USGS logging tool. Then the Karlsruhe University logging tool, which had been shipped to Norfolk harbour in November 2005 and started high resolution temperature (HRT) measurements from the top downwards. The logging was interrupted when the tool crashed at 780 m depth. After repair, a complete temperature profile was measured to 1400 m depth on December 6. In order to stop the artesian flow which had started immediately after the stop of circulation the well head was closed afterwards. On December 9 the well head pressure amounted to ~1.9 bar. After reopening of the well head, another temperature profile was recorded down to the end of the casing at 1130 m depth, because the lower open part was no longer accessible. After closing the well head the pressure raised to 2.13 bar.

In order to obtain a temperature profile, which is not disturbed by the artesian flow, it is necessary to stop this flow e. g. by a pipe erected above the well or a riser, through which the temperature can be logged. This experiment is envisaged for the end of March. Some kilometers away from the hole Eyre-B a test well STP2 has been drilled by USGS. The general lithology of this 823 m deep well and the resistivity and water salinity logs recorded in a 700 m deep groundwater observation well installed within the test hole has been published in EOS 85, no.39, 28 September 2004. Fortunately this hole was still accessible and not artesian. In this well the temperature could be recorded yielding an undisturbed profile with hydraulically interesting features. This profile can serve as a reference to the future temperature measurements in the ICDP Eyre-B hole.

The Eyre-B cores are not yet fully described. The present state is available at the corresponding ICDP website http://www.icdp-online.org/sites/chesapeake/news/news.html.

Our project was initiated by H. Burkhardt. It aims at describing the petrophysical and present geothermal conditions in the centre of the Chesapeake impact structure. The geothermal investigations will as well contribute to the study of the hydraulic regime of the impact structure which is one of the essential research aims of the ICDP Chesapeake drill hole.

We are grateful to Greg Gohn from USGS and his colleagues for technical support and administrative advice serving our intention to perform HRT measurements in the ICDP Chesapeake borehole.

IODP

Modes of fluid expulsion and its significance for forearc dewatering - IODP drilling proposal 633 to decipher deep fluid processes at an erosive convergent margin

Christian Hensen and Warner Brückmann
Leibniz Institut für Meeresforschung, IFM-GEOMAR, Kiel & 633-Proponent Group*

The active continental margin off Costa Rica and Nicaragua comprises a unique set of geological features that provide insight into deep fluid processes. The migration of fluids appears to be a major factor governing the evolution of the erosive convergent margin off Central America. Most free water along the plate boundary comes from dehydration of subducting sediments from depths >10km. The thermal structure of the subducting plate determines the area where the mineral-bound water is released. Extensional faulting caused by the collapse of the margin promotes the upward migration of these deeply rooted fluids. As much as 90% of the water provided by minerals in subducting sediment may be recycled into the ocean through mid-slope seepage related to mud volcanism and diapirism. Numerical modelling of ODP 170 data demonstrated that obviously only a small volume is transported along the décollement towards the deformation front.

Major sites of dewatering are mounds, positive sea floor anomalies, which are related mud diapirism/volcanism and precipitation of authigenic carbonates, and large-scale slides related to the subduction of seamounts. Vent fluids are characteristically depleted in chloride. Oxygen and hydrogen isotope ratios, thermogenic methane as well as elevated heat flow demonstrate that the fluid flow is initiated by smectite-illite transformation in the subducting sediments. Conspicuous differences in the geochemical composition allow a subdivision of a southern and a northern type of fluids, which may reflect differences in the input or a general south to north decrease in flow rates. Fluids of the southern type are enriched in boron and typically rise at high rates. In contrast, the northern type of fluids is strongly enriched in calcium and barium, which points to significant alteration along the flow path.

Convergence related seamount subduction and subduction-erosion are the primary reasons for slope instability, resulting in large-scale deformation structures. Fluid expulsion related to seamount subduction is largely unconstrained at present. Whereas seeps are rare at the top of the uplifted sediment bulge, massive discharge of methane-rich fluids is documented by lush tubeworm communities and significant methane plumes at the scarp planes. Recent estimates reveal that up to 65 Mg of methane per year may be released at a single structure, which may prove them as important as the mound structures in terms of fluid recycling.

In order to improve our current understanding of fluid recycling, to constrain long-term estimates of fluid flow, to systematize the variability of fluid geochemistry, and to fully understand the role of seamounts in the forearc it is proposed to drill several key sites of the most prominent dewatering structures within IODP.

IODP drilling 633-Full-2 proposes to drill sites of active fluid dewatering in order to elucidate fluid flow processes and constrain dewatering budgets at an erosive continental margin. The approach is based on a number of successful campaigns in the framework of

the collaborative research project (SFB) 574 at Kiel University and related projects offshore Central America margin over the last decade.

Drilling information is needed to understand the interrelationship between deformation and fluid generation in an erosive margin setting. The suggested drilling will not only improve our understanding of processes controlling and driving fluid flow, but also constrain volatile and material budgets of the erosive subduction system. In general, the following major hypotheses are to be tested:

- Mud diapirism/volcanism is a major dewatering pathway and provides a window into deep fluid processes.
- Seamount subduction creates major pathways for deep fluid advection and canalization.
- Release of deep, freshened fluids controls mud mobilization and hence the formation of the mounds and their internal build-up.

The selected mound-sites at Mound Culebra and Mound 11 are both clearly related to deep reaching fault systems, but show general differences in terms of their activity and stage of development. The proposed drill sites are chosen to penetrate below BSR depth in order to record changes in fluid geochemistry and microbiology along the flow path and hence, constrain preliminary estimates of the source depth of fluids and extruded material. Complementary, shallow holes at these sites will help to gather necessary data that will improve our understanding of mound hydrology (i.e. flow rates and development of shallow convection cells) and history of the mound build-up and consolidation (i.e. mud flows and authigenic carbonates).

At the selected target site to study seamount subduction, Jaco Scar, there is evidence for fluid flow as detected by geochemical anomalies in scar sediments and prominent methane plumes in the water column. Drilling of the proposed seamount site at Jaco Scar will give unequivocal evidence for the creation of deep-reaching conduits driven by the deformation of upper plate sediments and the continental basement wedge.

It is proposed to equip the 3 deep drill holes at Mound Culebra, Mound 11, and Jaco Scar with conventional CORKs for long-term observation of fluid geochemistry, heat flow and their relation to trigger mechanisms of seismic activity.

The Pacific margin offshore Costa Rica is one of the best-studied continental margins worldwide and processes observed here might be representative for erosive continental margins in general. Hence, the proposed drilling sites offer the unique opportunity to calculate real mass budgets of forearc recycling of fluids and volatile elements. This knowledge is of key importance in terms of a better understanding of the role of subduction zone processes in global biogeochemical cycles.

***633-Full-2 Proponent Group**

Noemi Fekete, Timothy Ferdelman, Andy Fisher, John C. Fry, Ingo Grevemeyer, Matthias Haeckel, Bo Barker Jørgensen, Sumito Morita, Tobias Mörz, Christian Müller, John Parkes, César R. Ranero, Timothy Reston, Volkhard Spiess, Ken Takai, Asrar Talukder, Klaus Wallmann, Andrew J. Weightman

IODP

Cyclic sedimentation processes and diagenetic alteration recorded in a deep-sea sediment drift (Antarctic Peninsula Pacific Margin)

D.A. Hepp[1,2], T. Mörz[2], J. Thiede[3] and W.-C. Dullo[4]
[1]Faculty of Geosciences, Bremen University, [2]Research Center Ocean Margins (RCOM), University Bremen, [3]Alfred Wegener Institute for Polar and Marine Research, Bremerhaven, [4]Leibniz-Institute of Marine Science (IFM-GEOMAR), Kiel - E-mail: dhepp@uni-bremen.de

Drift sediments are excellent archives for shelf ice dynamic signals. The sedimentary proxies are controlled by several geophysical and geochemical processes during and after sedimentation.

A series of eight sediment drifts on the upper continental rise of the western Antarctic Peninsula is directly associated with the glacial morphology of the outer continental shelf (Fig. 1). These sediment drifts are part of a complex glacial sedimentary feeder system composed of lobes and troughs on the outer shelf, a steep slope (average 16˚), and deep-sea channels separating the drifts on the upper rise. The channel system, separating the drifts from each other and the continental slope, is formed by downslope turbidity currents and alongslope bottom currents.

The drifts are primarily composed of fine-grained components from turbidity currents. Fine silt laminae, primarily observed in cores from distal drift sites, are interpreted as turbiditic spillover depositions from turbidity currents, channelled along the bathymetric depressions between the drifts.

We used sediment physical, geochemical records and x-ray images derived from Drift 7 (ODP Leg 178 Site 1095; Fig. 1) to show characteristics in glacial-interglacial cyclicity and associated sedimentary processes during Pliocene.

The data from three time sections of the uppermost early Pliocene (~3.6-3.8 Ma), middle early Pliocene (~4.0-4.2 Ma), and lowermost early Pliocene (~5.1-5.2 Ma) display two boundary types dividing half-cycles (Fig. 2):

Interglacial-to-glacial transition (IGGT) is distinct and characterized by a sharp decline in sediment lightness, an abrupt increase in Ca, magnetic susceptibility and bulk density and moderate decline in Fe values. This is expressed lithostratigraphically by an abrupt end of IRD and bioturbation at the IGGT and the onset of frequent silt lamination directly above. This drastic change is clearly displayed in x-ray images.

Glacial-to-interglacial transition (GIGT) is diffuse and characterized by a gradual decline in sediment bulk density but prominent changes in color reflectance a*, Fe, Ti and Ca. Consistently, all GIGT's are accompanied by a minima zone in magnetic susceptibility which comprises the upper portion of glacials and lower portions of interglacials. The diffuse character of this transition is lithostratigraphically expressed by a gradual onset of IRD across the GIGT and a synchronous decay in silt laminae frequency.

The GIGT accompanied by a minima zone in magnetic susceptibility (MMZ). This minima zone comprises the upper portion of glacials and lower portions of interglacials and is linked to diagenetic alterations that transform magnetic iron minerals to paramagnetic minerals.

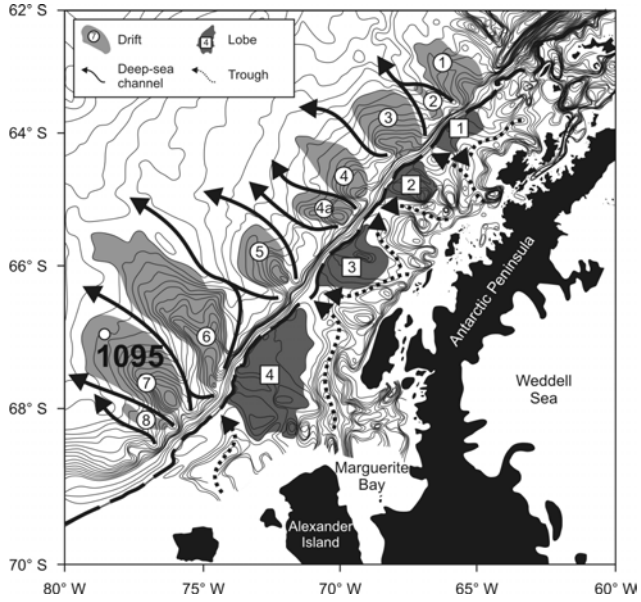

Fig. 1 Bathymetric map of the Antarctic Peninsula Pacific margin with ODP Leg 178, Site 1095 (modified after Lucchi et al., Mar. Geol. 189, 2002, Rebesco et al., Terra Antart. 5, 1998 and Rebesco et al., in: Deep-water contourite systems, 2002).

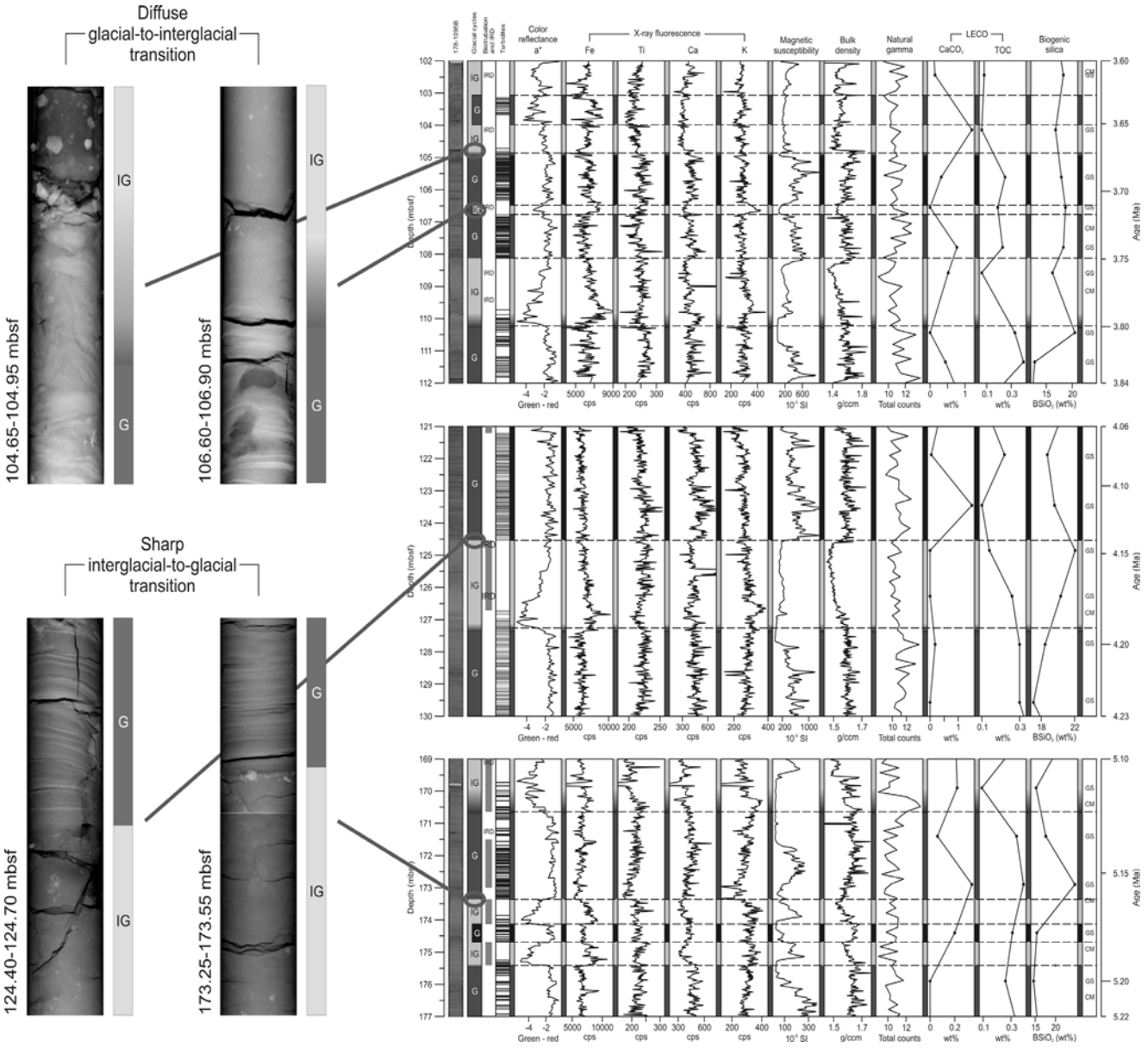

Fig. 2. Comparison of visual description, color reflectance, XRF, logging and biostratigraphic data from the (a) uppermost early Pliocene (~3.6-3.8 Ma), (b) middle early Pliocene (~4.0-4.2 Ma), and (c) lowermost early Pliocene (~5.1-5.2 Ma). The data show characteristic patterns of GIGT and IGGT (CM = clay minerals, G = glacial, GS = grain size, IG = interglacial, IRD = ice rafted debris). X-ray images show two characteristic types of glacial-interglacial boundaries: (a) a gradual decay of turbidite events vs. increase of IRD supply at GIGT, and (b) a sharp boundary dividing interglacial IRD supply from glacial turbidite events at IGGT. The IRD layer shown in image top left is interpreted as ice sheet collapse zone.

The nearly complete loss of magnetic susceptibility is coupled with glacial controlled cyclic decreases in sedimentation rate. We assume that this loss is caused by the anaerobic oxidation of methane (Fig. 3). This process leads to a depletion of sulfate at the sulfate/methane transition (SMT) and the alteration of iron oxides to iron sulfides. The MMZ is especially prominent in sections with a drastic decrease in sedimentation rate, which causes a stagnation of the SMT. This stagnation effects an enhanced diagenetic dissolution of ferromagnetic iron minerals within the sulfidic zone. A similar coherence between magnetic susceptibility low zones and diagenetic alteration is described for the western Argentine Basin (Riedinger et al., Geochim. Cosmochim. Acta 69, 2005). This area is characterized by highly dynamic depositional conditions. The MMZ in the investigated sites correlates with the recent position of the SMT. Linear profiles of sulfate pore water concentrations indicate constant low sedimentation rates for this periods of time and modeling of geochemical data suggest that the magnetic record is highly influenced by a drastic change in mean sedimentation rate.

Acquisition of additional pore water analyzes for ODP Leg 178 Site 1095 is not possible due to the storage time of seven years. Available shipboard data of methane and sulfate concentrations show down core trends and the position of the recent SMT, but sample intervals of 10 m are not sufficient for detailed analyzes on cycle scale. However, there is another way to locate the impact of diagenetic processes by paleoceanographic proxies of barium or barite (Fig. 3). The accumulation of solid phase barium is a proxy for productivity. The amount of barium in the sediment is dependent on the decay of organic matter in the water column. The diagenetic process of the AOM leads to the alteration of the primary barium signal. Dependent on the organic reservoir within the sedimentary sequence the alteration of barium signals can occur in greater sediment depths, where a complete depletion of sulfate promotes the remobilization of biogenic barium.

[Figure 3 next page]

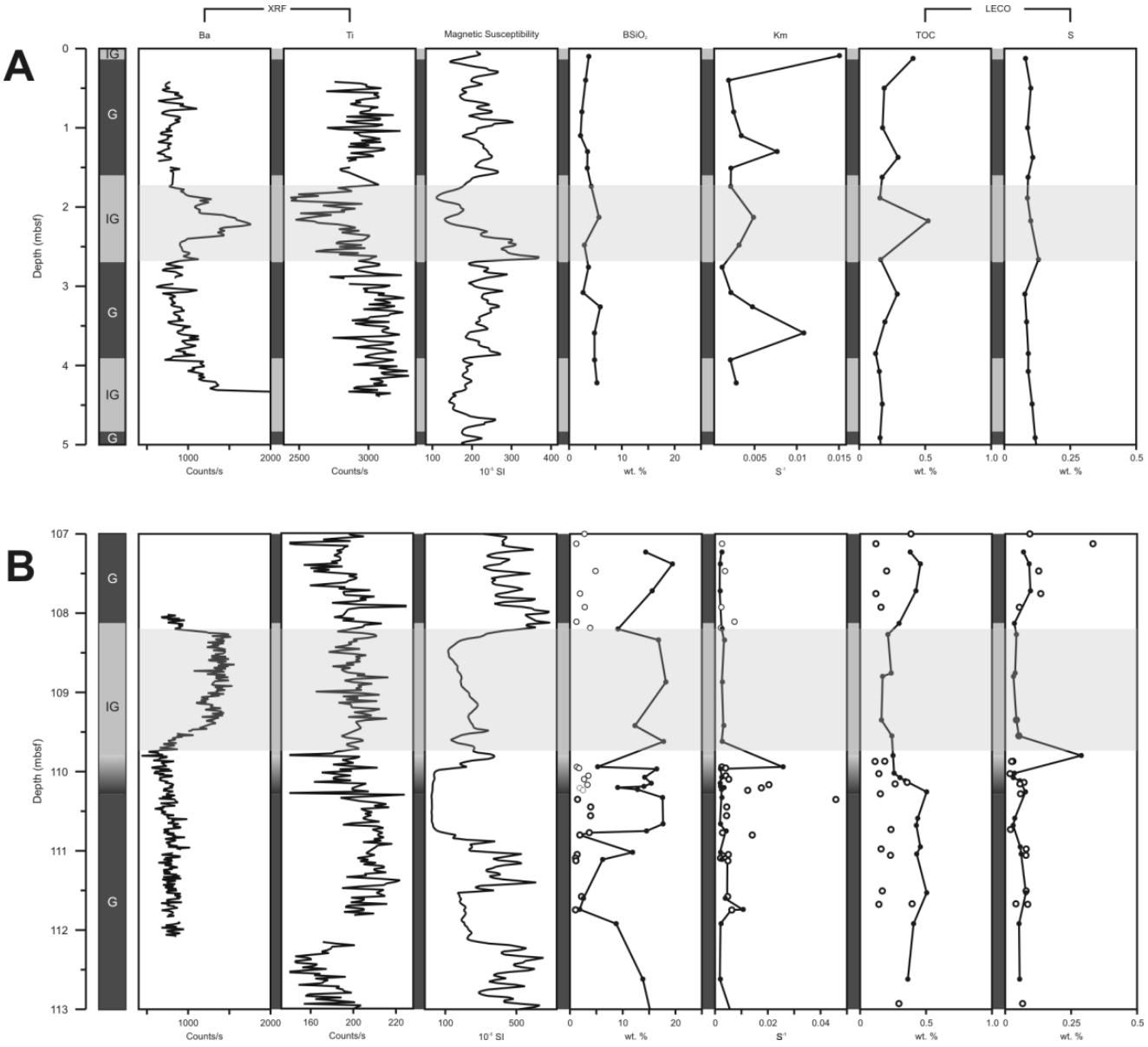

Fig. 3. Comparison of ODP Leg 178 Site 1095 core sections (A) with (at 0-5.0 mbsf) and (B) without (at 107.0-113.0 mbsf) minima zones. The light grey bar marks the barium peak. White circles shows turbidite samples and filled circles shows hemipelagic samples.

IODP

Authigenic barite formation triggered by black shale-fueled anaerobic oxidation of methane in the deep biosphere of ODP Leg 207

A. Hetzel[1], M.E. Böttcher[2,3], S. Arndt[1,4], M. Prieto[5], M. Gehre[6], H.-J. Brumsack[1]
[1]Institute for Chemistry and Biology of the Marine Environment, University of Oldenburg, P.O. Box 2503, D-26111 Oldenburg, Germany, (hetzel@icbm.de), [2]Max Planck Institute for Marine Microbiology, Celsiusstr.1, D-28359 Bremen, Germany, [3]Leibniz Institute for Baltic Sea Research, Seestr. 15, D-11815 Warnemünde, Germany, [4]Department of Earth Sciences, Utrecht University, P.O. Box 80.021, 3508 TA Utrecht, The Netherlands, [5]Departamento de Geología. Universidad de Oviedo C/Jesús Arias de Velasco, s/n. 33005-Oviedo, Spain, [6]UFZ Leipzig-Halle, Permoserstr. 15, D-04318 Leipzig, Germany

Biogenic barite in sediments is often used as a paleoproductivity-proxy. High productivity results in organic-rich sediments characterized by sulfate depletion due to microbial sulfate reduction during decomposition of organic material. Deeply buried Cretaceous black shales at Demerara Rise (ODP Leg 207, tropical Atlantic) provide a suitable substrate for ongoing metabolic activity in a deep biosphere several hundred meters below the present sediment surface. In this study we identify those processes that take part in the formation and modification of barite in the sediment column. Inorganic and stable isotope geochemical investigations were carried out on pore waters, bulk sediments and separated barites. The microbially driven pore water-sediment interaction forms the basis for diagenetic modeling.

High methane in combination with low sulfate concentrations indicate that organic matter degradation is still on-going in the deep-seated black shale sequence deposited almost 100 Ma ago. Upward diffusing microbial methane as well as downward diffusing sulfate are totally consumed in the course of anaerobic oxidation of methane (AOM). The lack of pore water sulfate within the black shale sequence promotes the remobilization of biogenic barite. Dissolved barium is diffusing upwards and reprecipitates as authigenic barite. The process is identified by the co-enrichment of heavy S and O isotopes. Different Ba/Sr ratios in the barite concretions indicate dynamics in pore water gradients in the course of diagenetic crystallization. Barite dynamics are controlled by the availability of sulfate and the rate of AOM, and thus by the upward flux of microbial methane from the black shale unit. The degradation of organic matter is the driving force behind these processes. We suggest that coexisting isotopically heavy barite and pyrite may serve as a new proxy for the occurrence of AOM.

IODP

Depositional environment of Cenomanian/Turonian black shales from Demerara Rise (ODP Leg 207) - Implications from trace metal patterns

A. Hetzel[1], A. Forster[2], H.-J. Brumsack[1]
[1]Institute for Chemistry and Biology of the Marine Environment, University of Oldenburg, P.O. Box 2503, D-26111 Oldenburg, Germany, (hetzel@icbm.de), [2]Royal Netherlands Institute for Sea Research (NIOZ), P.O. Box 59, 1790 AB Den Burg, Texel, The Netherlands

During ODP Leg 207 relatively expanded, shallowly buried Cretaceous sediments were recovered from Demerara Rise off Suriname, South America. Multiple sequences of Cenomanian and Turonian black shales evidence varying levels of bottom water dysoxia and/or enhanced surface water productivity. Under severe oxygen-depleted conditions, several redox-sensitive or sulfide forming elements are enriched within the sediments. Therefore, the C/T boundary (OAE 2) is characterized by a specific distribution pattern of diagnostic metals. It is suggested that trace metals provide useful information when reconstructing paleoenvironmental conditions.

High-resolution profiles for major as well as selected minor elements were investigated from black shale sequences of Sites 1258 and 1260, including the C/T-boundary, which is marked by a positive $\delta^{13}C_{org}$-excursion.

Element enrichment patterns indicate high bioproductivity comparable to recent coastal upwelling settings. An extended intense oxygen-minimum-zone (OMZ) is indicated by extremely low Mn/Al ratios. Chemical changes in the depositional environment during the OAE 2 are suggested from elevated Fe/Al and Co/Al values within the C/T interval, while above and below the C/T interval ratios are constant (close to average shale). This indicates euxinic conditions in the water column (sulfide forming) and at the same time reductive Fe and Co mobilization in oxygen-depleted nearshore sediments during OAE 2.

Beside these implications for the local depositional environment at Demerara Rise, the analysis of the trace metal (TM) profiles reveal information about the impact of global black shale deposition during the C/T event: Mo/Al, V/Al, and Zn/Al ratios are generally high throughout the analyzed sequence, but a significant depletion is notable exactly within the C/T interval. This depletion in TM/Al ratios may reflect the expansion of euxinic depositional areas during the event. Because hypoxic or even euxinic environments form a significant sink for TM in seawater, the global onset of black shale formation, particularly during OAE 2, led to a rapid drawdown of the seawater TM reservoir causing the decline in TM enrichment in Demerara Rise strata.

IODP

Carbon isotopic compositions of volatile fatty acids as proxies for biogeochemical processes in the deep marine biosphere

V. Heuer[1], M. Elvert[1], S. Tille[1], N. Finke[2], and K.-U. Hinrichs[1]
[1]Organic Geochemistry Group, DFG-Research Center Ocean Margins & Dept. of Geosciences, University of Bremen, P.O. Box 330 440, D-28334 Bremen, Germany; [2]Max Planck Institute for Marine Microbiology, Celsiusstr. 1, D-28359 Bremen, Germany

The Ocean Drilling Program has demonstrated the presence of viable microbes in sediments as deep as 800 mbsf. Considering the broad range of temperatures and pressures and the recalcitrant character of organic material in deep marine sediments, the existence and survival of an extensive deep marine biosphere is remarkable and poses basic questions for biochemistry and microbial ecology. However, biological activities appear to be generally low and studies oriented towards simulating the in situ processes in laboratory-based experiments are sometimes at the limit of their applicability.

Alternative approaches are needed and one option is to use the information encoded in the stable carbon isotopic composition of organic molecules as indicator of processes in situ. For low-molecular-weight metabolites, $\delta^{13}C$ values are routinely acquired for methane and used to examine details of its production and consumption. Likewise, $\delta^{13}C$ values of acetate, a ubiquitous intermediate in anaerobic metabolism, are potentially powerful probes to decipher the dominant carbon-transforming processes in situ. However, data on the isotopic composition of acetate and volatile fatty acids (VFAs) in natural environments is very rare.

The lack of information about carbon isotopic variations of VFAs in natural environments is due to a lack of methods suitable for their analysis at typical natural concentrations (i.e., molar in sediment pore-waters). We have developed a new analytical protocol for sensitive and accurate carbon isotopic analysis of VFAs by isotope-ratio-monitoring liquid chromatography/mass spectrometry (irm-LC/MS) (Heuer et al., in prep). This technique is based on the new Finnigan™ LC IsoLink interface that couples an HPLC to commonly used irm-MS-systems (Krummen et al., 2004). Our technique extends the previously accessible concentration range to lower concentrations and minimizes the required sample volume to 1-3 mL. The fully automated online operation allows for analysis of large sample sets.

We will present results from our systematic analysis of natural sediment/pore-water systems in coastal, open-ocean, and deeply-buried sedimentary environments. Our database on VFA isotopic composition reveals significant variability of $\delta^{13}C$-acetate values in different geochemical regimes. For acetate, we observe a carbon isotopic range from ~ 5 to 85‰, i.e., a similarly large range as known from methane. Highest values are associated with acetate consumption by acetoclastic methanogenesis while low values of ~ 50‰ are linked to autotrophic production of acetate. A special case are samples from a methane seep environment where cycling of strongly ^{13}C-depleted carbon appears to affect the acetate pool, resulting in $\delta^{13}C$ values as low as 85‰. Our findings demonstrate that carbon isotopic compositions of VFAs are highly sensitive to various biogeochemical processes and can aid elucidation of carbon-flow patterns in microbial ecosystems.

Heuer, V., M. Elvert, S. Tille, X. Prieto Mollar, L. Hmelo, M. Krummen, and Kai-Uwe Hinrichs (in prep): Online ?13C analysis of volatile fatty acids in sediment/porewater systems by liquid chromatography-isotope ratio-mass spectrometry. Limnology and Oceanography: Methods.
Krummen, M., Hilkert, A.W., Juchelka, D., Duhr, A., Schlüter, H.-J., Pesch, R., (2004). Rapid Communications in Mass Spectrometry, 18, 2260-2266.

IODP

Marine Diatomeen im Paläozän des SW - Pazifik, - Dokumentation des Produktivitätsmaximums

U. Hoff, Universität Hannover, Insitut für Geologie u. Paläontologie, Callinstr.30, 30167 Hannover + BGR Hannover, Stilleweg 2, 30655 Hannover
J.M. Fenner, BGR, Stilleweg 2, 30655 Hannover

Ein 30m langes Kerninterval aus dem Ober-Paläozän von ODP Bohrung 1121B, am Fuß des Campbell Plateaus, enthielt gut erhaltene Vergesellschaftungen marin planktonischer Diatomeen. Eine genaue taxonomische Analyse zusammen mit einer quantitativen Analyse der Artenhäufigkeiten sowie ein Vergleich mit existieren Ergebnissen zu den stabilen Kohlenstoff- und Sauerstoffisotopen ergab, dass das Intervall, in dem die Diatomeen am häufigsten sind und am besten erhalten sind, mit dem tertiären Produktivitätsmaximum im Ober-Paläozän zusammenfällt. Während dieses Produktivitätsmaximums nehmen wie zu erwarten die Dauersporen von für Hochproduktionsbedingungen typischen planktonischen Arten zu, korreliert mit den $\delta^{13}C$- Werten. Unter den die Vergesellschaftung dominierenden neritischen Arten sind die zwei Hauptgruppen: Stephanopyxis turris - Gruppe und Hemiaulus polymorphus - Gruppe invers mit einander korreliert. Die Dominanz der neritischen Diatomeen in diesen Tiefsee Sedimenten ist damit zu erklären, dass während des Paläozän ein breiter Schelf existiert hat, und die schon damals in dieser Region wirksamen Westwinde dieses Plankton ostwärts über die Kante des Campbell Plateaus verdrifteten, so dass diese neritischen Arten

verstärkt am Fuße des Plateaus in der Tiefsee zur Ablagerung kamen. Trotz des Meeresspiegelrückganges muß die Schelffläche während des Produktivitätsmaximums doch erheblich gewesen sein, denn benthische Arten und Süßwassereintrag sind in den untersuchten Proben praktisch nicht zu finden.

IODP

Impacts of orbital forcing and atmospheric CO_2 on Miocene global cooling

Ann Holbourn[1], Wolfgang Kuhnt[1], Michael Schulz[2] and Helmut Erlenkeuser[3]
[1]Institute of Geosciences, Christian-Albrechts-University, D-24118 Kiel, Germany (ah@gpi.uni-kiel.de); [2]Department of Geosciences and Research Center Ocean Margins, University of Bremen, Postfach 330 440, D-28334 Bremen, Germany; [3]Leibniz Laboratory for Radiometric Dating and Stable Isotope Research, Christian-Albrechts-University, D-24118 Kiel, Germany

About 13.9 million years ago, the Earth's climate cooled dramatically after an extended period of relative warmth. This key transition in Earth's climatic and biotic evolution, which marked the final stage of stepwise Cenozoic cooling, remains one of the most enigmatic episodes in Earth's Cenozoic climate history. High resolution time series spanning this critical climatic transition have remained extremely scarce, because sedimentary successions have all too often been strongly affected by carbonate dissolution or burial diagenesis or proven incomplete due to radical changes in ocean circulation. A further difficulty resides in the uncertainty in dating and inter-correlating records across basins, because age models for this time interval relied mainly on sparse biostratigraphic and magnetostratigraphic datums that were not directly calibrated to an astronomical timescale (Lourens et al., 2004). Yet, the middle Miocene offers a most tantalizing glimpse into a long and substantially warmer climate phase with much reduced ice-sheets, which ended with drastic global cooling. A better understanding of this interval will provide new insights into the climate dynamics of warm periods and the processes driving climate change, as well as help constrain modeling studies of past and future climate.

We present benthic foraminiferal oxygen ($\delta^{18}O$) and carbon ($\delta^{13}C$) isotope (4-5 kyr resolution) and x-ray fluorescence scanning (XRF) records (1 kyr resolution) in complete middle Miocene sedimentary sequences recovered at ODP Site 1146 (South China Sea; water depth: 2092) and Site 1237 (SE Pacific; water depth: 3212 m). We revised the 1146 and 1237 shipboard biostratigraphy, based on higher resolution sampling and ages derived from the new Neogene timescale ATNTS2004 (Lourens et al., 2004). The revised age models provided the framework to generate orbitally-tuned chronologies in Sites 1146 and 1237 for the interval 12.7-16.7 Ma (Holbourn et al., 2005; Figs. 1-2). Astronomically-tuned chronologies were developed by correlating the benthic $\delta^{18}O$ record in each site and the XRF Fe record in Site 1237 to computed variations of the Earth's orbit and solar insolation (obliquity and eccentricity in Laskar et al., 2004). These new chronologies permit correlations at unprecedented time resolution across the East-West Pacific.

Our results indicate that a conjunction of climatic forcing factors ultimately triggered middle Miocene ice-sheet expansion and global cooling at ~ 13.9 Ma (Holbourn et al., 2005). Using new chronologies, we found relatively constant low summer insolation over Antarctica coincident with declining atmospheric carbon dioxide levels at the time of Antarctic ice-sheet expansion and global cooling, suggesting a causal link. We infer that the thermal isolation of Antarctica played a role in providing sustained long-term climatic boundary conditions propitious for ice formation. Our data document that Antarctic ice-sheet growth was rapid, taking place within two obliquity cycles, and coincided with a striking transition from obliquity to eccentricity as the drivers of climatic change (Fig. 1). In short, our study demonstrates that the middle Miocene glacial expansion and global cooling were (i) associated with a transition from a 41-kyr to a 100-kyr world, (ii) probably triggered by a time period with low variation in orbital forcing and (iii) closely linked with major fluctuations of the global carbon cycle.

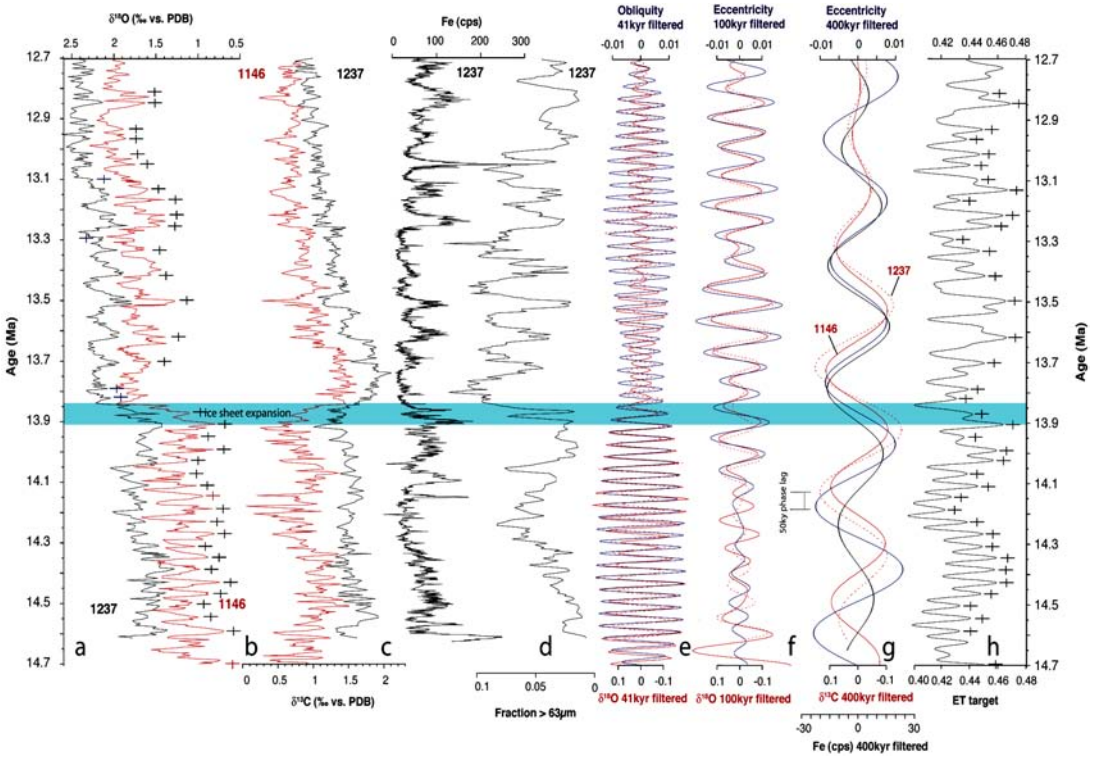

Fig. 1 Paleoceanographic records from ODP Sites 1146 and 1237 indicate that Earth's orbital configuration was the prime pacer of middle Miocene climate change. (a) Benthic foraminiferal 18O (age control points marked by crosses). (b) Benthic foraminiferal 13C. (c) Site 1237 iron content. (d) Site 1237 proportion of coarse fraction reveals increased carbonate preservation during colder periods after 13.9 Ma. (e-f) Filtered 41-kyr and 100-kyr components in 18O, obliquity and eccentricity exhibit similar amplitude modulation. (g) Comparison of filtered 400-kyr iron, 13C and eccentricity reveals 50-kyr phase lag of 13C. (h) Eccentricity-tilt tuning target (ET)

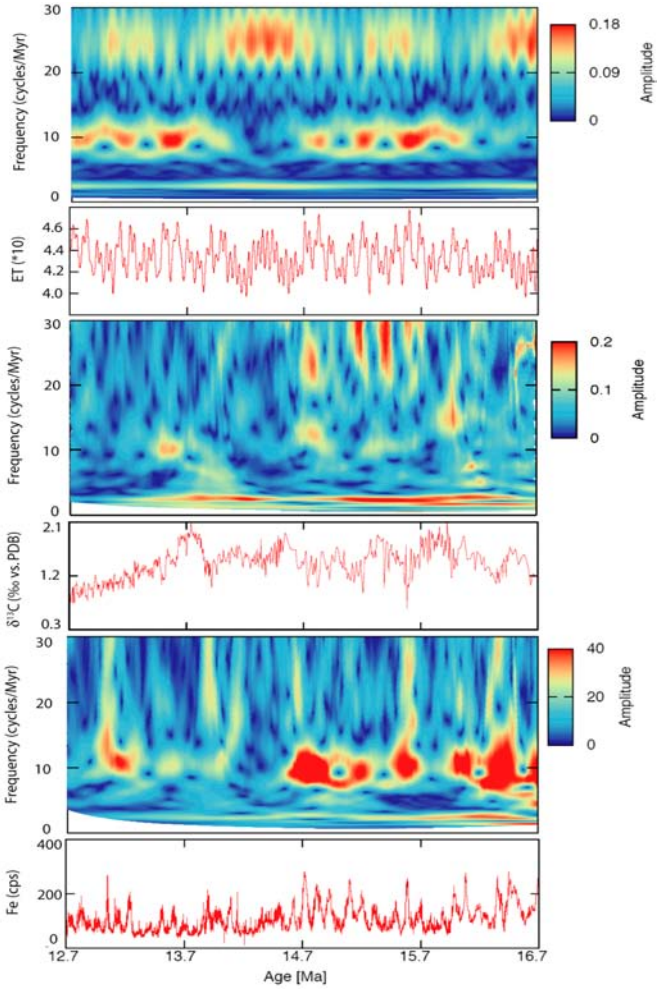

Fig. 2 Signal evolution in time-frequency space of 13C and XRF Fe in ODP Site 1237 and eccentricity-tilt (ET) tuning target (derived from Laskar et al., 2004). The amplitude evolution in the 100-kyr and 400-kyr bands of Fe closely follows the short and long eccentricity, whereas 13C predominantly exhibits the prominent 400-kyr eccentricity beat. Signal amplitudes are in same units as data analyzed.

A crucial factor influencing Antarctic glaciation after 13.9 Ma appears to have been a substantial decrease in atmospheric CO_2 partial pressure (pCO2). Marine $\delta^{13}C$ is closely linked to pCO_2 through productivity and organic carbon burial feedbacks resulting in lowest pCO_2 at $\delta^{13}C$ maxima and highest pCO_2 at $\delta^{13}C$ minima. A prominent feature of the Miocene $\delta^{13}C$ curve is the positive excursion starting at 13.92 Ma with maximum centered at ~13.7 Ma, which represents the final and most pronounced 13C increase within the "Monterey Excursion". The $\delta^{13}C$ increase started at 13.92 Ma before the onset of the major $\delta^{18}O$ shift and global cooling, suggesting that decreasing pCO_2 primed the dramatic response of the climate system, marking the final step into the "Icehouse". Atmospheric CO_2 fluctuations influencing Miocene climate evolution on orbital timescales have not been resolved by previous work and higher resolution pCO_2 proxy records are urgently needed to clarify the role of atmospheric CO_2 in Cenozoic climate cooling.

Enhanced carbonate preservation after 13.9 Ma may have further contributed to organic carbon burial, since the rate of burial also depends on the residence time of carbon in the mixed sediment surface layer, and hence carbonate accumulation rates. Increased carbonate preservation after 13.9 Ma is evident at the deeper Site 1237 (Fe and coarse fraction records in Fig. 1). It suggests an ocean-wide drop in the calcite compensation depth, probably related to a reduction of the shelf carbonate reservoir due to falling sea level and improved deep-water ventilation. On longer timescales (16.7-12.7 Ma), the 1237 Fe and $\delta^{13}C$ records exhibit low frequency variations, which are strikingly coherent with the 400-kyr eccentricity cycle (Fig. 2). Whereas Fe (carbonate dissolution) is in phase with the 400-kyr eccentricity cycle, $\delta^{13}C$ exhibits a ~50 kyr phase lag, indicating that the Pacific carbon cycle influenced $\delta^{13}C$. Thus, the 400-kyr eccentricity cycle appears to strongly influence the carbon cycle, and may even modulate long-term climate evolution.

Holbourn, A.E., Kuhnt, W., Schulz, M. & Erlenkeuser, H. Impacts of orbital forcing and atmospheric CO_2 on Miocene ice-sheet expansion. Nature, 438, 483-487 (2005).
Laskar J. et al. A long term numerical solution for the insolation quantities of the Earth. Astron. Astrophys. 428, 261-285 (2004).
Lourens, L., Hilgen, F., Shackleton, N.J., Laskar, J. & Wilson, D. in A Geologic Time Scale (eds Gradstein, F., Ogg J., Smith, A.) 409-440 (Cambridge University Press, 2004).

IODP

Perspectives for Scientific Drilling in the Levantine Basin (IODP)

Dr. Christian Hübscher, Institute of Geophysics, University of Hamburg; huebscher@dkrz.de, Tel. +49-(0)40-42838 5184, Fax. +49-(0)40-42838 5441

Salt tectonics and associated fluid dynamics are important mechanisms in basin formation. Owing to the special ductility, salt is capable of decoupling deep rooted tectonics from the supra-salt response. Salt tectonics controls the formation of complex traps for hydrocarbon or metals. Lateral salt flow may cause subaerial or submarine land slides. Salt diapirs are potential waste repositories. The interaction of fluids and salt may cause subrosion and subsequent surface collapses with a potential impact on civil infrastructures. Owing to their impermeability evaporites control fluid dynamics and hydrocarbon distribution. Furthermore, the high thermal conductivity of salt affects the thermal evolution and hence the hydrocarbon maturation properties of petroleum systems. The thorough understanding and prediction of salt tectonics and fluid dynamics is therefore fundamental in frontier research and it is crucial to develop ways in which man can optimise exploitation and risk assessment.

The semi-enclosed Levantine Basin in the easternmost Mediterranean represents a natural laboratory and world class site for the investigation of salt tectonics and associated fluid dynamics for several reasons.

1) The less than 6 Ma old Messinian evaporites are very young compared to the Permian Zechstein salt or the Mesozoic evaporites in the North Atlantic. The Levantine Basin is tectonically relatively quit since the collision between the African and the Anatolian plate turned from collision to strike-slip movement. Consequently, the salt structures are not or very little overprinted by plate tectonic processes and thus reflect almost pure salt tectonics caused by differential load and basin subsidence.

2) On the basin margins the thickness of the Post-Messinian (Plio-Quaternary) sediment cover varies between 1000 m (northern Israel) and 3000 m (Nile-Cone). In the central basin, the thickness is reduced to less than 500 m. The impact of differential sediment load on salt dynamics in terms of lateral salt flow can be therefore studied under varying, but well known conditions.

3) The marine environment is easily accessible for marine geophysical surveys, which are much faster than onshore measurements. The overall geometry of the basin, of the evaporitic layers and its overburden are very well known from academic pre-site surveys and reconnaissance surveys of the industry.

Scientific issues: The overall goal of the proposed drilling project is the reconstruction and prediction of salt and fluid dynamics as well as microbial activities related to methane and hydrocarbon turnover within a solitary basin of precisely defined geometry and external forcing. The Levantine Basin with its young Messinian evaporites is considered to represent an appropriate showcase example. This superior aim requires coercively the parameterisation of the evaporitic succession, its boundary layers and its overburden in terms of geological, geo-bio-chemical and

geo-mechanical properties by means of scientific coring.

The particular sub-topics can be described by the following keywords:

- Precipitational and depositional cycles,
- Properties and stratigraphy of evaporites and intercalated sedimentary facies,
- Sedimentation rates and lithology as indicators of onshore and shelf erosion,
- Salt tectonics and structural balancing,
- Salt microstructure as a key towards salt deformation,
- Modelling of basin subsidence, salt movement, and temperature history,
- Diagenetic inventory and processes reflecting palaeofluids,
- Presence, chemistry, and migration of intra- and sub-salinar fluids,
- Processes of gas generation in the sedimentary succession (sub- and supra-salt),
- Migration pathways of fluids and volatiles from the sub-salt into the overburden,
- Habitat of the deep biosphere and its influence on the hydrocarbon system.

ICDP

Lake Bosumtwi impact crater: physical properties and structural features in impact rocks determined from downhole measurements

Sabine Hunze & Thomas Wonik
Leibniz Institute for Applied Geosciences (GGA) Hannover; s.hunze@gga-hannover.de

The 1.07 Ma old Bosumtwi crater (Ghana, Africa) is a well-preserved complex impact structure that displays a pronounced rim and is almost completely filled by the 8 km diameter Lake Bosumtwi. Deep drilling in Lake Bosumtwi was performed (a) to study the subsurface structure (crater morphology and geometry) and crater fill (presence and composition of melt bodies), and (b) to obtain a complete 1 million year paleoenvironmental record (lake level changes) in an area so far only limited data exist for.

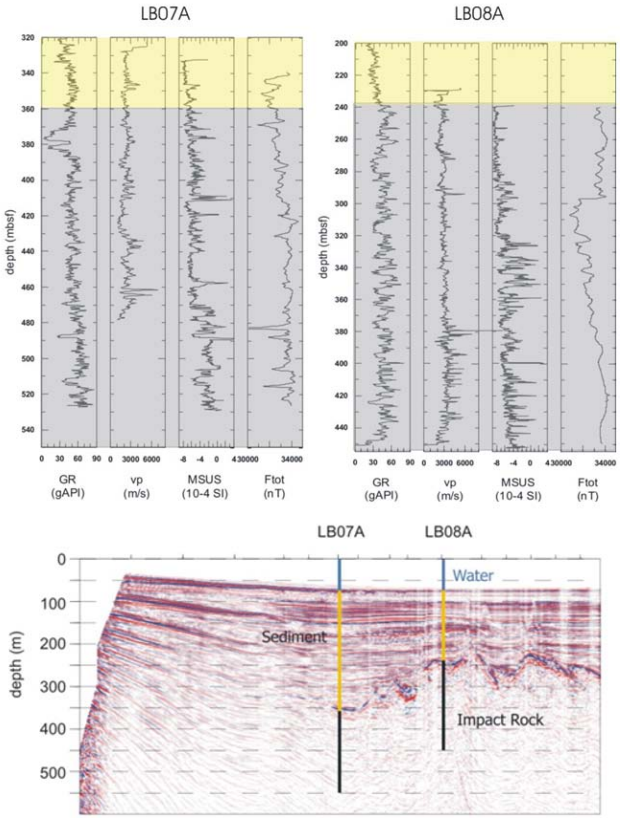

Figure 1: Seismic profile with the location of the drilled boreholes at Lake Bosumtwi and some important borehole measurements (natural radioactivity, p-wave velocity, magnetic susceptibility and total magnetic field) given for the hard rock drill sites LB07A (left) and LB08A (right).

Downhole logging data (such as resistivity, spectral gamma ray, susceptibility, and p-wave velocity) will be used to determine characteristic physical properties of impact rocks. Thus, borehole logging enables to obtain continuous, fine scale, in-situ physical and chemical parameters around the borehole walls.

We will translate downhole response data into lithologic and structural variations and will compare the characteristics of the Bosumtwi impact crater with those of craters like Ries, Barringer, and Tswaing. However, we will try to create a new way determining impact craters focusing on physical property data and downhole logs. These investigations are closely related to geophysical surface measurements (such as seismic, magnetic, and gravimetry) and petrophysical investigations on core plugs.

ICDP

Results of tilt observations around the KTB-site / Germany: Fluid induced deformation of the upper crust of the Earth

G. Jentzsch, T. Jahr, A. Gebauer
Department of Applied Geophysics, Institute of Geosciences, University of Jena, Burgweg 11, D-07749 Jena, Germany

In June, 2004, at the German deep drilling site KTB, a water injection experiment started in the pilot borehole (4000 meters deep), to be completed in May 2005. The injection had a medium rate of 180 liters/minute into the pre-hole. Beside monitoring of induced seismicity by a local network, a tiltmeter array was installed in the surrounding area of the KTB location in mid 2003 (Fig. 1), consisting of five high resolution borehole tiltmeters of the ASKANIA type (Weise et al., 1999). The aim of the research project was to observe the induced deformation of the upper crust at kilometer scale (Jahr, et al. 2005). Numerical modelling revealed that pressure built up by the given injection rate would cause a deformation of about 40 nrad within 4 months at the selected stations. The locations of the tiltmeter stations in the vicinity of KTB are at distances of 1.6 to 3.2 km. The instruments are installed in bedrock in depths between 24.5 and 45.5 m depending on the depth of the sediment cover, usually less than 20 m. The tiltmeters are equipped with a 3-D geophone set in order

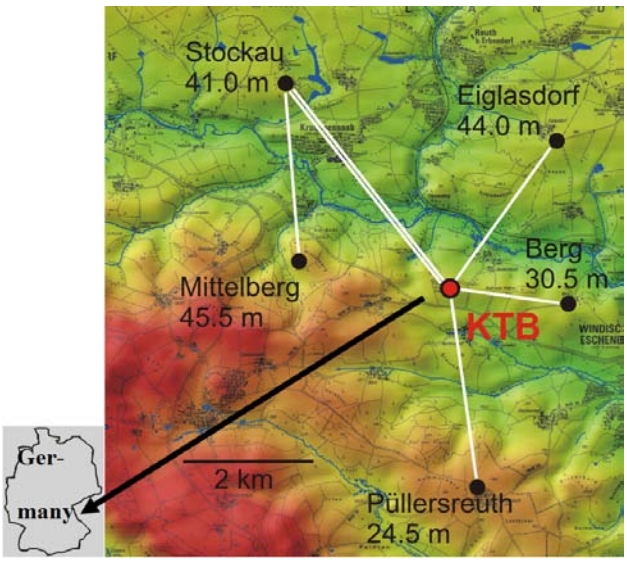

Fig. 1. The area around the KTB-site: The five tiltmeter stations were connected via WLAN to transmit the data on-line. Now the remaining stations Mittelberg, Püllersreuth, Berg and Eiglasdorf are running offline.

to complete the local seismic network. Next to each tiltmeter borehole in an additional drill hole the groundwater level is monitored as pore pressure variation. Tilt, groundwater level and seismic data were downloaded via a wireless LAN to KTB and further via Internet to the GFZ-Potsdam and the Institute of Geosciences, Jena. The project was carried out in close cooperation with seismologists of the GFZ-Potsdam who operated the seismic network and the WLAN. The wireless connections are given in Fig. 1 as well. Thus, the quality of the raw tiltmeter data and the remotely performed instrument calibration could be checked every day. We also installed a meteorological station at KTB to monitor barometric pressure and precipitation.

Fig. 2 shows the obtained data until the end of the year 2005. Due to technical problems and the end of funding we had to terminate the recordings at Stockau in August 2005 and the recording systems had to be replaced by systems without WLAN. The tilt data consist of long and uninterrupted sections. The comparison of the tidal amplitudes in the self-scaled plots reveals the different long-term drifts at each station: big tides denote small drifts.

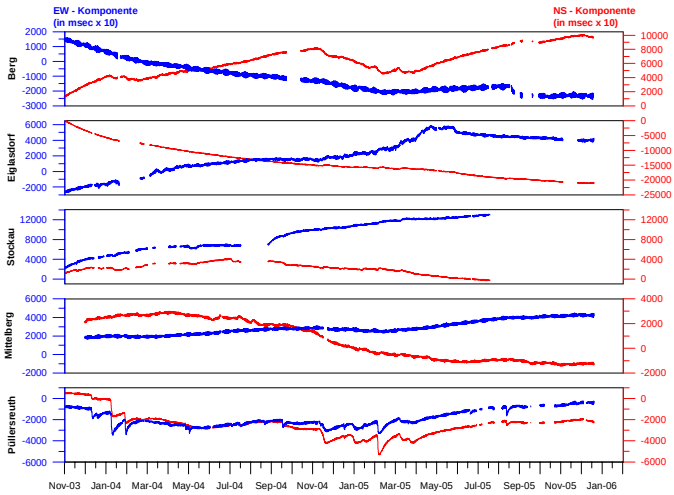

Fig. 2. After pre-processing the time series of the tiltmeter observations the drift behaviour can be visualised. The data is displayed in milliseconds of arc times 10 corresponding to about 100 nrad for the maximum tidal amplitudes. Mittelberg shows the lowest drift rates, while in Püllersreuth non-linear parts were caused by heavy precipitation. Data gaps at Eiglasdorf and Berg were caused by malfunctioning data loggers. In Stockau the tiltmeter failed in July 2004.

There are also different reactions to precipitation and local ground water changes. Heavy rainfall usually results in strong deviations with a relaxation of several days. The injection induced variations of tidal parameters, additional drifts of the records (in the order of the tidal amplitudes) and a characteristic movement of the tip of the tiltmeter pendulum (hodogram). The correction of the data for local meteorological effects (precipitation, air pressure) and ground water is in progress.

Although the obtained tidal parameters show a wide scatter, the variations at the individual stations correlate, either no variation or slight variations, respectively. Fig. 3 gives the results for the main tidal constituents M2 (semi-diurnal) and O1 (diurnal): There is a slight change in the parameters corresponding with the injection, here shown for the constituents M2 and O1: Three different periods can be distinguished, before, during and after the injection. The analyses show a slight increase of the parameters in the component North-South rather than in East-West. This corresponds to the findings regarding the seismicity which increased north of the KTB site. This can be interpretated as an injection induced change of the elasticity of the rock. This result is confirmed by the separated long-term drift. Although these drifts are still preliminary because local effects still have to be analysed and corrected, we can see common trends. Especially these drifts towards the injection center show a surface deformation correlating with the injection induced uplift of the KTB-site. Further, the hodograms reveal drift directions corresponding to geological strikes.

We can summarise that we found three different injection induced effects: Variations of tidal parameters, long-term drifts, and direct elastic tilts. These signals now need numerical interpretation.

The injection tests at KTB were accompanied by induced Seismicity (Shapiro et al., 2006). Here, we have a combination of surface deformation and seismicity which was already discussed by Jentzsch et al. (2001). The interpretation with regard to physical properties of the rock and concerning fluid induced processes (Fujimori et al., 2001) will be done by numerical modelling. We already modelled the expected deformation applying POEL (by R.J. Wang), but for a detailed modelling of the geologic structure we will use the Finite-Element-software ABAQUS. The first model is already under construction (Jahr et al., 2006).

We thank the KTB-working group and the Field Support Center for their help. Special thanks go to G. Asch and J. Kummerow (GFZ) for the organisation of the data collection and transfer. We wish to thank the Deutsche Forschungsgemeinschaft for the financial support, although it was not possible to receive funding for the completion of the work.

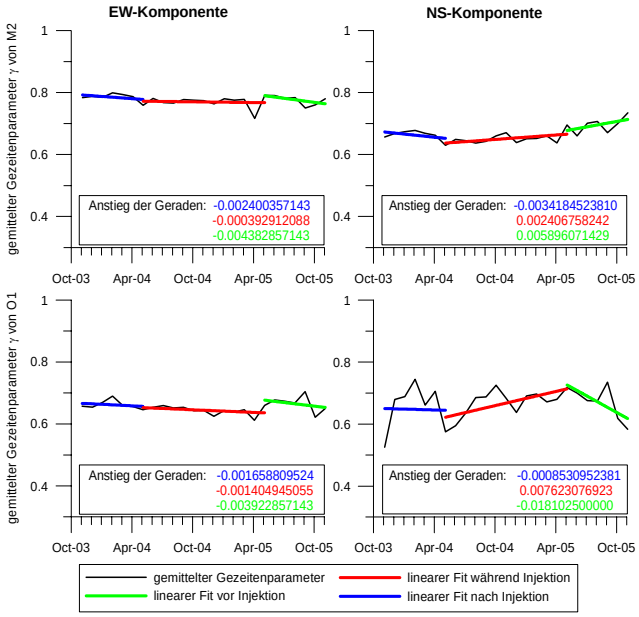

Fig. 3. Variation of tidal parameters of the main tidal constituents M2 and O1: Three different periods can be distinguished, before, during and after the injection. The effect is stronger in North-South than in East-West.

References

Fujimori, K., H. Ishii, A. Mukai, S. Nakao, S. Matsumoto, and Y. Hirata, (2001). Strain and tilt changes measured during a water injection experiment at the Nojima Fault zone, Japan. The Island Arc,10, 228 - 234.

Jahr, T., Jentzsch, G., Letz, H., Sauter, M., (2005) Fluid injection and surface deformation at the KTB location: modelling of expected tilt effect. Geofluids 5, 20 - 27.

Jahr, T., Letz, H. & Jentzsch, G., (2006) Monitoring fluid induced deformation of the earth´s crust: A large scale experiment at the KTB location/Germany. In: Jentzsch, G. (Ed.) Earth Tides and Geodynamics: Probing the Earth at Sub-Seismic Frequencies, J. of Geodynamics, Vol. 41, 1-3, 190 - 197.

Jentzsch, G., P. Malischewsky, M. Zaddro, C. Braitenberg, A. Latynina, E. Bojarsky, T. Verbytzkyy, A. Tikhomirov, and A. Kurskeev, (2001). Relations between different geodynamic parameters and seismicity in areas of high and low seismic hazards. Proc. 14th International Symposium on Earth Tides, Special Issue of the Journal of the Geodetic Soc. of Japan, 47/1, 82 - 87.

Shapiro, S. A., J. Kummerow, C. Dinske, G. Asch, E. Rothert, J. Erzinger, H.-J. Kümpel, and R. Kind, (2006). Fluid induced seismicity guided by a continental fault: Injection experiment of 2004/2005 at the German Deep Drilling Site (KTB). Geophys. Res. Let., Vol. 33, L01309, doi:10.1029/2005GL024659, 2006

Weise, A., G. Jentzsch, A. Kiviniemi, and J. Kääriäinen, (1999). Comparison of long-period tilt measurements: Results from the two clinometric stations Metsähovi and Lohja, Finland. J. of Geodynamics, 27, 237 - 257.

ICDP

The methodical limits of apatite fission-track temperature-time path modelling: mathematical, physical and geological data from the Kontinentale Tiefbohrung

Raymond Jonckheere, Gerald Van den Boogaart, Ralf Hielscher, Bastian Wauschkuhn, Carsten Weise, Eva Enkelmann, Lothar Ratschbacher
Technische Universität Bergakademie Freiberg

Apatite fission-track modelling rests on the assumption that the processes involved in annealing of induced fission tracks in lab experiments are also responsible for the annealing of fossil tracks on a geological timescale. This assumption is tested in experiments on age standards, borehole samples from the KTB Vorbohrung and ion- and neutron-irradiated samples. Experiments on age standards and KTB samples comprise dating experiments, length measurements and plateau experiments. Irradiation experiments provide a link with the physical experiments aimed at understanding the processes of track formation and annealing. The mathematical and modelling approach is designed to assess the performance of existing annealing equations in predicting the KTB profiles, fit new annealing equations to the KTB data; establish the limits of information contained in track length data and understand artefacts in the modelling procedures, resulting in a program for modelling complex data stacks.

Track formation (Chadderton et al., 2005). The identification of the PO4-unit as the agent in track formation and annealing distinguishes the phosphates from silicates; the phosphate group can cascade down sublattice channels and so be the agent for repair during particle assisted prompt anneal (PAPA) and defect assisted delayed anneal (DADA). The former dominates on the timescale of track formation so that even a fresh track is the frozen-in relict of a larger transient disordered region. The latter is of a magnitude sufficient to produce a decrease of the etchable track length in minutes to millions of years. The track structures (morphologies, intermittencies, characteristic distances and dimensions) depend upon a rapid drain of characteristic point defects: track to track, to surfaces, to interfaces and to extended defect sinks. This accords with the atomistic, transient, compound spike, not the macroscopic equilibrium thermal spike. Loss of point defects gives rise to a "skin effect". Latent track structures in insulating monazite and apatite are similar to those in fluorite and originate in the anion sublattice effect. Track etching studies show fission tracks in natural monazite to have lengths much less than those predicted by SRIM, due to the partial, homoepitaxial point-defect stimulation of PAPA. Latent tracks in bulk apatite are not amorphous, but appear to have a pseudo-monazite structure.

Age standards. Over 100 age determinations of apatites of known age (t_{REF}) demonstrate that their independent fission-track ages ($t\Phi$) determined with the external detector method are accurate ($t\Phi/t_{REF} = 1.009\pm0.010$). This implies that measurements of the thermal neutron fluence (Φ) with metal activation monitors are accurate and that value of the fission-decay constant recommended by the International Union of Pure and Applied Chemistry ($\lambda_F = 8.5\ 10^{-17}a^{-1}$; Holden and Hoffmann, 2000) is also accurate. Neutron fluence measurements with Al-0.1%Au and Al-1.0%Co monitors (Dr. Lin Xilei, Radiochemie, TUM) for seven irradiations in the FRM-II reactor, Garching, are consistent with results of irradiations and fluence measurements at the Thetis-reactor in Gent, confirming that both the pneumatic and hydraulic channels of the FRM-II reactor are well-suited for fission-track irradiations.

Age calibration. A deconvolution of the ζ-factor resulted in a multiple age-calibration (Jonckheere, 2003):

$$t = [\lambda\alpha]^{-1} \ln [(\lambda\alpha/\lambda_F)\ \zeta_0\ (\rho_S/\rho_i)\ I\ \sigma\ \Phi + 1] \quad (1)$$

with $$[\zeta_0]_{STD} = [\lambda_F / \lambda\alpha]\ [I\ \sigma\ \Phi_{St}]^{-1}\ [(\rho_S / \rho_i)_{St}]^{-1}\ [e^{\lambda\alpha\ t_{St}} - 1] \quad (2)$$

$$[\zeta_0]_{EXP} = [\rho_i]_{ed} / [\rho_i]_{ap} \quad (3)$$

$$[\zeta_0]_{CAL} = \tfrac{1}{2}\ [\eta q]_{ed} / [\eta q]_{ap}\ (I_f/I'_f)\ (I'_e/I_e) \quad (4)$$

The different ζ_0-values are consistent ($[\zeta_0]_{STD}/[\zeta_0]_{EXP} = 0.997\pm0.007$; $[\zeta_0]_{STD}/[\zeta_0]_{CAL} = 1.024\pm0.018$). The Φ-, Z-, ζ- and ζ_0-ages ($t\Phi$, t_Z, $t\zeta$ and $t\zeta_0$) of apatite samples are also in agreement; deviations from the mean (t_M) exceed the statistical uncertainties ($t_Z/t_M = 0.986\pm0.002$; $t\zeta/t_M = 1.016\pm0.003$; $t\zeta_0/t_M = 0.999\pm0.001$), but are $\leq$2% and traceable to statistical variation, including counting statistics and an extra-Poisson component due to the track identification criteria. The agreement between $t\Phi$ and t_{REF} and between $t\Phi$ and t_Z, $t\zeta$ and $t\zeta_0$ ($t\Phi/t_M = 1.000\pm0.001$) is not the result of cancelling systematic errors (Green, 1988) but an indication that these ages are, in fact, accurate (Enkelmann et al., 2005a).

Uranium measurements. The uranium concentrations in standard uranium glasses were calculated with an equation derived from (3) and (4), which takes into account the track registration geometries, counting efficiencies and track length deficits. The results are consistent with those of INAA, ENAA and TIMS (Enkelmann et al., 2005b). This is important because the reference values in this case are not the reference ages of geological age standards but the uranium concentrations of standard glasses that can be verified with other methods. The results are also not affected by partial annealing of the tracks and provide independent evidence for the conclusion that the fission-track ages are accurate.

Length measurements. The reduction of the fossil track length in age standards has no effect on their fission-track age. This has positive and negative consequences: in contrast to their current interpretation, Z- and ζ-ages are not "partially corrected", but like Φ- and ζ_0-ages, refer to the closure temperature of the fission-track system thus again assigning an unambiguous meaning to a fission-track age. On the other hand, the absence of a proportial relationship between the fission-track age and mean track length invalidates a fundamental assumption of T(t)-path modelling and can now be identified as the direct cause of the still ill-understood artefact known as the "worldwide recent exhumation".

Plateau experiments. Plateau-experiments on two apatites have demonstrated that their reduced fossil track length does not result in an increased resistance to annealing; the annealing kinetics of the fossil tracks are indistinguishable from those of the induced tracks in neutron-irradiated aliquots. This constitutes a direct violation of the principle of equivalent time (Jha et al. 1984), both as stated in terms of individual track length (Duddy et al. 1988) and in terms of mean track length (Jonckheere 2003). However, the fact that the principle of equivalent time is invalid, as stated, does not mean that its practical application in T(t)-path modelling must, perforce, also be invalid, because there is a fine distinction between the manner in which the principle is formulated and that in which it is applied. It does mean that the use of the principle of equivalent time in T(t)-path modelling rests entirely on an ad hoc assumption without any form of experimental justification under geological conditions.

Microprobe analyses. Microprobe analyses indicate that the KTB apatites possess a more or less homogenous but unusual, OH-rich, composition with little Cl. Calculations of the kinetic parameters (Ketcham et al., 1999) show that the samples are expected to have a low but constant resistance to annealing according to their Cl/F-ratio but a variable and higher resistance according to their OH-values. Except for an uncertain correlation between F-content and mean track length, which may be caused by other factors, there are no clear indications for either compositional effect in the KTB data.

KTB age profile. The fission-track age versus depth profile for the KTB-Vorbohrung is divided into an upper section with a constant mean age of ~65 Ma and a lower section where the age gradually decreases with increasing depth, which are interpreted as the present-day total stability zone and partial annealing zone. The ages determined with four dating methods (Φ, Z, ζ, ζ_0) are

consistent due to the consistent values of the calibration factors. There is excessive scatter in the age profile, perhaps due to compositional differences between the samples or extra-Poisson variation caused by spurious defects; the scatter does not result from post-Cretaceous tectonics.

KTB length profile. The mean-track-length versus depth profile is made up of an upper section in which the mean track length remains almost constant at ~13 μm, an intermediate section, where it decreases from ~13 μm to ~10 μm and a lower section with a limited decrease from ~10 μm to ~9 μm. Outliers are in most cases due to insufficient statistics in samples with few confined tracks. The track length versus orientation data seem consistent with the elliptical model of Donelick (1991) and Donelick et al. (1999). The angular bias is consistent with observations of Ketcham (2003; 2005) and Enkelmann et al. (unpubl.). In contrast to experimental data on induced tracks, there are no indications for accelerated annealing (Donelick, 1991; Donelick et al., 1999) or a segmentation of the tracks due to the appearance of unetchable gaps (Green et al., 1986; Hejl, 1995) in the most annealed KTB samples.

The calculated age and mean-track-length profiles for all existing annealing equations brought to light that: (1) they are determined by both the annealing model and the assumed observational bias models, (2) there are different bias models for the track counts and the confined-track-length measurements; (3) due to simultaneous track accumulation and annealing in geological samples, any combination of bias models causes a divergence of the age and track-length profiles at a certain depth; (4) whatever the true relationship between (ρ/ρ_0) and (l/l_0), the observed relationship between (ρ/ρ_0) and (l/l_0) in geological samples cannot be the same as that of induced tracks, in direct conflict with Green (1988). Further methodical considerations lead us to conclude that the age profile is a better diagnostic for evaluating the annealing equations whereas the length profile is better for evaluating bias models.

A comparison of the calculated and measured profiles shows that simple annealing equations are as good as more complex models. The curvilinear equations present no advantages over linear ones. A physical model such as that of Carlson (1990) is also not, per definition, less suited than empirical models. A reasonable fit is as often obtained with models based on Durango apatite as with models tailored to the specific composition of the KTB samples, whether in terms of Cl- concentration or OH-concentration. There is no proven advantage in accounting for composition and it is questionable whether its effects on the annealing kinetics of fission tracks are well understood. Our results lend support to the continuing preference for the fanning linear model of Laslett et al. (1987) for geological applications, despite the fact that it is one of the oldest models. It also lends support to the practice based on experience of setting the initial track length at a lower value than that of induced fission tracks.

Ion irradiation. Apatite mounts for track-length measurements have been irradiated with 300 MeV Xe and 800 MeV U at the GSI, to produce 20 m long host tracks for the confined tracks, and step-etched. The results indicate that: (1) this leads to a tenfold increase in the number of confined tracks; (2) the observational bias for confined track-length measurements depends on the irradiation conditions but the mean track length in a given orientation is not affected; (3) the elliptical model is over-constrained and does not provide the best fit to the confined-track-length versus orientation data. The increased number of confined tracks makes that the range of T(t)-solutions obtained with traditional software is no longer determined by statistics but by minor inaccuracies in the fundamental annealing equations.

T(t)-path modelling. In our current program, reverse modelling proceeds in steps: the 2n-dimensional phase space of all n-node first-order splines is searched using a most efficient method and a first-order grid with a mesh size of 10˚C/10Ma; the first-order grid is refined in subsequent searches. In view of the low resolution of fission-track data, the mesh-size is fine enough to detect good-fit solutions. If no solution satisfies the statistical criteria, the best-fit solution is retained as the starting point for the next search. All T(t)-paths start at the corrected sample age but this does not present a limitation because this limit is exceeded in subsequent searches with a finer grid around the best-fit solution. KS-statistic assesses the candidate T(t)-paths; other statistics will be added later. The program returns the best-fit solution, minimum and maximum palaeotemperature bounds at all t and the frequencies with which the nodes of good-fit solutions occur at each grid point. The forward precision gives the range of solutions for different samples from the calculated length distribution; the inverse precision gives the precision of the estimated T(t)-histories for the observed length distribution. The forward precision and prediction confidence bands for a known temperature history, e.g. the best-fit solution, are calculated brute force by repeated re-sampling of the calculated distribution and remodelling. A precise estimate of the variation can be obtained from the KS-bounds of just one re-sampled distribution because the assumptions of the KS-test are satisfied. Bootstrapping will be considered later. The inverse precision and the estimation confidence band are much more difficult to assess. Our first solution is to find all T(t)-histories which accept a stratified sample of the best-fitting distribution within the model.

Initial conclusions. (1) Apatite fission-track ages can be accurately determined with the independent and standard-based approaches, and have an unequivocal meaning in terms of closure temperature; (2) apatite fission-track temperature-time-path modelling rests on two unproven assumptions: the principle of equivalent time and the assumption that a single bias model applies to track counts and confined-track-length measurements; (3) the principle of equivalent time is invalid as stated but this does not disprove that it may apply to annealing of fossil tracks in the geological environment; (4) provided that some loss of resolution is accepted it is possible to model fission-track length data without using the principle of equivalent time; (5) a comparison of the calculated and measured KTB profiles reveals that different biases affect the track counts and length measurements; these need to be differentiated and understood; (6) ion-irradiation and step-etching increase the number of confined tracks to a point where the corresponding T(t)-paths are constrained by external factors; this points to inconsistencies in the fundamental equations, that need to be corrected, but also to the fact that sufficient statistics allow to put tighter constraints on the T(t)-solution than was considered possible; (7) the elliptical model is over-constrained and does not provide the best fit to the confined-track-length versus orientation data; (8) sophisticated annealing equations or those that account for composition-dependent annealing kinetics provided no better fit to the KTB data than the simpler time-tested equations of Laslett et al. (1987).

Although the equations must be adjusted and the fundamental assumptions revised, apatite fission-track temperature-time-path modelling can provide rather tight constraints on the thermal histories of rock samples; the required compromises are made good by the improved statistics resulting from ion irradiation.

IODP

Late Quaternary sea-surface temperature variability in the southeast Pacific and relationships to paleoenvironmental changes in southern Chile (ODP Site 1233)

Jérôme Kaiser[1*], Frank Lamy[1], Dierk Hebbeln[2], Ulysses Ninnemann[3], Helge W. Arz[1] and Joe Stoner[4]

[1]GeoForschungsZentrum-Potsdam, Telegrafenberg, 14473 Potsdam, Germany; [2]DFG Research Center Ocean Margins, Leobener Strasse, 28359 Bremen, Germany;

[3]Bjerknes Center for Climate Research, University of Bergen, Allégaten 55, 5007 Bergen, Norway; [4]Institute of Arctic and Alpine Research, University of Colorado, Boulder CO, 80309-0450, USA; * To whom correspondence should be addressed: kaiserj@gfz-potsdam.de or kaiserj@uni-bremen.de

ODP Site 1233 (Mix et al., 2003), located in the Southeast (SE) Pacific mid-latitudes (41˚S), has a well-constrained age model and presents unprecedented high sedimentation rates (ranging between ~1.5 and >3 m/kyr) over the last 70 kyr (Lamy et al., 2004; Kaiser et al., 2005), having therefore a huge potential to reconstruct past climate changes at multi-millennial to sub-centennial timescales in the still poorly studied Southern Hemisphere (SH). Site 1233 is located in a region under the influence of the major oceanographic and atmospheric circulation members of the SH mid-latitudes, respectively the Antarctic Circumpolar Current (ACC) and the Westerly winds, as well as close to the Patagonian Ice Sheet (PIS) which occupied a large area of southernmost South America during the last glacial time. In addition, the proximity of the site to the southern Chilean coast (~40 km) allows studying land and marine proxies within the same archive avoiding problems linked to age uncertainties.

The alkenone-based sea-surface temperature (SST) record at Site 1233 presents very similar millennial-scale fluctuations to the air temperature record from the well-dated Byrd ice-core (Blunier and Brook, 2001) over the last 70 kyr, suggesting an "Antarctic timing" in the SE Pacific on these timescales. During the last glacial time, at the same timescale, the SST record is closely correlated to sea-ice fluctuations in the SE Atlantic high-latitudes as well as to the dust content record of the EPICA Dome C ice-core (EPICA community members, 2004). This patterns suggest a mechanism similar to the modern Southern Annular Mode, a major interannual mode of variability in the SH mid- to high latitudes. During cold periods, the winds around Antarctica are strengthened and/or occupy a broader range of latitudes, resulting in and/or favoring an extension of the sea-ice. As a result, the ACC is shifted equatorward and supplies larger amounts of subantarctic cold waters into the SE Pacific. Other records of changes in the sea-surface water properties in the South Pacific and in the SE Atlantic show a similar pattern to the SST reconstruction at Site 1233. The proposed mechanism might thus be valid at a hemisphere-wide scale, and the SH high latitudes might have been less isolated as previously thought during the glacial time (Kaiser et al., 2005).

The apparent "Antarctic timing" of the SH mid-latitudes SST records suggests that the so-called thermal see-saw mechanism was operating during the last glacial in the SH mid-latitudes. The origin of the see-saw effect is generally considered to lie in a slowdown of the thermohaline circulation (THC) during the Northern Hemisphere (NH) Heinrich events, due to changes in the surface density in the North Atlantic realm, resulting in warm events in the Southern Ocean. However, as the SE Pacific region is not directly under the influence of the THC, changes in the SSTs and sea-ice extent around Antarctica might have played a significant role in either amplifying or even initiating these abrupt climate shifts as proposed by recent modeling studies (e.g., Knorr and Lohmann, 2003).

The South Pacific Eastern Boundary Current system (PEBCS), which is one of the most productive areas in the world ocean, acts like a conduit for heat exchange between the SH high latitudes and the eastern tropical Pacific. Its functioning during the last glacial time and the last deglaciation remains a challenging question for understanding SH and even global paleoclimates. By merging the SST results at Site 1233 with previously published SST records all along the PEBCS, it has been possible to draw major features of this system at different time-intervals over the last 70 kyr based on a SST gradient reconstruction. During cold periods as Marine Isotope Stage (MIS) 4 and 2 on the one hand, the temperature gradients were substantially stronger-than-today reflecting an equatorward shift of the subtropical gyre circulation by ~5˚ in latitude and resulting in a stronger supply of cold waters into the eastern tropical Pacific. On the other hand, the system was shifted poleward during the Holocene Climatic Optimum, when the climate was warmer-than-today (Kaiser et al., 2005).

In southern Chile, terrestrial peleoenvironmental records are mainly based on pollen assemblages and geomorphological evidences of glaciers fluctuations, and suggest latitudinal shifts of the Westerlies as being the main forcing mechanism. Part of these results suggests a climate linkage with the Northern Hemisphere (e.g., Denton et al., 1999; Moreno et al., 2001) in disagreement with the aforementioned SST reconstructions. Iron relative concentrations at Site 1233 were used as a proxy for PIS fluctuations during the last glacial time (Lamy et al., 2004; Kaiser et al., in press). The glacier advances as reconstructed on land correlate with iron maxima and cold offshore SST which would be in agreement with common latitudinal shift of the ACC/Westerlies system at a millennial timescale, bringing simultaneously subantarctic waters and higher rainfall feeding the ice-sheet. There is however a delay of the PIS retreats over the SST warmings of about 700-1000 years during MIS 4, late MIS 3 and MIS 2, suggesting a delayed response of the ice sheet to large-scale temperature changes as shown by the SST record. The strong dependence of PIS fluctuations on offshore SST changes in the SE Pacific has been independently derived from regional modeling studies (Hulton et al., 2002). The offset disappeared during the early and middle parts of MIS 3, a relatively warm time-interval of the last glacial, suggesting that the PIS was significantly reduced in its northern part, or even absent, and could thus react more rapidly to temperature and snow accumulation changes.

Spectral analysis on the short-term variability (<5 kyr) of both the iron and the SST records reveals three main, significant cyclicity-bands around 4.5-3.1 kyr, 2.4-2.2 kyr and 1.2-0.8 kyr (Kaiser et al., in press). The supposed origins comprise the so-called stochastic resonance mechanism for the 4.5-3.1 kyr band, which implies that the combination of a weak periodic signal with other signals might cause climate mode switches as the Dansgaard/Oeschger events. For the 2.4-2.2 kyr and the 1.3-0.8 kyr periodicity-bands, a solar origin can be assumed as similar cycles have been recognized in residual ?14C record from tree-rings. As proposed in several studies, changes in UV radiations could have ultimately an impact on the location of the mid-latitude storm tracks. Furthermore, spectral analyses of records from the Cariaco Basin, Greenland (GISP2 ice-core) and Antarctica (Byrd ice-core) show similar results suggesting global climate forcing.

The presence or absence of an equivalent to the Northern Hemisphere Younger Dryas (YD) event has been controversially discussed based on terrestrial records in Chile (e.g., Moreno et al., 2001; Bennett et al., 2000). A very high-resolution (~70 yr) SST reconstruction over the last deglaciation at Site 1233 shows a temperature plateau during the Antarctic Cold Reversal, followed by a ~2˚C warming during the later part of the Younger Dryas. This pattern is consistent with Antarctic ice-core records.

Finally, a high-resolution sea-surface salinity (SSS) reconstruction, together with iron (Fe) and titanium (Ti) relative concentration records, provide important new details on the interactions of the PIS and the oceanographic system at a centennial-scale evolution over the last deglaciation. Recent and better time-constrained records of the PIS fluctuations on adjacent land (e.g., Sugden et al., 2005) are in phase with the Fe and Ti relative concentrations, reinforcing the utilization of these proxies for PIS movements during older times. The SSS record at 41˚S suggests three main freshwater inputs linked to the melting of the PIS at ~17.5, 13 and 12 kyr BP. The first and main event at ~17.5 kyr BP occurred shortly after the last glacier advance as reconstructed on the adjacent land. The timing of the second event agrees well with the recently suggested drainage of a huge, ice-dammed lake into the Pacific Ocean linked to the separation of

the North and South Patagonian ice-fields (Turner et al., 2005). The third PIS melting event is probably related to the final melting phase of the PIS due to the 2˚C SST warming during the YD interval.

References:
Bennett, K. D., S. G. Haberle, and S. H. Lumley (2000), The Last Glacial-Holocene Transition in Southern Chile, Science, 290, 325-328.
Blunier, T., and E. J. Brook (2001), Timing of millennial-scale climate change in Antarctica and Greenland during the last glacial period, Science, 291, 109-112.
Denton, G. H., C. J. Heusser, T. V. Lowell, P. I. Moreno, B. G. Andersen, L. E. Heusser, C. Schluchter, and D. R. Marchant (1999a), Interhemispheric linkage of paleoclimate during the last glaciation, Geografiska Annaler Series a-Physical Geography, 81A, 107-153.
EPICA Community Members (2004), Eight glacial cycles from an Antarctic ice core, Nature, 429, 623-628.
Hulton, N. R. J., R. S. Purves, R. D. McCulloch, D. E. Sugden, and M. J. Bentley (2002), The Last Glacial Maximum and deglaciation in southern South America, Quat. Sci. Rev., 21, 233-241.
Kaiser, J., F. Lamy, and D. Hebbeln, 2005. A 70-kyr sea surface temperature record off southern Chile (Ocean Drilling Programm Site 1233). Paleoceanography 20, PA4009, doi:4010.1029/2005PA001146.
Kaiser, J., F. Lamy, H. Arz, and D. Hebbeln (in press), Dynamics of the millennial-scale sea surface temperature and Patagonian Ice Sheet fluctuations in southern Chile during the last 70 kyr (ODP Site 1233), Quaternary International.
Knorr, G., and G. Lohmann (2003), Southern Ocean origin for the resumption of Atlantic thermohaline circulation during deglaciation, Nature, 424, 532-536.
Lamy, F., J. Kaiser, U. Ninnemann, D. Hebbeln, H. Arz, and J. Stoner (2004), Antarctic Timing of Surface Water Changes off Chile and Patagonian Ice Sheet Response, Science, 304, 1959-1962.
Mix, A. C., R. Tiedemann, P. Blum, and Shipboard Scientists, (2003), Leg 202 Summary, pp.145, Ocean Drilling Program, College Station, TX.
Moreno, P. I., G. L. Jacobson, T. V. Lowell, and G. H. Denton (2001), Interhemispheric climate links revealed by a late-glacial cooling episode in southern Chile, Nature, 409, 804-808.
Sugden, D. E., M. J. Bentley, C. J. Fogwill, N. R. J. Hulton, R. D. McCulloch, and R. S. Purves (2005), Late-glacial glacier events in southernmost South America: a blend of "northern" and "southern" hemispheric climatic signals? Geografiska Annaler, Series A: Physical Geography, 87, 273-288.
Turner, K. J., C. J. Fogwill, R. D. McCulloch, and D. E. Sugden (2005), Deglaciation of the eastern flank of the North Patagonian Icefield and associated continental-scale lake diversions, Geografiska Annaler, Series A: Physical Geography, 87, 363-374.

IODP

A Middle to Late Miocene calcareous and terrigenous sedimentation in the incipient Benguela Upwelling system: Inferences from Silt Analysis

Mia Maria Kastanja[1], Jan-Berend Stuuta, Rüdiger Henrich[2]
[1] Research Center Ocean Margins, University of Bremen, Bremen 28334, Germany (kastanja@uni-bremen.de); [2]Faculty of Geosciences, FB.5, University of Bremen, P.O. Box 330440, 28334 Bremen, Germany

Deep-sea sediments from the SE Atlantic at ODP Leg 175 Site 1085 off the continental margin SW African provide a unique record of the Middle to Late Miocene sedimentation. In this study the results of a comprehensive data collection mainly from analysis of grain-size distribution, together with bulk geochemical analysis have been applied for reconstructing mechanisms and sediment transport pathways, and interpreting paleoenvironmental and paleoclimatic signals. The development of the Benguela Upwelling System and Miocene "Carbonate Crash" event were of the special focuses. The obtained multidisciplinary proxy records of the Late Miocene African climate development were coupled with the application of end-member modelling to understand controls of sediment transport variation in relation to paleoclimate change.

The result of grain-size analysis of the biogenic component shows that the entire interval is dominated by calcareous fine fraction with very low amounts of sand fraction, suggesting that calcareous nannofossils act as most important carbonate producers in the study area (Fig. 1). Two significant drops of CaCO3 concentration between 10.4 and 10.1 Ma and between 9.6 and 9 Ma are related to the Miocene "Carbonate Crash" events (Westerhold et al., subm.). The results showed that the driving process of these events was complex and differed compared to previous investigations in the other regions. The Miocene "Carbonate Crash" event in the eastern Equatorial Pacific (Lyle et al., 1995), western Equatorial Atlantic (King et al., 1997) and Caribbean Sea (Roth et al., 2000) are interpreted to be predominantly controlled by dissolution and shoaling of lysocline as a response to the closure of Central American Seaway. At the study area, the causes of these events are definitely different. Here, they are controlled mostly by changes in regional signals. The older drop of CaCO3 concentration at the study area is mainly controlled by variation in calcareous nannoplankton production (Fig. 1), while the younger crash event is caused by a combination of changes in calcareous nannoplankton production and dilution (Fig. 1). Interestingly, the same event was not detected in the open ocean settings on the Walvis Ridge, SE Atlantic, e.g., ODP Site 1265. It is thus questionable if the event can be called a 'global' event at all.

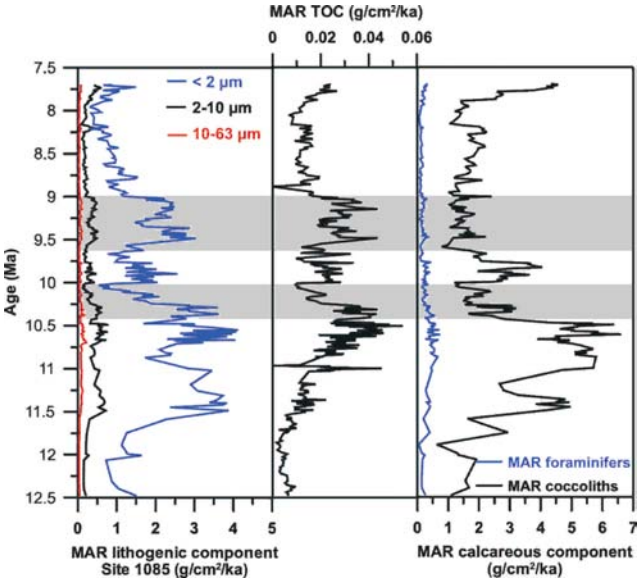

Figure 1. Temporal variation of mass accumulation rates (MAR) of lithogenic component, total organic carbon (TOC), and calcareous component at ODP Site 1085. (Grey bars are "Carbonate crash" events (Westerhold et al., subm.)

The Late Miocene terrigenous fraction of deep-sea sediments in the Cape Basin, SE Atlantic Ocean (ODP Site 1085), displays a temporal variation in grain size attributed to different transport mechanisms in relation to the paleoclimatic history. End-member modelling of carbonate free silt-size distributions (n = 216) is applied to distinguish the signals of varying sedimentation processes. This modelling resulted in four subpopulations, which are interpreted as weak and moderate hemipelagic mud and coarse and fine eolian dust. The results of end-member modelling together with geochemical analysis show that between 11 and 10 Ma, the input of terrigenous material is driven mainly by river supply from the Orange River (Fig. 2), indicating a humid climate in the hinterland. The initiation of trade wind transport of dust occurred at around 10.6 Ma (Fig. 2), signifying an establishment of the Benguela upwelling system. A prominent change of continental climate from relatively humid to relatively arid conditions in South Africa is noted at ~ 9.5 Ma (Fig.2), which probably was related to the expansion of the Antarctic ice-sheet and intensification of Southern Hemisphere winds.

References:
King, T.A., Ellis, J., Murray, W.G., Shackleton, N.J., Harris, S., 1997. Miocene evolution of carbonate sedimentation at the Ceara Rise: a multivariate data/proxy approach. In: Shackleton, N.J., Curry, W.B., Richter, C. and Bralower, T.J. (Eds.), Proc. ODP, Sci. Results, vol. 154. Ocean Drilling Program, College Station, TX, pp. 349-364.
Lyle, M., Dadey, K.A., Farrel, J.W., 1995. The Late Miocene (11-8 Ma) eastern Pacific carbonate crash: evidence for reorganization of deep-water circulation by the closure of the Panama gateway. In: Pisias, N.G., Mayer, L.A., Janecek, T.R.,

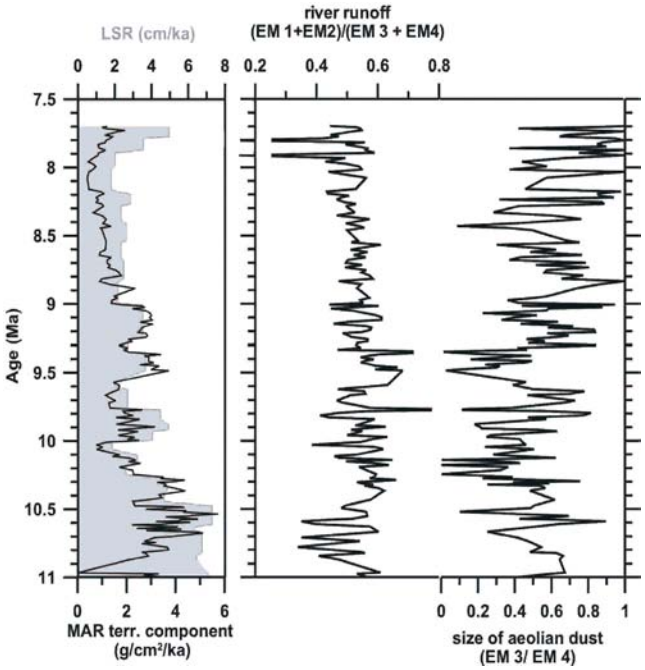

Figure 2. Temporal variation of linear sedimentation rates (LSR), mass accumulation rates of terrigenous component (MARterr), continental run off, and wind strength at ODP Site 1085.

Palmer-Julson, J. and van Andel, T.H. (Eds.), Proc. ODP, Sci. Results, vol. 138. Ocean Drilling Programm, College Station, TX, pp. 821-838.
Roth, M.J., Droxler, A.W., Kameo, K., 2000. The Caribbean carbonate crash at the Middle to Late Miocene transition: linkage to the establishment of the modern global ocean conveyor. In: Leckie, R.M., Sigursson, H., Acton, G.D. and Draper, G. (Eds.), Proc. ODP, Sci. Results, vol. 165. Ocean Drilling Program, College Station, TX, pp. 249-273.
Westerhold., T., Bickert, T., Röhl, U., subm. Miocene evolution of carbonate sedimentation in the eastern South Atlantic: High - resolution XRF-scanning records of ODP Sites 1085 and 1087. Submitted to Marine Geology

ICDP

Groundwater and Fluid Component Transport in the KTB SE1 and SE2 Fault Zones and a Possible Connection with the Eger Rift Valley

Winfried Kessels, Sonja Kuhlmann, Xuan Li
Leibniz Institute for Applied Geosciences, D-30655 Hannover, Germany
e-mail: w.kessels@gga-hannover.de; s.kuhlmann@gga-hannover.de

Hydraulic investigations in and between the two KTB boreholes have shown that groundwater flow is possible in great depths of the crystalline crust. Particularly in the fault zones SE1 and SE2 a remarkable permeability was found. The results from three-dimensional groundwater modelling (Graesle et. al., 2006) document the existence of a large-scale (more than 10 km) hydraulic reservoir in the crystalline crust. Fig. 1 shows the projection for the hydraulic pressure development in the KTB main (HB) and pilot hole (VB) resulting from the last long time pump and injection test calculated with this model. According to this calculation in 2009, 4 years after the end of the injection, still an overpressure of 0.4 MPa can be expected in KTB-HB. The good matching with the measured data confirms groundwater pathways in a scale of more than 10 km.

The isotopic water composition recovered from the pilot hole indicates a downward water flow along the SE2 fault zone, which is in contact with the Franconian Line. On the other hand, 60 km apart, in the western Eger Rift Valley, there is a deep up-going groundwater flow (Fig.2), indicated e.g. by the temperature signature and gas flow observations. Hence, the demand on fluid mass continuity needs a supplying down stream groundwater flow, likely to assume from the Franconian Line.

To see whether a hydraulic connection between Franconian Line and the Eger Rift Valley is possible, the question of potential driving processes must be answered. It needs a sufficient horizontal pressure gradient to allow groundwater flow in great depth between Franconian Line and the Eger Rift Valley. The density variations of groundwater with depth are most relevant for the calculation of horizontal pressure differences.

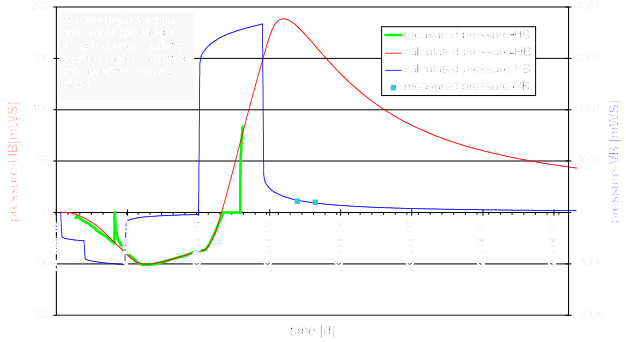

Fig. 1 Measured and calculated pressure in both KTB boreholes with different pressure scaling for both holes.

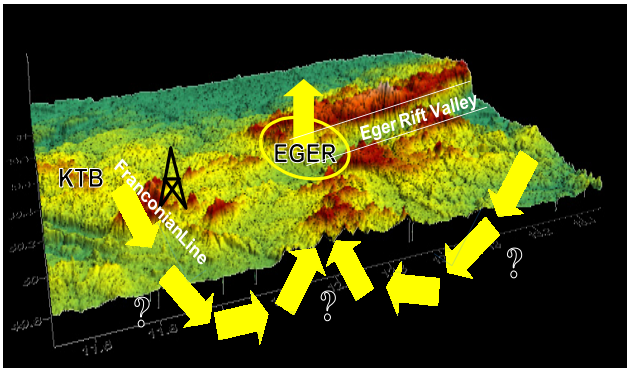

Fig. 2 Topographic map of the area between Franconian Line and Eger Rift Valley. Arrows indicate pathways for fluids.

A separation in 4 driving processes:

- The groundwater surface topography related to the groundwater recharge and mean regional distance between neighbourhood valleys
- Geothermal gradient and water density in dependency of temperature and pressure
- Different salt content in adjacent geological formations
- Gas content in the water and gas dissolution

results in the potentials for a horizontal flow given in Fig. 3 and in horizontal pressure gradients up to 0.5 MPa/km. For only 1 MPa pressure difference (low value check) between Franconian Line and the Eger Rift Valley with a distance of nearly 60 km we get (using the Darcy relation for the hydraulic KTB data):

Darcy flow density = 0.00025 to 0.001 [m/a]
Distance velocity = 1.0 to 5.0 [m/a]
Travel time for 60 km = 10 000 to 45 000 [a]

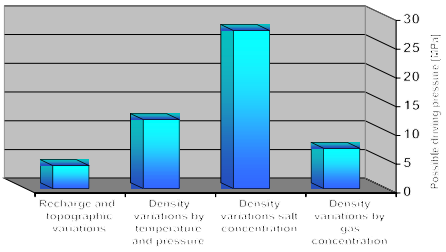

Fig. 3 Upper limit of driving pressures for different processes estimated for the range between Franconian Line and Eger Rift Valley.

This remarkable high groundwater velocity in this depth gives us a new view on the geodynamic processes in the crystalline crust.

To get a better understanding of the deep groundwater flow around the Eger Rift Valley we propose:

- First, a very thorough chemical and hydraulic testing of the SE 1 fault zone in 7200m depths in the KTB main hole.
- Second, a thorough chemical and hydraulic testing of the Eger Rift Valley.

The conditions to study the large-scale water and gas transport in the deep crust are unique in the area between KTB and Cheb (Eger Rift Valley).

References
Gräsle, W., Kessels, W., Kümpel, H.-J., Li, Xuan (2006): Hydraulic observations from a one year fluid production test in the 4000 m deep KTB pilot borehole. - Geofluids, 6, 8-23
Further Reading
Gräsle, W., Kessels, W., Li, X., Kuhlman, S. (2004): Transport processes in the fault zones of the crystalline crust. - Determination of the hydraulic properties at KTB area. - Poster, Fall Meeting American Geophysical Union; San Francisco, USA.
Gräsle W., Kessels, W., Rifai, H. (2003): A tracer based flow-log technique to assess hydraulic properties in deep fractured-porous aquifers of low permeability applied in the 4000 m pilot borehole of the KTB / Germany. - Int. Conf. on Groundwater in Fractured Rocks, 15.-19.09.2003, Prague.
Gräsle W., Kessels, W., Rifai, H. (2002): A new Flow-Log Technique Suitable for Small Flow Rates in Deep Drillings. - Eos Trans. AGU, 83 (47), Fall Meet. Suppl., Abstract H52B-0866.
Huenges, E., Erzinger, J., Kück, J., Engeser, B., Kessels, W. (1997): The permeable crust; geohydraulic properties down to 9101 m depth. - J. Geophys. Res., 102 (B8), 18,255-18,265.
Kessels, W., Kück, J. (1995): Hydraulic communication in crystalline rock between the two boreholes of the Continental Deep Drilling Project in Germany. - Int. J. Rock Mech. Min. Sci. & Geomech. Abstr., 32, 37-47.

IODP

Tropical Climate Dynamics during the past Glacial/Interglacial Cycle in (sub)annual resolution (Cariaco Basin and Mexican Lakes)

Ulrike Kienel[1], Gerald H. Haug[1], in cooperation with Larry C. Peterson[2], and David A. Hodell[3]
[1]GeoForschungsZentrum Potsdam, Climate Dynamics and Sediments, Telegrafenberg C, 14473 Potsdam Germany; [2]Rosenstiel School of Marine & Atmospheric Science, University of Miami, USA; [3]Dept. of Geological Sciences, University of Florida, Gainesville, USA

The reconstruction of tropical climate and ITCZ dynamics on a high-frequency scale (El-Niño-Southern Oscillation - ENSO, North Atlantic Oscillation - NAO) is pivitol to understand the role of the Tropics in global climate change. Our sediment-core locations sit within the area of seasonal change of the ITCZ position that determines the hydrological cycle and rainfall distribution in Mesoamerica, i.e, along a transect from the Cariaco Basin (off N Venezuela) across Yucatán and Central Mexico to the Pacific coast.

From those laminated sequences, we currently obtain data in ultra-high time resolution applying µXRF-element scanning and varve microfacies analyses. These data, together with radionuclide dates (^{14}C, ^{137}Cs, ^{210}Pb) and tephrochronology, form the basis for a robust, varve-based chronology. Our data has the potential to provide a new history of mean state, frequency, and amplitude of ENSO, and to disentangle the interplay between high versus low latitude forcing of ITCZ dynamics in the region during the past Glacial/Interglacial cycle (the Cariaco Basin) and focused on the past 1000 yr (the Mexican lakes). We will discuss our paleoclimate data in light of the societal development in west Central Mexico and Yucatán. We show new data from two lakes of volcanic origin in México (Hoya La Alberca and Lago Crater) in sub-annual resolution.

The varved sequence from Hoya La Alberca in the Central Mexican Volcanic Belt covers the period AD 1846 - 1975. The chronology is supported by three tephra layers dated to 1903, and 1998 from Colima and to 1943 from Paricutín. The varve micro facies reflect the seasonality with summers rich in precipitation and clastic input and the dry winter half year with diatom production and precipitation of Calcite. This is tracked by the µXRF-derived element chemistry with high Fe and Ti counts vs. high Ca counts. Toward the top of the sequence, rising Ca counts and calcite layer density reflect increasing evaporation in parallel with descenting lake levels. Nevertheless, detrital element counts (Fe, K, Al, Ti) tend to increase as a consequence of increased erosion related to an enlargement of the catchment area in the maar crater that run synchronous with the lowering of lake level and / or to the destruction of the vegetation cover.

The upper 70 cm of the sediment sequence of hypersaline Lago Crater on Isla Isabela, 30 km off Nayarít in the Pacific, span roughly 500 yr. In contrast to the only two-part annual layers (varves) from Central Mexican Hoya La Alberca, the sublayer succession in the Lago-Crater sequence is complex with five distinguishable laminae (see table). This may be due to the maritime influence that alleviates the contrast of the dry season (late-fall to early-spring) and the wet season in summer. A decreasing trend of the counts of detrital elements (Fe, Ti, Al, K) is likely to reflect a trend towards lower external input / lower precipitation to the lake as a consequence of drier conditions. The opposite development of Cl counts may indicate a synchronous salinity increase. Maximum peaks of Ca and Sr occur in cycles offset to those of external input and seem to reflect chemical precipitation events, either as a consequence of high productivity or evaporation.

These data would substantiate that our µXRF-data reflect the cyclic development of the hydrologic balance in the lake.

Layer Code	Organismus	External input precipitation	Season	Sediment color	Diatoms	Ostracods	Pollen	Element maximum peaks	Calcite XX / Calcite detritus
O1	Diatom bloom, vegetation bloom	low / low	fall stratification	green	amphora bloom	none	abundant, small		none / none
O2	Diatom bloom	low / low	winter/srping overturn	intensive green / yellow brown	amphora bloom	much	some		none / none
P_1	(Algal bloom bacteria)	rapid increase high	summer onset rainy season	light yellow / green	amphora (Gomphonema, Nitzschia)	broken shells	rare	Fe, S, Ti, Si, K, Al	scattered / scattered
P_2	(Bacteria)	high / high	summer	light yellow / green	amphora (Gomphonema, Nitzschia)	much	rare	Ca, Sr	concentrated
P_{FU}	none	decreasing / low	fall end rainy season	colorless	none	none	none	Cl	none / none

Table: Isla Isabela, Lago Crater - Sublayer sequence in varves.

IODP

2-Methylhopanoids as biomarkers for Cretaceous bioproductivity of cyanobacteria

Björn Klein[1], Simon C. Brasell[2] and Jürgen Rullkötter[1]
[1]Institute for Chemistry and Biology of the Marine Environment (ICBM), Carl von Ossietzky University of Oldenburg, PO Box 2503, D-26111 Oldenburg; e-mail: b.klein@icbm.de; [2]Biogeochemical Laboratories, Department of Geological Sciences, Indiana University, Bloomington, IN 47405-1403, USA

The sediments drilled during ODP Leg 198 on Shatsky Rise in the Pacific Ocean cover an age range of the Cretaceous through the Paleogene. Within this time interval several abrupt and transient climatic changes occurred, which are associated, amongst others, with drastic changes in primary production in ocean surface waters and in the marine environmental conditions.

Previous organic geochemical analyses of these sediments lead to the assumption that a high phytoplanktonic productivity significantly contributed to the abundant sedimentary organic matter exceeding 30 % Corg in certain intervals (Dumitrescu & Brassell, 2005). Cyanobacteria are important members of phytoplanktonic communities. A problem in determining the amount of cyanobacterial contribution to the sedimentary organic matter is the lack of fossil remains, which would allow a simple estimation. An alternative assessment is the determination of the amount of 2-methylhopanoids either as free molecular biomarkers in the bitumen extractable from the sediment or as bound components which were preserved after incorporation into the insoluble kerogen. 2-Methylhopanoids are specific for a number of cyanobacteria (Summons et al., 1999) and like the A-ring-unmethylated hopanoids readily detectable by standard analytical methods.

A succession of sediment samples drilled during ODP Leg 198 was analysed using pyrolysis-gas chromatography/mass spectrometry (PY-GC/MS) in order to identify the biomarker composition of the organic matter. It is suggested that the ratio of regular hopanoids to their methylated analogues provides a method for estimating the amount of cyanobacterial input into the sediment.

By now 34 samples from ODP Hole 1207B representing a depth interval from 565.23 to 566.42 mbsf and 27 samples from hole 1213B representing a depth interval from 256.84 to 257.91 mbsf were analysed. Both profiles represent pelagic records of the early Aptian Oceanic Anoxic Event (OAE1a), when one of the climatic changes mentioned above occurred.

Dumitrescu, M., Brassell, S.C. (2005) Biogeochemical assessment of sources of organic matter and paleoproductivity during the early Aptian Oceanic Anoxic Event at Shatsky Rise, ODP Leg 198. Organic Geochemistry, 36, 1002-1022.
Summons, R.E., Jahnke, L.L., Hope, J.M., Logan, G.A. (1999) 2-Methylhopanoids as biomarkers for cyanobacterial oxygenic photosynthesis. Nature, 400, 554-557.

IODP

Opaque phase petrology and geochemical modeling as a guide to abiotic organicsynthesis in the Mid-Atlantic Ridge 15ºN area: Results from ODP Leg 209

Frieder Klein and Wolfgang Bach, Universität Bremen, FB 5, Postfach 330440, 28334 Bremen

One of the most intriguing aspects of peridotite-hosted hydrothermal systems is the strongly reduced nature of the vent fluids, due to the production of hydrogen by hydrolysis of ferrous components in the ultramafic host rock. The levels of dissolved hydrogen in these systems are so high that reduced dissolved carbon species are more stable than dissolved inorganic carbon.

We investigate oxide/sulfide/native metal assemblages in hydrothermally altered peridotites (serpentinites) from the ODP Leg 209 area in the Mid-Atlantic Ridge (MAR) 15ºN area. These assemblages are indicative of temperatures as well as oxygen and sulfur fugacities during serpentinization. Certain phases, such as awaruite ($Ni_{2-3}Fe$) are also considered to be important surface catalysts for organic synthesis reactions. Phase petrology and geochemical modeling will be employed to estimate temperature, fluid flux, pH, and redox conditions during serpentinization and to calculate the thermodynamic driving force for organic synthesis reactions under the prevailing conditions of fluid-peridotite interaction.

We here report on first results from a project that started last fall. Initial screening of samples from Leg 209 Sites 1268 and 1274 by electron microprobe indicates awaruite-heazlewoodite (Ni_3S_2)-magnetite assemblages representing very low oxygen and sulfur fugacities during initial stages of serpentinization in Hole 1274A. Site 1268 represents a system with higher integrated fluid fluxes. Oxygen and sulfur fugacities increase during prolonged peridotite-seawater interaction, when the reducing capacity of the rock is exhausted. Such conditions are indicated by millerite as the dominant Ni-sulfide and pyrite and/or phyrrhotite as Fe-sulfides. Using amino acids and organic acids as examples, we show that many organic synthesis reac-tions are exergonic only if redox conditions are set by parageneses that include alloys/metals.

It has been proposed (Seyfried et al., 2004) that vent fluids from mid-ocean ridge serpentinization systems equilibrate with magnetite-heazlewoodite assemblages. In those calculations, the stability field for heazlewoodite is very large, because reduced Ni-phases, except native Ni, have not been considered. An assessment of hydrothermal fluid equilibria with FeNi alloys has so far been impossible due to the lack of solubility data for these phases. We have used standard formation thermochemical data for awaruite and tetrataenite (NiFe) (Howald, 2003) to calculate equilibrium constants for the precipitation of these alloys from aqueous fluids at high temperatures. Our results indicate the existence of two additional phases, awaruite and tetrataenite, between the stability fields of heazlewoodite and nickel. These data will now be used to re-evaluate fluid-mineral equilibria in peridotite-hosted hydrothermal systems such as the Logatchev field in the MAR 15ºN area.

ICDP

Fold-origin of the Sudbury Igneous Complex, Canada: Fold-adjustment flow in the core of its NE-lobe

Christian Klimczak[1] and Ulrich Riller[2]
[1]Freie Universität Berlin, Institut für Geologische Wissenschaften, Malteser Strasse 74-100, D-12249 Berlin, e-mail: christian.klimczak@museum.hu-berlin.de; [2]Humboldt-Universität Berlin, Institut für Mineralogie, Invalidenstrasse 43, 10115 Berlin, e-mail: ulrich.riller@museum.hu-berlin.de

The synformal geometry of the 1.85 Ga Sudbury Igneous Complex (SIC), an impact melt sheet resulting from large-magnitude meteorite impact, attests to post-impact deformation. However, in contrast to the overlying Onaping Formation, a heterolithic impact melt breccia, the SIC shows little evidence for pervasive mesoscopic ductile strain. This pertains in particular to its NE-lobe characterized by a curvature of about 100˚ in plain view. This curvature has been interpreted either as a fold or as a primary feature. In order to test these scenarios, a detailed structural analysis was conducted in the core of the NE-lobe, which consists of rocks of the Onaping Formation.

Structural measurements and lithological observations made at a total of 1300 stations collectively led to the construction of a detailed structural map of the Onaping Formation in the NE-lobe. The map displays a non-systematic pattern of higher-order domes and basins evident by individual units of the Onaping Formation. The fold axes of the domes and basins trend approximately NE-WS and are collinear to the uniformly SW-dipping planar mineral shape fabrics (see Figure below) suggesting a genetic link between these structures. Next to km-scale discontinuities, which in the field and digital elevation models are evident by their strong gradients in topography, the strike of the mineral fabrics assumes that of the discontinuities. In terms of scale and structures developed, deformation of the Onaping Formation in the core of the NE-lobe is, therefore, highly heterogeneous.

Based chiefly on the shape-preferred alignment of metamorphic minerals, the intensity of shape fabrics was visually estimated in the field. Fabric intensity is strongest at the top of the

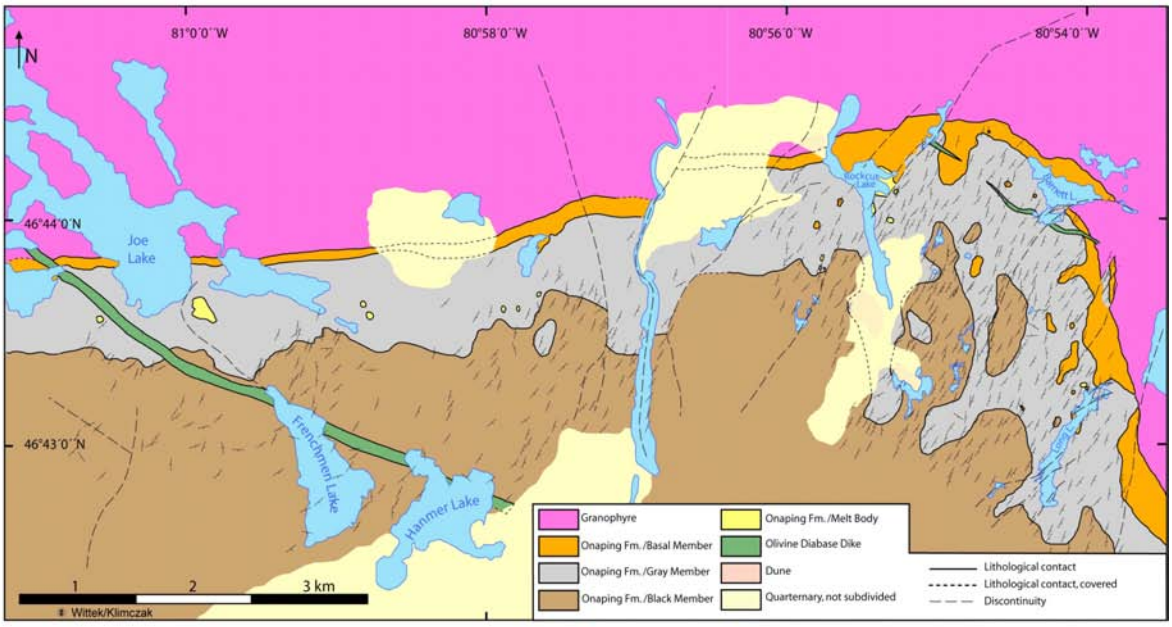

Onaping Formation but decreases dramatically towards its contact with the SIC. This intensity gradient corresponds well with the size of matrix minerals as well as with granitoid and metasedimentary fragments, which increases toward the base of the Onaping Formation. Apart from this lithologically controlled correspondence, shape fabric intensity is maximal in the central portion of the NE-lobe and, along with the axial-planar geometry of the planar mineral fabrics, attest to generation of the NE-lobe be folding of the SIC around a south-westerly plunging axis. During such folding, deformation of the mechanically less competent Onaping Formation was accomplished heterogeneously, evident by the highly variable fold geometry and shape fabric intensity. Such heterogeneous deformation is typical for fold-adjustment rock flow in fold hinge zones of mechanically more competent rocks, i.e., the SIC.

ICDP

Magnetic mineralogy and rock magnetic properties of impact breccias and crystalline basement rocks from the Bosumtwi crater drilling project, Ghana

A. Kontny and J. Just
Geological-Palaeontological Institute, Ruprecht-Karls University, Im Neuenheimer Feld 234, D-69120 Heidelberg, Germany. (agnes.kontny@urz.uni-heidelberg.de)

The Bosumtwi crater drilling project (BCDP) provides core samples of the impact and crystalline basement lithologies from two bore holes (LB-07A and LB-08A) down to a depth of 540 and 450 m, respectively. One main interest of this project is to obtain a complete record of impactites at the central uplift and in the crater moat of the largest young impact structure known on Earth to understand the formation and effects of medium-sized impact craters (Koeberl et al. 2006). Our study contributes rock magnetic and magnetic mineralogy data of the drilled lithologies, which will better constrain the interpretation of the aeromagnetic anomaly pattern and the magnetic borehole measurements. Such data contribute to the understanding of the formation of magnetic minerals and the mechanisms creating and modifying magnetic properties like the remanent magnetization and magnetic susceptibility during impact-related processes.

In general, magnetic susceptibility (k) and natural remanent magnetization (NRM) correlate positively, with largest values up to $20x10^{-3}$ SI units and up to 100 A/m, respectively in a metavolcanic rock sample from 375.6 - 376.1 m. Impact breccias show k values below $0.5x10^{-3}$ SI units and NRM intensities between 0.4 and 200 mA/m, similar to the majority of basement rocks. Therefore, no significant difference was found for these rock magnetic parameters between the basement rocks and impact breccia. However all values, especially for the basement rocks, are distinctly higher than the one reported by Plado et al. (2000) for surrounding rocks of lake Bosumtwi (0.1 - 39 mA/m).

In all lithologies rock magnetic properties are carried mainly by pyrrhotite (T_C: 310-320˚C). In some metavolcanic target rocks, magnetite (T_C: 580˚C) or a magnetite-near phase (T_C: ~450˚C) occurs in minor amounts. Few Fe-hydroxide (T_C: ~160˚C) and probably greigite (T_C: ~350˚C) occur in some samples, mostly from the upper part of the drill core. In the basement rocks, pyrrhotite appears as small (< 10 μm), relics in pyrite indicating a transition from pyrrhotite to pyrite. The sulfide assemblage pyrite, pyrrhotite and arsenopyrite show overgrowth of the schistosity and sulfides grew into open space affirming a genesis after the Birimian metamorphosis. Beside pyrite alteration, a replacement of ilmenite by Fe-sulfides and rutile was observed. In a first step ilmenite is decomposed to pyrrhotite and rutile and in a second step, with increasing sulfur fugacities, pyrrhotite is decomposed to pyrite and rutile. Therefore changing redox conditions accompanied the rock history before the impact event. Mostly pyrite is strongly cataclased in the impact breccias, while pyrrhotite does not show a similar strong deformation, which is odd if pyrrhotite has been formed before the impact. Probably, the small grain size of pyrrhotite (10-20 μm) prevented it from brittle deformation but caused only (rotational?) movement. Transmission electron microscopy will help to solve the question of pyrrhotite formation in relation to the shock event. Small grain sizes of pyrrhotite are magnetically confirmed by the absence of field-dependence of k and relatively high medium destructive fields between 10 and 65 mT, indicative of hard magnetic behavior.

Surprisingly, the supposed high content of melt rocks was not observed and only few porous glass fragments have been found in the impact breccia. The main shock deformation mechanism seems to be brittle under low temperature conditions (<200˚C?). Indications for a post-impact hydrothermal system are scarce. Probably a shock-induced remagnetization of the preexisting pyrrhotite is responsible for the several times higher magnetization compared to the surrounding fall-out suevite.

References

Koeberl, C., et al. (2006) Meteoritics & Planetary Science, in press.
Plado J., Pesonen L.J., Koeberl C. and Elo S. (2000) Meteoritics & Planetary Science, 35, 723-732.

IODP

NanTroSEIZE: The Nankai Trough Seismogenic Zone Experiment, a complex drilling proposal within IODP

Achim J. Kopf[1] & NanTroSEIZE proponents[2]
[1]RCOM, Univ. Bremen, PO Box 330440, 28334 Bremen, Germany; akopf@uni-bremen.de, Tel +49-421-21865800, Fax +49-421-21865805; [2]for full list see: http://ees.nmt.edu/NanTroSEIZE/603-CDP-REV3_pub.pdf

The foremost goal of the NanTroSEIZE (Nankai Trough Seismogenic Zone Experiment) Program is to understand the mechanics and dynamics of seismogenesis and rupture propagation along the active plate boundary faults of a subduction zone, in terms of direct in situ sampling and instrumentation at depth. Nankai Trough is a unique place to study the mechanism and energy budget of great earthquakes in the subduction zone as emphasized in the complex drilling proposal (CDP). Advantages include a long historical earthquake record, extensive DSDP and ODP drilling efforts further to the west, a wealth of pre-site survey data, a huge seismological data set by the Japanese scientists, etc. Also, a cabled observatory network in the Kumano Basin area has just been funded to carry out long-term observation in shallow sediments.

With RV Chikyu, penetrations at a range of depths from ~1 km below sea floor to the seismogenic zone (6.5-7 km bsf) are critical in testing many of the key hypotheses stated in the CDP, which are related to (a) progressive down-dip and along-strike changes in fault mechanical state and frictional properties, (b) fault strength and the role of fluids, (c) temporal changes in strain, micro-seismicity, pore pressure and temperature within the fault zone, and (d) the partitioning of slip between seismic and aseismic periods along faults at different P-T conditions within the system.

All drill sites (and namely the shallow holes) are extremely well suited for complementary studies by other geoscientific disciplines. Non-riser as well as riser-drilling will take place into the incoming plate sediments, incoming seamounts, the toe region of the accretionary wedge, the upper slope of the wedge, into rapidly deposited forearc basin fills, to name just a few. For this exercise, consecutive ship time in excess of 400 days has been allotted for 2007, using both RVs Joides Resolution and Chikyu.

IODP

Calcareous nannofossils in the SE-Atlantic during the middle to late Miocene: Coccolithophorid carbonate budgets and fine-fraction stable isotopes

R. Krammer, K.-H. Baumann, T. Bickert, R. Henrich
Fachbereich 5 - Geowissenschaften, University of Bremen

The Cenozoic is characterized by major changes in the global climate system from ‚greenhouse' conditions in the Early Paleogene towards ‚ice-house'-regime in the Neogene (e.g. Zachos et al., 2001). The opening and closing of oceanic gateways and mountain uplift episodes are assumed to be the main factors inducing these global climate changes resulting in an intensification of circumpolar currents and thermal isolation of Antarctic waters from the subtropics.

The main object of our study was to document and understand the role of coccolithophores as the main carbonate producers in relation to changes in ocean circulation and global climate during the Middle to Late Miocene. For this purpose ODP Sites 1085 (continental margin off Namibia) and ODP Site 1092 (northern slope of the Meteor Rise) were investigated. The nannoplankton contribution to the bulk carbonate production as well as the stable isotopic composition of the coccolith carbonate were explored.

The data show that calcareous nannofossils constitute a significant part of the carbonate fraction. At Site 1085, highest numbers of nannofossils were observed during the intervals 9.9 to 9.7 Ma and 8.7 to 8.0 Ma, probably linked to the initiation of the Benguela Upwelling system at about 10 Ma. Diminished numbers of coccoliths during 9.6 to 9.0 Ma probably indicate time periods of weakened nannofossil productivity resulting in a decrease in nannofossil carbonate content. This decrease in calcareous nannoplankton productivity is one possible explanation for the 'Carbonate Crash' (Lyle et al., 1995) between 9.6 and 9.0 Ma. Therefore, a correlation between productivity in the initiated Benguela Upwelling and carbonate production by coccolithophores seems reasonable. At Site 1092, analyses of calcareous nannofossils show a rise in productivity associated with changes in nutrient availability between 8.8 and 8.6 Ma. Additionally, analyses on polyspecific nannofossil carbonate stable isotopes were performed to reconstruct environmental changes in surface waters. The potential of nannofossil stable isotopes as indicators of conditions in the shallow mixed-layer was shown by comparing these records with those of co-existing planktic foraminifers. Based on the data set of Site 1085, nannofossil carbonate isotopes reflect surface-water hydrographic conditions of the late winter-early spring period when relatively cool, nutrient-rich subsurface water mass is entrained into surface waters by vertical mixing. In contrast, foraminiferal isotopes reflect the post-deep-mixing, relatively warmer (late spring to fall) stratified water masses. This seasonality effect on plankton production offers the possibility to quantify paleoseasonality.

This study showed, that coccolithophores provide important paleoenvironmental informations. They are a useful tool to reconstruct paleoproductivity and changing surface-water conditions in the eastern South Atlantic during the Middle to Late Miocene. Now, we propose a research project in the Northern Atlantic (ODP Site 982) to prove the potential of coccolithophorid stable isotopes as proxy to reconstruct the surface water variability and climatic development.

References:

Lyle, M., Dadey, K.A., Farrell, J.W., 1995. The late Miocene (11 - 8 MA) eastern Pacific carbonate crash: evidence for reorganisation of deep-water circulation by the closure of the Panama gateway. Proc. ODP, Sci. Res. 138, 821-838.
Zachos, J., Pagani, M., Sloan, L., Thomas, E., Billups, K., 2001. Trends, rhythms, and aberrations in global climate 65 Ma to present, Science, 292, 686-693.

IODP

Towards a Baltic IODP - New results from a seismic pre-site survey in the Kattegat area and the southern Baltic Sea

S. Krastel[1], T. Andrén[2], O. Benike[3], R. Endler[4], J. Harff[4], V. Spieß[1], B. Wagner[4]
[1]Bremen University; [2]Stockholm University; [3]Geological Survey of Denmark and Greenland, Copenhagen; [4]Baltic Sea Research Institute Warnemünde

In 2004 a group of scientists from countries around the Baltic Sea submitted a pre-proposal for a Baltic IODP "Paleo-environmental evolution of the Baltic Sea Basin through the last glacial cycle". The general aims of the project are to use the high resolution sedimentary record of the Baltic Sea in order to reconstruct the climatic response of Northern Europe to the forcing of the Northern Atlantic atmospheric and oceanic circulation changes during the last c. 130 000 years. Eemian interglacial and Early Weichselian interstadial sequences are expected in the Kattegat area. The southern Baltic Sea which is regarded having been ice free before the Last Glacial Maximum at c. 20 000 yrs BP is prospective for complete records of the Early and Middle Weichselian interstadial deposits, whereas the Northern Baltic Sea hosts Late Weichselian to Holocene varved clay sediments.

During a first field campaign He244 (06.02.06-16.02.06) using the German R/V "Heincke" a pre-site survey has been carried out in five areas prospective for IODP drilling sites in the Kattegat and the southern Baltic Sea: Kattegat: "Anholt Loch"; Southern Baltic Sea: "Arkona Basin", "Kristiansø Horst", "Ivar Crater" and "Hanö Bay". Two methods have been deployed during the survey: Air gun profiling and sediment echosounding.

Due to the shallow water depth (<80m) and the large lateral variability of the Quaternary sediments in the survey area we used a combination of two streamer systems for recording the seismic data. An especially designed 50 m-long shallow water streamer with single hydrophones at a spacing of 1 m allows imaging of the Quaternary deposits with extremely high lateral resolution but

causes problems in determining sediment velocities and the suppression of multiples. Therefore we additionally used a 300 m long 48 channel streamer with a group spacing of 6.25m. These data will allow a precise velocity analyses which is essential for distinguishing between (low-velocity) Quaternary deposits and (high-velocity) bed rocks. Both data sets were recorded simultaneously. A 0.4 l GI-Gun was used as a source for both streamer systems. Based on a preliminary processing and first interpretation of the data, three of the surveyed areas represent promising locations for the proposed IODP-drilling campaign.

The "Anholt Loch" within the southern Kattegat is situated in a tectonically active zone at the border of the Fennoscandian Shield: The seismic data show a northwest striking erosional valley that hosts on top of (Jurassic ?) bedrock a sequence of interglacial, glacial, late glacial, and Holocene sediments. Based on a sedimentary sequence penetrated by a well on Anholt Island the sediments deposited in the "Anholt Loch" are expected to represent Weichselian and older (Eemian and Saalian) sand and clay sequences overlain by well stratified late glacial clay and Holocene mud.

In the southern Baltic the isolated basin of Hanö Bay is assumed to host glacial and interglacial sediments sheltered from glacial erosion during the last Weichselian ice advances. Here an extended seismic data set of very high quality revealed several sedimentary facies which may be attributed to longer records of glacial and limnic processes. .A first interpretation of the seismic data indicates the possible occurrence of a thick, relatively transparent sequence of sediments with some internal reflectors below a relatively thin till cover of Late Weichselian age. The lower unit is assumed to be of Eemian, Early or Mid Weichselian age. The whole area is covered by Holocene mud and clay. These data indicate that this site may be the most promising drill site investigated during the "Heincke"-cruise.

In the Arkona Basin a glacially (most probably pre-Weichselian) eroded, more or less E-W oriented valley was identified on the seismic data. This valley protected the basin fill from erosion by the last Weichselian ice-flow from north and northeast with only a last weak ice advance from almost due east. The basin fill shows a seismic stratigraphy typically for the southern Baltic Sea: below appx. 20 m of Holocene mud, late glacial clay and till is an up to 100 m thick imaged as acoustically transparent unit with several internal reflectors. These sediments are assumed to have deposited in a lake that existed in the southern Baltic Sea before the last ice advance between 40 000 and 20 000 yrs BP. Sediments of the above listed areas will be sampled during an expedition using R/V "Maria S. Merian" between March 27 and April 5, 2006. Core data together with processed seismic data gained during the "Heincke"-expedition will be used for the full proposal for a Baltic drilling campaign to be submitted to the IODP panel by October 1, 2006.

ICDP

Noble Gases in Olivine Phenocrysts Derived From the 3109 m to 3340 m depth interval of the HSDP-2 Drill Core Section of Mauna Kea Volcano

Krüsmann, T., Niedermann, S. and Erzinger, J.
GeoForschungsZentrum Potsdam

Noble gas concentrations and isotopic compositions will be analysed in olivine phenocrysts from the 3109 m to 3340 m depth interval of the Hawaii Scientific Drilling Project (HSDP) phase II drill core recovered in 2004/2005. The existing hole from 1999 was deepened in 2004/2005 starting at the bottom of the 1999 hole at 3109m. As of Feb 2005 the drilling had reached 3340 m, recovering 231m core. Samples of this depth interval have recently been taken and olivine is now being separated for the noble gas measurements to be accomplished in March/April 2006. The aim is to integrate the data record to greater depths in order to achieve information on the chemical and isotopic composition of the early stages of the Mauna Kea volcanism. The knowledge about the origin and evolution of the Mauna Kea magmas is still incomplete; therefore uncovering the chemical and isotopic composition of the early Mauna Kea lavas will contribute to the interpretation of the evolution and structure and to a refinement of geochemical models of the Hawaiian plume.

The equipment for the determination of noble gases consists of (1) a high temperature ultrahigh vacuum extraction furnace to release gases from the olivine samples, (2) a gas purification line, (3) two cryostatic adsorbers to separate the noble gases from each other, and (4) the noble gas mass spectrometer VG 5400. The noble gases are extracted from the minerals at several temperature steps. The aim of the sequential extraction of noble gases through stepwise heating is to take advantage of the different release patterns of components with different origin and locations within the sample (Ozima and Podosek, 2002).

The results of the noble gas analysis of the 3109 m drill core recovered in 1999 during phase II of the HSDP (Althaus et al., 2003) led to the following conclusions. He, Ar, and sometimes Ne start to reveal their mantle signature at extraction temperatures from 1200˚ to 1400˚C, becoming more evident at melting temperatures (1700˚-1800˚C). While the 3He/4He ratios show a temporal trend, which is characterized by an increase in the subaerial section of the drill core, Ne and Ar do not reveal a comparable evolution with time. The dominant 3He/4He in the submarine samples is around 12 R_A (R_A is the atmospheric $^3He/^4He$) , but there are short "spikes" of a few lava flows between 2000 and 2600m characterized by elevated $^3He/^4He$ up to 21 R_A (Althaus et al., 2003). The hypothesis that high $^3He/^4He$ values represent the Hawaiian plume center leads to the assumption that Mauna Kea sampled pulses of magma of the upwelling plume, represented by the high $^3He/^4He$ spikes, but was never directly over the plume centre, hence the return to values ranging about 12 R_A, which dominate the submarine section (Kurz and Solow, 2004). The isotopic signature of Ne shows a typical trend in those samples and correlates within error limits with the Loihi-Kilauea line as defined by Honda et al. (1991), thereby indicating a plume derived origin (Althaus et al., 2003). $^{40}Ar/^{36}Ar$ varies widely between 360 and 3300 due to different contributions of components with air-like isotopic signatures. Krypton and xenon isotopic signatures remain air-like throughout the drill core.

Althaus T., S. Niedermann, and J. Erzinger (2003) Noble gases in olivine phenocrysts from drill core samples of the Hawaii Scientific Drilling Project (HSDP) pilot and main holes (Mauna Loa and Mauna Kea, Hawaii). Geochem. Geophys. Geosyst. 4(1), 8701, doi:10.1029/2001GC000275.

Honda M., I. McDougall, D. B. Patterson, A. Doulgeris, and D.A Clague (1991) Possible solar noble-gas component in Hawaiian basalts. Nature 349(6305), 149-151.

Kurz M. D. and A. Solow (2004) Rapid helium isotopic variability in Mauna Kea shield lavas from the Hawaiian Scientific Drilling Project. Geochem. Geophys. Geosyst. 5(4), Q04G14, doi:10.1029/2002GC000439.

Ozima M. and F.A. Podosek. (2002) Noble Gas Geochemistry- 2nd ed. Cambridge University Press.

ICDP

Interpretation of Injection-induced Micro Seismicity at the German Deep Drilling Site (KTB)

J. Kummerow[1,2], G. Asch[1,2], S.A. Shapiro[2], C. Dinske[2], E. Rothert[2]
[1]GeoForschungsZentrum Potsdam; [2]Freie Universität Berlin

Introduction

The KTB site in Southeastern Germany provides a dual borehole configuration, with the 4.0 km deep pilot hole and the 9.1 km deep main hole at only 200 m surface distance. This offers an unique potential to study the physical rock parameters, rheology and dynamics of the continental crust. Two fluid injection experiments were previously carried out near the open-hole section of the main hole at 9 km depth, which triggered intense microseismicity (Zoback & Harjes 1997, Baisch et al. 2002).

Recently (2004-2005), a third, long-term (12 months) injection experiment was performed. Unlike the previous cases, the fluid

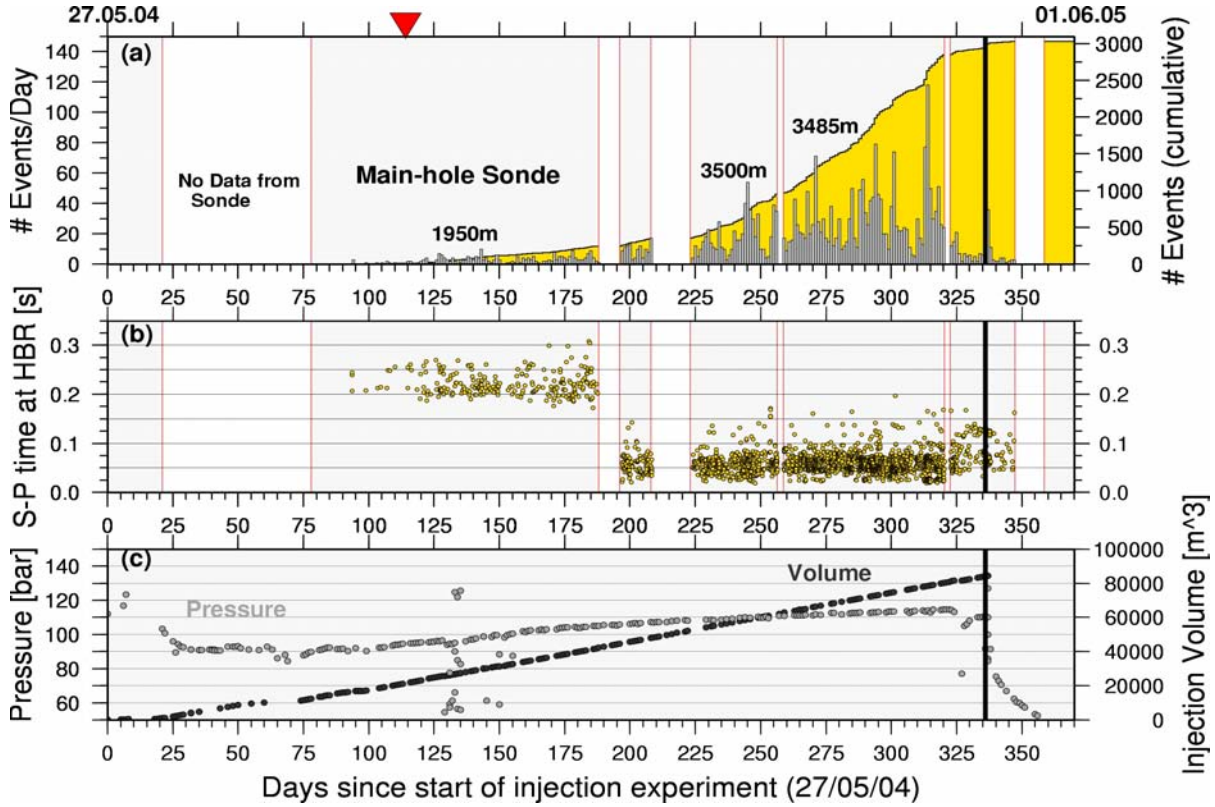

Fig. 1: (a) Rate of induced events observed at the sensor in the KTB main borehole. Numbers mark the changing installation depths of the geophone. (b) Travel time difference between S and P onsets at the main hole geophone. (c) Rate of well-head pressure and injection volume.

was injected directly into a continental fault system (named SE2 reflector) at the bottom of the pilot hole at 4 km depth. The seismicity was monitored by a borehole sensor in the main hole at 1.9/3.5 km depth, and additionally by a near-surface seismic array. The injection phase was preceded by an one-year fluid production test in 2002/2003.

Precise absolute and relative event locations were performed, and the spatio-temporal characteristics were analysed in order to determine the hydraulic behaviour of the fault. We tested the effect of the velocity model on the absolute location of the KTB events, and optimized the arrival time data set by calculating waveform cross correlation. We relocated the hypocenters by applying a relative location method.

An approach to estimate the hydraulic diffusivity of rocks using microseismicity (Seismicity Based Reservoir Characterisation, SBRC) uses a spatio-temporal analysis of the cloud of fluid-injection induced events (e.g. Shapiro et al. 2002). This approach has already been applied to the previous injection experiments at the KTB site (see Shapiro et al. 1997 and Rothert et al. 2003). Here, we present results for the most recent injection test in 2004/2005.

Seismic monitoring of the KTB2004/2005 injection experiment

Seismicity was monitored for a period of almost two years, starting six months before the initiation of the injection experiment and ending four months after the termination of the injection. The main components of the KTB seismic monitoring system were: A 15 Hz geophone in the KTB main hole, with a horizontal distance of about 200 m to the injection source in KTB pilot hole. Installation depth was variable (1950 m/3500 m). A network consisting of seismic near-surface stations. These instruments and the main hole sensor were integrated into an on-line monitoring system based on wireless LAN technology with a radius of about 2.5 km from the KTB. About 15 offline seismic instruments which temporarily supplemented the on-line monitoring system. They where deployed mostly within a distance of 5 km from the KTB.

Induced seismicity

During the KTB 2004/2005 injection experiment, a total volume of 84600m3 water was injected in the pilot hole at 4 km depth (Fig. 1). Injection rate was constant at 200 l/min. The first micro event was recorded on July 30, 2004, i.e. 64 days after the injection start. This time roughly coincided with the time, when the fluid volume extracted during the previous production test (22000m3) had been re-injected. The seismicity rate steadily increased until days 300-320 of the experiment with peak values of >100 events per day. Simultaneously, the pressure increased from 90 bar to 115 bar. The recorded seismic activity ceased within two weeks after the injection experiment. Magnitudes of the detected events are in the range of about -2.5 to +0.4.

Event location

Absolute location of the induced events was performed within a local 3D gridded velocity model using the NonLinLoc software package (Lomax et al. 2000). In order to achieve a better accuracy in arrival time picks, we calculated differential travel times by waveform cross-correlation and combined them with the original picks. Using an inversion algorithm adopted from Shearer (1997) we obtained an adjusted, more consistent arrival time data set. The effect on the locations is a further improvement in scatter and data fit (mean rms residual of ~ 6 ms).

The epicenters define an elongated, NW-SE trending zone, coinciding with the strike direction of the SE2 fault system. The distance from the injection source is about 250-800 m. The largest hypocentral depths seem to be limited by the depth of the injection point in 4.0 km (Fig. 2). We refined the locations using the double difference method (Waldhauser & Ellsworth 2000). The relocations yield a narrower seismically active zone and a stronger clustering.

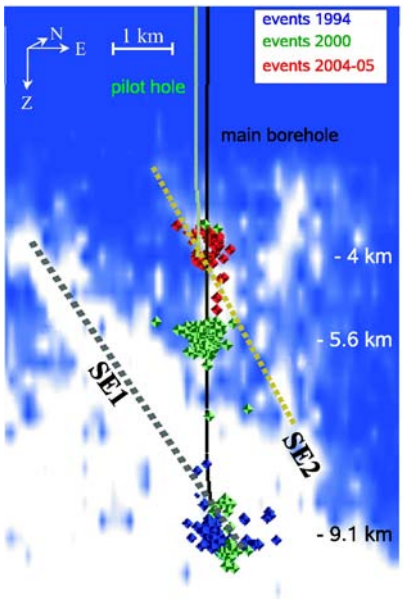

Fig. 2: Depth migrated image ISO89-3D. The seismic reflection intensities are shown in blue-white colour. Seismicity induced by KTB injection experiments is also plotted (diamonds).

Microseismicity and hydraulic parameters

In its simplest version, the SBRC approach uses an equation describing the spatial position r of the so-called triggering front in an effective isotropic homogeneous poroelastic medium with the scalar hydraulic diffusivity D at time t:

$$r=(4\pi Dt)^{1/2}$$

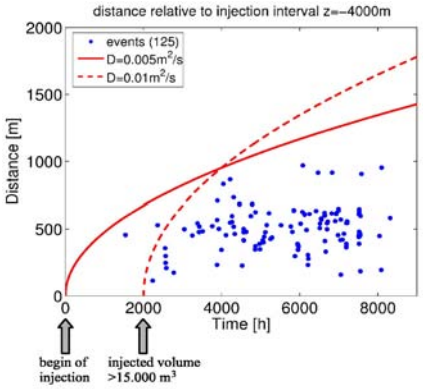

Fig. 3: Estimates of the microseismic triggering front for the injection in 2004/ 2005

Fitting the cloud of events by a parabolic envelope (Fig. 3) provides the effective scalar estimates of the hydraulic diffusivity. The standard SBRC formulation requires an injection experiment without any preliminary fluid extraction i.e., the excess pore pressure build-up must start at time zero. Applying the envelope fitting (red solid line) without taking into account the fluid extraction and recovery phase leads to underestimating hydraulic diffusivity. When using instead the onset of significant seismicity at time zero, the obtained estimates of the hydraulic diffusivity are of the order of 0.01 - 0.02 m2/s. These values are higher than the diffusivity at the depth of 5.4 km (0.004 m2/s to 0.01 m2/s). This is also in good agreement with the slightly enhanced seismic reflectivity of the SE2 fault system in respect to the surrounding rocks. Furthermore, the hydraulic diffusivity is smaller than the values obtained at 9 km depth for the injection experiments in 1994 and 2000 (0.05 m2/s to 2 m2/s), which are strongly influenced by the SE1 fault system (see Figure 2).

Conclusion

The influence of the orientations of pre-existing natural fracture systems on the triggering of microseismicity is obvious. Recent (2002-2005) hydraulic experiments at the KTB indicate several unique features of microseismicity related to properties of the seismic SE2 reflector. Firstly, it seems that this fault is seismically more stable than rock volumes stimulated during previous (1994 and 2000) injections. It produces less seismicity for the same order of averaged injection pressure and much larger injection fluid volume. The seismic reflectivity is positively correlated with the hydraulic permeability. The SE2 reflector is characterized by permeability up to one order of magnitude higher than that of surrounding rocks. For pressure perturbations in the order of tens of bars, this fault has non-linear hydraulic properties (permeability increasing with pore pressure, according to flow-pressure data of the recent production and injection experiments).

References

Baisch, S., Bohnhoff, M., Ceranna, L., Tu, Y. and Harjes, H.-P. [2002] Probing the Crust to 9-km Depth. Fluid-Injection Experiments and Induced Seismicity at the KTB Superdeep Drilling Hole, Germany. Bull. Seism. Soc. Am. 92(6), 2369-2380.

Lomax, A., Virieux, J. , Volant, P. and Berge, C. [2000] Probabilistic earthquake location in 3D and layered models: Introduction of a Metropolis-Gibbs method and comparison with linear locations. Advances in Seismic Event Location, Ch. Thurber and N. Rabinowitz (eds.), 101-134. Kluwer, Amsterdam.

Rothert, E., Shapiro, S.A., Buske, S. and Bohnhoff, M. [2003] Mutual relationship between microseismicity and seismic reflectivity: Case study at the German Continental Deep Drilling Site (KTB). Geophys. Res. Let. 30(17), doi:10.1029/2003GL017848.

Shapiro, S.A., Huenges, E. and Borm, G. [1997] Estimating the crust permeability from fluid-injection-induced seismic emission at the KTB site. Geophys. J. Int. 131, F15-F18.

Shapiro, S.A., Rothert, E., Rath V. and Rindschwendtner, J. [2002] Characterization of fluid transport properties of reservoirs using induced microseismicity. Geophysics 67, 212-220.

Shearer, P.M. [1997] Improving local earthquake locations using the L1 norm and waveform cross correlation: Application to the Whittier Narrows, California, after shock sequence. J. Geophys. Res. 102, 8269-8283.

Waldhauser, F. and Ellsworth, W.L. [2000] A double-difference earthquake location algorithm: Method and application to the northern Hayward fault, Calif.. Bull. Seism. Soc. Am. 90, 1353-1368.

Zoback, M. and Harjes, H.-P. [1997] Injection induced earthquakes and the crustal stress at 9 km depth at the KTB deep drilling site. J. Geophys. Res. 102, 18477-18492.

ICDP

Detection of fluid movements, caused by the Fluid Injection Test from 2004 till 2005, in great depths at KTB-site

Laaß, D., Danckwardt, E., Petzold, G. (Leipzig, Institute of Geophysics and Geology)

Introduction

In a depth of nearly 4,000 meters, the KTB pilot borehole situated near Windischeschenbach in the Upper Palatinate passes through a fault zone which belongs to an area where two continental shelves have collided 320 million years ago. So, it is possible to carry out field studies about processes of fluid movements in continental fault systems e.g. by injection experiments. Our studies, as presented below in greater detail, are based on measurements of the geoelectrical and self-potential field. They should contribute to a better characterization of transport phenomena.

Fluid Injection Test from 06/2004 till 05/2005

The fresh water injection of more than 80,000 cubic meters during a period of 12 months caused an increase of the electrical resistivity of the fluids at the borehole-site. The saline crust water was stirred and displaced by injected fresh water. Because of the large contrasts in electrical conductivity, geoelectrical methods are predestined for the detection of the inflow of natural fluids as well as for estimation of the direction of movements and the depth of flows, bound to fractures and cracks of the fault.

Geoelectrical methods

Inhole-measurements

Inhole-logs gave an overview about vertical variations of the electrical conductivity with increasing depth in the uncased part of the pilot borehole (3,850 m - 4,000 m). The resistivity meter Geotom and the Vertical Electrode System (VES) were used for a dipole-dipole configuration of electrodes (spacing of 25 m) that

provides a horizontal investigation depth of about 25 m around the borehole. First geoelectrical measurements after the injection test took place in September 2005, three months after the injection was finished. Higher electrical resistivity values than those measured in 2003 after the KTB production test were detected. The repeat of the measurements in November 2005 partially proved the inflow of new built saline crust water close to the pilot borehole, since only little changes in electrical resistivity had been detected (fig. 1). In addition, measurements planned for spring of this year should provide more information about the situation of balance - is the redress the balance still in progress or not.

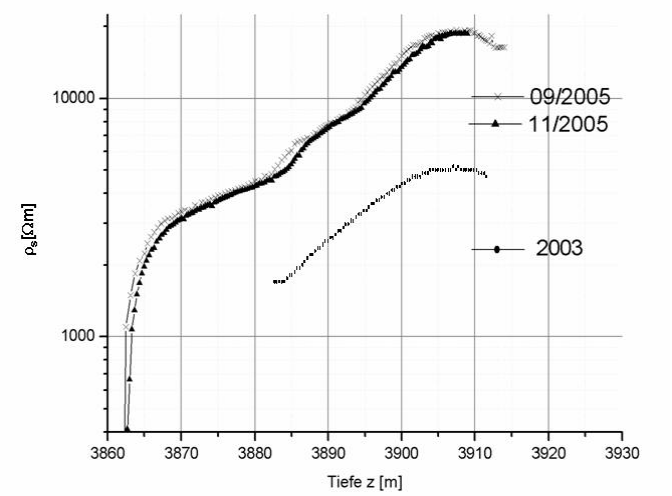

Fig. 1: Little changes in electrical resistivity (inhole-logs) in the uncased part of the pilot borehole between September (cross) and November (triangle) 2005, for comparison values after Fluid Production Test in 2003 (dot).

Surface-hole-measurements

Combined surface-hole-experiments provide clear information about the depths of inflow and their direction of movement as well as processes of stabilization in larger distances to the pilot borehole. Currents of 5 - 7 A were injected with the Scintrex TSQ-4 at 11 dipoles (dipole length = 250 m) around the pilot borehole (average distance = 1,000 m). The potential was registered in the uncased part of the pilot borehole at each of the 7 dipoles (dipole lengths of 25, 50 and 100 m) using Texan 125 data loggers.

Registration of the natural electrical field

The natural electrical field was recorded at the surface with two crossing dipoles (l = 200 and 290 m, very close to the pilot borehole) by the transient recorder Texan 125 in November 2005. A single spectrum of the measurements in the depth of 3876.5 m is shown in fig. 2. Next to the peak of 16 2/3 Hz (train) two undefinable distinct maxima (about 0.14 and 2.5 Hz) appear. Schumann resonances generate peaks of nearly 8 Hz and their harmonic of 14 Hz. Measurements of the natural electrical field should give clear evidence of the correlations between variations of the natural electrical field and fluid movements caused by the fluid injection test.

Outlook and conclusions

Geoelectric measurements are predestined for registration of changes in conductivity, even in a large scale system. Inhole-logs could give a first indication of fluid inflow displaced by injected fresh water last year. Whether such decreases in electrical resistivity signify the beginning of reaching balance or an end to the fluid's movements, is difficult to say without knowledge of the results of forthcoming measurements in spring this year. Because there was no reference measurement permitted before the injection test was started, the third field work is essential for final interpretation.

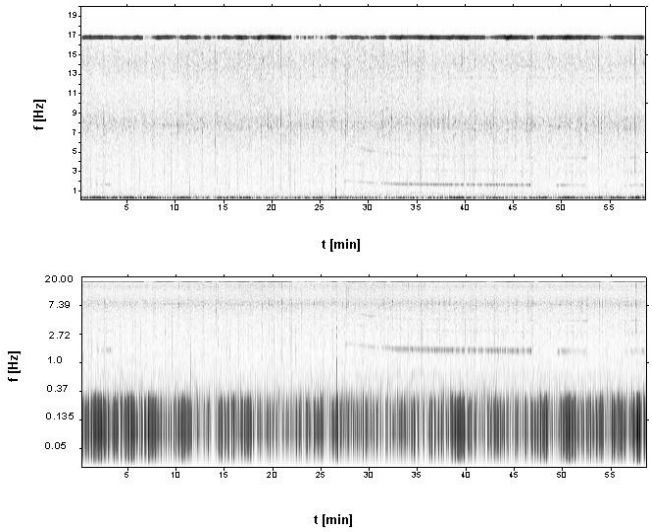

Fig. 2: Example of frequency-time-spectrum (linear on top, logarithmic on bottom) of the natural electrical field in a depth of 3876.5 m from 04:00 p.m. till 05:00 p.m.; high amplitude: black, low amplitude: white.

The analysis of our data is still under way, yet updated results will be presented at the conference.

Acknowledgment

We gratefully acknowledge financial support by DFG grants DA 317/4-1and 4-2.

IODP

High Resolution SST record from the Southeast Pacific provides new insights in interhemispheric climate pattern during Termination 1

Frank Lamy[1*], Jérôme Kaiser[1], Helge W. Arz [1], Dierk Hebbeln[2], Barbara Stenni[3]
[1]GeoForschungsZentrum-Potsdam, Telegrafenberg, 14473 Potsdam, Germany; [2]DFG Research Center Ocean Margins, Leobener Strasse, 28359 Bremen, Germany; [3]University of Trieste, Via E. Weiss 2, 34127 Trieste, Italy; *To whom correspondence should be addressed: flamy@gfz-potsdam.de

There is a general consensus that the deglacial warming in the Southern Hemisphere mid- and high latitudes started earlier than in the north. In addition, the warming trend was interrupted by a millennial-scale cooling event (Antarctic Cold Reversal, ACR) that began at or around the time of the Bölling/Alleröd (B/A) warming and ended close to the beginning of the Younger Dryas cold phase observed in the Northern Hemisphere. In Antarctic ice-core records, the timing of the ACR is relatively well constrained as large swings in methane records allow a relatively close synchronisation to the Greenland records though the partly large gas age/ice age offsets may introduce significant uncertainties. However, before ca. 15 kyr B.P and back to ca. 28 kyr BP (gas ages), methane fluctuations are much smaller making the exact timing of the beginning of deglacial warming and short-term events before more ambiguous.

Here, we present a new, well-dated (14C-AMS), and high resolution sea-surface temperature (SST) record from Ocean Drilling Project Site 1233 located within the northernmost Antarctic Circumpolar Current off southern Chile (41˚S). In previous works, we showed that the complete ca. 70 kyr-long SST record closely follows millennial-scale temperature fluctuations as observed in Antarctic ice cores. We now substantially increased the time resolution during the deglaciation in order to resolve centennial-scale events. Deglacial warming starts at ca. 18.7 kyr BP. with an abrupt SST increase of nearly 5˚C until 17.5 kyr BP. Therafter, temperatures remain nearly stable until the beginning of a second warming step of ca. 2˚C between ca. 12.7 and 12 kyr BP. Superimposed on these general trends, minor SST variability with amplitudes in the order of 1˚C can be observed.

A comparison to the methane-synchronised temperature record of the Western Antarctic Byrd ice-core suggests a close correspondence in the timing of the beginning of the deglacial

warming and the second warming step at the end of the ACR. These major trends are also observed in inland ice cores such as Dome C (applying a methane synchronisation time-scale). In contrast to the ice-core records, our Pacific SST record shows a much faster initial warming that starts exactly at the time of the beginning of cooling in Greenland towards Heinrich Event 1. In addition, we do not observe a cooling at the beginning of the ACR but a warming at its end (during the Younger Dryas). These observations may suggest that the mid-latitude Pacific reacts more rapid to reductions of the North Atlantic Thermohaline Circulation (THC) than inland Antarctica. Conversely, a cooling during the resumption of the THC (as during the B/A) appears to be more prominent in Antarctica and only minor in the subpolar Pacific. Shorter-term temperature fluctuations during the deglaciation as observed in our record appear in a similar shape in the coastal ice-core sites (Byrd and Law Dome) but are basically absent in the more continental Dome C record. Finally, the close correspondence of our SST record in particular to the Byrd ice core records may help to improve the ice core stratigraphy during those time-intervals where methane records only show minor fluctuations.

ICDP

Gasgehalte und mikrochemische Charakteristika von Impaktgläsern der Bosumtwi-Struktur (Ghana) und Tektiten der Elfenbeinküste

F. Langenhorst[1], A. Deutsch[2], U. Bläß[1], K. Heide[1]
[1]Institut für Geowissenschaften, Friedrich-Schiller-Universität Jena, Burgweg 11, D-07749 Jena, Germany, Falko.Langenhorst@uni-bayreuth.de ; [2]Institut für Planetologie, Westfälische Wilhelms-Universität Münster, Wilhelm-Klemm-Straße 10, D-48149 Münster, Germany, deutsca@uni-muenster.de.

Die Bosumtwi-Struktur in Ghana, Westafrika, ist ein junger (~1.07 Ma), gut erhaltener Impaktkrater, der im Rahmen des International Continental Drilling Projects (ICDP) im Oktober 2004 erbohrt wurde. Unter den derzeit bekannten irdischen Kratern ist Bosumtwi die größte (Ø=10.5 km) komplexe Impaktstruktur mit einer zentralen Aufwölbung. Im Zusammenhang mit Bosumtwi sind Gläser aus drei unterschiedlichen Quellen bekannt: (1) die Tektite der Elfenbeinküste, (2) ein Mikrotektitstreufeld vor der afrikanischen Küste und (3) Impaktgläser in oberflächlich aufgeschlossenen Sueviten. Gläser konnten bislang kaum in den Kernen der ICDP-Bohrung nachgewiesen werden.

Die Bohrkerne enthalten im Wesentlichen verschiedene brecciierte Sedimentgesteine des Deckgebirges, die von Grauwacken bis hin zu Schiefertonen und Tonschiefern reichen. Die Breccien dokumentieren insgesamt einen erstaunlich niedrigen Grad der Stoßwellenmetamorphose, d.h. Impaktglas-Partikel oder diaplektische Gläser sind weitgehend unbekannt. Im Gegensatz dazu sind Impaktgläser in den Rückfall-Sueviten nördlich des morphologischen Kraterrandes weit verbreitet. Für die vorliegende Studie wurden Glas-reiche Suevite aus dem Gebiet zwischen Nyameani and Nkowinkwanta nahe des nördlichen Kraterrandes gesammelt. Zusätzlich wurden vom Max-Planck-Institut für Kernphysik in Heidelberg Tektite der Elfenbeinküste zur Verfügung gestellt. Die schwärzlichen Tektitkugeln stammen aus den (süd)östlichen Landesteilen der Elfenbeinküste (Adzope, Daoukro, und Nzi-Nziblekro). Um einzugrenzen, aus welchen der erbohrten Lithologien sich die Tektite und Suevitgläser zusammensetzen und welche Abkühlungsgeschichte die Gläser durchlaufen haben, wurden vergleichende petrologische, analytische und mikrostrukturelle Untersuchungen mittels Polarisationsmikroskopie, DEGAS-Gasanalytik (Kopplung von Thermogravimetrie und Massenspektrometrie) und analytischer Transmissionselektronenmikroskopie (TEM) durchgeführt.

Die an der Krateroberfläche beprobten Rückfall-Suevite enthalten verschiedene Gläser, die von Coesit-führenden diaplektischen Quarzgläsern über Mineralgläser mit Fließstrukturen bis hin zu heterogenen blasenreichen Glassplittern mit Schlieren reichen. DEGAS-Analysen der blasenreichen Gläser weisen auf kleine Konzentrationen von Wasser (Freisetzung bei 320˚C) und Spurengehalte von CO_2/CO, Kohlenwasserstoffen (aliphatische Komponenten bzw. CH_4), SO_2 und H_2 hin (geordnet entsprechend abnehmender Konzentration). Die Wassergehalte sind aufgrund des Verlaufs der Spektren zum Großteil auf geringe Beimengungen von Tonmineralen zurückzuführen. Im deutlichen Gegensatz dazu sind die Tektite der Elfenbeinküste vollständig entgast, was möglicherweise auf ihre sehr hohen Bildungstemperaturen zurückzuführen ist.

TEM-Untersuchungen wurden bislang an den blasenreichen Gläsern durchgeführt. Dabei konnten starke chemische Heterogenitäten bezüglich des Al/Si-Verhältnisses nachgewiesen werden. Die Gläser zeigen eine Glas-Glas-Entmischung, wobei die Matrix SiO_2-reich ist, während die entmischten Glaskügelchen sehr hohe Al_2O_3-Gehalte (bis zu 56 Gew.% Al_2O_3) aufweisen. Dieses Entmischungsgefüge deutet auf eine langsame Abkühlung im Glasübergangsbereich hin. Die insgesamt hohen Al2O3-Gehalte (im Mittel ca. 22 Gew.% Al_2O_3) sind nur mit Staurolith-führenden Glimmerschiefern erklärbar, die als Fragmente in den Sueviten auftreten.

IODP

Application of Texture Analysis in Electrical Borehole Wall Images

Margarete Linek[1], Matthias Jungmann[2], Thomas Berlage[2], Renate Pechnig[2,3], Christoph Clauser[1]
[1]Applied Geophysics, RWTH Aachen University; [2]Fraunhofer Institute for Applied Information Technology, St. Augustin; [3]Geophysica Beratungsgesellschaft mbH, Aachen

Within the Integrated Ocean Drilling Program (IODP), image logging tools are routinely deployed using the Formation MicroScanner (FMS) tool. This method is based on resistivity measurements at the borehole wall and is consequently sensitive to conductivity contrasts, which are converted into colour scale images. These images are commonly used to study the structure of sedimentary rocks and the oceanic crust (petrologic fabric, fracture and vein occurrence, etc.).In IODP, the mapping of lithology from electrical images is currently based on visual inspection and subjective interpretation. We apply pattern recognition techniques on electrical borehole images in order to develop a method, which augments objective rock identification. Pattern recognition is the study of how machines can learn to distinguish certain patterns. There are object- or texture-based methods. We apply a supervised texture analysis for rock type classification, which studies the spatial distribution of grey level. Supervised texture classification involves three processes: image acquisition, feature generation in image intervals of known rock types, and classification of the entire data set. In order to extract texture features, a grey level co-occurrence matrix (GLCM) is computed by counting the number of occurrences of a pair of grey levels that are a certain distance apart. Once the GLCM is computed, we are able to calculate so-called Haralick texture features such as contrast, energy, entropy, homogeneity, and autocorrelation. In addition, we use the wavelet-transform in order to localise frequencies in space. The wavelet transform decomposes the image signal into frequency-dependent sub-images enhancing horizontal, vertical and diagonal texture features. The combination of wavelet transform and Haralick texture features provides a wide variety of image attributes. We assign characteristic texture features to different rock types by reducing the image information into a small set of descriptive features. Once an appropriate set of texture features is computed, we define a suitable classification algorithm to assess the discriminative power of these features. Rock classification based on texture analysis enables objective lithology mapping and is characterised by a high repeatability in contrast to subjective image interpretation.

IODP

Novel heterotrophic Archaea dominate deeply buried sulfate-methane transition zones in sediments off Peru.

Julius S. Lipp[1], Jennifer Biddle[2,3], Helen F. Fredricks[4], Marcus Elvert[1], Jean E. Brenchley[2,3], Andreas Teske[5], Christopher H. House[3,5], Kai-Uwe Hinrichs[1,4]
[1]Organic Geochemistry Group, Dept. of Geosciences, University of Bremen, D-28334 Bremen, Germany Email: khinrichs@uni-bremen.de; [2]Dept. of Biochemistry and Molecular Biology & [3]PennState Astrobiology Research Center, Pennsylvania State University, University Park, PA, USA; [4]Dept. of Geology and Geophysics, Woods Hole Oceanographic Institution, Woods Hole, MA, USA; [5]Department of Marine Sciences, University of North Carolina, Chapel Hill, NC, USA; 6Dept. of Geosciences, Pennsylvania State University, University Park, PA, USA.

Using a multidisciplinary approach involving lipid biomarkers, stable carbon isotopic compositions of lipids, whole cells and various other sedimentary carbon pools, rRNA derived molecular phylogeny, and geochemical and bioenergetic modeling, we have studied four deeply buried sulfate-methane transitions zones (SMTZs) at burial depths ranging from ~10 to 90 mbsf (Fig. 1) recovered during ODP Leg 201 (Biddle, Lipp et al., 2006). Three of four of these sediment horizons, in which methane is consumed at the expense of sulfate, exhibited conspicuously elevated counts of total intact cells (D'Hondt et al., 2003). In the most extreme case, cell counts at the lower SMTZ at Site 1229 exceeded those in surface sediments (Fig. 1b).

Our study was designed to address whether the similar organisms mediate the anaerobic oxidation of methane (AOM) in deeply buried sediments as in surface environments such as marine methane seeps (e.g., Hinrichs and Boetius, 2002). In a collaborative project involving three laboratories, three molecular lines of investigation were applied in parallel to adjacent samples to provide a view on the composition of the subsurface communities: analysis of intact polar membrane lipids (IPLs) as markers of living subsurface prokaryotes (Sturt et al., 2004), sequencing of extracted rRNA, considered to be indicative of only the most active fraction of the community, and microscopic observations of

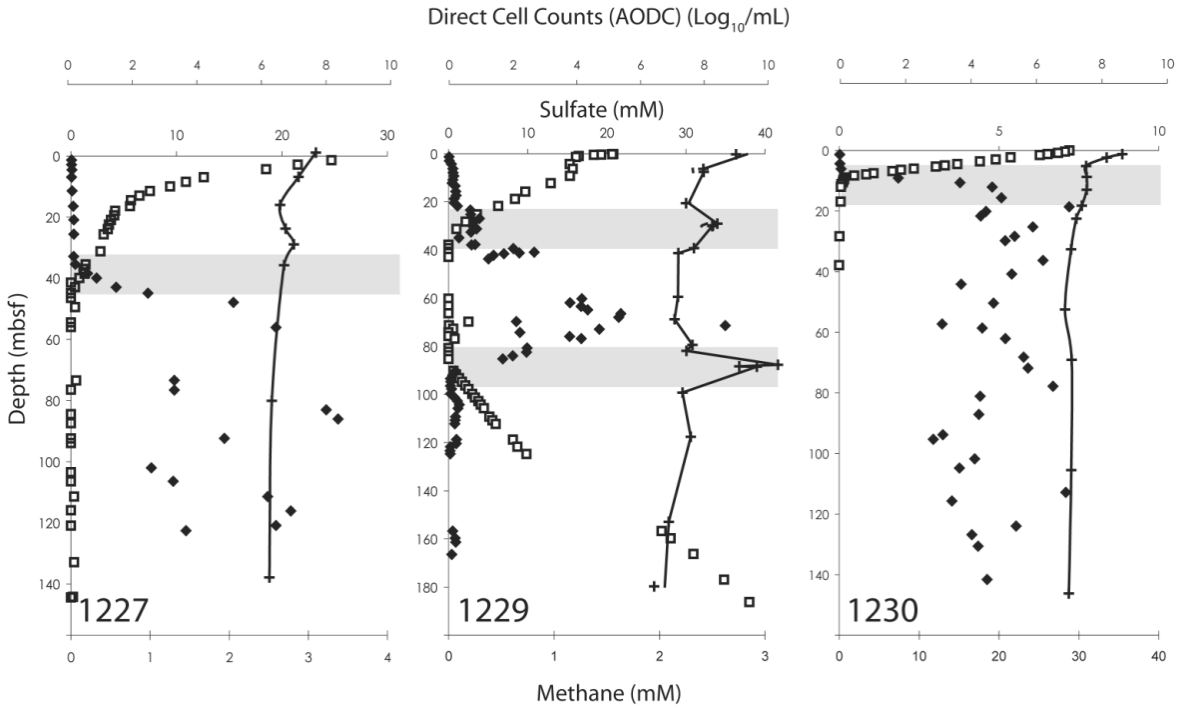

Fig. 1. Porewater profiles of sulfate (open squares), methane (closed diamonds) and cell numbers determined by acridine orange direct counts (all data from D'Hondt et al., 2003).

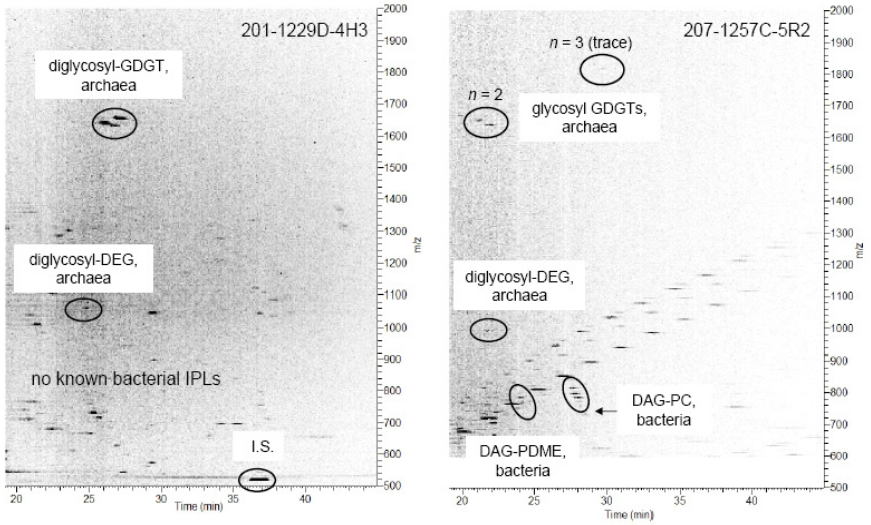

Fig. 2. Density maps derived HPLC-MS analysis of lipid extracts from representative subsurface sediments from ODP Leg 201 and 207 (the latter modified after Fredricks and Hinrichs, submitted). The gray background noise is consistent with very low concentrations of IPLs. Circled are IPLs that have been unambiguously identified as archaeal or bacterial IPLs. Slightly lower retention times in the sample from Leg 207 are due to slightly different analytical conditions.

cells targeted by domain-specific fluorescent probes (fluorescence in situ hybridization, FISH). The distribution of IPLs in both sediments within and outside SMTZs off Peru suggests a general predominance of Archaea. The IPLs from these sediments are dominated by archaeal glycerol-dialkyl-glycerol-tetraethers (GDGT), followed by dialkylether-glycerol (DEG), both types attached to diglycosidic polar headgroups (Fig. 2). The presence of calditol-based IPLs and crenarchaeol-derived alkyl chains (Fig. 2) are indicators of crenarchaeotal community members, in agreement with rRNA results, which indicate a predominance of crenarchaeotal phylotypes that were observed previously in subsurface environments. Counts of cells hybridized to a domain-specific archaeal FISH probe support the IPL data and suggest archaeal predominance. Notably, methanotrophic archaea that dominate methane-rich surface environments (Hinrichs and Boetius, 2002) were not detected.

In the past few years, we have systematically surveyed IPL inventories in a broad range of aquatic environments, incl. water column samples, surface sediments, deeply buried sediments and hydrothermal environments. Our data show that IPLs provide diagnostic fingerprints of environmental prokaryotic communities. The low yields of bacterial IPLs appear to be a unique feature of deeply buried sediments from the Peru Margin (cf. Fig. 2). While the archaeal diglycosidic GDGTs appear to be present in almost all deep subsurface sediments, the bacterial IPLs are consistent with a higher overall diversity among bacteria in subsurface environments. For example, sediments from ODP Sites 1257 and 1258, Demerara Rise, contain phosphatidylcholine (PC) and phosphatidyldimethylethanolamine (PDME) diacylglycerol (DAG) (Fredricks and Hinrichs, submitted) (Fig. 2) while sediments from Hydrate Ridge contain phosphatidylglycerol (PG) and phosphatidylethanolamine (PE) IPL derivatives (Orcutt, Lipp, Hinrichs, unpubl. data).

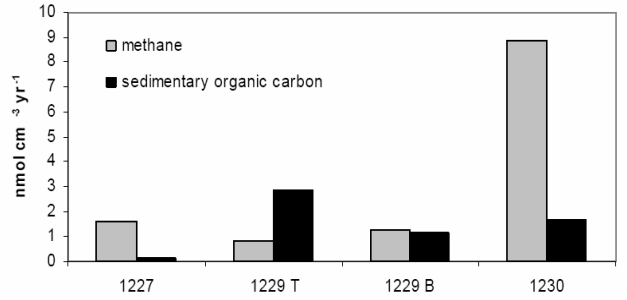

Fig. 3. Turnover rates of sedimentary organic carbon and methane in four SMTZs off Peru (ODP Leg 201), estimated using a diagenetic model and sedimentary porewater profiles (Biddle, Lipp et al., 2006).

In SMTZs off Peru, the stable carbon isotopic compositions of both IPLs and whole archaeal cells, the latter determined by secondary ion mass spectrometry of FISH-labeled cells (Orphan et al., 2001) suggest that the community members predominantly utilize sedimentary organic carbon for biosynthesis (Biddle, Lipp et al., 2006). This is surprising as geochemical modeling indicates that methane oxidation accounts for an important to dominant fraction of the total carbon turnover in these sedimentary strata (Fig. 3). Consequently, if subsurface archaea were to assimilate methane-carbon like methanotrophic archaea in seep environments do (e.g., Hinrichs et al., 1999), this should be detectable in the isotopic composition of archaea. We therefore hypothesize that novel archaea are involved in the anaerobic oxidation of methane in deep subsurface sediments off Peru. Apparently, these archaea do not assimilate methane.

References

Biddle, J.F., Lipp, J.S., Lever, M., Lloyd, K., Sørensen, K., Anderson, R., Fredricks, H.F., Elvert, M., Kelly, T.J., Schrag, D.P., Sogin, M.L., Brenchley, J.E., Teske, A., House, C.H., Hinrichs, K.-U. Novel heterotrophic Archaea dominate sedimentary subsurface ecosystems off Peru. Proceedings of the National Academy of Sciences, U.S.A., in press.

D'Hondt, S, Jørgensen, B.B., Miller, J. & ODP Leg 201 Shipboard Scientific Party. (2003) Proceedings of the Ocean Drilling Program, Initial Results 201, online: http://www-odp.tamu.edu/publications/201_IR/201ir.htm.

Fredricks, H.F., Hinrichs, K.-U. Data report: Intact membrane lipids as indicators of subsurface life in Cretaceous and Paleogene sediments from Sites 1257 and 1258. Proceedings of the Ocean Drilling Program, Scientific Results 207, in review.

Hinrichs, K.-U. and Boetius, A. (2002) The anaerobic oxidation of methane: New insights in microbial ecology and biogeochemistry. Ocean Margin Systems (ed. G. Wefer et al.), Springer Verlag, Berlin-Heidelberg, pp. 457-477.

Hinrichs, K.-U., Hayes, J.M., Sylva, S.P., Brewer, P.G., and DeLong, E.F. (1999) Methane-consuming archaebacteria in marine sediments. Nature, 398, 802-805.

Orphan, V.J., House, C.H., Hinrichs, K.-U., McKeegan, K.D., & DeLong, E.F. (2001) Methane-consuming archaea revealed by directly coupled isotopic and phylogenetic analysis. Science, 293, 484-487.

Sturt, H.F., Summons, R.E., Smith, K.J., Elvert, M., and Hinrichs, K.-U. (2004) Intact polar membrane lipids in prokaryotes and sediments deciphered by ESI-HPLC-MSn - new biomarkers for biogeochemistry and microbial ecology. Rapid Communications in Mass Spectrometry, 18, 617-628.

ICDP

Implications for the timing of gas release: crush degassing Experiments (lab), continuous gas monitoring (near-field) and analysis of >1.5 Ma old crustal fluids (regional), Witwatersrand Basin, South Africa

J. Lippmann-Pipke[1], S. Niedermann[1], J. Erzinger[1], M. Zimmer[1], T.C. Onstott[2]
[1]GFZ Potsdam, Germany; [2]Princeton University, USA; lippmann@gfz-potsdam.de, nied@gfz-potsdam.de, erz@gfz-potsdam.de; weihe@gfz-potsdam.de; tullis@princeton.edu

Deep crustal fluids (0.8 to 3.3km) and quartz veins (3.3km) from the Witwatersrand Basin, South Africa, were investigated with methods of noble gas geochemistry and isotope hydrology to further specify the fluid dynamics and geochemistry in the ultra-deep continental crust. We understand the ultra-deep fissure waters to be a mixture of paleometeoric water and components of billion-year-old hydrothermal fluids (0.8 to 2.5Ga). The quartz veins are remains of these hydrothermal fluids that precipitated during geologic times.

Subsurface model ages of the ultra deep fissure water samples were quantified by means of dissolved radiogenic and fissiogenic noble gas concentrations $^{4}He_{rad}$, $^{40}Ar_{rad}$, $^{134}Xe_{fiss}$, $^{136}Xe_{fiss}$ and ^{36}Cl data: minimum ages of all individual fissure water samples are constrained based on ^{36}Cl data to be older than 1.5Ma; noble gas model ages range up to some 20Ma.

Both, the ultra-deep fissure water as well as some vein quartz material show a) unusually high nucleogenic ^{21}Ne-concentrations and exceptional $^{21}Ne/^{22}Ne$ ratios. This supports our idea that the hydrothermal fluids (that once carried gold and uranium) influenced both, the quartz veins and the ultra-deep fissure water. As noble gases- among other fluids - can be stored in fluid inclusions in quartz veins over geologic time scales, the question is when and how are they released from the fluid inclusions and eventually accumulate in fissure waters.

The gas content of fluid inclusions will eventually be released by diffusion, alteration or during seismic forces and may get dissolved in pore fluids and accumulate therein with time. With the ongoing ICDP-project "Quantification of gases released during seismic events: long-term, on-site borehole monitoring in deep active faults, South Africa." we intend to better understand the processes and the timing of gas release. An on site long-term gas monitoring system is meant to employ this unusually high $^{21}Ne/^{22}Ne$ ratio (as well as other gas concentrations) as a tracer for the gas release from rocks during seismic events.

The monitoring system will analyze in real-time the ambient atmosphere and will take gas samples from inside a 40m long borehole, 3.6km deep underground that penetrates a fault system which cuts through the gold reefs. Here mining induced seismic events of up to magnitude 3 are expected to occur within the next years. We will analyze background gas composition for N_2, CH_4, He, H_2, O_2, Ar and CO_2 prior to the events and eventually changes

in gas composition during and after seismic events. Off-line samples for isotope analysis are taken on a regular basis. The off-line sampling rate will be increased during and after seismic events.

This near-field experiment shall enhance our understanding of crustal fluid dynamics and the geochemical behavior of gases in rocks (source) and ultra deep crustal waters (sink).

ICDP

Lake Van Drilling Project, Turkey "PaleoVan" - a new ICDP initiative

Thomas Litt (University of Bonn, Germamy), Sebastian Krastel (University of Bremen, Germany), Michael Sturm (EAWAG Zürich, Switzerland), Nüzhet Dalfes (Istanbul Technical University, Turkey), Sefer Örcen (Van University, Turkey), Georg Heumann (University of Bonn, Germany), Feliz Demirel-Schlüter (University of Bremen, Germany), Frank Niessen (AWI Bremerhaven, Germany)

Lake Van in Turkey is an excellent paleoclimate archive comprising long high resolution annually laminated sediment records. The lake is situated on the high plateau of eastern Anatolia and has a surface area of 3,522 km2. Its maximum depth is 451 m and its length is 130 km. It is the fourth largest of all terminal lakes in the world and contains highly alkaline waters. Following the successful completion of a pre-site survey in 2004 that included a seismic reflection and coring campaign, we present results of the multidisciplinary scientific work on short cores (5m - 10m sediment depth) including magnetic susceptibility, physical properties, stable isotopes, pollen and spores, and absolute datings. Based on a single sediment core obtained already in 1990, Landmann et al. (1996) assumed extreme water level changes after the Last Glacial Maximum, and they postulated that the approximately 500 m deep Lake Van became completely dry within less than 4000 years. They described an oolith layer at the lowermost part of the core as an indicator for shallow water. If this interpretation is correct that the lake was dry around 15 ka BP, it would have strong implications for using long sediment records from Lake Van as a paleoclimate archive. In this case sedimentation gaps and unconformities must be taken into account.Our new profile VAN04-2 (water depth 375 m), which was identified as a potential ICDP drill site in the seismic data, gets deeper in time than all the other Lake Van cores obtained to date. First palynological data indicate that profile VAN04-2 encompasses a continuous sequence from the LGM to the present time. Our preliminary results show that the hypothesis by Landmann et al. (1996), that Lake Van fell completely dry between 20 and 15 ka BP, is very unlikely. We have no evidence of aragonite crusts or similar layers as indication of extreme low stands between the LGM and the onset of the Lateglacial. During that time a continuous sedimentation took place in our record. The seismic data also do not show any indications that the deepest part of Lake Van (Tatvan Basin) was dry or almost dry in past times. Based on the new seismic profiles we mapped in fact erosive channels, deltaic sequences and unconformities. However, these features only occur in the shallower parts of the lake showing that the lacustrine shelf was dry several times. None of these features was found in water depth >250m, hence indicating that Tatvan Basin was not dry in the past. Both the seismic and coring data show that Lake Van is a most interesting object for large lake drilling within ICDP. Therefore, the research initiative PaleoVan announces an international workshop to be held in Van, Turkey, on June 6 - 9, 2006 under the auspices of the ICDP. Specific goals of the PaleoVan project are to reconstruct: (1) Palaeoclimate development in a sensitive semiarid region based on proxy data and modeling; (2) dynamics of lake level fluctuations and hydrogeological development; (3) formation and age of Lake Van; (4) history of volcanism and volcanic activity based on tephrostratigraphy; (5) variations of the earthmagnetic field; (6) tectonic, palaeoseismic and earthquake activity; (7) interaction between man and environment since prehistoric time.

ICDP

Fission-track dating at drill cores from the CCSD/ICDP Donghai Drill Holes, China

S. Liu[1], U. Weber[2], Z.-Q. Xu[3], U.A. Glasmacher[4,2], G. A. Wagner[2]
[1]Guangzhou Institute of Geochemistry, Guangzhou, China, [2]Max-Planck-Institut für Kernphysik, Heidelberg, [3]Beijing Institute of Geology, Chinese Academy of Geological Sciences, China, [4]Geologisch-Paläontologisches Institut, Ruprecht-Karls Universität Heidelberg, email: ulrich.a.glasmacher@urz.uni-heidelberg.de

The Qinling-Dabie-Sulu (QDS) orogen in East-Central China results from the Triassic collision and attempted subduction of the Yangtze continent (SCB; South China Block) beneath the Sino-Korean continent (NCB; North China Block). Petrologic and structural studies indicate that the Hong'an and Dabie regions in the East of the Qinling-Dabie branch of the QDS orogen were subducted to ~150 km prior to the early Triassic. First exhumation in Triassic time (240 and 225-210 Ma) transported subducted UHP and HP-HT rocks from mantle to crustal levels. From the Late Jurassic to Early Cretaceous (140 and 120 Ma) those rocks were exhumed from a depth of 15-30 km to upper crustal levels.

Fission-track data of the western Dabie-Sulu ultrahigh pressure metamorphic (UHPM) belt show that uplift continued through the Cenozoic to the present [1]. The CCSD/ICDP Donghai drill site is located in the eastern part of the Dabie-Sulu UHPM belt between North China Plate and the Yangtze Plate [2]. The CCSD/ICDP-pre-pilot holes (PP1; PP2) and the main CCSD/ICDP-drill holes at Donghai, China, are keyholes that allow the continuous reconstruction of the medium to low temperature history of the eastern part of the Dabie-Sulu-UHPM belt. Integration of petrological and structural data allows transferring the fission-track T-t paths into a post-orogenic exhumation history [3].

In the frame of this research project, 43 samples from the drill core were processed (Fig. 1). Samples were taken in a nearly even spacing of 100 m covering all major lithologies such as eclogite, amphibolite, paragneiss and orthogneiss. 38 samples yielded enough apatite for fission-track dating. In addition, 9 of the 38 samples yielded apatite grains in excess to prepare a second mount for 252Cf-irradiation. Those 9 mounts were used to measure confined track length. Nearly all apatites bear dislocations, fluid and solid inclusions. In addition, most of the apatites from eclogites have very low uranium contents. Therefore, together with the Autoscan Ltd. Company, we further developed the Autoscan dating system. An external measuring system was adapted to the 3-axes computer-driven stage to increase the reproducibility from about 5 µm to 0.2 µm on long distance movements (~several cm). Integration of a Pelletier-cooled CCD-colour camera and change of the software lead to the ability to date at two screens simultaneously.

Apatite fission-track (AFT) age data have a spread between 98.6 (17.0) Ma (1887 m) and 3.2 (1.3) Ma (3899 m). The surface sample revealed an age of 87.1 (11.2) Ma. With increasing depth the fission-track age pattern varies significantly indicating movement along major normal and reverse faults at various times in the past (Fig. 2). The first major normal fault appears at a depth of 350 m with a vertical displacement of ~400 m. Movement along the third major normal fault is younger than 25 Ma. Three major reverse faults occur at about 2450 m (RF3), 3050 m (RF4) and 3250 m (RF5), respectively. The vertical displacement between RF4 and RF5 is about 500 m in total and younger than ~10 Ma.

Exhumation rates calculated from age-depth relationship in the uppermost part of the drill core account for 23 m/myr between 95 Ma and 80 Ma. Between the major reverse faults RF2 (depth: 1550 m) and RF3 (depth: 2450 m) appears to be a segment where fission-track age data show no continuous age-depth trend. The segment could be interpreted as a major tectonized zone. The bimodal confined track-length distribution indicates a three step exhumation history with a fast exhumation at the beginning, followed by a longer phase of slow exhumation and a final increased exhumation.

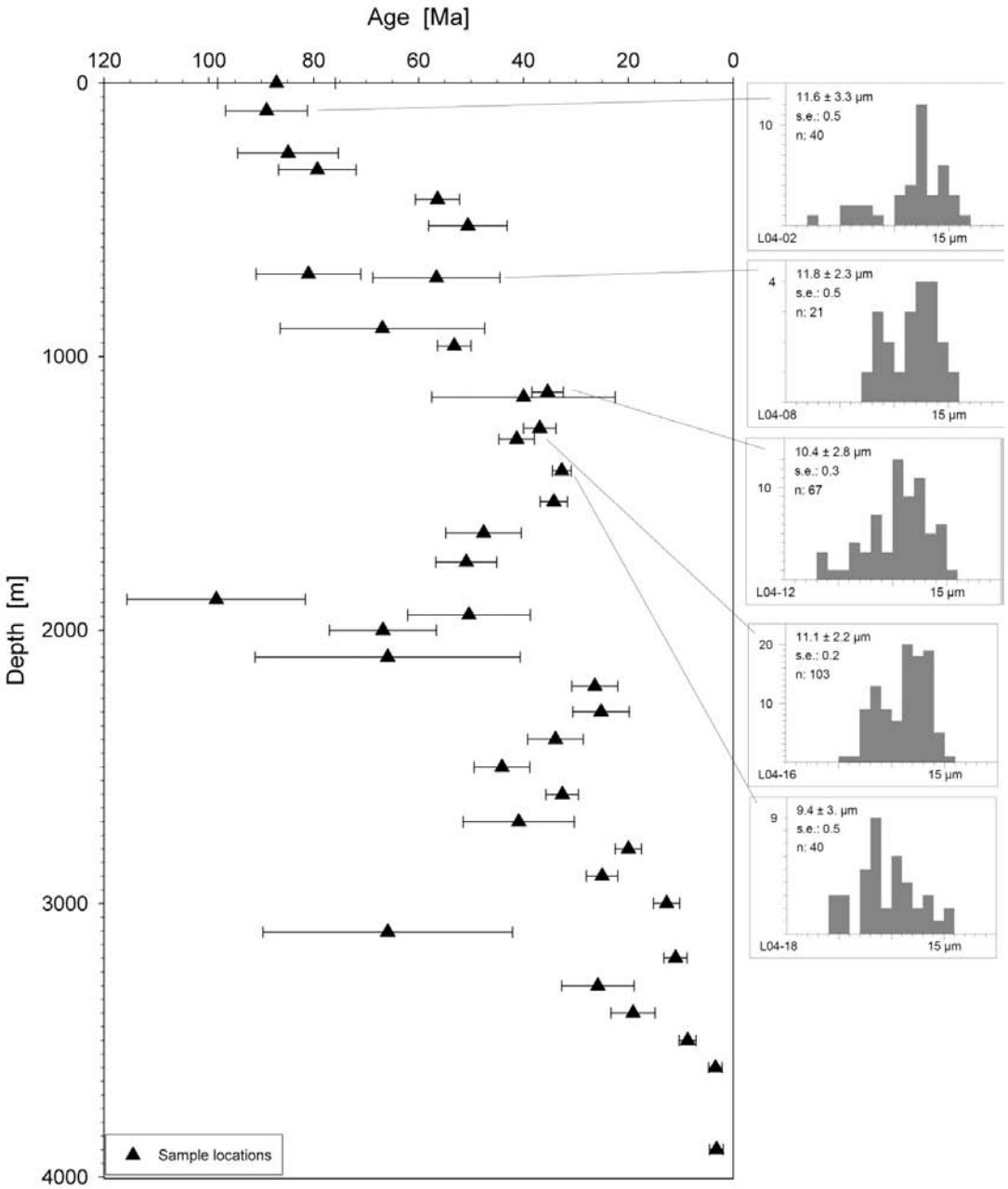

Fig. 1: Age-depth relationship of apatite fission-track data of the CCSD/ICDP drill hole in Donghai, China. Histograms show confined fission-track length distribution of selected samples.

]Fig. 2: next page]

References

[1] Grimmer J.C., Jonckheere R., Enkelmann E., Ratschbacher L., Hacker B.R., Blythe A.E., Wagner G.A., Wu Q., Liu S., and Dong S., 2002. Cretaceous - Cenozoic history of the southern Tan-Lu fault zone: apatite fission-track and structural constraints from the Dabie Shan (eastern China). Tectonophysics 359, 225-253.

[2] Liu, F.L., Xu, Z.Q., Yang, J.S., Zhang, Z.M., Xu, H.M., Li, T.F. 2004. Geochemical characteristics and UHP metamorphism of granitic gneisses in the main drilling hole of Chinese Continetal Scientific Drilling Project and its adjacent area. Acta Petrologica Sinica 20, 9-26.

[3] Xu, Z., Wencai, Y., Jingsui, Y., Zeming, Z., and Fulai, L., 2000. Chinese Continental Scientific Drilling Program in the Sulu Ultrahigh Pressure Metamorphic Belt. ICDP Newsletter, 2: 13 - 16.

IODP

Monsoonal variability and oxygen minimum zone intensity in the northern Arabian Sea: Status of a mature IODP drilling proposal

A. Lückge[1], W. J. Zachariasse[2], U. von Rad[1], L. Lourens[2], G.-J. Reichart[2], C.Rühlemann[1], H. Schulz[3] and co-proponents of IODP Proposal 549

[1]Bundesanstalt für Geowissenschaften und Rohstoffe, Stilleweg 2, 30655 Hannover, Germany, [2]Institute of Earth Sciences, Utrecht University, NL-3508 TA Utrecht, The Netherlands, [3]Institut für Geowissenschaften, Universität Tübingen, D-72076 Tübingen, Germany (a.lueckge@bgr.de)

In the northeastern Arabian Sea a stable oxygen minumum zone and high productivity favour the deposition and preservation of organic-rich laminated (varved) sediments. This provides an ideal climate archive for the high-resolution study of the response of seasonal components of the Indian monsoon to orbital and suborbital forcing during the late Neogene.

High-resolution sediment cores of Holocene to late Pleistocene age show monsoon variability on centennial to millennial time scales with a high degree of correspondence in event timing and structure with records from the North Atlantic, central Greenland, as well as with records from the South China Sea and the Bay of Bengal. The primary mechanisms responsible for the coupling between the monsoons, other tropical climate features and the North Atlantic climate regime remain, however, poorly understood.

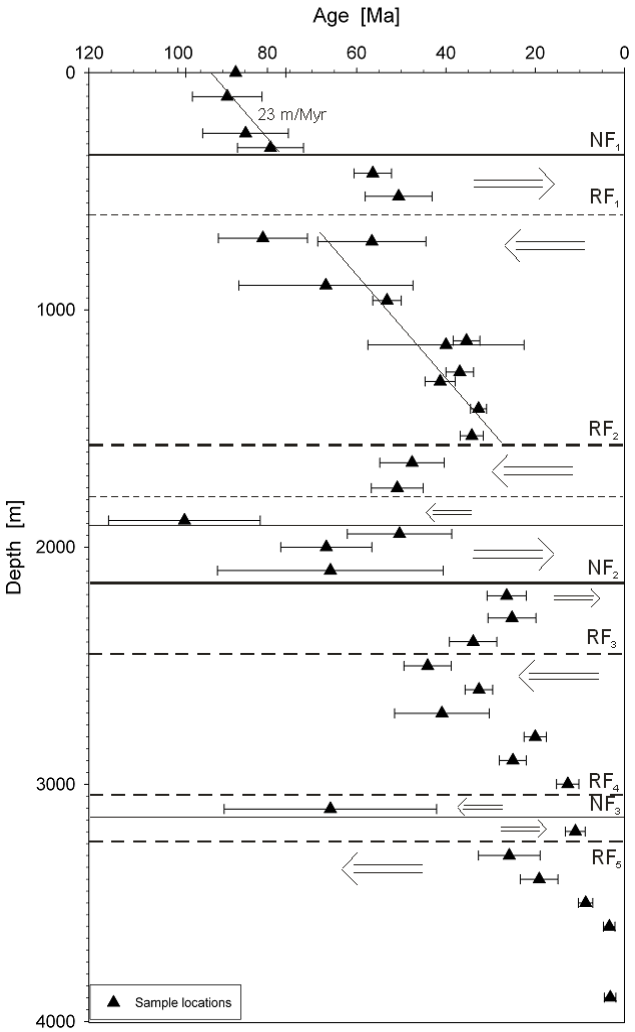

Fig. 2: Interpretation of the fission-track age-depth relationship. Major normal (NF1) and reverse faults (RF1) are shown by solid and dashed lines, respectively. [to Abstract Liu et al.]

Our aim is to recover fully intact sequences of Late Neogene hemipelagic sediments in the northern part of the Arabian Sea to study the history of the Indian monsoon and OMZ on annual to tectonic time scales. We propose to drill a transect of three, about 400 m deep, triple-APC-cored holes into Quaternary hemipelagic sediments of the Pakistan Margin and a transect of four triple-APC-cored sites into Quaternary to Late Miocene sediments of the Murray Ridge. The proposed drill sites offer a unique opportunity to study the following objectives:

- Late Neogene evolution of millennial-scale variations in monsoon-influenced OMZ intensity. Annual to (sub)Milankovitch variability in Indian monsoon climate studied over millions of years under different boundary conditions may provide new insights in forcing mechanisms and teleconnections between low and high latitude climate and in the causes of changing boundary conditions for rapid switches of OMZ variability.
- Biogeochemical cycles including organic carbon production, preservation and diagenesis within and below the OMZ in the context of the so-called "productivity versus anoxia dispute".
- Astronomical pacing of the Indian monsoon during long global cooling. Phase stationarity of the monsoon system relative to the Earth's orbital cycles can be tested for both the summer and winter monsoon.
- Tectonic-scale paleoceanographic and climate changes (e.g., documentation of the response of winter and summer monsoon to Tibetan uplift and the inception of large northern ice sheets; influence of the closure of the Indonesian gateway on the aridification in East Africa 3-4 Ma ago).
- "Deep Biosphere" (abundance, diversity and extent of deeply buried sedimentary microbial communities in anaerobic environments).

ICDP

Geochemical and mineralogical studies on different impact melt products; the Lake Bosumtwi Impact structure, Ghana, W. Africa

Sabine Luetke[1], Alex Deutsch[1], Falko Langenhorst[2], Birgit Kreher-Hartmann[2]
[1]Institut für Planetologie, Westfälische Wilhelms-Universität Münster, D-48149 Münster, Germany, luetke.s@uni-muenster.de;
[2]Institut für Geowissenschaften, Friedrich-Schiller-Universität Jena, D-07749 Jena, Germany

The L. Bosumtwi crater offers the possibility of multidisciplinary studies in the fields of palaeo-climate, geophysics, petrology, geochemistry, and impact science. The 1.7 Ma young and large (Ø 10.5 km) crater, is exceptional well-preserved, and source of one of only four known tektite strewn fields.

In the context of the ICDP Bosumtwi Core Drilling Project (BCDP) 14 sediment and two hard rock cores (BCDP-7A, crater moat; BCDP-8A, flank of the central uplift) were drilled. BCDP-8A shows a cyclic sedimentary sequence of mainly greywackes and shales (Deutsch et al., 2006). These are target lithologies and constitute about 87 vol%. of the total of ~214 m drilled "hard rocks". Remaining 23 vol. % consist of different types of impact breccias, mainly intercalated in the upper part of the core.

Our project focuses on the study of impact melt products that originate according to current views during different stages of the cratering event and by different mechanisms. The term "impact melt products" comprises melt rocks, glass particles within impact breccias, tektites, microtektites, and microcrystites. Main scientific goals by studying glasses produced in the Bosumtwi event are to identify the precursor rocks by geochemical and isotopic fingerprinting and to understand the processes that yield these different types of melt lithologies. Melt particles are also important to estimate the level of shock metamorphism (Deutsch and Langenhorst, 2006). Likewise a better understanding of mixing processes, constraining high-temperature chemistry and redox conditions in vapor plumes, as well as deriving the different cooling paths of impact glasses are in the focus of this project. Why, for example, does only a small fraction of impact events result in the formation of tektites and microtektites? What are the diagnostic tools to distinguish microtektites from volcanic glass spherules? To answer these questions we combine optical, scanning (SEM) and transmission electron microscopy (TEM) with electron microprobe (EMP) and isotope analysis techniques (thermal ionization mass spectrometry - TIMS; laser ablation ICPMS - LA-ICPMS).

We started to prepare Ivory Coast and related microtektites for LA-ICPMS. In addition, delicate samples from the transition of impact breccias to post-impact sediments are currently investigated for the presence of glassy fall-back spherules.

At the meeting, we will present first analytical results for target and impact lithologies (microscopic and SEM studies, XRD and XRF data, Rb-Sr and Sm-Nd isotope data).

References

Deutsch, A., Heinrich, V., Luetke, S., (2006). Lunar Planet. Sci. Conf. XXXVI, Abstract #1292

Luetke, S., Deutsch, A., Langenhorst, F., Kreher-Hartmann, B. (2006). Lunar Planet. Sci. Conf. XXXVI, Abstract #1811.

Deutsch, A. and Langenhorst, F. Conference Abstract, this volume.

We appreciate support by DFG grants De 401/19 and La 830/71

Ackowlwgements. Drilling was funded by ICDP, the U.S. NSF, the Austrian FWF, the Canadian NSERC, and the Austrian Academy of Sciences. We appreciate support by DFG grant De 401/19, skillful technical assistance by M. Ude (Jena), H. Baier and U. Heitmann (Münster).

IODP

Indication for deep microbial populations in sediments below the Challenger Carbonate Mound in the Porcupine basin, offshore Ireland (IODP Leg 307)

Kai Mangelsdorf[1], Klaus-G. Zink[1], Rolando di Primio[1], Tim Ferdelman[2], Barry Cragg[3], Brian Horsfield[1], Jean Pierre Henriet[4] and the IODP Expedition 307 scientific party

[1]GeoForschungsZentrum Potsdam (GFZ), Telegrafenberg, D-14473 Potsdam, Germany; [2]Max-Planck-Institute for Marine Microbiology, Celsiusstr. 1, D-28359 Bremen, Germany; [3]School of Earth, Ocean and Planetary Sciences, University of Cardiff, PO Box 914, Cardiff, CF10 3YE, UK; [4]Renard Centre of Marine Geology (RCMG), Ghent University

In recent years the examination of microbial life in deep sedimentary successions has become a new and exciting challenge in today's geosciences. Within this area intriguing questions concern the kind of microbial populations, their extent in deep sediments, their ability to adapt to extreme environmental conditions, and their potential carbon and energy sources to survive in the deep subsurface.

In April to May 2005 IODP Leg 307 investigated the Porcupine basin area offshore Ireland. Sediment material from three drill sites on and adjacent to the Challenger mound in the Belgica carbonate mound province was sampled taking strict precautions to avoid microbial surface contamination. Preliminary results (AODC counts) show that microbial populations within the mound interval are only below the average prediction line of the trend observed in other IODP or ODP sites [1]. In contrast to this, at and below the mound base the cell counts together with the number of dividing cells increase and plot above the average prediction line, indicating active population growth in this sedimentary interval. Concomitantly, this increase is accompanied by significant methane contents and a decrease in pore water sulphate, suggesting methane oxidation and/or methanogenesis is taking place at these depths.

Computer simulations of the basin history, undertaken at GFZ Potsdam [2] in the previous Geomound project, revealed that below the carbonate mounds in the Belgica mound province specific sandstones represent important migration pathways for natural gases to the surface. Thus, investigations of microbial biomarkers and the isotopic signal of natural gases at the mound base will help to elucidate whether hydrocarbon gases could have migrated to the mound base stimulating microbial activity in this interval.

[1] Parkes, R. J., Cragg, B. A., Wellsbury, P. (2000). "Recent studies on bacterial populations and processes in subseafloor sediments: A review." Hydrogeology Journal 8(1): 11-28.

[2] Naeth, J., di Primio, R., Horsfield, B., Schaefer, R.G., Shannon, P.M., Bailey, W.R., Henriet, J.P., 2005. Hydrocarbon seepage and carbonate mound formation: a basin modelling study from the Porcupine Basin (offshore Ireland). Journal of Petroleum Geology, 28 (2), p. 43-62.

IODP

Gas hydrate quantification in continental margin sediments using a combined geochemical and geophysical approach: first results from ODP Leg 170 off Costa Rica

Mathias Marquardt[1], Thomas Temmler[2], Christian Hensen[1], Christian Müller[2]

[1]IFM-GEOMAR, Wischhofstr. 1-3, 24148 Kiel, Germany; [2]BGR, Stilleweg 2, 30655 Hanover, Germany.

The proposed project HYDRA aims at developing a new approach to quantify the amount of gas hydrate in continental margin sediments by the complementary use of geochemical models and the implementation of the effective medium theory for seismic modelling and inversion. In spite of intense research on gas hydrates over more than two decades, the published estimations of the total quantity of hydrocarbon gas in the form of hydrates vary within orders of magnitude. Early estimates of up to $7.6 \cdot 10^{18}$ m^3 (e.g. Dobrynin et al., 1981) were continuously corrected downward to the most recent estimates between $>2 \cdot 10^{14}$ m^3 (Soloviev, 2002) and $1\text{-}5 \cdot 10^{15}$ m^3 (Milkov, 2004). Since the late 1980s gas hydrate amounts have been estimated by either interpretation of seismic data or the use of available pore water data (usually restricted to ODP drill sites). However, the results derived from these two methods at the same site may reveal differences of up to an order of magnitude. A combined approach, which cross-evaluates the results and uses them for the improvement of respective parameterisations has never been tested before.

Preliminary results of the project show that the prediction of gas hydrate inventories by seismic methods is highly sensitive to the accurate determination of porosities. This may cause large uncertainties, which can be reduced by calibration against a numerical reactive-transport model (constrained by pore water data from ODP-sites). The present model scheme (after Hensen & Wallmann, 2005) considers major processes controlling the formation of CH_4 and gas hydrate such as the sedimentation and compaction of the sediments, the input and degradation of organic material (POC), diffusion and advective fluid flow, and the anaerobic oxidation of CH_4.

Based on the data of ODP Sites 1040 and 1041 the model predicts average gas hydrate concentrations in the sediments of about 1.9 vol.% (pore space) within the zone of gas hydrate occurrence. The contribution of upward migrating thermogenic gases to the overall gas hydrate could be shown to be negligible in this area (Lückge, 2002). Sites of mud volcanism are considered to have only a minor effect on the total amount of gas hydrate inventories (Milkov, 2000) and were preliminarily neglected. Variations of about ± 0.25 vol.% are likely due to the regional heterogeneity of major control parameters (pressure/temperature conditions, input and composition of POC, POC-degradation rates, fluid flow). Model-derived degradation rates of POC are between $1.6 \cdot 10^{-3}$ and $1.23 \cdot 10^{-4}$ nmol/$g_{sediment}$/day corresponding to methane formation rates between $8.9 \cdot 10^{-6}$ at the surface and $1.2 \cdot 10^{-7}$ nmol methane produced/$g_{sediment}$/day at the bottom of the sediment column. These results are in agreement with rates of methanogenesis recently determined by Colwell et al. (2005). We will present model predictions constrained by all available ODP data from Leg 170, which will enable the prediction of regional parameter variabilities that can be used for empirical predictions of the GH inventory and distribution.

References:

Dobrynin, V., Yu. Korotajev, D. Plyuschev, 1981. Gas hydrates - a possible energy resource. In: Meyer, R., J. Olson (eds.), Long term energy resources, Boston, Pitman, S. 727 - 729.

Colwell, F., Lorenson, T., Boyd, S., Delwiche, M.E., Reed, D., and Newby, D.(2005): Experimentally determined rates of methanogenesis in methane hydrate bearing sediments. Salt Lake City Annual Meeting, Paper No. 224-2.

Hensen, C. and Wallmann, K. (2005): Methane formation at Costa Rica continental margin - constraints for gas hydrate inventories and cross-décollement fluid flow. EPSL (Vol. 236), S. 41 - 60.

Lückge, A., Kastner, M., Littke, R., Cramer, B. (2002): Hydrocarbon gas in the Costa Rica subduction zone: primary composition and post genetic alteration. Org Geochem. (Vol. 33), S. 933 - 943.

Milkov, A.V. (2000): Worldwide distribution of submarine mud volcanoes and associated gas hydrates. Mar. Geol. (Vol. 167), S. 29 - 42.

Milkov, A. V. (2004): Global estimates of hydrate-bound gas in marine sediments: how much is really out there? Earth Sciences Reviews (Vol. 66), S. 183 - 197.

Soloviev, V.A.(2002): Global estimation of gas content in submarine gas hydrate accumulations. Russ. Geol. Geophys. (Vol. 43), S. 609 - 624.

IODP

Plio-/Pleistocene palynostratigraphy in the Central Arctic Ocean (Lomonosov Ridge, Expedition 302)

Jens Matthiessen[1], Jan Backman[2], Henk Brinkhuis[3], Martin Jakobsson[4], John King[4], Martin Frank[5], Kate Moran[4], Matt O`Regan[4]

[1]Alfred Wegener Institute for Polar and Marine Research (AWI), Bremerhaven, Germany; [2]Stockholm University, Department of Geology and Geochemistry, Stockholm, Sweden; [3]Utrecht University, Laboratory of Paleobotany and Palynology, Utrecht, The Netherlands; [4]University of Rhode Island, Narragansett Bay Campus, Narragansett, United States; [5]University of Kiel, Leibniz Institute for Marine Science, Kiel, Germany

Dinoflagellate cysts and other palynomorphs are currently studied on Expedition 302 sediments in order to establish a high-resolution biostratigraphy for the Central Arctic Ocean. In

these almost carbonate and opal-free sediments dinoflagellate cysts are the only microfossil group that have a somewhat regular occurrence in Plio-/Pleistocene sediments. Together with a magnetostratigraphy, 10Be stratigraphy and some additional calcareous nannofossil and planktic foraminifer datums, a preliminary stratigraphic framework has been developed that is supported by a correlation to relatively well-dated ODP Leg 151 holes and "Polarstern" cores. The new chronostratigraphy confirms that sedimentation rates on Lomonosov Ridge in the Central Arctic Ocean were on the order of cm/ka. This model of relatively high sedimentation rates is in contrast to the long-held belief that central Arctic Ocean Plio-Pleistocene sedimentation rates have been on the mm/ka-scale, or even sub-mm/ka-scale, estimated from numerous short gravity or piston cores.

ICDP

Petrophysical Investigations within the Chicxulub and Chesapeake Bay Impact Scientific Drilling Projects (CSDP and USGS)

Mayr S.[1], Burkhardt H.[1], Popov Yu.[2], Wilhelm H.[3]
[1]Department of Applied Geosciences, Technical University Berlin, Germany; [2]Moscow State Geological Prospecting University, Russia; [3]Geophysical Institute, University of Karlsruhe, Germany

Based on investigations of the Yaxcopoil-1 well, drilled within the Chicxulub Impact Crater (Yucatan, Mexico) (see e.g. Popov et al. 2004, Wilhelm et al. 2004, and Mayr et al. 2005) a joint approach of extensive laboratory measurements of various physical rock properties on densely sampled cores and high resolution temperature measurements in the Eyreville borehole, drilled in the inner basin of the Chesapeake Bay impact structure, will contribute to a better understanding of the influence of the impact on the petrophysical properties and on the geothermal and hydraulic fields. The experimental petrophysical data, supported by mineralogical and structural analysis, will be interpreted with respect to the internal structure of rocks by numerical modelling and by correlations between different parameters and used for calibration and control of geophysical borehole logs, as well as for constraints to geophysical interpretation and modelling of the impact structure.

Chicxulub Impact Scientific Drilling Project (CSDP):

Thermal parameters, porosity and density were measured on 450 rock samples of the Yaxcopoil-1 well, drilled within the Chicxulub Impact Crater (Yucatan, Mexico). Various other petrophysical properties were determined on representative subgroups of samples: Petrophysical modelling and empirical correlations yield detailed physical property logs (Popov et al. 2004 and Mayr et al. 2005).

New results on hydraulic permeablity and micro morphology

Internal surface Spor, formation factor F, NMR-T2 relaxation times and hydraulic permeability k were measured on some selected samples for the estimation of permeability (Popov et al. 2004) and analysis of "micro morphology". Hydraulic permeability k is estimated using the classic Kozeny-Carman-equation (class. KC): $k = 1/(2\ F\ S_{por}^2)$ (1)
and the fractal PaRiS-model (Pape et al. 1987):

$$k\ [Darcy] = 475.3\ /(F * S_{por}^{BET}\ [1/\mu m])^{3.1085}\ q^{3.1085} \quad (2)$$

In addition hydraulic permeability k is estimated from NMR-T2 relaxation time (Kenyon, 1997). The PaRiS-model was developed for sandstones. With the factor q differences of the fine structures ("micro morphology") can be taken into consideration, for sandstones it equals 1. In rocks with an enhanced structured surface due to lamelar structures q is greater than 1, in rocks with smoother surfaces smaller than 1 (Pape et al. 1987). The factor *q* had to be estimated for the investigated samples by means of micro morphology.

Next to grain and pore size distribution, the internal surface reflects the "micro morphology" (Schön, 1997). Four groups with decreasing internal surface can be found (Figure 1): (1)upper suevite and brecciated impact melt rock; (2)post-impact limestones type 1; (3)anhydrites; (4)limestones type 2 together with calcarenites, dolomites and the lower suevite. The fine structure of the grain surfaces has to be known for better permeability estimation by means of scanning electron microscopic (SEM)-pictures of selected samples.

The investigations of these four groups with SEM shows the following:

- Dolomites, carbonates and some limestones (Type 2) have a smoother fine structure in 100nm range than most post-impact limestones (Type 1) resulting in a smaller internal surface.
- Melt-rich impact breccias of the sub units upper suevite and brecciated impact melt rock contain abundant silicate melt particles that underwent hydrothermal alteration to clay minerals (like smectites and illites). These clay minerals are most likely the main cause for the higher internal surfaces measured in these rocks.
- The lower suevite is distinctly different from the overlying upper suevite and brecciated impact melt rock: The measured lower internal surface Stot correlates with higher contents of massive carbonates in both the matrix and the clasts as well as a lower content of clay minerals leading to a less structured surface (see Schmitt et al. 2004 for bulk geochemical data).

The estimated permeability is shown in Figure 2. For anhydrites, where no information about the "micro morphology" is available and for post impact limestones type 1 $q = 1$ is used. In case of the melt-rich impact breccias overlying the lower suevite, having an enhanced structured surface q is set to 1.5 leading to higher estimated permeability. As the internal surface of calcarenites and dolomites is very smooth the class. KC-equation is used. For lower suevite, having a smooth internal surface, $q = 0.5$ is assumed.

In general, the different estimations and measurements are in satisfactory accordance, taking the complicated nature of permeability into account. This is particularly true for the estimated values from NMR-measurements (open symbols) and from the PaRiS-model / class. KC (solid symbols), i.e. from two completely independent methods. Directly measured permeabilities for samples YAX-1_562.43 (Φ=25.8%) and YAX-1_656.08 (Φ =17.1%) are distinctly lower than the estimated ones. These two samples are clearly layered. Since the gas-permeability could only be measured perpendicular to the layering and the estimated permeabilities are bulk values, the measured values are probably underestimated due to anisotropy. Permeability of sample YAX-1_617.53 (Φ =1.7%) with approximately 10^{-5} mD was at the resolution limit of the instrument. Measured data by Vermeesch and Morgan (2004) are in the same magnitude as our estimations and measurements.

The internal surface gives a tool for investigation of the internal structure, i.e. grain, pore size distribution and "micro morphology" which can be influenced by e.g. hydrothermal alteration of silicate melt particles to clay minerals.

The resulting permeabilities should give at least a rough estimate for the order of magnitude for the intrinsic bulk permeabilities of the section. Despite very high porosities (up to 35%) the permeabilities are in general below 10 mD, i.e. the rocks are characterised by large pores with minor interconnections. These small bulk permeabilities indicate that the effective hydraulic properties of this formation should be dominated by macroscopic effects.

Chesapeake Bay Impact Scientific Drilling Project (USGS)

Two partly overlapping boreholes were drilled between September 15, 2005 - December 4, 2005 into the central crater of the Chesapeake impact structure in Virginia, USA: the borehole Eyreville A (0 to 940.9 m) and Eyreville B (737.6 to 1,766.3 m). The USGS logger collected a natural gamma log and a temperature log for nearly the entire length of combined holes A and B. The

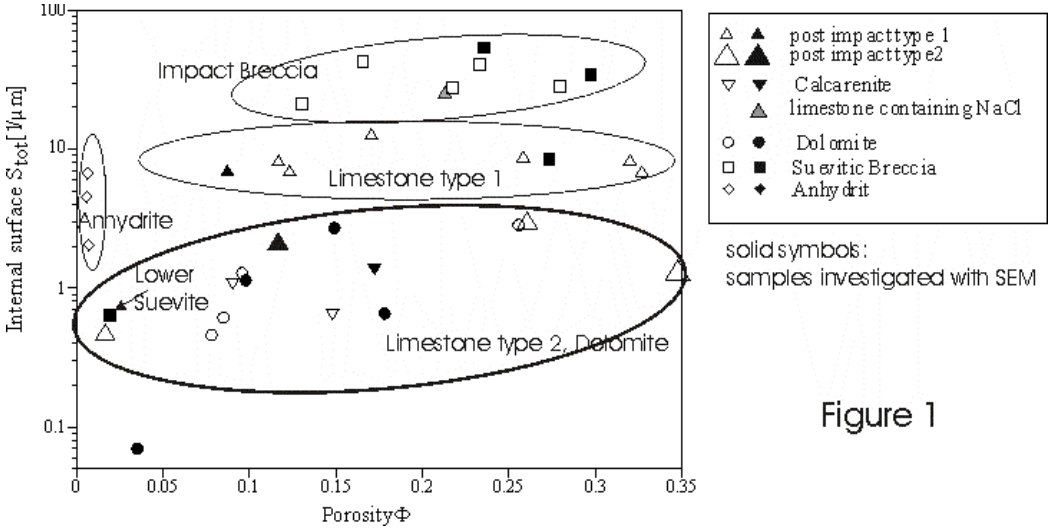

Figure 1

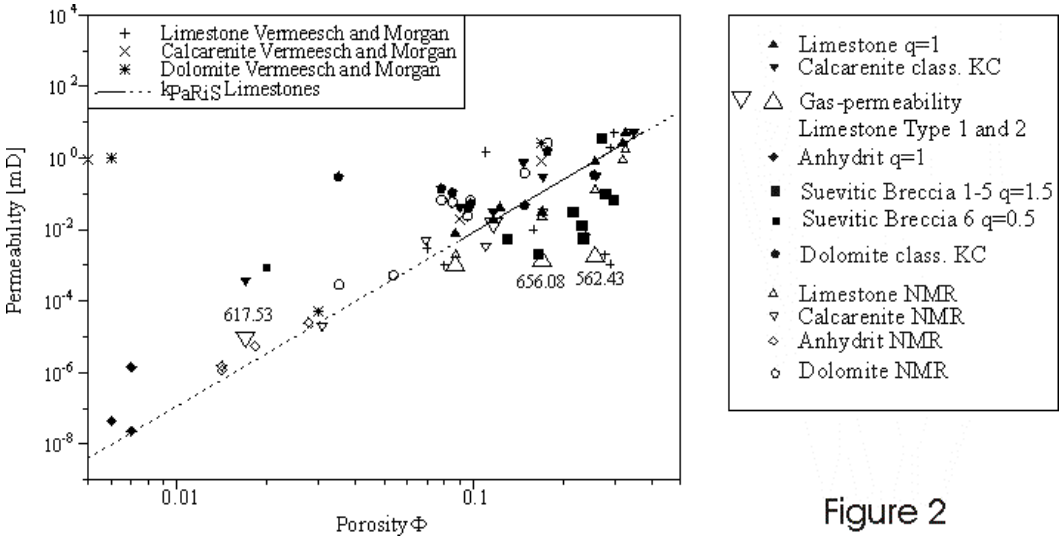

Figure 2

Karlsruhe University temperature probe also was run in the hole (cf. Heidinger et al. 2006). The uncased hole below 1,100.9 m probably cannot be accessed in future. In the cored interval between 125.6 m and 1,766.3 m the core recovery is good. The preliminary generalised lithologic column is (Principal Investigators, 2006):

0 to 444 m	Post-impact sediments
444 to 1,096 m	Exmore sediment-clast breccia and sediment megablocks
1,096 to 1,371 m	Granitic megablock(s)
1,371 to 1,393 m:	Lithic blocks in sediment
1,393 to ca. 1,550 m	Suevite and lithic breccia
Ca. 1,550 to 1,766 m	Schist and pegmatite; breccia veins

The sampling party is scheduled for March 19-21, 2006. A dense sampling by our group is needed for physical characterisation of the cored lithology, further emphasised by the fact, that geophysical borehole logging is severely restricted due to technical difficulties. A close co-operation with Prof. Popov (MSGPU), Prof. Wilhelm (UKA), Dr. Safanda, Praha and L. Pesonen (University of Helsinki) is planned.

As one of the main scientific objectives Chesapeake drilling project is the "understanding of processes and products of a marine impact and its consequences for the groundwater resource management" next to measurements of thermal and elastic properties special emphasis will be laid on estimation of permeability.

References:
Heidinger P. Wilhelm H., Burkhardt H., Šafanda J. 2006, this session.
Kenyon, W.E. 1997. Log Analyst 38(2):21-43.
Pape H., Rieper L., and Schopper J.R., 1987. Colloids and Surfaces, 27, 97-122.
Principal Investigators, 2006. UPDATE: The Chesapeake Bay Impact Crater Drilling Project, January 13.
Popov Yu., Romushkevich R., Bayuk I., Korobkov D., Mayr S., Burkhardt H. and Wilhelm H., 2004. Meteoritics and Planetary Science (MAPS) 39, No 6, 799-812.
Mayr S., Burkhardt H., Popov Yu., Romushkevich R., Bayuk I., Wilhelm H., 2005. Poster. ICDP-IODP Joint Meeting - Euro-Forum, Potsdam, March 14-16.
Schmitt, R.T., Wittmann, A., and Stöffler, D., 2004. MAPS 39, No 6, 979-1001.
Schön, J.H. 1997, Seismic Exploration on CD-ROM - Elsevier Science Ltd.
Vermeesch P.M. & Morgan J.V., 2004. MAPS 39, No7,1019-1034.
Wilhelm H, Heidinger P, Šafanda J, Cermak V, Burkhardt H, and Popov Y, 2004, MAPS, Nr 6, 813-819.

ICDP

A geomechanical facies model to investigate the coupled hydraulic-geomechanical processes at the KTB site

McDermott, C.I.[1], Lodemann, M.[2], Ghergut, I.[2], Tenzer H.[1], Sauter M.[2], Kolditz, O[1].
[1]Center for Applied Geoscience, University of Tübingen, Sigwartstr. 10, 72076 Tübingen, Germany; [2]Geoscientific Centre at the University of Göttingen,

Georg-August University of Göttingen, Goldschmidtstr. 3, 37077 Göttingen, Germany.

Fracture systems dominate the movement of geofluids in crystalline rocks where the rock matrix is almost impermeable. Investigation of the coupled processes and parameters controlling the flow, mass and heat transport in such systems is important for the later utilisation of such systems, e.g. in the extraction of geothermal energy. Several authors have shown the scale dependency of hydraulic parameters and mechanical parameters. In this abstract the combination of data from several scales of investigation are combined in a three dimensional numerical model of the KTB site to investigate the non-linear coupling of hydraulic flow and mechanical deformation.

Much data is already available in the literature, as exemplified by Emmermann and Lauterjung (1997). Here recent field scale experimental work involving a one year long pumping test (June 2002 - July 2003) to investigate the hydraulic characteristics of the fractured basement rock is combined with laboratory scale elastic compression tests, drilling records, geological, geophysical and hydrogeological data and numerical investigation techniques.

Large scale geophysical surveys Harjes et al. (1997) indicating the presence of reflectors, considered to be pathways for geofluids, geological investigations particularly structural and tectonic interpretations Hirschmann et al. (1997), and fluid bearing fracture zones (Lodemann et al., 1998) provided the basis for a three dimensional fracture network model. Geologically individual fault

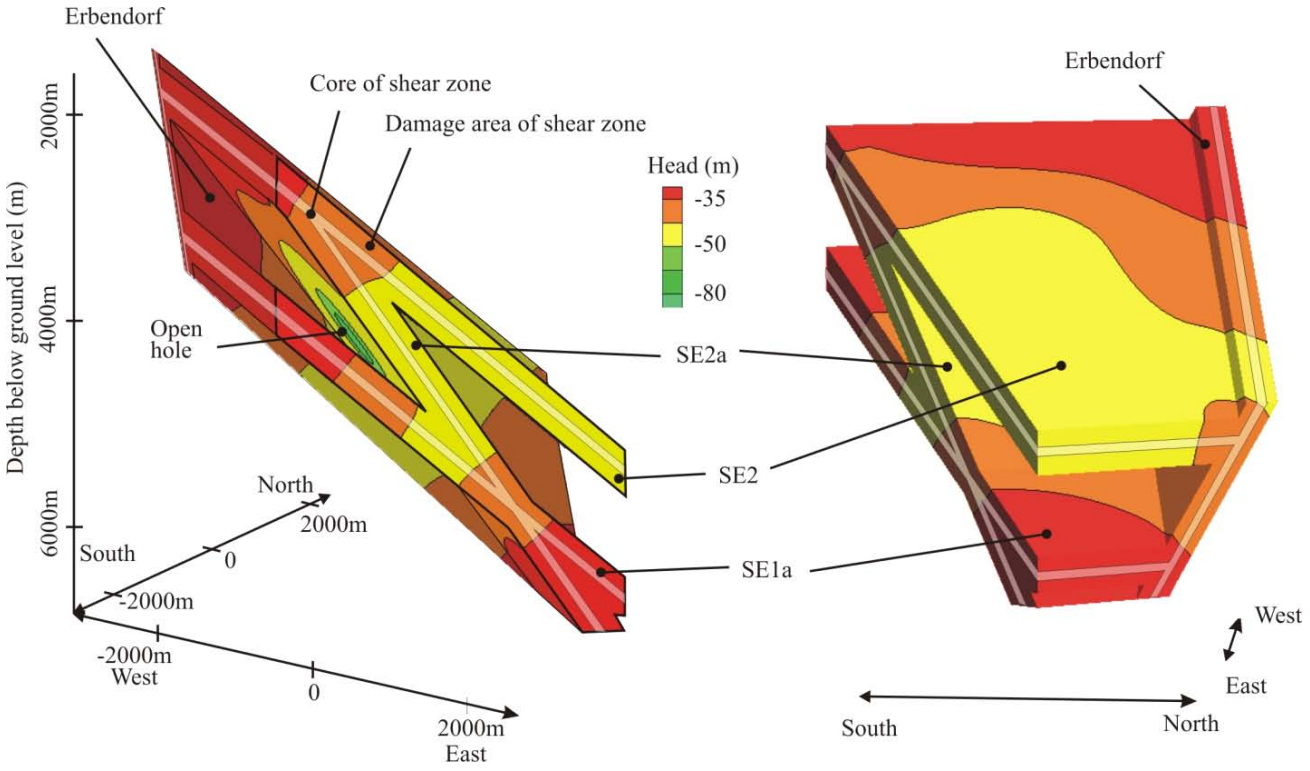

Figure 1: KTB Geomechanical facies, after McDermott et al. (2006)

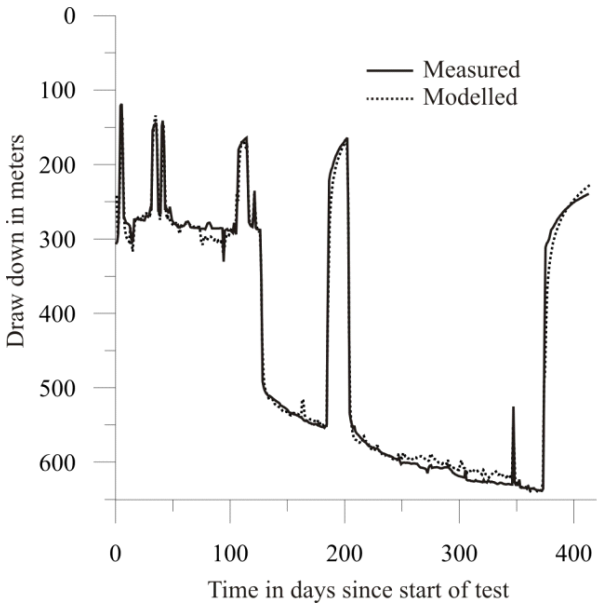

Figure 2: KTB long term pump test

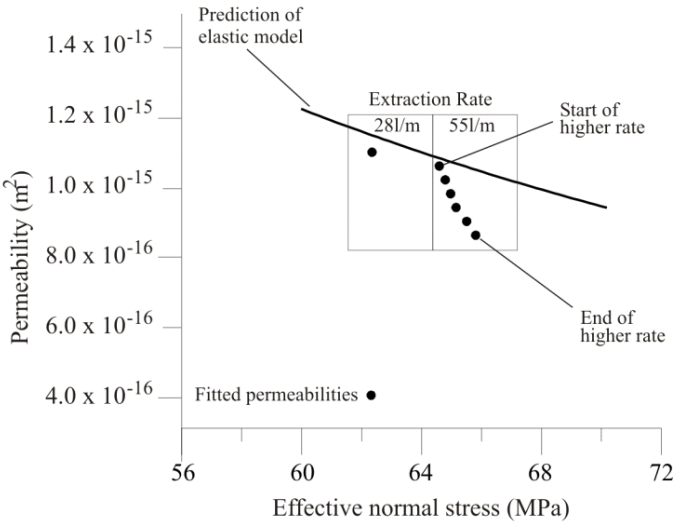

Figure 3: Matching of elastic interpretation

planes are seldom encountered, and in reality one is dealing with a whole swarm of similarly orientated fractures extending sometimes over considerable distances, within which the movement responsible for the formation of the fractures is accommodated as is flow within the fractures. Therefore we introduce the concept of shear zones to represent the major geological tectonic features observed in the pilot and main boreholes. A shear zone in this modelling context is a plane with a certain thickness comprising nfr discrete interacting fractures. Several analyses of the tectonic features at the KTB site have been undertaken, particularly the KTB work group under Hirschmann provided much detailed fracture picking information. Winter et al. (2002) analysed drill cuttings from the KTB main hole from 1700 m to 2400 m and from 4500 m to 5000 m. Their results indicate that cataclastic shear zones can be found in the cuttings extending well over one hundred meters thickness.

It is clear that geological deposits are not just random groups of deposits but rather there is both depositional and structural process control on the in situ properties. This consideration has led to the concept of architectural elements within geological deposits, particularly sedimentary deposits. An architectural element defines a principal building block of the geological deposit being considered to which specific parameters are assigned. Adapting this for a hydrogeological and geo-mechanical situation, i.e. the coupling of hydraulic, mechanical and later thermal properties, allows the definition of geomechanical facies. In the context of the KTB site, a geomechanical facies approach allows the description of separate architectural elements of the shear zone with definite

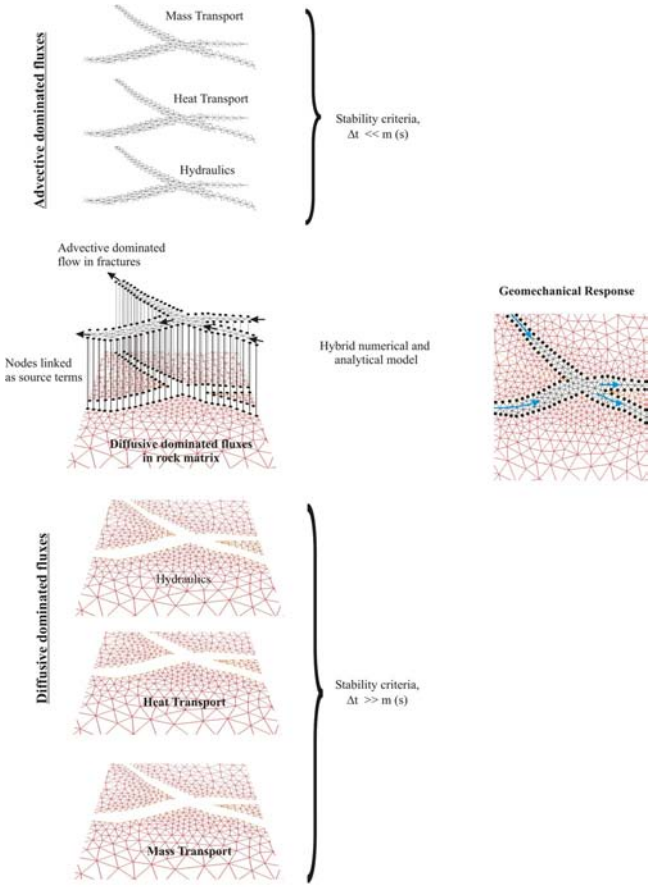

Figure 4: Use of multiple meshing for the numerical investigation of several coupled processes in heterogeneous multi continuum media

flow, transport and mechanical characteristics. In the current model the shear zone is divided into a core zone where flow and transport is more prevalent and a damage zone where there is an increase in micro-cracking. Between the shear zones there is an undisturbed zone where the action of shearing has not influenced the material. This conceptual structure is illustrated in Fig. 1.

The final results of several hundred model runs (Fig. 2) to match the pump test signal gained from the KTB site indicated that there is no one ubiquitous set of parameters which can fit the entire hydraulic range. The almost perfectly fitted set of data was achieved using a time dependent permeability and storage parameters. The elastic analysis, Fig 3, indicated short term changes could be accounted for, but a none elastic process was operating to cause the longer term changes.

The complex fracture systems, and in this case the characteristics of the geomechancial facies can be further identified with the use of transport experiments (Push Pull tests) investigating both the mass transport of several tracers as well as heat as a tracer. Numerical evaluation of the so called push-pull tests offer a method of characterising the nature of the in situ fracture network Ghergut et al. (2006). Experience from recent literature Helmig, Braun and Manthey (2002; Dietrich et al. (2005; McDermott et al. (2006) show that in such complex scale dependent systems a hybrid model combining several approaches to modelling the processes and geometry provides the best method of simulating the signal. Numerically it is possible to reduce the computational effort of process description by introducing the concept of multiple meshes. Each mesh has a limited number of processes operating on it, and is optimised for the numerical requirements of the processes in terms of size, structure and location of the individual elements. Where several processes are operating there exists several meshes.

Exchange between the processes operating on different meshes is controlled by key time state exchange, analytical functions or source and sink terms dependent on the state variables dominating the meshes. An example of this concept is given in Fig 4. Evaluation of the data provides the basis for the integration of analytical and numerical solutions into a multiple mesh representation of the geomechanical facies.

Conclusion

A geomechancial facies approach coupled with a multiple meshing of the KTB site offers a number of significant computational and investigation advantages in the characterisation of deep seated crystalline fractured systems.

References

Dietrich, P., Helmig, R., Sauter, M., Hötzl, H., Köngeter, J. and Teutsch, G., 2005. Flow and Transport in Fractured Porous Media. Springer, 450p.

Emmermann, R. and Lauterjung, J., 1997. The German Continental Deep Drilling Program KTB: overview and major results. Journal of Geophysical Research, 102: 18179-18201.

Ghergut, I., McDermott, C.I., Herfort, M., Sauter, M. and Kolditz, O., 2006. Reducing ambiguity in fractured-porous media characterization using single-well tracer tests. IAHS Publ. (in press), 8 pp.

Harjes, H.P., Bram, K., Durbaum, H.J., Gebrande, H., Hirschmann, G., Janik, M., Klockner, M., Luschen, E., Rabbel, W., Simon, M., Thomas, R., Tormann, J. and Wenzel, F., 1997. Origin and nature of crustal reflections: results from integrated seismic measurements at the KTB superdeep drilling site. Journal of Geophysical Research, 102: 18267-18288.

Helmig, R., Braun, C. and Manthey, S., 2002. Upscaling of two-phase flow processes in heterogeneous porous media: Determination of constitutive relationships. IAHS AISH Publication, 277: 28-36.

Hirschmann, G., Duyster, J., Harms, U., Kontny, A., Lapp, M., de-Wall, H. and Zulauf, G., 1997. The KTB superdeep borehole: petrography and structure of a 9-km-deep crustal section. Geologische Rundschau (DEU), Band 86, Heft Suppl: 3-14.

McDermott, C.I., Lodemann, M., Ghergut, I., Tenzer, H., Sauter, M. and Kolditz, O., 2006. Investigation of Coupled Hydraulic-Geomechanical Processes at the KTB site: Pressure dependent characteristics of a long term pump test and elastic interpretation using a geomechanical facies model. Geofluids, 6: 67-81.

Winter, H., Adelhardt, S., Jerak, A. and Kuchenhoff, H., 2002. Characterization of cataclastic shear-zones of the KTB deep drill hole by regression analysis of drill cuttings data. Geophysical Journal International, 150(1): 1-9.

IODP

Influence of lateral advection on Feni drift deposits (ODP Leg 980) - an integrated, conceptual approach

Helge Meggers[1], Karl-Heinz Baumann[1], Michael Frenz[2], Jan-Berend Stuut[1], Christoph Vogt[1] and Thomas Wagner[3]
[1]Department of Geosciences, University of Bremen, Germany; [2]Southampton Oceanography Centre, United Kingdom, Challenger Division for Seafloor Processes, UK; [3]School of Civil Engineering and Geosciences, University of Newcastle upon Tyne, UK

A better understanding of the mechanisms and effects of the various types of sediment supply on the marine paleoclimatic record has recently gained more attention in the scientific community. This interest is mainly due to the fact that differential supply and movement of fine- and coarse-grained sediment does substantially influence the interpretation of paleoceanographic records and thus accurate insights into past ocean circulations. Lateral sediment displacement may play a conspicuous role for the accurate interpretation of geochemical and micropaleontological marine records. Therefore we carried out a systematic and high-resolution investigation on a sediment core from the Feni Drift (ODP Site 980) integrating information from grain-size studies with mineralogy, micropaleontology and bulk organic and isotope geochemistry. These complementary sets of data essentially improve our understanding on the effects of lateral advection on deglacial-Holocene drift sediments on the sedimentary record as a climate archive in the northern North Atlantic for the last 20,000 years. We elaborate a first continuous high-resolution sedimentological record to validate the indirectly inferred variations in NADW vigour and to assess the advantages and disadvantages of the "sortable silt" and "end-member modelling" approaches (Mc Cave et al., 1996, Prins et al., 2002). Sediment grain-size as the central issue provides detailed information on the current strength variability over the past 20,000 years (Fig. 1). We discriminate the ice-rafted from the current-sorted proportion by applying an end-member modelling algorithm to the sediment grain-size distributions. The sedimentological study is further supported by three independent lines of evidence. These are the issues of (1) "old" organic carbon, (2) resuspended coccoliths and coccolith (alkenone)-derived sea surface temperatures and (3) imported clay minerals.

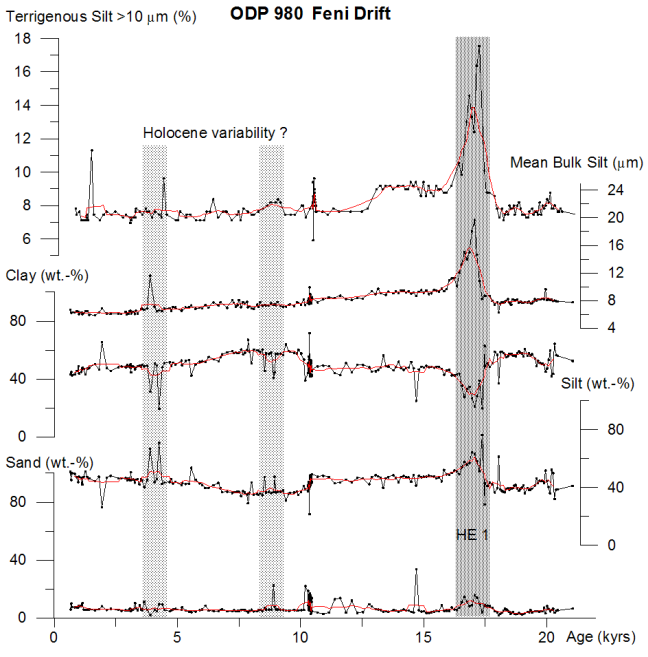

Fig. 1: Sand, silt and clay fraction content of ODP Leg 980 in the northern North Atlantic (Feni Drift) in the last 20 kyrs in comparison to the mean of the bulk silt fraction and the sortable silt fraction. Heinrich Event 1 is indicated with a grey bar.

References:
McCave, I. N., Manighetti, B., and Robinson, S. G. (1995). Sortable silt and fine sediment size/composition slicing: Parameters for palaeocurrent speed and palaeoceanography. Paleoceanography 10, 593-610.
Prins, M. A., Bouwer, L. M., Beets, C. J., Troelstra, S. R., and Weltje, G. J. (2002). Ocean circulation and iceberg discharge in the glacial North Atlantic: Inferences from unmixing of sediment size distributions. Geology 30, 555-558.

ICDP

Opening up a unique high-resolution climate archive of the last 1.3 Ma from the Qaidam Basin, China

Steffen Mischke
Institute of Geological Sciences, Freie Universitaet Berlin, Germany

The Qaidam Basin in northwestern China contains an unprecedented thickness (3.2 km in its center) of Quaternary fine-grained and fossil-rich continental sediments. The high sedimentation rates in the basin allow a high-resolution record to be obtained and contrast markedly with other proxy records for Central Asia that produce lower-resolution data and/or are of shorter duration. In contrast to the present-day arid conditions, petroleum exploration boreholes in the proposed drill region reveal that most of these sediments continuously accumulated in a large freshwater lake, possibly up to 70,000 km² in size. During high lake-level stands this lake would have been regionally significant as a continental moisture source, having a profound influence on local and regional climate.

This proposed research aims to obtain a 1.3 km long core from these sediments to provide a record of environmental change spanning the last 1.3 Ma. This target depth is determined from two existing cores, which span the period from 1.3 Ma to ~2.8 Ma, and the possibility to obtain a new archive for environmental change in Central Asia covering the last ~2.8 Ma. Due to the long-term high sediment accumulation rates in the Qaidam Basin, the cores will allow the investigation not only of the complete Quaternary climate evolution of the region but also of selected periods of climate change based on close sediment sampling of the core. Furthermore, the lake sediments from the Qaidam Basin contain a number of sedimentological, geochemical and palaeontological proxies of environmental and climate change which cannot be investigated using comparable long-term non-marine records such as the loess-palaeosol sequences of the Chinese Loess Plateau, speleothems or ice cores.

The proposed drilling project will contribute to the understanding of the linkages between drainage and lake evolution in response to the glaciation and uplift of the northern Tibetan Plateau and will help to better understand the formation of oil and gas sources, and reservoir sediments in the Qaidam Basin.

To prepare for the proposed drilling and accompanying investigations in the Qaidam basin, a workshop is planned as a first step towards information exchange, project conception and interdisciplinary cooperation. An initial group of 21 scientists from 7 countries covering all the relevant scientific aspects of the proposed project has been established and has agreed to attend the workshop.

The main objective of this project is to develop a new archive of sediments from one of the world's thickest successions of Quaternary continental deposits. This will enable a high-resolution record of the nature of Quaternary environmental change in NW Tibet to be reconstructed.

The planned workshop aims to collate all the existing relevant data and discuss the potential to drill a new continuous core. This will be used:

1. to reconstruct the Quaternary lake evolution and hydrologic history
2. to provide quantitative information on long-term environmental and climate change using transfer functions based on existing regional surface-sample training sets
3. to study the history of the Siberian-Mongolian high pressure cell on a timescale pertinent to understanding dust deposition

within the lake,

4. to trace the glaciation and uplift threshold conditions of northern Tibetan Plateau, which likely helped force a shift from a large lake environment sometime in the Late Pleistocene to the present-day dry conditions
5. to investigate the linkages between the evolution of the drainage systems of large rivers, such as the Yellow and Qinglong River, which possibly had contributed to the Qaidam Basin in the early Quaternary
6. to improve the understanding of oil and gas formation, and the nature and distribution of reservoir sediments within the basin

ICDP

Tectonic evolution of the northern Malawi rift, East Africa: sediment dispersal in a large lake basin.

Estelle Mortimer

The Malawi Rift is an integral part of the East African Rift system (EARs), the type example of a rift system in its youthful stages of development. Understanding the spatio-temporal evolution of this rift system provides insights into the past histories and controls on more ancient rift basins. Fundamental questions remain regarding the structural styles, partitioning, and sediment dispersal patterns within large lacustrine basins that are common to young rifts. Such basins are particularly useful recorders of climatic fluctuations. In areas with pronounced climatic variability and high evaporation/precipitation ratios this may lead to, often transient, basin isolation that may dramatically affect sediment and facies distribution.

We investigate the structural evolution and sedimentation patterns of the North basin, Malawi Rift. We utilise two seismic reflection data sets: the first, collected by project PROBE, records the entire basin-fill (Sequences 1-3) at medium resolution; the second provides a closely-spaced high-resolution survey of the past ~1 Ma (Sequence 3). These data document the development of the basin-bounding and intra-basin faults. Throughout its history, the basin-bounding fault has accommodated the greatest strain and therefore exerted the fundamental control on the distribution of sediment within the rift. Present-day sediments enter the basin axially, although there is evidence that transverse supply was also important in the past. We identify 11 intra-basin structures that strike parallel or sub-parallel to this border fault. These intra-basin faults, active from the earliest stages, have initial segment lengths of ~30 km, but rapidly reach lengths in excess of 80 km in the north of the basin, and 60 km in the south. Much of the sedimentation along the faults occurred during Sequence 2 (~2.7-1.6 Ma), a period of relative over-filling of the basin. While the basin-bounding fault controls the overall sediment architecture, all 11 intra-basin structures have remained active and have, in particular during the most recent depositional history, played an important role in sediment dispersal within the basin during lake-level lowstands. Such long-lengths and long-lived activity on almost exclusively synthetic intra-basin faults is, however, unusual. This pattern is possibly attributed to one or a combination of factors including: underlying structural fabrics; the geometry of the detachment at depth; sediment loading at the mouths of feeder systems; or loading by a volcanic centre to the north.

IODP

PRESS (Pressurised Core Sub-sampling and Extrusion System)

In-situ Sampling, Transfer and Investigation Methods in Scientific Drilling, Technology Progress Report from IODP Leg 311, Cascadia, and Beyond

Wolfgang H. Müller, Erik Anders, Hans Amann
TU Berlin, Inst. für Mechanik, Lehrstuhl für Kontinuumsmechanik und Materialtheorie, LKM

In order to understand the complexities of the environment in which we live and on which we are utterly dependent, we need to study it accurately. More than 50% of the Earth's surface compose of the deep sea floor. Precondition to achieve unbiased and true findings is research in pristine habitat. In-situ sampling, transfer and analysis of specimens while maintaining unchanged environmental parameters, i.e., mainly pressure and temperature, opens up new frontiers of research into the study of gas hydrates and of barophilic micro-organisms living in the sub-seafloor biosphere. As opposed to traditional ex-situ methods, remote and substantially different natural processes and their parameters can thus be directly determined under laboratory conditions. Such progress is particularly valid for studying deep sea ephemeral processes and will contribute to increased knowledge of the environment. Understanding the sub-seafloor biosphere is of great commercial and scientific interest and may help to define potential hazards, significant regional and global earth flux components, the limits of life on Earth and allow potentially useful organisms for biotechnology to be identified.

Teams from the Technische Universität Berlin, Lehrstuhl für Kontinuumsmechanik und Materialtheorie, LKM, and its predecessor MAT, Marine Technology, are developing in various national and international research projects methods and tools for in-situ sampling technology. The EU Projects HYACE and HYACINTH (EVK3-CT 2001 - 00060) have achieved hardware prototypes of in-situ sampling and subsampling for ocean drilling. The HYACE Rotary and the Fugro Percussion Corers (HRC and FPC) were used, also with support of Deutsche Forschungs-gemeinschaft (DFG), for Leg 204 of Ocean Drilling Program (ODP), and now for Leg 311 of Integrated Ocean Drilling Program (IODP). In the latter project, PRESS, the downstream pressurised sub sampling and transfer system, was used as a pilot in research facilities of the Canadian Geological Service (CGS) in Sidney, BC (November 2005) with support by DFG (MU 1752/9-1) and complemented its successful technical feasibility tests on pressurised gas hydrate cores from the US Joint Industry Project in the Gulf of Mexico (May 2005). The assistance by DFG and CGS is acknowledged with gratitude.

Axial subsampling of the very centre of the core, almost swarf free liner cutting and controlled sterilisation of hazardous parts were enhanced and investigated during the progress of development and could minimise the peril of contamination. Videoobserved extrusion of subsamples (~80 mm length, 20 mm) and their diversion into several pressurised microbiological cultivation chambers were achieved and inaugurate new dimensions of applied in situ deep biosphere science. Moreover geochemical and bio-geochemical reactions such as methane oxidation and sulphate reduction for gas hydrate bearing sediments can be measured under quasi in-situ conditions.

Further technical development and scientific applications of in-situ methods and tool systems, including subsampling and transfer, concentrate on the extension of the present pressure rating from 250 bar to 400-600 bar and ultimately up to 1100 bar, with simultaneous consideration of scaling down and simplifying the apparatus. Enhancements are needed to eventually investigate all parts of the pressure dependent deep sea floor, the largest geo-bio habitat world wide. Improved functioning of the novel tools, contamination control during sampling, storage, sub sampling and safety engineering continue to guide further technology efforts. Advanced design and high performance materials such as carbon, high strength fibre composites, ceramics and Titanium alloys shall be applied. Clearly the anisotropic behaviour of the composites and/or the brittle nature of ceramics might require a partial redesign of the in-situ sampler so that full use can be made of the advantages these materials have to offer. Finite element calculations will be used during the redesign process as well as in general to validate the safety and reliability of the whole construction from a pressure vessel / boiler code point-of-view.

Future routine industrial tools should be cost-effective, easily interfaced with dedicated downstream tools for very different and

specific scientific tasks and should withstand a minimum of 1000 high load cycles. The recent successful beginning of in situ technology in scientific drilling continues into broad applications and further development during the forthcoming years.

IODP

Investigation of blueschist and serpentinized harzburgite from the Mariana forearc: Insights into the mechanisms of element mobilization in subduction zones and storage of fluid-mobile elements in the mantle wedge

Sonja Pabst[1], Thomas Zack[1], Rainer Altherr[1], and Ivan Savov[2]
[1]Mineralogisches Institut, Universität Heidelberg, Germany; [2]Department of Terrestrial Magnetism, Carnegie Institution of Washington, USA

Subduction zones are the most complex geological structures and contribute significantly to the diversity of rock types on Earth. In this case, we want to gain insight into the mobilization of fluids and fractionation of associated trace elements within the forearc of active subduction zones.

The serpentine mud volcanoes from the forearc of the Mariana subduction zone yield a unique opportunity for studying samples from both the dehydrating slab (blueschist-facies mafic samples) as well as samples from the overlying mantle wedge (serpentinized harzburgite samples). These crustal and mantle rocks have been transported to the ocean floor in a serpentine mud matrix directly from the slab-mantle interface. They have been subject of intense studies and several authors gave detailed information about the petrology as well as the pressure and temperature regime in such depths.

The aim of this project is to investigate the trace element inventory of serpentinized harzburgite and blueschist-facies mafic rocks from two serpentine mud volcanoes, the Conical seamount (ODP Leg 125) and the South Chamorro seamount (ODP Leg 195). To estimate fluid fluxes in the Mariana forearc, we will investigate fluid-mobile elements (mostly Li and B, but also Sr, REE, Sb, Cs and Pb) in the crystal structure of minerals from both mafic and ultramafic samples by in situ techniques. The following questions are of particular interest.

1: To what degree is oceanic crust loosing fluid and fluid-mobile elements at a depth of ~20 km (beginning dehydration of mafic oceanic crust)? Thus, trace element abundances of the blueschist-facies mafic clasts will be compared with compositions of basaltic oceanic crust by using B isotope fractionation as an index.
2: The available ultramafic samples are only partly serpentinized with different generations of serpentine minerals. Thus, we can investigate fluid infiltration in detail with attention to storage of trace elements into the serpentine crystal structure, and to the amount of fluid transported through the observed veining network.
3: To what extend do serpentinite clasts interact with the surrounding fluids in the serpentine mud during ascent from 20 km depth to the seafloor? Hence, we will analyze serpentines that have formed before entrainment into the serpentine mud. The later interaction with the serpentine mud can be evaluated by comparing the first generation serpentines with whole rock data from the same samples.

In this project several in situ methods will be employed: the scanning electron microscopy (SEM) will be used to work out micro-textural relationships in the samples, electron-microprobe analyses (EMPA) will specify the mineral composition of the samples, micro-Raman serves to distinguish serpentine polymorphs. The secondary ion mass spectrometer (SIMS) in Heidelberg is in the center of this study as it has been optimized to study light elements at high spatial resolution (e.g. δ^{11}B-measurements can be conducted at a resolution of 30μm). Li and B mapping with the Time-of-Flight SIMS (TOF-SIMS) at the Smithsonian Institution will guide these measurements. Additionally, measurements of the other fluid-mobile elements by laser ablation inductively coupled plasma mass spectrometry (LA-ICP-MS) will complement this data set.

Thus, with these (high-resolution) in situ geochemical analyses important new information can be gathered on the trace element budget in the serpentinites and the blueschist-facies mafic clasts. Due to the existence of complex network of thin veins of serpentine minerals in the serpentinites that show crosscutting relationships, we hope that we can ultimately estimate the temporal evolution of slab-derived serpentine producing fluids. The recognition of trace element patterns associated with specific textures within the serpentinites and blueschist-facies rocks are thought to reflect specific subduction zone processes and will help to better understand the "subduction factory".

IODP

Paleoclimate and paleoecology of the northern lowland Neotropics, Phase I: Limnological survey of modern aquatic environments of the Peninsula Yucatán, a contribution to the Lake Petén-Itzá, Guatemala, Drilling Project

Liseth Pérez[1], Evgenia Vinogradova[1], Wolfgang Riss[2], Burkhard Scharf[1] & Antje Schwalb[1]
[1]Institut für Umweltgeologie, Technische Universität Braunschweig, Pockelsstrasse 3, D-38106 Braunschweig, Germany; [2]Institut für Evolution und Ökologie der Tiere, Westfälische Wilhelms-Universität Münster, Hüfferstr. 1, D-48149 Münster, Germany

Phase I of our contribution to the Lake Petén-Itzá, Guatemala, Drilling Project consists of a Limnological survey of modern aquatic environments of the Yucatán Peninsula. Yucatán is characterized by a steep precipitation gradient from the dry northern lowlands to the humid mountainous areas in the south and is thus an ideal region to study the location of aquatic system proxies on the regional climatic gradient. Our goal is to (1) improve the role of microfossils as indicators of past environmental and climate changes and (2) to use this information for the interpretation of species assemblages from long cores retrieved from Lake Petén-Itzá, during February 2006. In a multidisciplinary approach we combine aquatic geochemistry, isotopic signatures from ostracode valves, modern and paleofauna of chironomids and ostracodes to characterize environments and habitats.

Here we present first results from a sampling campaign along a transect across the Peninsula Yucatán including lakes in Guatemala, Belize and Mexico. From November to December 2005 water samples and surface samples from a total of 14 lakes were collected. Analysis of water samples for major and minor ion composition, $\delta^{18}O$, $\delta^{13}C_{DIC}$ and ^{87}Sr is in progress. Surface and littoral sediments were sampled to determine modern species assemblages of ostracodes and chironomids, and the stable isotope signature from ostracode valves. In addition, samples for cladocerans, diatoms, thecamoebians, pollen and charcoal to be analyzed by cooperation partners were taken. In Lake Petén-Itzá a more detailed survey program was carried out. Water samples from the water column and surface sediments along a depth-transect were collected. This will serve as calibration for the reconstruction of past lake levels. Four short cores were retrieved in order to determine sedimentation rates by ^{210}Pb and for the reconstruction of recent lake system and climate change.

Results from this survey will contribute to reconstruct environmental parameters such as precipitation, evaporation, and lake level changes from Lake Petén-Itzá long core sediments in phase II of our project. This will provide information on how the overall setting of Lake Petén-Itzá and its response to climate forcing in the Neotropics has changed through time.

IODP

Hydrocarbon potential of ODP Hole 1276A, the first deep well on Newfoundland Margin

T. Pletsch[1]*, J. Kus[1], J. Pross[2], H. Wehner[1], G. Scheeder[1], M. Arnaboldi[3]
[1]Bundesanstalt für Geowissenschaften und Rohstoffe, Stilleweg 2, 30655 Hannover, Germany; [2]Geologisch-Paläontologisches Institut, Johann-Wolfgang-Goethe-Universität Frankfurt, Senckenberganlage 32-34, 60054 Frankfurt, Germany; [3]Department of Geological Sciences, University of Michigan, 3520 CC Little Building, 1100 North University Avenue, Ann Arbor, MI 48109-1005, USA

More than six hundred meters of mid-Cretaceous, dark, organic rich mudstones alternating with turbidites and debrites were recovered in Ocean Drilling Program (ODP) Hole 1276A, at the toe of the SE facing Newfoundland Margin. Laminated black shales with elevated marine organic carbon content, some of which correlate with Cretaceous Oceanic Anoxic Events (OAE), are intercalated with the mudstone sequence. Organic matter in the mudrocks is dominantly terrigenous and recycled from previously buried sediments with occasional intercalations of more marine organic matter at times corresponding to OAEs. Marine organic matter has suffered from degradation, probably as a result of its long travel through an oxygenated water column.

Two alkaline basalt sills, 10 and approximately 20 meters thick, intruded into the mudstones when these were still poorly indurated. Radiometric ages and structural evidence suggest that the upper sill intruded first. Both mudrocks and black shales are immature over much of the section down to 1700 meters below seafloor (mbsf), except for the narrow thermal aureoles close to the igneous sills. Within the aureoles, maturity increases sharply, but reaches overmature levels only immediately adjacent to the igneous contacts. The subdued impact of igneous heating on the maturity of the enclosing sediments is attributed to the advection of relatively cool pore waters through the poorly compacted sediments.

Most hydrocarbons generated within the aureole above the upper sill were not trapped but escaped to the hydrosphere. Hydrocarbons generated in the aureole of the lower sill migrated upward and accumulated in a high-porosity interval of plastic clays between the two sills that is characterised by elevated methane concentrations. Significant undercompaction and the retention of volatile hydrocarbons testify to the sealing efficiency of the overlying sill and mudstones. Hydrocarbons generated below the recovered section may have been trapped beneath the lower sill. Depending on sill geometry, intrusion age, and structural position, sills elsewhere on the Newfoundland Margin may acts as top seals of economic hydrocarbon reservoirs.

ICDP

Efficient computational formulation of elastovisco-plasticity for 3D modeling of strain localization in lithosphere: first step of thermo-mechanical modeling of San Andreas Fault System

A. A. Popov and S. V. Sobolev
GeoForschungsZentrum, Germany (anton@gfz-potsdam.de / Phone: +49-331-288-1281)

The aim of this project is 3D thermo-mechanical modeling of the evolution of the San Andreas Fault System (SAFS) in California in lithospheric scale during the last 10-20 M.Y. The scale and the nature of the complicated coupled thermal and mechanical process in SAFS require development of special numerical methods, which is the major focus of this particular presentation.

The most complicated phenomenon exhibited by the Earth materials is the formation of shear bands and macroscopic discontinuities (fracture). Conventional modeling of this process by means of strain softening may cause ill-posedness of mathematical description of the problem, thus leading to physically unacceptable results. More adequate description is provided by the non-local and gradient-enhanced damage models or even by switching to the analysis of contact interaction along localized internal interfaces. In this work, however, we confine our interest to the conventional models of creep and plasticity without strain softening and demonstrate that even this simplified approach can still be useful for the three-dimensional modeling of strain localization in the lithosphere. Specifically, we employ extended non-associative Drucker-Prager elastoplastic model along with arbitrary combination of diffusion, dislocation and Peierls creep mechanisms.

Numerical modeling of mechanical processes in geodynamics is indeed an inherent part of computational mechanics in the sense that many difficulties are shared with the other areas of application, of which engineering is the most productive. Many powerful techniques, that form a qualitative level of computational formulation, were initially designed for engineering applications. We are striving to adopt this extensive experience for the purposes of computational geodynamics as far as possible in our work. Namely, we utilize Hughes-Winget incrementally objective implicit time integration algorithm which allows an arbitrary combination of rheological mechanisms (elastic, viscous and plastic) within a single finite element model. For this approach to make sense, elastic strains must remain vanishingly small - behavior closely followed by the Earth materials. However the magnitude of plastic and viscous strains is not restricted. An approximate linearization of discrete equilibrium equation is employed in order to use time step which is limited only by the characteristics of the mechanical process that we simulate and can be orders of magnitude larger than Maxwell time. Details of material tangent operator derivation are discussed in addition, along with stable element formulation and robust solver for linear equation system. We present a set of benchmarks and simplified models in order to validate our approach.

IODP

The Miocene carbonate crash: First results from carbonate budgets and silt grain size analysis (ODP Sites 927, 928)

Inga Preiß-Daimler and Rüdiger Henrich

Several sharp drops in carbonate content have been reported from different sites in the Atlantic, Carribbean, Pacific and Indian Ocean (see Roth et al., 2000 for review) in the middle to late Miocene transition (12-8 Ma). These Carbonate Crash Events occur in a period of the onset of NADW formation and prominent tectonic-climatic reorganisation on land and in the ocean basins. During the crash events carbonate MAR's dropped significantly, as reported from the East Pacific and are attributed to the closure of the Panama gateway and thus reorganisation of deep water circulation (Lyle et al., 1995). This incident leads to a re-establishment of NADW due to the increased northward export of warm saline waters out of the Carribbean and an influx of corrosive southern-sourced intermediate water into the Carribbean. Recent results from sites off Namibia (Sites 1085, 1087) indicate that the Miocene crash events in this region were at least partly influenced by terrigeneous dilution (Kastanja et al. in review). Based on coarse fraction data, Diester-Haas et al (2004) assumed that carbonate dissolution was not a prominent cause in this region. However, the major cause here appears to be shifts in carbonate production, predominantly in coccolith accumulation (Krammer et al. in press).

Our first results from geochemical and sedimentological investigations at Ceara Rise indicate a minimum in carbonate content at both sites lasting from 10.1 to 9.8 Ma can be related to the Carbonate Crash Event 5 (Roth et al., 2000). The coarse fractions show a decline in the carbonate minimum. In the same interval these subfractions reveal a shift from coarser to finer grain sizes: the portion of the fraction 63-125µm increases and the portion of the 250-500µm decreases relative to the bulk coarse fraction. This might be indicative of fragmentation processes to be

further confirmed by a conservative planktic foraminifer fragmentation index, that is presently being compiled.

Silt grain-size analysis will provide proxies for bottom current speed (sortable silt according to McCave et al., 1995) and deep water regime. The hypothesis whether lower bottom current velocities is related to reduced NADW production and thus worse carbonate preservation will be checked. The calcareous silt (CS mean and mode of the grain size spectra) will be used to describe the state of foraminiferal preservation. The fine fraction is recently prepared for Sedigraph measurments.

References:

Diester-Haass, L., Meyers, P.A. and Bickert, T. (2004) Carbonate crash and biogenic bloom in the late Miocene: evidence from ODP Sites 1085, 1086 and 1087 in the Cape Basin, southeast Atlantic Ocean. Paleoceanography 19(1): 1-19.

Kastanja, M.-M., Diekmann, B. and Henrich, R. (in review) Controls on carbonate and terrigenous deposition in the incipient Benguela upwelling system during the Middle to the Late Miocene (ODP Sites 1085 and 1087). Paleogeogr. Paleoclimatol. Paleoecol.

King, T.A., Ellis, J., Murray, W.G., Shackleton and N.J., Harris, S. (1997) Miocene evolution of carbonate sedimentation at the Ceara Rise: a multivariate data/proxy approach. In: Shackleton, N.J., Curry, W.B., Richter, C. and Bralower, T.J. (Eds.), Proc. ODP, Sci. Res., vol. 154. Ocean Drill. Progr., College Station, TX. 349-364.

Krammer, R., Baumann, K.-H., Henrich, R. (2005 in press) Middle to Late Miocene fluctuations in the incipient Benguela Upwelling System revealed by coccolith assemblages (ODP Site 1085A). Palaeogeography, Palaeoclimatology, Palaeoecology.

Roth, M.J., Droxler, A.W. and Kameo, K. (2000) The Caribbean carbonate crash at the Middle to Late Miocene transition: linkage to the establishment of the modern global ocean conveyor. In: Leckie, R.M., Sigursson, H., Acton, G.D. and Draper, G. (Eds.), Proc. ODP, Sci. Results, vol. 165. Ocean Drilling Program, College Station, TX. 249-273.

ICDP

Thermo-hydraulic conditions in the area of the "Gulf of Corinth Deep Geodynamic Laboratory": Interpretation from well-logging and modeling

Rettenmaier, D.[1], Giurgea, V.[1], Förster, A.[2], Hötzl, H.[1]
[1]University of Karlsruhe, Dept. of Applied Geology (AGK); [2]GeoForschungsZentrum Potsdam (GFZ)

Background and Objectives

European research activities in the Gulf of Corinth are targeted at the development of an In-Situ Laboratory for obtaining data on earthquake sources and fault mechanics and for investigating the role of faults on fluid flow in this seismically active area. In that regard it is important to know the subsurface temperature and hydraulic conditions and the heat flow from greater depth. The ICDP/DGLab AIG10 borehole (Fig. 1), which intersects at depth the Aigion fault on the southern graben shoulder of the gulf, constitutes the first key activity in this framework and provides for the first time direct access to the conditions above and below this seismically active fault zone. GFZ and AGK supervised the drilling and the geological interpretation of the 1000-m-deep AIG10 borehole. The DFG supported through the SPP ICDP research on the thermo-hydraulic conditions.

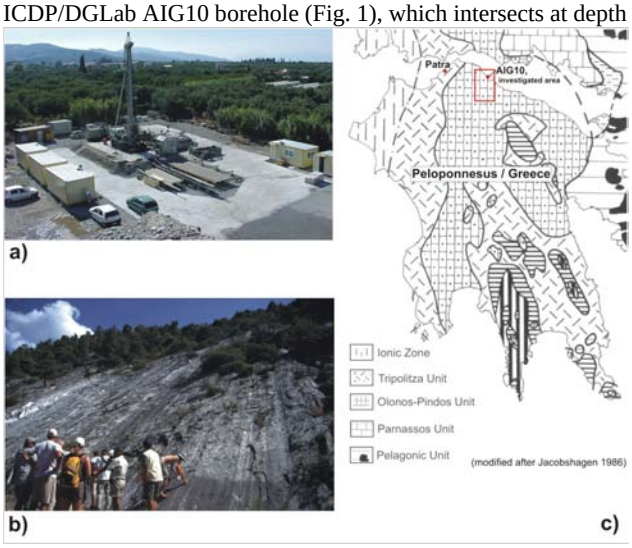

Fig. 1: (a) The drill rig at the AIG10 site near the harbour of Aigion. The spud-in point was selected to intersect the Aigion normal fault at depth within the Olonos Pindos platy limestones and not in the overlying Corinth graben fill. (b) The larger Aigion area is characterized by syn- and antithetic normal faults, (here Eliki fault), which are responsible for strong recent seismic activities. (c) As a result of the Alpine orogeny the Peloponnesus peninsula can be separated into several tectonic thrust nappes. The rectangle marks in the Olonos-Pindos tectonic unit the 80 km2 area around the AIG10 borehole, which was the target of our study.

The heat-flow situation in the Gulf of Corinth is unknown. A general problem in obtaining conductive heat flow onshore Greece is that most boreholes were drilled into permeable formations allowing underground water circulation with an advective overprint of the thermal subsurface conditions.

We use a thermo-hydraulic approach to determine the surface heat flow in the area of the AIG10 borehole including (i) geological surface investigations [1], (ii) hydraulic testing, (iii) petrophysical well-log analysis, (iv) optical-fiber temperature sensing, (v) laboratory measurement of thermal conductivity and porosity, (vi) investigation of water chemistry, and (vii) numerical modeling to evaluate overprints of conductive heat flow by fluids.

Results

The Olonos-Pindos Unit (Fig. 1c) is allochthonous and exhibits a complex geological structure. Imbrications, duplex structures as well as thrusts and thrusted folds cause an alternation of several stratigraphic sequences, which results in changes in lithology over short distances. Gaining knowledge of the geological-tectonical structure was a key for interpreting the succession encountered in the AIG10 borehole (Fig. 2) [2, 3]. The borehole has crossed at least one thrust-fault zone and a major normal-fault zone (the Aigion normal fault) at 760 m. This fault zone separates well-fractured platy, micritic limestone in the hangingwall from highly fractured radiolarite in the footwall, both of the Olonos-Pindos tectonic unit [2].

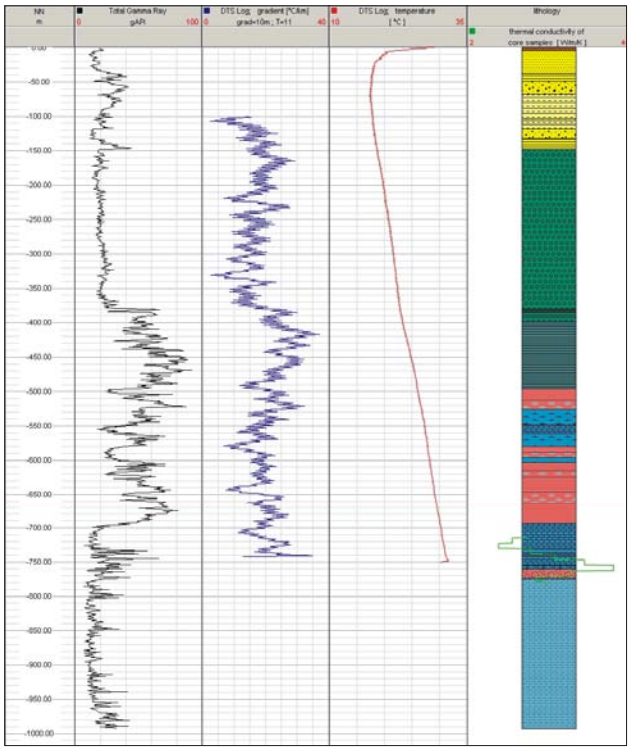

Fig. 2: from left: Gamma-log; temperature gradient (calculated from DTS log), temperature (DTS) log, and interpreted litho-log from cutting, core and log interpretation

Geologic-tectonic mapping (scale 1:10 000) in an area with the size of 80 km² and the generation of a 22-km long N-S geological cross section through this area helped to define the model architecture. A 7-km cutout of the geological cross section then is

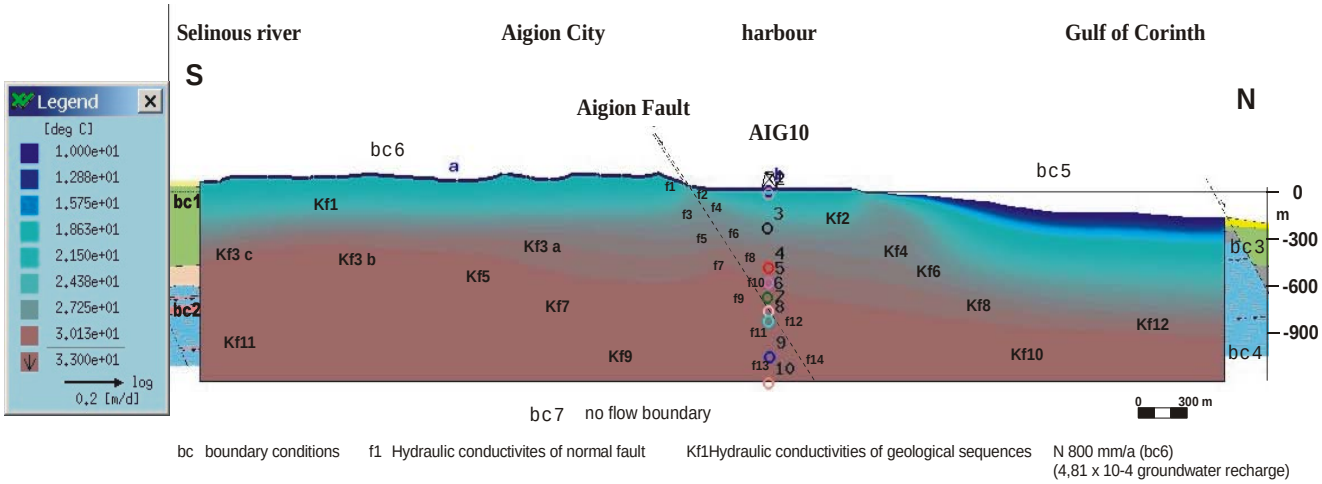

Fig. 3: Preliminary numerical model using FEFLOW® (explanations see text)

the basis for numerical calculations. Hydrochemical analyses of water from 89 springs and pumping stations as well as from six pumping tests were used for calibrating and verifying the conceptual model [4, 5]. The hydraulic conditions also were constrained by two open-hole pumping tests and one artesian production test performed in the AIG10 borehole [6].

Below the Aigion fault zone, pressure and flux increased suggesting karstic water-flow conditions. A water-pressure difference of > 0.5 MPa between the hanging wall and the footwall provides evidence that the Aigion fault zone acts as an impervious zone.

Different hydraulic parameters such as porosity (derived from geophysical logs and laboratory measurements), permeability (k_f), flux rate, etc. were verified in the conceptual hydrogeological model. After calibrating the hydrogeologic flow model, the fluid dynamics in the numerical model was verified by variation of the hydraulic parameters Kf1-Kf10 (for lihological units) and f1-f17 (for fault behaviour) (Fig. 3). Afterwards, the groundwater-flow model near faults was extended to a coupled fluid heat-flow model where data from thermal well-logging (Fig. 2) and thermal properties of rock samples also were incorporated. In this model, a constant basis temperature (33˚C) at depth, the measured temperature-depth profile, and the thermal conductivity determined for the different lithotypes were used.

Heat flow determined by the interval method (in depth intervals above the Aigion fault) averages to 55+/-5 mW/m². This value resembles "normal" crustal heat flow, not suggesting any impact by the magmatic arc of the Hellenic subduction zone. However, the preliminary results of thermo-hydraulic modelling (Fig. 3) indicate that heat flow is slightly affected by fluid flow in aquifers above the fault. Effects from fluid flow in the karst unit below the heat-flow determination interval (below 772 m) is not indicated in the model if values of hydraulic conductivities are taken into account that are realistic or in the range measured.

The model calibrated by the pressure data shows average horizontal velocities of 10-2-10-1 m/d for the karst and of 10-4 m/d for the platy limestones. Modeled temperature, using this range of velocities, is constant from the lowermost model boundary in the footwall up to the fault and identical with the bottom-hole temperature and with the constant temperature of 30-32˚C measured during the production test in AIG10. Whether the thermal conditions in the karst below the fault are not affected by water flow needs to be substantiated in final modelling runs.

References

[1] Rettenmaier, D., 2002: Europäische Erdbebenzone Golf von Korinth: Geologisch-tektonische und hydrogeologische Untersuchungen in der Region Egion und Klokos (NW-Peloponnes, Griechenland), Diploma Thesis, Dept. of Applied Geology, University of Karlsruhe, 116 p., 81 figs., 3 maps, 1 plate, 1 CD, Karlsruhe.

[2] Rettenmaier, D., Giurgea, V., Förster, A., Hötzl, H., 2004: The AIG10 drilling project (Aigion, Greece): interpretation of the litho-log in the context of regional geology and tectonics: C.R. Geoscience, 336, 415-423.

[3] Lemeille, F., Chatoupis, F., Foumelis, M., Rettenmaier, D., Unkel, I., Micarelli, Bourdillon, C., Guernet, C., Müller, C., 2004: Recent syn-rift deposits in the hangingwall of the Aigion Fault (Gulf of Corinth, Greece):C. R. Geoscience, 336, 425-434.

[4] Unkel I., 2003: Europäische Erdbebenzone Golf von Korinth: Geologisch-hydrogeologische Untersuchungen in der Region Aigion, im Umfeld der kontinentalen Tiefbohrung AIG 10 (NW-Peloponnes, Griechenland), Diploma Thesis, Dept. of Applied Geology, University of Karlsruhe, 153 p., 113 figs., 4 maps, 1 plate, 1 CD, Karlsruhe.

[5] Bauer, E., 2004: Europäische Erdbebenzone Golf von Korinth: Geologisch-hydrogeologische Untersuchungen südlich Aigion in der Region Melissia (NW-Peloponnes, Griechenland), Diploma Thesis, Dept. of Applied Geology, University of Karlsruhe, 160 p., 99 figs., 3 maps, 1 plate, 1 CD, Karlsruhe.

[6] Giurgea, V., Rettenmaier, D., Pizzino, L., Unkel, I., Hötzl, H., Förster, A., Quattrocchi, F., 2004: Preliminary hydrogeological interpretation of the Aigion area from the AIG10 borehole data: C. R. Geoscience, 336, 467-475.

IODP

Detrital carbonate (Heinrich-type) Layers during Glacial Stages of the Bruhnes Chromozone at IODP Site 1302/03 (North Atlantic, off Newfoundland)

Romero, O.E. and the IODP Expedition 303 Shipboard Scientific Party
Department of Geosciences, University Bremen, POBox 33 04 40, 28334 Bremen, Germany; oromero@uni-bremen.de / Phone: +49 421 21865537

The region off Newfoundland in the NW Atlantic has provided the most detailed marine record of Laurentidae Ice Sheet (LIS) instability in the form of rapidly-deposited detrital layers intercalated in background hemipelagic sediments. Site 1302/03, drilled at 50˚10.0'N, 45˚38.3'W during IODP Exp 303, is well positioned to monitor LIS instability and serves as an important reference location for detrital (Heinrich-type) layers and their correlation to Greenland ice cores over. Although Heinrich events are well-documented for the past glacial period, less is known about whether similar events occurred during older glacial periods. Using the Avaatech XRF core scanner at the University of Bremen, we measured a full suite of elements between Al and Ba (e.g., Al, Si, p, S, K, Ca, Ti, Mn, Fe, Sr, Ba) at 1-cm resolution in the upper 90 m of the spliced composite section of Site 1302/03, corresponding to the last 800 k.y., ensuring a high-resolution record (mean sedimentation rates estimated to be ~13 cm/k.y.). We found that the Ca/Sr and Ti/Al ratios are excellent proxies for detrital carbonate layers. Because the Sr/Ca partition coefficient is much greater for biogenic carbonate, detrital carbonate events are uniquely identified by peaks of Ca/Sr. At Site 1302/03, at least 8 distinct Ca/Sr and Ti/Al peaks occurred during the last glacial period corresponding to Heinrich Events. These 8 layers were originally described by Heinrich (1988) as "cemented marls" an each is also marked by an increase in sediment bulk density

measured by gamma ray attenuation. Similar detrital carbonate layers, identified by peaks of Ca/Sr, Ti/Al and density, are tentatively identified during Marine Isotopes (MIS) 6, 8, 10, 12, and 14. On the basis of the density data alone, detrital carbonate events occur prior to MIS 15 at Site 1302/03 and are thus not only limited to periods of large ice volumes associated with the "100-k world" in the latest Pliocene. We conclude that Ca/Sr and Ti/Al ratios provide an excellent proxy for the rapid, non-destructive recognition of detrital carbonate layers in North Atlantic sediments. Detailed geochemical analysis is needed to verify the source areas of these older detrital carbonate layers. The occurrence, timing and pacing of these older detrital carbonate layers may provide some important constraints on the origin and cause of the Heinrich events in the North Atlantic.

IODP

Carbonate veins from oceanic core complexes: Tracing different stages of sub-seafloor alteration

Martin Rosner[1], Wolfgang Bach[2], Holger Paulick[3] and Jörg Erzinger[1]
[1]GeoForschungsZentrum Potsdam; [2]University Bremen; [3]University Bonn

Hydrothermal alteration of uplifted blocks of gabbro and peridotite by circulation of large volumes of seawater at slow-spreading Mid-ocean Ridges (MOR) is a phenomenon with important consequences for the thermal structure and rheology of the oceanic lithosphere, geochemical budgets of the oceans, and microbial processes within and at the seafloor.

Carbonate veins are a common alteration feature of the ocean crust and record physico-chemical conditions and timing of precipitation. To gain insight into different stages of sub-seafloor alteration we studied trace element concentrations and stable and radiogenic isotope compositions of aragonite and calcite veins from the 15˚20'N Fracture Zone area at the Mid-Atlantic Ridge drilled during ODP Leg 209 ("MAR Peridotite"; Figure. 1).

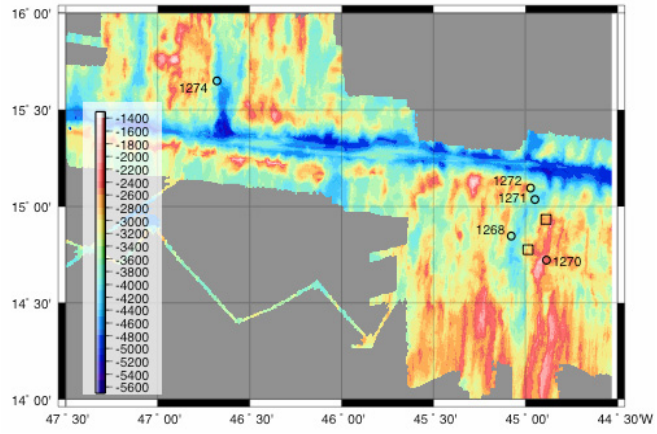

Figure 1:
Map of the 15˚20'N Fracture Zone area with locations of Leg 209 drill sites (circles) and SPP 1144 focus sites, including the Logatchev vent field (squares). Bathymetric data are from Fujiwara et al., 2003, G3).

Veins types and formation environment:

Carbonate veins recording different stages of seawater-basement interaction are present in cores of Leg 209. Three vein types have been distinguished on the basis of mode structural und mineralogical criteria as well as formation temperature (deduced from ?18O). The most abundant vein type are extensional aragonite veins (Fig. 2 A, B) that formed during the latest stage of subseafloor alteration under cold (<12˚C), oxidizing conditions.

A second vein type is extensional, low-temperature calcite veins in melt-impregnated peridotite overlying a gabbroic intrusion at Site 1275.

A third carbonate type is developed only in talc-serpentine schists from the uppermost basement at Sites 1270 and 1271: It is calcite deformed and intergrown with fibrous serpentine (Fig.2 C).

The syntectonic formation mode and elevated formation temperatures of 90 to 220˚C indicate that these carbonates precipitated from hydrothermal fluids percolating within the active detachment fault.

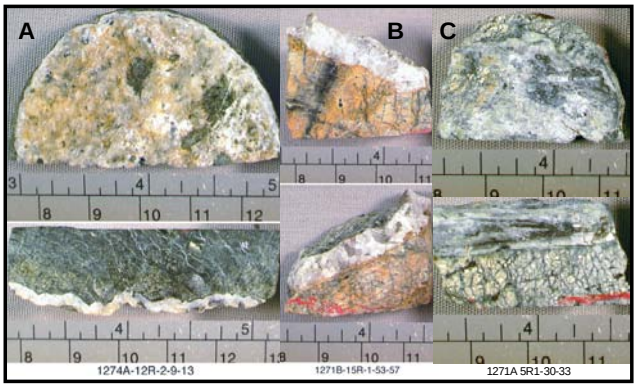

Figure 2:
Photographs of handspecimen with carbonate veins: extensional aragonite veins (A, B) and calcite in serpentine-talc-tremolite schists (C).

Age:

Radiocarbon (NOSAMS, Woods Hole) and U-Th disequilibrium ages (Laura Robinson, WHOI) suggest that the aragonite veins are much younger then hypothetical exposure ages of 700 to 1500 kyrs calculated from half-spreading rates and the distance of the drill site to the fault termination. Ages of aragonite veins from Site 1274 are 2-12 kyrs, and those from Site 1271 are 38 to 120 kyrs. The majority of aragonite veins from Site 1274 yield ages around 8 kyrs. These young ages indicate recent fracturing and fluid flow in the history of the sampled core complexes, indicative of prolonged fluid-basement interaction during exhumation and uplift of lithospheric mantle in these settings. The high-T calcites from the detachment fault rocks are radiocarbon-dead, and attempts of U-Th disequilibrium dating (Jan Scholten, U Kiel) have failed thus far, due to the extremely low U concentrations (<10 ppb) of these samples.

Geothermal gradient:

Given the uniformly young ages (around 8 kyrs) and assuming that circulating fluids and basement were thermally equilibrated, we used the $\delta^{18}O$ values to calculate a geothermal gradient for the basement at Site 1274. The $\delta^{18}O$ profile (Fig. 3) indicates a geothermal gradient of 100-150˚C/km. A steady state conductive

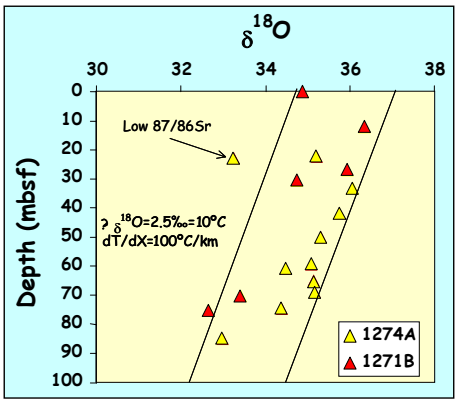

Figure 3:
ϋ^{18}O vs depth of aragonites of Sites 1271B and 1274A. Parallel lines highlight trend downhole trends in ϋ^{18}O.

thermal gradient in the area is between 40 and 70ºC/km. This estimate is derived from an assumed temperature at the base of the lithosphere of 1300 ºC and from high-pressure liquid lines of descent of Atlantic MORB and estimations from thermobarometry on olivine-plagioclase-two pyroxene-spinel cumulates at Site 1275, which suggest a conductive boundary layer thickness of 20-30 km (Kelemen et al., 2003, Proc. ODP, Init. Repts., 209). The high geothermal gradient indicates either that the basement is

not at steady state or that an internal heat source plays a role. Exothermic serpentinization reactions in the mid-crust would be a potential heat source that might steepen the mid- and upper-crustal thermal gradient, as enthalpies of serpentinization reactions can be as high as 600 J/g serpentine.

Water-rock interaction

Late-stage: Progressive water-rock interaction with increasing subseafloor depth is recorded by increasing δ^7Li values and chemical indicators for fluid maturity, such as Mg/Ca (Fig. 5), in aragonites of sites 1271 and 1274. We attribute the large δ^7Li range of aragonites and increasing δ^7Li values with depth to progressive depletion of ^{6}Li over ^{7}Li as seawater penetrates the basement and water-rock interaction progresses. Strontium isotope compositions, on the other hand, are nearly uniform very similar to modern seawater, due to limited Sr exchange between circulating seawater and the basement at low temperatures.

Detachment faulting: High-T calcites have Sr and Li isotope compositions as low as 0.70385 (^{87}Sr/^{86}Sr) and +3.3‰ (δ^7Li), indicating that Sr and Li are isotopically equillibrated with the basement. These calcites veins have Li and Sr isotope compositions very similar to high temperature vent fluids from the Logatchev and Rainbow hydrothermal sites (^{87}Sr/^{86}Sr = 0.7037-0.7041; Douville, 1999, PhD Thesis, Brest; and δ^7Li~ 6.6‰; Bray et al., 2001, AGU 2001 Fall Meeting). By comparision with hydrothermal vent fluids, we infer that the calcite-precipitating fluids had peak-temperatures of more than >350ºC prior to precipitation and underwent significant conductive cooling within the detachment fault. This interpretation is corroborated by the C isotopic composition of calcite that ranges from δ^{13}C values as heavy as 8 ‰ to light values of -7 ‰. The only reasonable explanation for the heavy δ^{13}C compositions is thermogenic methanogenesis, which requires temperatures in excess of 350˚C (McCollom and Seewald, 2001, GCA).

Figure 4:

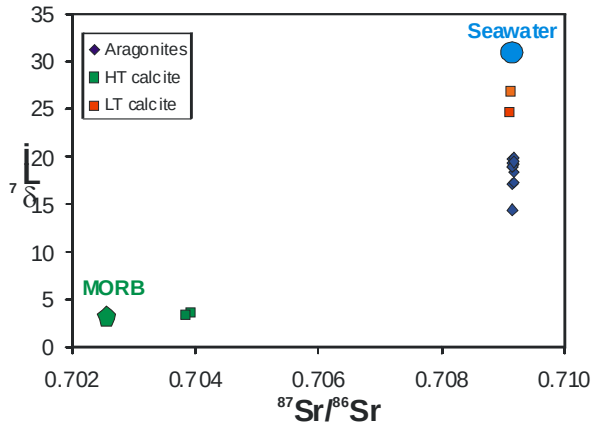

Lithium and Sr isotope compositions of different types of carbonate veins from ODP Leg 209. The variability of ῡ^{7}Li values at constant Sr isotope composition suggests that Li isotopes are very sensitive indicators of fluid-basement interactions at low temperatures. Evolutions paths of fluids in Sr-Li isotope space will be useful tracers of seawater-basement interaction studies.

The fact that temperatures recorded by O isotopes (90-220˚C) are much lower that the estimates peak temperatures of > 350˚C constitutes strong evidence for conductive cooling and, hence, slow rates of fluid advection. The low upwelling velocities of fluids were accompanied by conductive cooling of the fluids. Conductive cooling has facilitated partial re-oxidation of thermogenic methane, which can account for the heavy δ^{13}C values.

The combined Sr-Li-O-C isotope variations allow unique insights into fluid evolution pathways. The carbon isotope variability indicates that high-temperature thermogenic methanogenesis was followed by partial re-oxidation of methane when the fluids migrated up the detachment fault and underwent significant conductive cooling.

Figure 5:

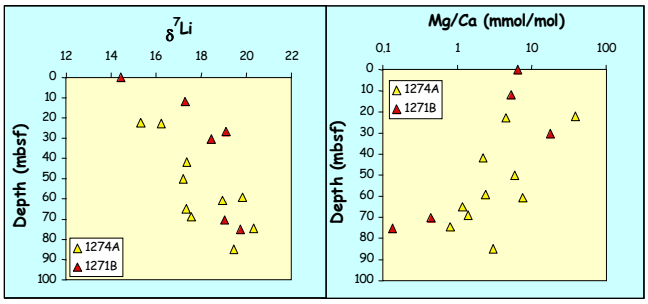

Downhole variations in ῡ^{7}Li and Mg/Ca showing progressive water-rock inter-action with increas-ing depth.

Lithium fractionation in the deep ocean:

Lithium isotope data of the Leg 209 carbonates that have seawater-like Sr isotope compositions show a wide range of δ^7Li values (Figs. 2, 4, 5). However, these data are generally consistent with experimentally determined fluid/mineral isotope fractionation factor for aragonite and calcite (Mariott et al., 2004, Chem. Geol.; Fig. 4). Our data show that fractionation factors for calcite are smaller than for aragonite, but additionally imply that δ^7Li Fluid - δ^7Li Aragonite in the deep ocean is ~16‰ at about 4ºC (Fig. 4). This fractionation factor is slightly larger than a Li isotope fractionation factor at 25˚C of 12‰ during aragonite precipitation proposed by Mariott et al. (2004, Chem. Geol.). This difference in fractionation factors can be due to the lower temperature, faster precipitation kinetics, effects of fluid chemistry (e.g. different Mg/Ca), or a combination of these different effects. At temperatures of around 350ºC, δ is 0.996 (Chan and Edmond, 1988, GCA); hence, fluids corresponding to the lowest δ^7Li value of 3.3‰ equate to a δ^7Li of ~7‰, consistent with the uniform value for vent fluids 6.6±1.2 ‰ (Bray et al., 2001, AGU 2001 Fall Meeting).

IODP

Reconstruction of Mid-Miocene climate in Southwest Africa: first results from ODP records in the Benguela upwelling area (Project RCOM TP A5/A6)

B. Roters[1] and R. Henrich
University of Bremen; Department of Geosciences; P.O. Box 330 440; 28334 Bremen; Germany; [1]bastian.roters@uni-bremen.de

In the Miocene a general trend of falling temperatures is observed. The Mid-Miocene itself shows several periods of short-term glaciations on East-Antarctica, but also periods of warming. For ODP Site 1085 three glaciation periods in the Mid-Miocene are recognized in the δ^{18}O record (Westerhold et al., 2005).

The aim of this study is to reconstruct the regional climate in Southwest Africa in the Mid-Miocene. We hypothesise that waxing and waning of the Antarctic ice-sheet had an effect on the regional climate. Therefore aeolian and fluvial silt are used as proxies for recording wind-strength and humidity in this region. During colder periods the Subantarctic Front shifts northwards, thus increasing trade-wind and aridity on land. For humidity no direct correlation is known so far.

Our study focuses on the silt fraction of two sites: ODP site 1085 off the Orange River mouth and DSDP site 530 at the northern edge of the Walvis Ridge. The working strategy is to sample the cores in a 100-kyr interval first to get an overview about the grain size distribution. In a second step we want to refine the sampling resolution to 20 - 50 kyr. Here, we present silt grain size data derived from Sedigraph measurements from 38 samples

of site 1085 from the interval between 11,0 and 14,5 Myr. Ages are based on an age model published by Westerhold et al. (2005).

We suppose that the carbonate-free silt originates from the African continent only. Beside aeolian and fluvial transport we have to take ocean-current transport into account as transport processes for the silt. It is proposed for the future to model the terrigeneous silt's grain size distribution depending on transport processes with the End Member Modelling Algorithm (Weltje, 1997) using the refined, complete sample-sets.

The sedimentation rate shows values between 1.0 and 3.0 cm/kyr for the interval from 13.9 to 11.7 Myr. Between 11.7 and 11.0 Myr the the sedimentation rate increases up to 11.0 cm/kyr. This interval shows an increasing trend with strong peaks for the sedimentation rate. The overall silt fraction plot (weight-% against age) reveals two patterns: In the older part between 14.5 and 13.2 Myr the plot shows a cyclic variation. These cycles last between 400 and 500 kyr and they are also found in the sand fraction. In the younger part from 13.2 Myr on we find a decline in the bulk silt and the sand fractions, so the clay fraction increases. In contrast the younger part from 13.2 Myr on is generally dominated by the clay fraction, while the bulk silt and the sand fractions decrease. This possibly indicates an increasing marine productivity.

Weltje, G. (1997): End-member modelling of compositional data: Numerical-statistical algorithms for solving the explicit mixing problem.- Math. Geol., 29(4): 503-549; New York.

Westerhold, T. et al. (2005): Middle to Late Miocene Oxygen Isotope Stratigraphy of ODP Site 1085 - SE Atlantic.- Paleo 3, 217: 205-222; Amsterdam.

IODP

Mobilization of platinum group elements in altered oceanic crust: outlook to studies on a complete section of upper oceanic crust (Expedition 312)

Scheibner, B.[1,2], Stosch, H.-G.[2]

[1]Geowissenschaftliches Zentrum Göttingen, Abteilung Geochemie, bscheib@gwdg.de; [2]Universität Karlsruhe (TH), Institut für Mineralogie und Geochemie.

It is well established that Platinum-Group Elements (PGE) show, in the absence of metals, chalcophile behaviour during magmatic processes in the Earth's mantle and crust and that sulphides are the major host of the PGE in mantle peridotite. In addition, recent studies indicate that most mafic igneous rocks display Pt/Pd ratios lower than the primitive mantle and that this feature is explained by the presence of additional (exotic) phases such as metal alloys or by postmagmatic alteration. However, so far no study has systematically investigated the effects of hydrothermal alteration on the PGE budget of a complete section of oceanic extrusive and intrusive rocks. We propose to fill this gap by studying an entire profile of altered upper oceanic crust and the uppermost gabbroic section, formed at the East Pacific Rise some 15 Ma ago and drilled at the multicruise ODP-borehole 1256D (Expeditions 206, 309, and 312). Ocean Drilling Program (ODP) borehole 1256D is the first hole prepared with the infrastructure desirable for drilling an entire and complete in situ section of oceanic crust. In this hole, the expected Sheeted Dike Complex - Gabbro transition (Layer2/3) was drilled at 1406.6 meters below seafloor (mbsf). Previously, only ODP-Hole 504B on 6.9-Ma-old crust on the southern flank of the Costa Rica Rift, had sampled a large section of oceanic crust, but only down to the upper Sheeted Dike Complex. Prior to borehole 1256D the Sheeted Dike Complex - gabbro transition had never been drilled, despite being considered to be the most critical zone in deciphering crustal accretion processes at mid-ocean ridges. ODP Borehole 1256D is located at 6˚44'N, 91˚56'W beneath 3635m of water in the Guatemala Basin on the Cocos Plate. This section of oceanic crust was generated by superfast spreading (~220 mm/yr). Between November 2002 and December 2005, a complete in situ section of oceanic crust was drilled at borehole 1256D, covering the lithologies of the Volcanic Zone, the Sheeted Dike Complex and the uppermost part of the gabbro. The degree of alteration increases sharply within the Sheeted Dike Complex from greenschist facies to amphibolite facies within about 100 meters with amphibolite-facies assemblages prevailing below 1350m. The lower Sheeted Dike basalts are characterized by the occurrence of Ca-rich plagioclase + hornblende and show a granoblastic texture. The Transition Zone between the Sheeted Dike Complex and the Volcanic Zone has the potential to host massive sulphide deposits of elements such as Zn, Cu and subordinate amounts of PGE. Sulphur isotope evidence indicates that some seawater sulphate has been reduced to sulphide, forming secondary sulphides around primary igneous sulphides to produce deposits at axial vents. The root zones for these ore-forming deposits are preferentially located at the transition between Sheeted dikes and gabbros, as observed in ophiolites. Through this study we wish to evaluate the PGE mobility during alteration of ocean crust and study the behaviour of PGE systematically along the hydrothermal fluid path from the root zone to noble metal deposits; the PGE will be analysed by ID-fire assay/ICP-MS, laser ablation ICP-MS, and synchrotron-μXRF.

IODP

Development and Application of New Quantitative Molecular Ecological Techniques to Study the Abundance and Activity of Microorganisms in the Marine Deep Subsurface

Axel Schippers*[1] and Lev N. Neretin[1,2]

[1]Section Geomicrobiology, Federal Institute for Geosciences and Natural Resources, Stilleweg 2, 30655 Hannover, Germany. E-mail: a.schippers@bgr.de; Tel.: (+49) 511 643 3103; Fax: (+49) 511 643 2304. [2]Department of Biogeochemistry, Max Planck Institute for Marine Microbiology, Celsiusstrasse 1, 28359 Bremen, Germany

Deeply buried marine sediments may harbour over half of all prokaryotic cells on Earth (Whitman et al., 1998), despite the fact that only about 1 % of the total marine primary production of organic carbon is available for deep-sea microorganisms (Whitman et al., 1998; Schippers et al., 2005). The huge number of prokaryotes has been calculated from numerous microscopic acridine orange cell counts (AODC) in sediment cores of the Ocean Drilling Program (ODP, Parkes et al., 1994; 2000). Since AODC detects living, but also dormant or even dead cells (Kepner and Pratt, 1994), the abundance and diversity of living prokaryotes in deeply buried sediments remained questionable.

The deep biosphere of sediments from the Equatorial Pacific and the Peru continental margin has been intensively studied in ODP Leg 201. Different research teams enriched and isolated prokaryotes (D´Hondt et al., 2004; Lee et al., 2005), measured microbial activities using different radiotracers (Parkes et al., 2005; Schippers et al., 2005), and explored the microbial diversity using 16S rRNA gene clone libraries (Sørensen et al., 2004; Parkes et al., 2005; Biddle et al., 2006; Inagaki et al., 2006).

Within this DFG funded project, the first direct quantification of living Bacteria for deep sediment samples using rRNA targeting Catalyzed Reporter Deposition - Fluorescence In Situ Hybridisation (CARD - FISH) was provided (Schippers et al., 2005; Teske, 2005). A large fraction of the sub-seafloor prokaryotes was shown to be alive, even in very old (16 Ma) and deep (>400 meters below sea-floor (mbsf)) sediments. Bacteria were detected at the open-ocean and ocean-margin Leg 201 sites using CARD-FISH (Fig. 1). Depth profiles of AODC and numbers of Bacteria determined by CARD-FISH and quantitative, real-time PCR (Q-PCR) showed that AODC were generally higher at the ocean-margin sites than at the open-ocean sites, consistent with earlier results (Parkes et al., 1994; 2000). A large proportion of AODC were detected by CARD-FISH analysis: about one third for the open-ocean and up to one tenth for the ocean-margin sediments. The abundance of Archaea was too low to be quantified using CARD-FISH, indicating that Bacteria were the dominant prokaryotes in these deeply buried marine sediments. The predominant detection of Bacteria over Archaea was supported by

the Q-PCR analysis of 16S rRNA genes of deep sediment samples from the Peru margin (Schippers et al., 2005; Inagaki, et al., 2006; Schippers and Neretin, 2006a), in contrast to recent FISH and cell membrane lipid data (Biddle et al., 2006).

Using CARD-FISH, living Bacteria could also be quantified in two Cretaceous black shale samples from ODP Leg 207. AODC values were 2 x 10^7 and 9 x 10^6 cells cm^{-3} wet sediment, whereas the values for the living Bacteria were considerably lower: 4 x 10^5 and 5 x 10^5 cells cm^{-3} wet sediment, respectively (Schippers and Neretin, 2006b).

In addition to CARD-FISH, Q-PCR allowed a comparative quantitative microbial community analysis in near-surface and deeply-buried marine sediments from the Peru continental margin (Fig. 2). The 16S rRNA gene copy numbers of prokaryotes and Bacteria were almost identical with a maximum of 108 to 1010 copies cm-3 in the near-surface sediments. Archaea exhibited one to three orders of magnitude lower 16S rRNA gene copy numbers. The 18S rRNA gene of Eukarya was always at least three orders of magnitude less abundant than the 16S rRNA gene of prokaryotes. The 16S rRNA gene of the Fe(III)- and Mn(IV)-reducing bacterial family Geobacteraceae and the dissimilatory (bi)sulfite reductase gene (*dsrA*) of sulfate-reducing prokaryotes were abundant with 10^6 to 10^8 copies cm^{-3} in near-surface sediments but showed lower numbers and an irregular

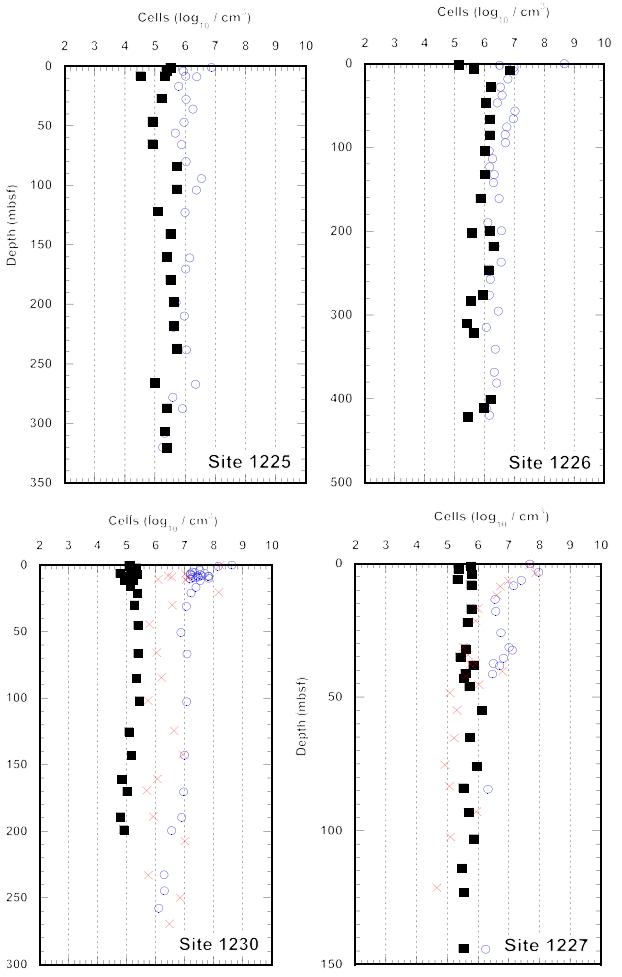

Figure 1. Depth profiles of AODC (circles) and numbers of Bacteria determined by CARD-FISH (squares) and Q-PCR (crosses) for ODP sites in the Equatorial Pacific (Sites 1225, 1226) and in the Peru margin (Sites 1227, 1230). For each site, the mean standard deviation of the CARD-FISH counts was 0.4 cells (log10 cm-3). Figure from Schippers et al. (2005).

distribution in the deep sediments. The copy numbers of all genes decreased with sediment depth exponentially. The depth gradients were steeper for the gene copy numbers than for numbers of total prokaryotes (AODC), which reflects the ongoing degradation of the high-molecular weight DNA with sediment age and depth. However, the occurrence of eukaryotic DNA also suggests DNA preservation in the deeply-buried sediments.

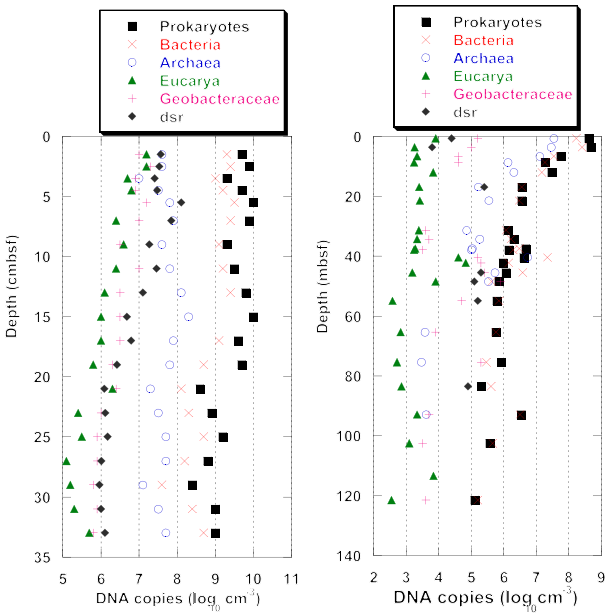

Fig. 2. DNA copy numbers of the 16S rRNA genes of prokaryotes, Bacteria, Archaea, and Geobacteraceae, the 18S rRNA gene of Eukarya, and dsrA in the near-surface sediment (0-0.34 mbsf) from Station 2MC (R/V SONNE 147, left) and in deep sediments (0-121mbsf) from ODP Site 1227 (right) on the Peru continental margin. Figure from Schippers and Neretin (2006a). Note different units and scales.

Schippers, A., and L. N. Neretin. 2006a. Quantification of microbial communities in near-surface and deeply buried marine sediments on the Peru continental margin using real-time PCR. Environ. Microbiol., in press.

Schippers, A., and L. N. Neretin. 2006b. Data Report: Microbiological AODC and CARD-FISH analysis of black shale samples from the Demerara Rise, ODP Leg 207 In: Proceedings Ocean Drilling Program (ODP), Scientific Results, 207 [Online]. D. C. Mosher, J. Erbacher, and M. J. Malone (eds.). Available from World Wide Web: http://www-odp.tamu.edu/publications/207_SR/207sr.htm.

Schippers, A., L. N. Neretin, J. Kallmeyer, T. G. Ferdelman, B. A. Cragg, R. J. Parkes and B. B. Jørgensen. 2005. Prokaryotic cells of the deep sub-seafloor biosphere identified as living bacteria. Nature 433: 861-864 (selected as "Research Highlights", Nature Reviews Microbiology 2005, 3 (4): 274).

D'Hondt, S. L., B. B. Jørgensen, D. J. Miller, A. Batzke, R. Blake, B. A. Cragg, H. Cypionka, G. R. Dickens, T. G. Ferdelman, K.-U. Hinrichs, N. G. Holm, R. Mitterer, A. Spivack, G. Wang, B. Bekins, B. Engelen, K. Ford, G. Gettemy, S. D. Rutherford, H. Sass, C. G. Skilbeck, I. W. Aiello, G. Guèrin, C. H. House, F. Inagaki, P. Meister, T. Naehr, S. Niitsuma, R. J. Parkes, A. Schippers, D. C. Smith, A. Teske, J. Wiegel, C. N. Padilla, and J. L. Solis Acosta. 2004. Distributions of microbial activities in deep subseafloor sediments. Science 306: 2216-2221.

IODP

Examples of mass wasting and hemipelagic sedimentation of Brazos-Trinity Basin IV and Ursa Basin, Northern Gulf of Mexico, IODP Expedition 308

J. Schneider[1], T. Moerz[1], A. Bartetzko[1], G.J. Iturrino[2], P.B. Flemings[3], J. Behrmann[4], C. M. John[5], and the Expedition 308 Shipboard Scientific Party[5]

[1]Research Center of Ocean Margins, University of Bremen, Bremen, Germany; [2]Lamont-Doherty Earth Observatory, Columbia University, Palisades NY; [3]Dept. of Geosciences, Penn State University, University Park PA; [4]Geologisches Institut, Albert-Ludwigs-Universität Freiburg, Freiburg, Germany; [5]Integrated Ocean Drilling Program, College Station TX

Pore pressure evolution in sedimentary basin sequences is a complex function of sedimentation rates, sediment type and depositional processes. A thorough understanding of a given pore pressure situation in a sedimentary sequence requires a time resolved knowledge of many sediment-physical- and visco-elastic parameters, commonly not accessible through direct measurements. Integrated Ocean Drilling Program Expedition 308 was dedicated to study overpressure and fluid flow on the Gulf of Mexico continental slope, examining how sedimentation,

overpressure, fluid flow, and deformation are coupled in passive margin settings. Results of Expedition 308 allow to compare a normally consolidated sequence with quasi hydrostatic pore pressures (Brazos-Trinity Basin IV) to an underconsolidated, overpressured sequence at Ursa Basin using comparable data sets. We propose to characterize and classify both sequences with regard to depositional units and physical properties independently of changes caused by consolidation, using logging while drilling, wire line and sedimentological data. Depositional unit thickness and time constrains together with consolidation and dewatering parameters derived from geotechnical testing will feed a back stripped finite element model to reconstruct sedimentation/erosion, consolidation and pore water pressure evolution over time. In situ pore pressures acquired during Expedition 308 will act as boundary conditions, guiding the modeling process.

In this research project we combine sedimentology, physical properties, downhole logging, and modeling to investigate the influence of sedimentation history on formation pressure conditions in the two basins drilled during Expedition 308. In detail, the goals of the project are:

- To investigate the stratigraphic record and identify single depositional units (hemipelagic sedimentation, turbidites, mass wasting deposits) and to determine sedimentation rates exclusive of short-term mass wasting events.
- To characterize single units by their physical properties, to reconstruct the influence of consolidation on physical properties and to classify depositional types of sediments independently of changes in physical properties caused by consolidation.
- To model the entire depositional sequence to identify the specific factors and conditions in the Gulf of Mexico that influence sediment consolidation and formation of overpressured horizons.

As preliminary work, a first comparison between electrical borehole images and core descriptions from Expedition 308 Sites U1320 and U1322 was done. We investigated thickness and frequency of single depositional events in the two basins and did a first estimate of the mass wasting/hemipelagic mass accumulation rates ratio. These first comparisons show that turbidites predominate at the Brazos-Trinity Basin IV while mass flow deposits such as slumps are important in the Ursa Basin. The results of these first investigations were integrated into a preliminary age model.

IODP

Diagenetic alteration of periplatform sediments of the Great Bahama Bank

J. Schwarz, S. Steinke, and R. Rendle-Bühring
Research Center Ocean Margins, University of Bremen, Bremen, Germany (johanna.schwarz@uni-bremen.de / Phone: +49-(0)421-21865884)

Mineralogical, geochemical and sedimentological analyses of periplatform sediments at the two ODP Sites 633 (Exuma Sound) and 1006 (western Great Bahama Bank) have been carried out in order to characterise early diagenetic processes. Layers of carbonate nodules have been observed as major diagenetic products in distinct intervals of Late Pliocene to Holocene age in both cores. These nodules are white, irregularly rounded concretions with a micritic matrix that contain whole tests and fragments of planktonic foraminifera. The matrix is composed of coccolithophorids, biogenic debris, rare aragonite needles, and few low-magnesium calcite cements. Oxygen and carbon isotope analyses of the micritic matrix suggest an in situ formation in equilibrium with bottom water. On the western side of the Bahamas (Site 1006) nodules occur only during glacial periods, and only from marine isotope stage (MIS) 44 until 22 and in MIS 10. In contrast, the eastern margin (Site 633) is characterised by a consistant abundance of nodules during the late Plio-/ Pleistocene until MIS 23, while thereafter they are mainly restricted to glacial periods.

Glacial periods have generally higher amounts of sand-sized material (>63 µm) than interglacials, which is caused by a lower input of fine material from the platform top/margin due to a lower sea-level. Winnowing of fine sediments due to higher bottom water current intensities may has amplified the coarsening of the sediments, leading to a higher pore space in the surface sediment. This enhances the formation of nodules in the glacial layers; as they pass through the dissolution and cementation zones below the sediment surface, pore waters can easily circulate through these layers and trigger diagenetic processes. The nodules in the glacial layers even intensify the signal of the coarse fraction from an amount of approx. 35% to up to 70%. Therefore, the grain size signal can not be interpreted as primary. So far, grain sizes of carbonate sediments have been considered as a proxy for deposition and transport processes in response to environmental changes (e.g. sea level). Our study shows that this kind of proxy must be handled with care.

The occurrence of nodules is generally linked to periods of low aragonite values. We assume that the formation of the nodules is caused by aragonite dissolution and cementation during early diagenesis. Dissolution of aragonite could be intensified by the supply of organic material during periods of higher productivity. These environmental conditions could have been changed in relation to the 41 ky to 100 ky climate transition ("Mid-Pleistocene Revolution") at MIS 23 (approx. 0.9 Ma), causing the distinctive cut in the temporal distribution of nodular layers.

IODP

High-Temperature Hydrothermal Venting at Submarine Volcanoes on the Tonga Arc, SW Pacific

Ulrich Schwarz-Schampera[1], Peter Stoffers[2], Tim J. Worthington[2] Mark D. Hannington[3]
[1]BGR, [2]Universität Kiel, [3]University of Ottawa

The first submarine hydrothermal vents and associated seafloor mineralization on the Tonga arc have been found during the 2005 SITKAP cruise with the PISCES submersibles. Venting occurs in the summit calderas of two shallow-water volcanoes, greatly extending the known areas and diversity of seafloor hydrothermal activity in the western Pacific region. The highest temperature vents (245-265 ˚C) occur at water depths of 385-540 m near the summit of a large volcano at 24˚S. They comprise clusters of large (to 10 m high) barite, anhydrite, and sulfide chimneys surrounded by extensive deposits of Fe-oxy-hydroxides. The chimneys are characterized by vigorous venting of clear fluids with temperatures on the seawater boiling curve. There is abundant evidence of phase separation, which can be seen as flame-like jets of steam (H2O vapor) discharging from the chimney orifices. Pyrite, marcasite, sphalerite, and chalcopyrite line the interiors of the highest temperature vents, similar to black smoker chimneys on the mid-ocean ridges. A second, spatially distinct, vent field occurs at water depths of 850-985 m within a large caldera on the western side of the volcano. Venting is more diffuse and at lower temperature in this field (to 112˚C), which features large clusters of Fe-oxy-hydroxide and silica chimneys at its core. Both vent fields are spatially related to basaltic dike swarms. Low-temperature venting (to 152˚C) was also found on a second volcano at 21˚S. There, venting occurs at the southern end of a chain of young explosion craters, and is most intense in water-depths of 160-210 m. Large fields of mussels and white filamentous bacteria cover the seafloor around these craters, and the vents are characterized by voluminous gas streaming (most likely CO2 bubbles) through sulfur-cemented ash.

Our findings indicate that the Tonga suprasubduction zone represents a favorable tectonic setting for the generation of epithermal-style deposits. The southern Tonga arc is affected by the collision and subduction of the intensely altered aseismic Louisville ridge. The style of magmatism and associated hydrothermal activity at volcanoes along the collision zone suggest

mobilization and enrichment of volatiles in the subduction zone and their recycling during magmatic processes. Partial melting at elevated oxygen fugacities and the enrichment in fluid-mobile elements lead potentially to elevated contents of chalcophile elements in the arc volcanic rocks and associated hydrothermal fluids and precipitates. The present sampling of the southern Tonga arc indicates a large potential for Au and Cu-Zn-Pb mineralization in this area.

IODP

Transport in microporous rocks studied by in situ FTIR microscopy - implications for hydrothermal alteration of the oceanic crust

Anna Simonyan[1], Stefan Dultz[1], Harald Behrens[2], Ulrich Schwarz-Schampera[3]
[1]Institute of Soil Science, University of Hannover, Herrenhäuser Str. 2, D-30419 Hannover; e-mail: a.simonyan@mail.ru; [2]Institute of Mineralogy, University of Hannover, Callinstr. 3, D-30167 Hannover; [3]Federal Institute of Geosciences and Natural Resources (BGR) Stilleweg 2, 30655 Hannover

Changes in seawater chemistry during circulation through ridge flanks can be significant for global budgets of several elements. The rate of seawater/rock interaction and the alteration of the oceanic crust depends on the permeability and on the accessible specific surface of the rock. Large portions of the available specific surface are located in micro or macro pores inside of unfractured rock fragments. Diffusion and reaction processes within these pores have strong influence on mobilisation and immobilisation of elements in hydrothermal fluids.

In this study we use the rock samples from ODP leg 169 at Middle Valley, Juan de Fuca Ridge as an example to investigate systematically the role of pores and permeability on element turnover in oceanic hydrothermal systems. The central drilling hole 856h provides an excellent set of samples ranging from strongly altered sediments to the nearly unchanged igneous basement.

Our approach includes various analytical and spectroscopic techniques for characterization of samples separated from drilling cores, in particular the determination of pore size distribution and its change by formation of secondary minerals. These findings will be combined with experimental studies on fluid migration and reactions within interconnected pores.

The pore volume of samples was measured by Hg-porosimetry and by analysing the H2O content released from water filled samples below 200˚C using Karl-Fischer titration. The samples were examined by optical and electron microscopy to identify the main phases and to select samples with homogeneously distributed pores and minimum amounts of cracks and impurities. Anionic and cationic composition was investigated by wet chemistry. Bulk water content was measured by Karl-Fischer titration.

To study diffusion in the pore systems, we use a new experimental cell in which the sample is surrounded by a continuous flux of an aqueous solution. During the experiment, the temperature and concentration of the solution can be maintained constant providing stable conditions on the solution/rock interface. The cell is designed so that diffusion processes of aqueous species within a pore space of samples can be measured in situ by FTIR spectroscopy. One edge of the sample was open to the surrounding liquid so that one-dimensional diffusion conditions are established. During the experiment, IR spectra are continuously recorded at a fixed position on the sample, which is typically 1.5 - 2.5 mm away from the open edge. The solution can be exchanged within a few seconds allowing an exact definition of the starting time.

We present here the first results of the H2O-D2O exchange experiments with the rocks obtained in a temperature range of 10-45˚C. In order to apply the results to the hydrothermal system in the deeper, hotter oceanic crust, such experiments are required also for elevated temperatures and pressures. We plan to develop new experimental tools to study fluid permeation and diffusion/reaction processes at temperature up to 250˚C and pressures up to 200 bar.

IODP

Rekonstruktion und Modellierung Neogener Ozeane - Zwischenstand

Peter Smolka, Geologisches Institut, Universität Münster, smolka@uni-muenster.de

Das jüngere Neogen (ab ca. 6 Ma) ist sowohl durch Treibhausklimate gekennzeichnet (ca. 3˚ C über präindustriellen Werten, z.T. ausgedehnte Gebiete erhöhter Temperaturen) als auch - in der Norwegensee - durch konsistentes Auftreten eistransportierter Gerölle ab ca. 6 Ma. Dieser IRD tritt in der Norwegensee auch während pleistozäner Warmzeiten auf. Die rekonstruierten Temperaturverteilungen (warme tropische Ozeane in Verbindung mit arktischem Meereis) erzeugen im Winter erhebliche Temperaturgradienten. In Verbindung mit der Polarnacht (Ergebnisse eines von den SSTs angetriebenen GCMs) entstehen im NH-Winter extrem niedrige Temperaturen auf den Nordkontinenten. Die Sommer sind (4-5 Ma) den rezenten Vergleichbar. Dies begünstigt ab ca. 4-5 Ma. die Bildung von ausgedehnten Glazialen. Die Orbitalparameter modulieren dies zusätzlich. Dies gilt für das Pliozän und das Pleistozän.

Die bislang durchgeführten Untersuchungen sind Gleichgewichtsrechnungen (Rekonstruktionen gekoppelt mit Modellrechnungen). Klimaveränderungen können dann als besser verstanden gelten, wenn es gelingt, nachgewiesene Klimaschwankungen (Vostok, GRIP, GISP-Kerne, Cariaco-Becken, ODP-Kerne u.a.) transient zu modellieren. Aufgrund der langen Zeiten ist es erforderlich ein GCM entsprechend zu beschleunigen.

Es wurde in zeitintensiven Modellbereichen ein Zeitgewinn von mehreren hundert Prozent erzielt. Die entsprechenden Rechenvorgänge kommen in vielen Modellbereichen (Atmosphäre, Land, Ozean) vor. Da sich die Rechenzeitgewinne z.T. multiplizieren, wird ein Gesamt-Rechenzeitgewinn von Faktor 5000 bis 10000 weiterhin für realistisch gehalten. Der sehr hohe Rechenzeitgewinn wird auch deshalb für möglich gehalten, weil bei den realisierten Verfahren in vielen Fällen auf eine explizite Berechnung verzichtet wird. Das Klimamodell benötigt dann ein mehrfaches an Zeit zum Start, wird danach aber schneller aufgrund der eliminierten numerischen Berechnungen.

Die Ergebnisse sind dann sowohl im Bereich des IODP als auch im Bereich des ICDP (terrestre Kerne) verwendbar. Die transiente Modellierung der letzten 3 Ma wird weiterhin als Fernziel festgehalten.

IODP

The Paleogene ("Greenhouse") Arctic Ocean paleoenvironment: Implications from organic-carbon records (IODP-ACEX Expedition 302)

R. Stein and P. Weller
Alfred Wegener Inst. f. Polar and Marine Research, 27568 Bremerhaven, Germany

A major element in the global climate evolution during Cenozoic times has been the transformation from warm Eocene oceans with low latitudinal and bathymetric thermal gradients into the more recent modes of circulation characterized by strong thermal gradients, oceanic fronts, cold deep oceans and cold high-latitude surface waters (e.g., Zachos et al., 2001). In this context, however, continuous sedimentary records to be used to establish chronologic (high-resolution) sequences of climate and environmental change through Cenozoic times, were missing for the Arctic Ocean. Now, the recovery of an about 420m thick sequence of late Cretaceous/Cenozoic sediments on Lomonosov Ridge/central Arctic Ocean during the IODP-ACEX Expedition 302 in 2004 (Moran et al., 2006) allows for the first time a detailed reconstruction of the paleoclimatic history of the early pre-glacial Arctic Ocean. Our study of these unique ACEX sediments will focus on the Arctic Ocean organic carbon cycle and its relationship to the long- and short-term paleoenvironmental /paleoceanographic evolution during Paleocene-Eocene times. Applied methods include elemental analyses (TOC, C/N, C/S), Rock-Eval pyrolysis, biomarker studies using GC and GC/MS techniques, and stable

carbon isotopes of the organic matter and specific biomarkers.

Whereas the Pleistocene to Miocene interval is characterized by low TOC contents (< 0.4%) of terrigenous origin (very similar to numerous Late Quaternary organic carbon records known from the central Arctic Ocean; e.g., Stein et al. 2003 and further references therein), the Eocene - Paleocene interval displays high organic carbon contents of 1 to > 6%. Elevated hydrogen index values of 150 to 350 mgHC/gC suggest increased amounts of (marine and/or freshwater) algae material being preserved. Low C/S ratios of <1 indicate dominantly suboxic/anoxic conditions. Increased primary production, increased freshwater input, and/or increased preservation under suboxic/anoxic conditions have probably caused this organic carbon enrichment during Eocene/ Paleocene times. The Paleocene/Eocene Thermal Maximum (PETM) Event as well as the lowermost Eocene "Azolla Event" are also obvious in the organic carbon data, suggesting that at these times maximum (algae-rich) organic carbon was burried.

References

Moran, K., Backman, J., Brinkhuis, H., Clemens, S.C., Cronin, T., Dickens, G.R., Eynaud, F., Gattacceca, J., Jakobsson, M., Jordan, R.W., Kaminski, M., King, J., Koc, N., Krylov, A., Martinez, N., Matthiessen, J., McInroy, D., Moore, T.C., Onodera, J., O'Regan, A.M., Pälike, H., Rea, B., Rio, D., Sakamoto, T., Smith, D.C., Stein, R., St. John, K., Suto, I., Suzuki, N., Takahashi, K., Watanabe, M., Yamamoto, M., Frank, M., Jokat, W., and Kristoffersen, Y., 2006. The Cenozoic palaeoenvironment of the Arctic Ocean. Nature, in press.

Stein, R., Schubert, C.J., Macdonald, R.W., Fahl, K., Harvey, H.R., and Weiel, D., 2003. In: Stein, R. and Macdonald, R.W. (Eds.), The Organic Carbon Cycle in the Arctic Ocean, Springer-Verlag, Berlin, pp. 295-314.

Zachos, J., Pagani, M., Sloan, L., Thomas, E., and Billups, K., 2001. Science, 292: 686-693.

IODP

Late Neogene-Quaternary variability in North Atlantic paleoceanography: Preliminary results of IODP Expedition 306

R. Stein, J. Hefter and the 306 Scientific Party

Alfred Wegener Institute for Polar and Marine Research, 27568 Bremerhaven, Germany

Understanding the mechanisms and causes of abrupt climate change is one of the major challenges in global climate change research today. In this context, the paramount importance of the North Atlantic as a possible major driver of global climate change has to be mentioned. Thus, new IODP Expedition 303/306 sites were drilled at key locations in the North Atlantic to extend the present knowledge of millennial-scale climate variability over the last few million years. Of special interest is the long-term evolution of millennial-scale variability in surface temperature, ice sheet dynamics, and thermohaline circulation. These sites will give the unique possibility for detailed studies of organic carbon and biomarker records as tool for high-resolution reconstruction of sea-ice cover, sea-surface temperature, sea-surface salinity, and sea-surface productivity, to be done within the AWI-303/306 project. Of special interest will be the correlation between biomarker-based paleotemperature and paleosalinity records with Heinrich Events and related IRD and meltwater pulses. Within IRD-/Heinrich-type intervals, specific terrigenous biomarkers indicative for IRD sources will be quantified.

Preliminary shipboard results from a limited number of samples show that solvent extractable organic matter at Site U1313 consists primarily of odd-numbered C25-C35 n-alkanes and long chain C37-C40 alkenones. Variations in proportions of these compound classes reflect a change in the organic matter composition with respect to terrigenous and marine sources. Alkenone-derived sea-surface temperatures show variability from ~13 to 19˚C in the Pleistocene, whereas temperatures of ~20 and 22˚C were obtained for the late Pliocene and the latest Miocene, respectively (Fig. 1).

Reference:

Lisiecki, L.E. and Raymo, M.E., 2005. A Pliocene-Pleistocene stack of 57 globally distributed benthic d18O records. Paleoceanography, 20, PA1003, doi:10.1029/2004PA001071.

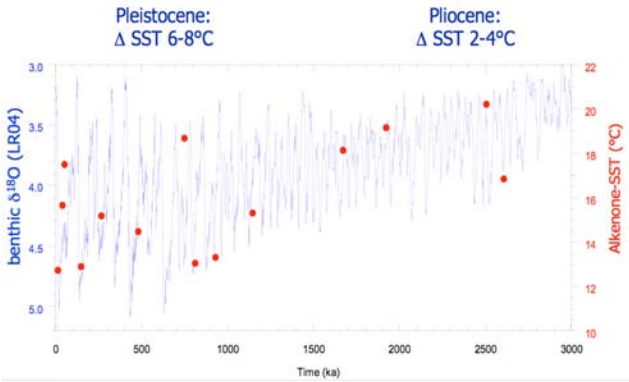

Fig.1. Global benthic oxygen isotope stack (Lisiecki and Raymo 2005) and sea-surface temperatures at Site U1313 (preliminary shipboard data)

IODP

Pelagic carbonate records during the Upper Pleistocene on Walvis Ridge (ODP Leg 208 Sites 1264-1266): Evaluation and enhancement of proxies

J. Steinlöchner*; R. Henrich*

*: FB Geowissenschaften, Univ. Bremen, Postfach 330440, D-28334 Bremen, Germany

With a combination of different established and new carbonate dissolution proxies, we intend to estimate the paleoclimatic influence on pelagic carbonate production in the SE-Atlantic. An additional aim of this study is a reconstruction of the carbonate ion concentration of different water masses in this region. Due to the process of carbonate dissolution in the water column, there is a progressive breakdown of calcareous particles during their sinking to the sea floor as well as close to or at the sediment/water interface. This process leads to changes in bulk sediment parameters such as grain-size distribution (in particular the sand fraction) and within the carbonate content.

The current project investigates the preservation stage of planktic foraminifers as one of the major calcareous plankton groups in order to assess the pelagic carbonate budget. Planktic foraminiferal assemblages are modified by preferentially removing dissolution susceptible tests (i.e. surface dwellers like G.ruber). Therefore, thick walled, more robust shells (i.e. some deep dwellers) will be enriched in the sediment. Two additional processes can influence this effect: (1) dilution with non-carbonate material and (2) ecological variations of the planktic foraminiferal assemblage through time. To minimise the dilution effect through terrigenous input analyses will start on Holocene to Upper Pleistocene material from ODP Leg 208 where foraminiferal nannofossil oozes with very high carbonate content (in excess of 90%) cover the Walvis Ridge (Zachos, 2004).

First results show increasing carbonate dissolution with increasing water depth reflected in the decreased CaCO3- and sand content of samples from Site 1266 (3798m) in the comparison to samples from Site 1264 (2505m). Preliminary results from additional examinations of the fine fraction in both sites with a Micromeritics SediGraph 5100 show a similar trend within the investigated sections; a rapid increase of the clay fraction in the older part of both cores can be noticed. This could be caused by two different processes (1) an increasing dissolution or (2) a change in the productivity of the different planktic organisms. Examination of the coarse fraction in regard to foraminiferal assemblages will be utilised to identify the two processes. To avoid a misinterpretation of the foraminiferal record we intend to establish a species-specific planktic foraminifer fragmentation proxy.

Reference:

Zachos, J.C., Kroon, D., Blum, P., et al., 2004, Early Cenozoic Extreme Climates: The Walvis Ridge Transect Sites 1262 - 1267, proc. ODP, Init.Rpts., 208.

IODP

High-resolution reconstruction of North Atlantic photic zone dynamics in the Late Pleistocene using coccolithophore-based proxies

Katharina Stolz[1], Karl-Heinz Baumann[1], Katharina Janke[1], Rüdiger Henrich[1], Patrizia Ziveri[2]

[1] Fachbereich Geowissenschaften, University of Bremen, Postfach 330 440, 28334 Bremen, Germany (kstolz@uni-bremen.de); [2]Department of Paleoclimatology and Geomorphology, Faculty of Earth & Life Sciences, Vrije Universiteit, De Boelelaan 1085, 1081 HV Amsterdam, The Netherlands

Main focus of the project is the establishment and evaluation of coccolithophores as a tool for the reconstruction of environmental conditions and their forcing factors in the North Atlantic region in the last 150.000 years. Therefore biological and chemical proxy indicators derived mainly from coccolithophores are used for these reconstructions. It is well known and documented from Greenland ice core records that short term intervals of climate variability occurred within this interesting time interval of the last 150.000 years. This work wants to investigate those events using mainly the primary producers coccolithophores as a palaeoclimatic tool.

The investigations of mainly coccolithophorid assemblages are carried out on a late Pleistocene sediment sequence from the Rockall Plateau (ODP Leg 162 Site 980). The sedimentary record provides a good succession from the late Marine Isotope Stage (MIS) 6 up to MIS 1.

The studies of coccolithophorid assemblages show that contents of coccolithophores rapidly increase with the beginning of MIS 5e (Eemian) and remain at relatively high contents during MIS 5, being dominated by the species Emiliania huxleyi and Gephyrocapsa muellerae. In comparison to this, coccolith contents decrease with the beginning of MIS 4, whereas G. muellerae disappears almost completely. During MIS 3 reworked Cretaceous nannofossils are found, which correspond with the occurrence of Heinrich events. Those changes in coccolithophore assemblages point out that they strongly react to climatic changes. The described changes of floral assemblages indicate adaptations of species to different kinds of water masses.

The present study needs to be extended in more detail. In addition, special emphasis will be given to species specific isotope analyses in the near future. As a first step the separation of the size fraction <20µm and of the clay fraction (coccoliths <5µm) has already started. Later on, species specific separations will be performed and complement the investigations on the sediment core.

IODP

Pre-eruptive magmatic conditions of the Kerguelen large igneous province: an experimental study

Strauß H, Nowak M, Holtz F

Institut für Mineralogie, Universität Hannover, Callinstraße 3, 30167 Hannover, Germany; email: H.Strauss@mineralogie.uni-hannover.de

In Earth's history the formation of large igneous provinces (LIP) is considered synchronous with global atmospheric and hydrospheric changes. These events are discussed to correlate them with mass extinction events. The knowledge of pre-eruptive volatile contents such as SO_2, HCl, and CO_2 is important to estimate the degassing potential of LIP basalts and to elucidate possible impacts of LIP formation to the climatic system and the biosphere. A combination of olivine hosted glass inclusion studies and of the experimental investigation of phase equilibria and volatile solubilities of the magma composition using high pressure/high temperature methods can shed light on pre-eruptive volatile contents. The petrology and geochemistry of Kerguelen plateau basalts in the Southern Indian Ocean is well known from numerous ODP cruises and thus this province is ideal to investigate the degassing potential of LIPs.

For the high P / high T crystallization experiments we synthesized a batch of 100g basaltic glass with the composition of re-equilibrated olivine hosted glass inclusions (SiO_2: 49, TiO_2: 4, Al_2O_3: 13, FeO: 10, MgO: 8, CaO: 11, Na_2O: 3, K_2O: 2, in wt%) of a picritic basalt. This composition is assumed to be near the parental melt of the active volcanic episode 20Ma ago (Borisova et al., 2002). Partial crystallisation experiments with this glassy starting material were performed at subliquidus/supersolidus conditions (950 - 1150˚C, 400MPa, dry to H_2O-saturated) in an internally heated argon-pressure vessel (IHPV). For this purpose Au80Pd20-capsules were filled with 60mg glass powder and different ratios of water and silveroxalate as CO2-source to adjust the H2O activity of the fluid phase and thus the H_2O content of the melt. Experiments were run in an IHPV for approximately 24 hours. The intrinsic oxygen fugacity of this IHPV was determined to be close to QFM+4 (QFM = quartz-fayalite-magnetite buffer). The synthetic magma chamber was quenched rapidly to room temperature with about 200˚C $s^{-1}$to avoid quench crystal formation of the low viscous melt during cooling.

For further experiments at lower oxygen fugacity conditions it was necessary to estimate the minimum runtime in an IHPV to reach an near equilibrium state. Short runtimes at lower oxygen fugacity conditions are important to prevent iron loss from the melt into the capsule material used at temperatures above 1050˚C ($Au_{80}Pd_{20}$). For this purpose we used (1) a basalt with fluid phase ($xH_2O_{initial}$ = 0.2) and (2) a nominally dry basalt doped with S, Cl, and F to perform time series experiments between 1 min and 18 h to get kinetic information.

Crystalline phases and glass pools of the quenched synthetic magma were large enough to determine the compositions using an electron microprobe Cameca SX-100. The H_2O content of the melt was determined using the "by-difference" method (total volatiles equal 100wt % minus the measured major element analytical total) (Devine et al., 1995).

The results of the phase equilibria experiments at oxidizing conditions are compiled in Fig 1. Crystalline phases stable within the experimental conditions are magnetite, ilmenite, pseudobrookite, chromium spinel, olivine, clinopyroxene, amphibole and plagioclase. Chromium spinel (Cr_2O_3 > 20wt %) is the liquidus phase at high H2O activity. At lower temperatures magnetite is replaced by pseudobrookite. Olivine is stable at low H2O activity and moderate temperatures (1050 - 1150˚C) while plagioclase is stable at low H_2O activity and low temperatures (≤1050˚C).

Fig 2 shows the temporal development of melt composition for nominally anhydrous basalt. Two short time experiments (t = 1min; 20min) still contain unaltered glass grains that are similar to the starting material on the spatial resolution of the EMA. However, X-Ray powder diffraction measurements reveal crystalline phases within the shortly tempered glass grains. XRD diffraction patterns of samples with a longer run time are similar to the patterns of the short time runs. We suggest that crystal seeds form in a very early state during an experiment. After t = 100min melt pools and crystal phases can be determined by using EMA. Between t = 3h and 24h the compositions of the phases (melt and crystalline phases) remain constant within error. Experimental products show an increase in size of crystal phases for longer run times. These observations for a fluid-free system have been confirmed for experiments conducted with a fluid phase. This kinetic study demonstrates that 3 h run time are sufficient (1) to attain near equilibrium conditions and (2) to get crystal sizes that are large enough to determine chemical composition with EMA (Fig. 3).

Determination of partition coefficients of major and trace elements between crystalline phases and glass are in progress to determine the effect of dissolved H2O content on element partitioning (e.g.: Ni partitioning between olivine and glass) and to develop a possible "geohygrometer". Phase equilibria experiments at more reducing conditions and the addition of volatiles like chlorine, fluorine and sulfur are in progress.

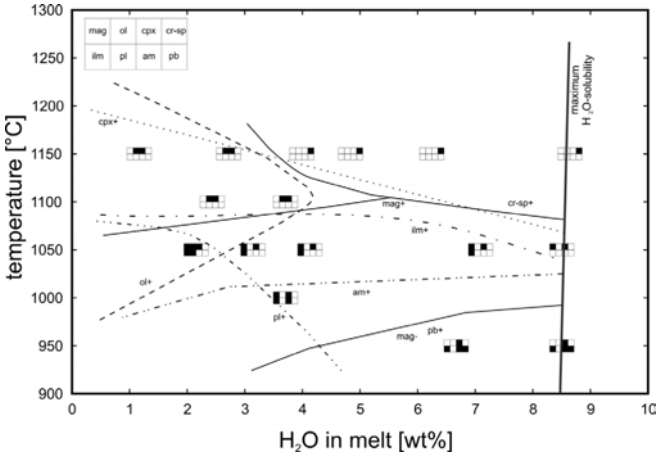

Fig. 1: Stability fields of mineral phases for different temperatures and H2O contents at 400 MPa. Crystalline phases are magnetite (mag), olivine (ol), clinopyroxene (cpx), chromium spinel (cr-sp), ilmenite (ilm), plagioclase (pl), amphibolite (am) and pseudobrookite (pb).

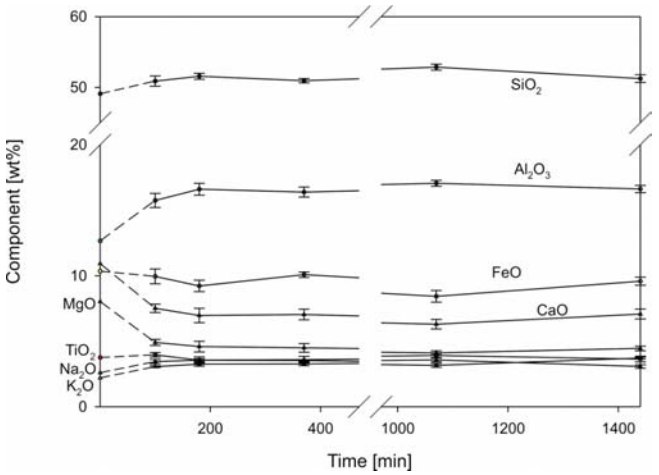

Fig. 2: The diagram shows different major element concentrations of the melt (total composition normalized to 100wt%) depending on the experimental run time. Concentrations for t = 0 represent the composition of the starting material.

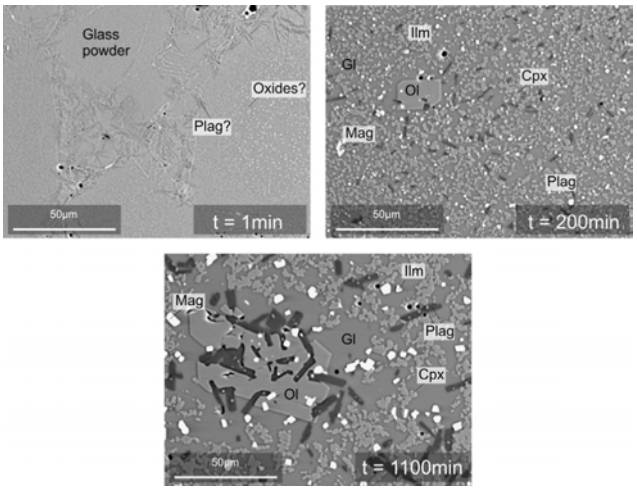

Fig. 3: Back scattered electron images showing experimental products performed under the same experimental conditions (4kbar, 1100˚C, aH2O=0) at different run times.

References:
Borisova et al. Chem. Geol. 183: 195-220, 2002
Devine et al. Am. Mineral. 80: 319-328, 1995

IODP

Development of an orbitally tuned time scale for the time interval 2.4-12 Ma (Leg 202)

Arne Sturm and Ralf Tiedemann
AWI Bremerhaven (asturm@awi-bremerhaven.de)

The astronomical tuning technique is at present the most accurate absolute dating method for sediment records spanning the time interval of the last 35 Ma for which astronomers provide a valid and precise orbital solution for variations in Earth's orbital parameters (eccentricity, obliquity, precession). The orbitally tuned geological time scale already became the standard chronology for the Pleistocene and Pliocene (0-5.3 Ma). Our goal is to expand and to astronomically calibrate the 'Magnetic Polarity Time Scale', the oxygen isotope stratigraphy and biostratigraphy to 12 Ma at South Pacific Site 1237 (Leg 202). So far, this is the only marine site that meets nearly all critera of providing a complete Neogene reference section by integrating the excellent framework of both magnetostratigraphy and biostratigraphy into an orbitally tuned oxygen isotope stratigraphy.

So far, we generated orbitally tuned time scales for Pacific Sites 1237 and 1241 that span the time interval from 2.4-6 Ma and extended the record at Site 1237 back to 9 Ma. The Atlantic-Pacific comparison of benthic $\delta^{18}O$ and $\delta^{13}C$ records indicated that the late Miocene and early Pliocene $\delta^{13}C$ signal is globally correlative and better structured than the $\delta^{18}O$ signal (Tiedemann et al., in press). Although the spectral variability of both parameters is dominated by 41-kyr cycles with relatively constant phase relationships, the clarity and correlative nature of the 41-kyr cycles is generally better developed in $\delta^{13}C$ records. This demonstrated that the benthic $\delta^{13}C$ records are not only a powerful medium for orbital tuning, but also a valuable tool for chronostratigraphic correlations that could assist the Miocene benthic oxygen isotope stratigraphy. This finding was very important for adopting our strategy and for extending our astronomically calibrated time scale (ATS) from 6 Ma to 9 Ma.

Our tuned oxygen isotope stratigraphy for the interval <4.9 Ma is in agreement with the 5.3-Myr stack of benthic $\delta^{18}O$ records recently published by Lisiecki and Raymo (1995), but deviates by more than one obliquity cycle in the older part before 4.9 Ma. The ages of the polarity reversals at Site 1237 agreed well with those of the generally accepted astronomical polarity time scale between the base of Réunion (2.17 Ma) and the top of Thvera (5.24 Ma) (Hilgen, 1991a,b; Shackleton et al., 1995; Lourens et al., 1996, 2004), except for the Kaena chron (3.11-3.16 Ma). Our astronomical ages for the base and top of Kaena are one and two obliquity cycles older, respectively. Our estimates for the time interval from 5 to 9 Ma are very close to the ages suggested by Hilgen et al. (1995, 2003) that were summarized in the ATNTS2004 timescale of Lourens et al. (2004).

IODP

Rapid climate change during the formation of the Lower Cretaceous OAE 1b

Isabel Stüsser[1], Peter Hofmann[1], Thomas Wagner[2], Stefan Schouten[3], Jaap S. Sinninghe Damsté[3] and Jens O. Herrle[4]
[1]University of Cologne, Institute for Geology and Mineralogy, Zülpicherstr. 49a, 50674 Köln, Germany (i.stuesser@uni-koeln.de); [2]School of Civil Engineering and Geosciences, University of Newcastle, Newcastle upon Tyne, NE1 7RU, UK; [3]Department of Marine Biogeochemistry and Toxicology, Royal Netherlands Institute for Sea Research, Den Burg, Texel, The Netherlands; [4]Southampton Oceanography Centre, School of Ocean and Earth Science, European Way, Southampton, SO14 3ZH, UK

The Cretaceous is characterized by several perturbations of the global carbon cycle, resulting in the so-called Oceanic Anoxic Events (OAEs). During the Lower Cretaceous the OAE 1b is one of these major pertubation associated with black shale deposition. It is documented in Albian deposits from the North and Central

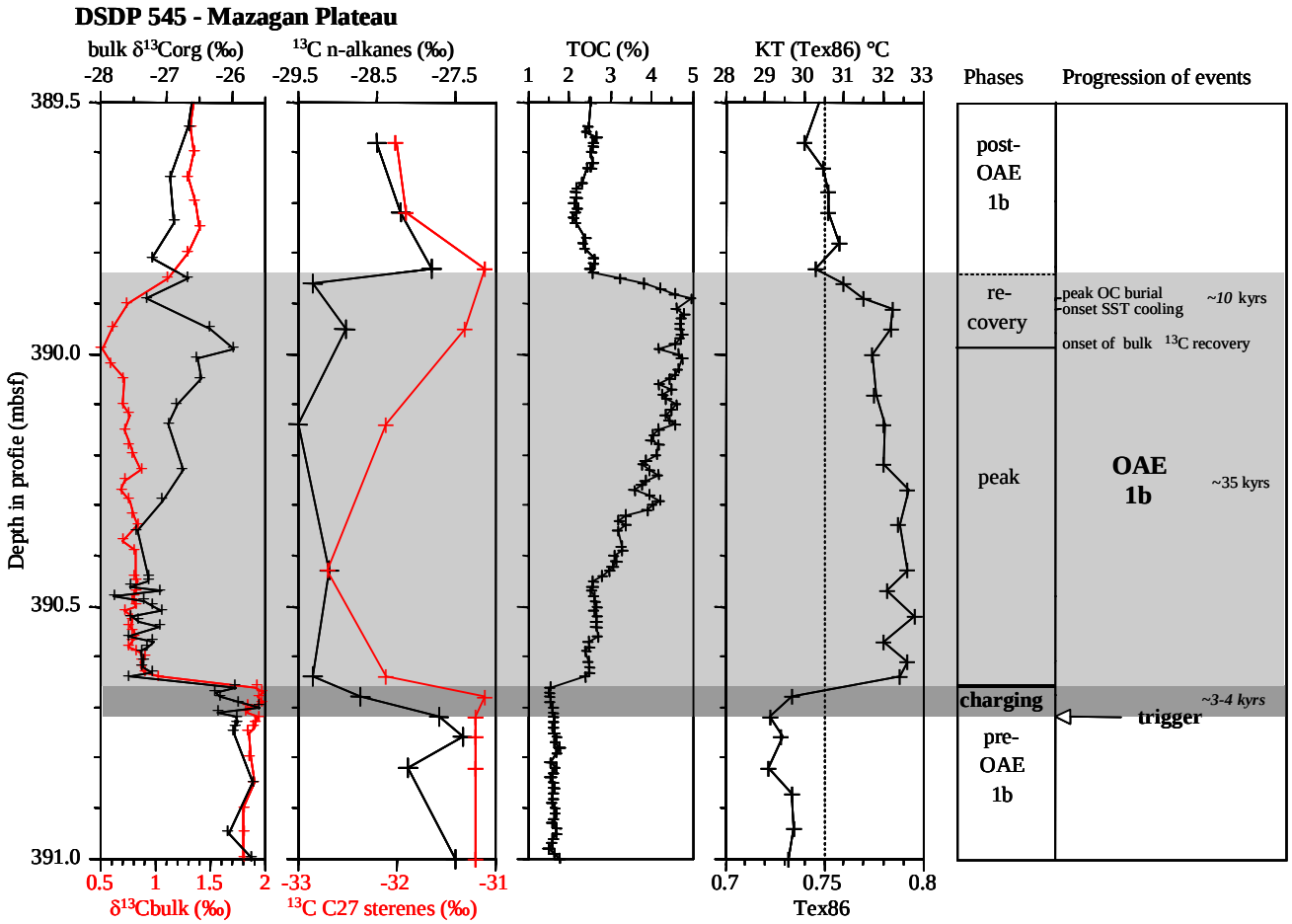

Figure 1: Geochemical record of the organic composition from DSDP Site 545. Focused on the black shale interval (light-grey). Carbon isotopes for the bulk carbon and bulk organic composition are shown at the left side. The compound-specific isotopes for the atmospheric and the marine signal are displayed by the n-alkanes and C27-sterenes and the SST is measured with the TEX86.

Atlantic region as well as from the western Tethys area and is therefore considered a supra-regional black shale. OAE 1b is associated with a pronounced negative shift in various carbon isotope reservoirs. Negative shifts in the carbon isotopes are also observed for the Toarcian OAE and the early Aptian OAE 1a and are thought to result from the catastrophic release of methane from marine gas hydrates.

Aim of the present study is to elucidate the global controls for OAE 1b and to quantify local climate changes. Therefore, high-resolution geochemical records for two paleogeographically distinct sites were established. Detailed organic and inorganic geochemical analyses were performed on a 6-meter record from DSDP Site 545 (North Atlantic, Mazagan Plateau) and a 14-meter record from the Vocontian Basin (SE-France). DSDP Site 545 is located in the lower Albian northern tropical climate belt offshore Morocco. The Vocontian Basin was situated in the subtropical Albian climate belt in the western Tethys region.

Our results document that the OAE 1b interval can be defined by the bulk carbonate and bulk organic carbon $\delta^{13}C$ isotope records. The black shale interval starts and ends simultaneously with the negative isotope excursion at both sites. Compound-specific carbon isotopes for the tropical site 545 show furthermore, that the perturbation of the carbon cycle occurred synchronously in the oceanic- and atmospheric carbon reservoirs (Fig. 1). This is indicated by the stable isotopic composition of biomarkers for terrestrial higher plant waxes (n-alkanes) and marine algal lipids (C27 Sterenes).

Strikingly, an abrupt 3 C˚ rise in sea surface temperature (SST, TEX86) at the tropical site 545 is observed parallel to the negative shift in the carbon isotopes. A temperature increase is also indicated for the onset of the OAE 1b interval in the Vocontian Basin and at ODP Site 1049 Blake Nose, suggesting rapid global warming for that time period. This global temperature rise has different effects on the investigated locations. For the pre-OAE stage at the Mazagan Plateau, fluctuations in the terrestrial composition indicate cyclic warm-cold variations (Fig. 2), which are in good agreement with a postulated upwelling system. The detrital input (Si/Al) is dominated by the eolian dust, delivered by the NE-trade wind system from the African continent. With the onset of OAE 1b the upwelling cell slows down as indicated by the decreasing ratios of the wind derived proxies (Fig. 2).

The Vocontian Basin represents a more restricted shallow marine environment surrounded by carbonate platforms. Prior to OAE 1b low amplitude cyclic variations in the siliciclastic fraction are dominant indicating climate controlled sediment supply (eg. Si/Al, CIA Fig. 2). During the black shale interval enhanced amplitudes of the cyclicity suggest stronger climate contrasts.

For both investigated sites climate proxies indicate more humid climate conditions (CIA = Al/Al+K+Na) during the black shale interval. After the black shale event both systems remain disturbed for several thousand kyrs before pre-OAE conditions are reestablished. Prior to reestablishment, at the tropical site 545 detrital input remains low similar to the black shale interval. At the subtropical site the cyclic variation ceases during the post-OAE interval.

The cyclic variation of the geochemical proxies for temperature and weathering intensity display in the tropics a strong excentricity signal, while the subtropics record is characterized by precession cycles (Fig. 2). In addition, a long-term trend in the carbon isotope curves and the temperature

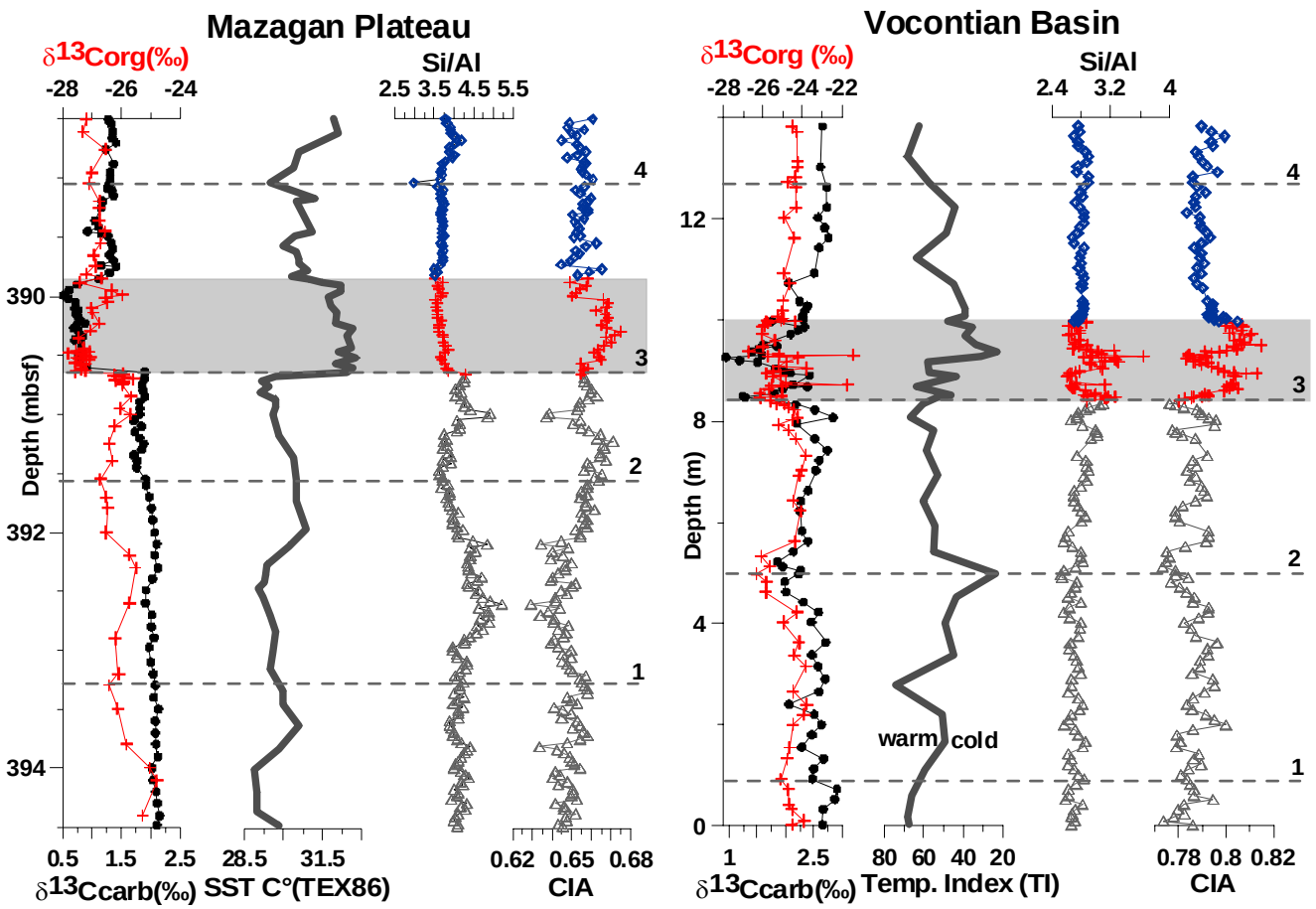

Fig. 2: Comparison of both sites. The grey-shaded interval marks the OAE 1b. The carbon bulk isotope excursion defines the black shale. The SST is derived from TEX86 and a calcerous nanofossil temperature index. Si/Al- and the CIA-ratio display terrigenous input and the degree of alteration. Line 1-4 are time lines based on the structure of the $\subset^{13}$Ccarb isotope curve.

proxies at both sites appear to record excentricity driven climate fluctuations.

The major climatic pertubations associated with OAE 1b also had consequences for the biota at the two investigated locations. At the Mazagan Plateau the organic matter production increased even though the upwelling which had prevailed for more than 200 ka prior to the event weakened, probably due to an increased influx of nutrients from the adjacent African Continent. The bioproduction of the Vocontian Basin shifted towards bacterial dominated communities as indicated by selected isoprenoids (e.g., PME). An enhanced siliciclastic input also suggests an increased runoff from the adjacent continents for this sites. Our data demonstrate a warming pulse during OAE 1b resulting in a weakening of the tropical trade wind system and higher climate contrasts for subtropical regions.

The trigger mechanisms leading to the abrupt onset and termination of OAE 1b, however, are still under debate. The gas hydrate release as trigger mechanism for the OAE 1b formation, as postulated for the Toarcian OAE and OAE 1a, appears to be unlikely because of the shape of the δ^{13}C isotope curve for various carbon reservoirs at DSDP 545. There, the magnitude of the isotope excursion remains constant over several ten thousand years. A single methane blast would strongly affect the atmospheric signal, but the concentration of light carbondioxid would than constantly exhaust. Hence, the record rather suggests a constant supply of 13C-depleted CO2 during the entire black shale interval. Further high resolution studies from other locations are needed to elucidate the nature of the ultimate trigger mechanism.

IODP

Erste geochemische Ergebnisse aus Untersuchungen der Gabbros des IODP Legs 305 (30˚N, Mittelatlantischer Rücken)

G. Suhr[1,2] und Leg 305 Scientific Party
[1]Geologisch-Mineralogisches Institut, Uni Köln, 2 Max Planck Institut Chemie, Mainz; guenter.suhr@uni-koeln.de

IODP Leg 305 vertiefte die während Leg 304 abgeteufte Bohrung 1309D von 401 auf 1415 m (siehe auch Fahrtbericht Suhr und Hellebrand im Abstract-Band). Die Bohrung 1309D hatte aufgrund umfangreicher Voruntersuchungen die berichtigte Hoffnung, frische Mantelgesteine zu erreichen. Sie ist lokalisiert auf dem Top eines "ozeanischen Kernkomplexes", d.h. eines tektonisch exhumierten Bereichs nahe des Mittelatlantischen Rückens. Ähnliche Settings waren schon das Ziel der Bohrungen 735B (Leg 118/176) und 1275 (Leg 209) und hatte dort jeweils zu hervorragendem Kerngewinn mit vorwiegend Gabbrogestein geführt. 1309D reiht sich nun nahtlos in diese Serie ein und brachte entgegen aller Erwartungen 96% Gabbro zu Tage. Wir präsentieren hier Ergebnisse der Mikrosondenanalytik des Intervalls zwischen 840 und 1250 m (an 47 Shipboard Slides) sowie - mit besserer räumlicher Auflösung - des Intervalls von 1198 bis 1242 m (72 Proben).

In einer stark vereinfachten Klassifizierung wurden zwischen 840 und 1000 m Teufe meist noritische Gabbros erbohrt, zwischen 1000 und 1100 m meist Olivin Gabbros, und zwischen 1100 und 1250 mbsf meist Olivin-reiche Troktolite. Unter 1250 m sind dann wieder noritische und Oxid-Gabbros vorherrschend. Im Detail sind die meisten Lithologien miteinander verwoben, wobei die wichtige Beobachtung an Bord gemacht wurde, daß stärker fraktionierte Lithologien intrusiv in primitivere Gesteine sind. Im Extremfall, z.B. bei 1240 m Teufe, ist Oxidgabbro (Mg# im cpx 60) intrusiv

in Olivin-reichen Troktolith (Mg# im cpx 87). Ein wesentliches Problem besteht nun darin zu klären, durch welchen Prozeß diese Gabbroabfolge gebildet wurde.

Bis auf die Oxidgabbros zeigen alle untersuchten Proben am Kornrand eine starke Anreicherung an TiO2 und Verarmung von Cr_2O_3 im cpx, z.B. Kern 0.4% TiO_2, Rand 0.8 bis 1.2% TiO2. Auch opx ist zoniert. Die späte Migration einer evolvierten Schmelze hat daher sicher eine bedeutende Rolle gespielt. Dies ist auch von Gabbros der Legs 176 (SW Indischer Rücken), 153 (Kane Fracture Zone, Atlantik) und 147 (Pazifik, Hess Deep) bekannt. Vermutlich ist diese Intergranularschmelze auch verantwortlich für die Bildung der z.T. extrem großen poikilitischen Klinopyroxene (bis zu 10 cm).

Bei Betrachtung der Cr_2O_3 Konzentrationen in cpx-Kernen (d.h. vermutlich zeitlich gesehen vor der Überprägung durch intergranulare Schmelze), kann mit etwas gutem Willen zwischen 800 und 1100 m eine übergeordnete geochemische Fraktionierung erkannt werden. Inwieweit die texturell markanten olivinreichen Troktolithe das primitive Endglied dieser übergeordneten Abfolge sind (NiO im Olivin bis zu 0.27%, Cr_2O_3 im cpx bis zu 1.4%) oder eine separate (ehemalige Mantel-) Einehit, kann bisher nicht eindeutig geklärt werden:

Im Vergleich zu den Olivin-Gabbros mit NiO ~ 0.11 im Olivin und Cr_2O_3 ~ 0.2-0.3 im cpx sind die Olivin-reichen Troktolithe ganz erheblich erhöht im Gehalt an kompatiblen Elementen und führen Cr-Spinell. Zum anderen liegen die Olivin-reichen Troktolithe aber noch im möglichen Bereich primitiver Kumulate. Deutlich positive Hinweise auf einen an Bord heiß diskutierten Ursprung als geochemisch überprägtes Mantelgestein fehlen bisher. Allerdings ist eine simple Bildung aus einer Mantelschmelze mit einem Gleichgewichtsolivin von Mg# 90 und 0.37% NiO allein durch Olivin-Fraktionierung nicht möglich. Der Grund ist, dass die beobachteten Olivine eine zu niedrige Mg# haben. Um innerhalb eines Kumulatmodells die olivin-reichen Troktolithe zu erklären, müsste auch für sie eine Equilibrierung mit einer evolvierten Schmelze zur Erniedrigung der Mg# angenommmen werden.

IODP

Controls on Ca isotope fractionation in porewaters of the Cascadia margin (ODP Leg 204)

B.M.A. Teichert[1], N. Gussone[2], A. Eisenhauer[3]
[1]Bundesanstalt für Geowissenschaften und Rohstoffe, Stilleweg 2, 30655 Hannover, Germany, b.teichert@bgr.de; [2]DFG Forschungszentrum Ozeanränder, Universität Bremen, Leobener Str., 28359 Bremen, Germany, gussone@uni-bremen.de; [3]Leibniz Institut für Meereswissenschaften IFM-GEOMAR, Wischhofstr. 1-3, 24148 Kiel, Germany

Methane-derived authigenic carbonates in the sediments of cold seep sites are a significant calcium sink. The strong depletion of dissolved Ca in the porewaters of shallow sedimentary sections (centimeters to tens of meters) due to authigenic carbonate formation has been widely observed. Our study of porewaters from ODP Leg 204 at Hydrate Ridge shows that, in addtion to carbonate chemistry, the Ca isotopes are highly influenced by several other processes. Here we present the data of 4 sites (Sites 1244, 1245, 1250, 1251) in an east to west and north to south profile across the accretionary prism. These sites can be grouped into three different hydrogeologic environments. Sites 1244 and 1245 are typical of sites drilled in the western flank of southern Hydrate Ridge. Site 1250 characterizes the southern summit in the region of active seafloor venting. Site 1251 was drilled in a slope basin to the east of the summit. All sites show a strong decrease in $\delta^{44/40}Ca$ of up to 0.8 permill in the upper ~60 mbsf indicating the release of light Ca isotopes at about 50-60 mbsf due to shallow diagenetic processes. The decrease in alkalinity and solid calcium carbonate as well as the increase in Ca concentration in porewaters below 60 mbsf at Site 1245, suggest dissolution of carbonates. The Ca isotopes comprise even more information and indicate that authigenic carbonates, once precipitated in shallow, near-seafloor sediments, are being dissolved here. The Ca isotope signal of porewater in the deeper sedimentary sections suggests a deep sourced fluid with a distinct signature characterized by high Ca concentration and light Ca isotopy. The influence of this fluid increases with distance from the accretionary toe due to increasing compaction and dewatering, as has been previously shown based on strontium and chloride geochemistry. This deep fluid seems to be as well transported into shallower sediment depths along a horizon (Horizon B) at Site 1244 which is visible as a strong seismic reflection and composed of a cluster of multiple turbidites.

IODP

X-ray Computer Tomography and Image Analyses as tool for coral quantification and identification in cold-water coral mounds (Challenger Mound, Porcupine Seabight, IODP Expedition 307)

J. Titschack[1], A. Foubert[2], A. Freiwald[1], T. Ferdelman[3], A. Kano[4], T. Williams[5], J.-P. Henriet[2] and IODP Exp. 307 Scientists
[1]Institute of Palaeontology, Erlangen University, Germany, juergen.titschack@pal.uni-erlangen.de ; [2]Renard Centre of Marine Geology, Gent University, Belgium; [3]Max-Planck-Institute for Marine Microbiology, Bremen, Germany; [4]Department of Earth and Planetary Systems Science, Hiroshima University, Japan; [5]Lamont-Doherty Earth Observatory, Palisades, USA

Cold-water coral environments, dominated by the azooxanthellate corals Lophelia pertusa and Madrepora oculata, are well-known along the European continental margins in water depth ranging from 40 m to 1000 m. The Porcupine Seabight, west of Ireland, represents an exceptional hotspot for such cold-water coral environments with over thousand mound structures constructed and covered by cold-water corals. Although many of the mounds are buried nowadays by hemipelagic drift sediments, several mounds are still active in terms of coral growth. The mounds are grouped in three distinctive mound provinces and can reach heights of up to 200 m and several kilometres length at their base. Intense biogeological and oceanographic research during the last years on and around these fascinating mound structures culminated recently in the IODP Expedition 307 Modern Carbonate Mounds: Porcupine Drilling in spring 2005. Despite being the target of over 20 scientific cruises during the last year, none of the operations could penetrate the mounds interior deeper than 10 m, therefore leaving much space for controversial and fruitful debates on the origin and evolution of the mounds.

The main goals of the IODP Expedition 307 were to shed light on the processes involved in mound nucleation, mound evolution and growth as well as to establish a stratigraphic framework for the slope/mound system by the identification and correlation of regional erosional surfaces and mound growth phases in line with global oceanographic changes. IODP Expedition 307 targeted the asymmetrically buried, 170 m high Challenger Mound. For the first time in history, a cold-water coral mound was drilled, revealing a sedimentary record of 155 m dominated by cold-water coral float- and rudstones with a muddy matrix. Multiple cycles could be identified in the physical properties, which correlate with changes in facies.

However, to get a better insight into mound evolution, it is of utmost importance to identify active mound growth phases, represented by intervals of high coral densities. X-ray Computer Tomographic scans and digital image analyses were used for the quantification of the coral content. The CT scans were performed with a SOMATOM Sensation 64 of the Siemens Medical Solution Centre in Forchheim. Altogether, 18 m of core were scanned with a spatial resolution of 0.4 mm. The advantage of analysing CT scans is (1) that the coral content estimation is based on the whole core volume and not on small sediment aliquots, (2) the possibility to evaluate coral orientation and fragmentation, an hint for the kind of preservation, in situ versus transported, and (3) the method is non-destructive. A comparison of the CT-scans with the quantification of the coral content from digital surface pictures (by using the AnalySIS software) will shed light on potential quantification errors due to the reduction from a 3-dimensional- to

a 2-dimensional-based coral density estimation. In a second stage, the quantification of the coral content can be used to correlate active mound growth phases with other datasets such as physical properties, colourmetry, grain-size analysis or chronostratigraphic datasets. Important will be the later comparison of the coral quantities with aragonite dissolution patterns obtained from examining the dissolution pattern in the coral Lophelia pertusa for the differentiation of primary facies changes to changes caused by secondary aragonite dissolution.

ICDP

Hot-spot related crustal magnetization and magnetic petrology of basalts from the Reykjanes peninsula (IDDP-site) and the Stardalur drilling, SW-Iceland (KO1514/3)

C. Vahle, A. Kontny, F. Dietze
Geological-Paleontological Institute, Ruprecht-Karls-University, Im Neuenheimer Feld 234, 69112 Heidelberg, Germany
(agnes.kontny@urz.uni-heidelberg.de, carsten_vahle@urz.uni-heidelberg.de)

Rock magnetic and magneto-mineralogical data contribute to our understanding of the growth history and tectonic evolution of volcanic structures and are important for the interpretation of magnetic anomalies. The aim of this project is to evaluate the effect of magnetic mineralogy and texture on the development of high and low crustal magnetization in basalts, which is responsible for stripe-like and localized magnetic anomalies. During a first sampling on Iceland, surface samples from the Reykjanes peninsula and drill cores from the Stardalur volcanic complex have been selected for detailed investigations.

The Reykjanes high-temperature system is located at the boundary where the submarine Reykjanes Ridge passes over into the rift zone of southwestern Iceland. Surface geology is characterized by the historic Stampar fissure eruption from 1226, a picritic lava shield and intercalated pillow basalt - hyaloclastite ridges probably formed during the last glacial episode (14.5 - 20 thousand years). The geothermal field, which coincides with a magnetic low in the aeromagnetic anomaly map, is situated within a dense NE-SW fissure and fault zone. Within the frame of IDDP, a 3 m drill core was recovered from a depth of 2245 - 2248 m of the RN-19 borehole in May 2005, which entirely consists of a dense dolerite intrusion. Different rock magnetic and magneto-mineralogical investigations were carried out on different volcanic surface rocks from three profiles across the peninsula and the drill core to correlate rock magnetic and magneto-mineralogical properties with magnetic field intensity. Koenigsberger (Q) ratios are high (17-132) for all surface samples, indicating that the remanent magnetization dominates. Natural remanent magnetization (NRM) is between 2.5 and 33 A/m with high values in the youngest flow. The high NRM coincides with the magnetic high, while samples from flows of older age with lower NRM and susceptibility occur within the area of magnetic low. We observed that NRM is especially high in the scoria of young flows, while it is lower in the vesicular and dense basalt of the more central parts of flows. First temperature dependent magnetic susceptibility data (k-T) reveal homogeneous titanomagnetite with Tc at about 60 ˚C, pure magnetite (Tc = 580 ˚C) and an irreversible titanomaghemite with Tc at about 450 ˚C in the area of the magnetic low. The occurrence of magnetite and the low-temperature behavior of k-T curves below -150 ˚C indicate exsolution textures typically forming during high-temperature oxidation.

The Stardalur volcanic complex 20 km NE of Reykjavik forms a localized very strong positive magnetic anomaly of Olduvai age (ca. 1.8 my, normal polarity). Drill cores from a 200 m deep borehole, drilled in the years 1969-70 into the area of maximum intensity, revealed about 45 m of fresh olivine tholeiitic lava flows and tuffs with low magnetic intensity. Below that depth until at least 140 m, strongly magnetic early Quaternary lavas follow. Susceptibility measurements on the drill cores gave high values ranging between 20 and 73 * 10E-03 SI below 44 m. Laboratory measurements on standard cylinders revealed an almost linear correlation between NRM intensity and susceptibility reaching very high values up to 121 A/m and 148 * 10E-03 SI, respectively, suggesting a high content of opaque minerals. Temperature dependent susceptibility measurements (in argon) give Curie temperatures of ca. 580 ˚C and microscopic observations (reflected light and SEM) revealed magnetite/maghemite as the carrier of the magnetic properties. Most of the magnetite is the product of oxy-exsolution of originally titanomagnetite, but also grains formed by hydrothermal alteration are present. Additionally, shrinkage cracks and a mottled texture of the grains point to maghemitization. Therefore the unusually high natural remanent magnetization of the Stardalur basalts is not a TRM, but a CRM of different origin, carried predominantly by maghemite.

IODP

Bulk mineral assemblage of IODP Leg 302-Arctic Coring Expedition (ACEX) cores-implications on paleoceanography and early diagenesis

Christoph Vogt[1] , Rüdiger Stein[2] & Reinhard X. Fischer[1]
[1]Kristallographie, Fachbereich Geowissenschaften, Universität Bremen, cvogt@uni-bremen.de; [2]Alfred-Wegener-Institut für Polar- und Meeresforschung, Bremerhaven

As part of the intensive international effort to investigate the unique sediment sequence retrieved by the Arctic Ocean Coring Expedition (ACEX) we focus on the X-ray diffraction analysis (XRD) of the bulk sediment fraction. By applying the most sophisticated quantitative phase analysis (QPA) available for Arctic Ocean sediments (Vogt et al., 2002) the project aims on (1) improving the reconstruction of Quaternary changes in the sedimentation record beyond Marine Isotope Stage 6; (2) performing a detailed investigation of central Arctic Ocean paleoenvironmental changes preserved in Late Cretaceous to Quaternary sediments, (3) deciphering the sources of the terrigenous sediment component, and (4) recognizing the diagenetic overprint in particular in the sequences with massive carbonate dissolution and authigenic carbonate precipitation as well as in the sequences with Fe-Sulfides, Fe- and Mn-(Hydr)Oxides precipitation.

230 samples have been measured during the onshore phase of the ACEX Scientific Party at the Crystallography Laboratory Bremen in November 2004 and subjected to a three step QPA since then. The XRD information has already been used to support the lithostratigraphic sectioning of the combined ACEX cores. The Cretaceous basement rocks for example are sandstones rich in quartz and feldspars while the Tertiary sequence above has much lower contents of quartz and feldspar. The mineralogical data permit to correlate the ACEX composite section to shorter well dated cores on the Lomonosov Ridge retrieved by RV "Polerstern" earlier. Increased quartz and feldspar contents most probably are related to the increased ice rafted debris derived mainly from the Barents and Kara Sea regions. Intercalated peaks of dolomite which also stratigraphically correlate to the neighboring cores and are interpreted as deglaciation iceberg events from the Canadian Arctic Archipelago (c.f. Vogt, 1997; Nørgaard-Pedersen et al., 1998, 2003). Ages below 4 m were difficult to assign in those cores. In the ACEX cores the Brunshes/ Matuyama paleomagnetic boundary (ca. 780.000 years) was recognized at about 16 mcd, multiple small magnetic events might be related to known events and provide more age fix points as calcite microfossils are sparse. At least below 28 mcd ACEX cores received a diagenetic overprint, authigenic carbonate minerals like siderite and rhodocrosite occur. In the early Tertiary section a full opal-opal CT-zeolite diagenetic sequence has been observed combined with massive authigenic pyrite.

Vogt, C., Lauterjung, J. and Fischer, R.X., 2002. Investigation of the clay fraction (<2 μm) of the clay mineral society reference clays. Clays and Clay Minerals, 50(3): 388-400.
This work is funded by Deutsche Forschungsgemeinschaft project number Fi-442/10-1. Laboratory work has been extensively supported by the ACEX Scientific Onshore Party and the IODP Core Repository Bremen.

IODP

Developing a high temperature magnetometer to study oceanic basalt magnetisation carriers

Michael Wack, Maxim Alexutin and Juergen Matzka
Department of Earth and Environmental Sciences, University Munich, Theresienstr. 41, 80333 Munich, MichaelWack@gmx.net

It has been recognized early in the study of oceanic basalt magnetism that the natural remanent magnetisation (NRM) is behaving in a peculiar way during the classic stepwise thermal demagnetisation. In order to get an overview of the various kinds of thermal demagnetisation behaviour of oceanic basalts, we thermally demagnetised more than 100 DSDP, ODP and IODP samples from all oceans representing oceanic crust with various age and state of alteration. Typically, the thermal demagnetisation behaviour resembles that of a multicomponent NRM where the individual components are characterised by different unblocking temperatures. This is especially observed for oceanic basalts older than approximately 10 Ma. In contrast to this finding, there is no indication for a multicomponent NRM from alternating field (AF) demagnetisation experiments. Rock magnetic experiments also indicate the presence of only one magnetic mineral phase, which is a titanomaghemite with a Curie temperature around 300 ˚C. Our hypothesis to make the complex multicomponent thermal demagnetisation behaviour consistent with the simple single phase magneto-mineralogy is that the titanomaghemite undergoes alteration during thermal demagnetisation and that the alteration product inherits the titanomaghemites original NRM. However, AF demagnetisation and rock magnetic experiments are not the most suitable methods for identifying the carrying mineral of the NRM and it is not easy to understand how alteration products can inherit an original NRM. One way to test our hypothesis is to continuously monitor the NRM at high temperature during heating steps. This is not possible with standard paleomagnetic equipment. A new magnetometer "Hotspin 2" is therefore being developed to measure ocean basalt NRM at high temperatures. It is an advanced version of the already existing "Hotspin" instrument which is limited to the measurement of only two of three components of a sample's magnetisation. A hot air heating was developed and is ready to be used in "Hotspin 2" to avoid the use of electrical heating with unpredictable magnetic effects on the samples. Our redesigned instrument will have some additional features like the possibility to measure multiple samples at the same time and an advanced analysis software. In contrast to the original Hotspin, it's an off axis spinner magnetometer, which means that the sample is not located on the spinning axis but at a distance of 15 cm to it. This allows the determination of all three components of the magnetisation, which is essential to obtain the full paleomagnetic information. For our project the main aim here is to distinguish between the unblocking of viscous magnetic overprints and magnetisation changes related to thermal alteration. The ambient field is compensated by three orthogonal Helmholtz coils with a size of 2 meters surrounding the instrument. The components of the magnetic field generated by the specimen are measured with six fluxgate sensors. For each of the three components the signal difference of two sensors is used. This reduces the influence on the measurement signal by temporal changes in the ambient fields, which can be substantial at our current location in the centre of Munich. Special care was taken to optimise the sensor geometry and the signal amplifying and filtering electronics to achieve a sensitivity of 50 mA/m which basically represents the limits of the fluxgate sensors. We use a standard PC with a LabView based software to control the instrument and to process the data. One main problem is currently the maximum temperature of the hot air heating. Up to now we reached 320 ˚C maximum temperature. By increasing the heating power and the flow of hot air through our oven we hope to achieve temperatures of more than 400 ˚C in the future. This maximum temperature will be sufficient to distinguish between viscous magnetic overprints and magneto-mineralogical alterations of the titanomaghemites, which take place between 300 ˚C and 400 ˚C. In its final version, the "Hotspin 2" instrument will be set up at the Paleomagnetic Laboratory Niederlippach at a location with significantly reduced disturbances of the ambient magnetic field.

IODP

Joint ICDP and IODP data management for MSP expeditions

Wallrabe-Adams, H.-J.[1], Huber, R.[1], Klump, J.[2], Conze, R.[2], Graham, C.[3], Krysiak, F.[4]
[1]MARUM, University of Bremen, [2]GeoForschungsZentrum Potsdam, [3]British Geological Survey Edinburgh, [4]smartcube GmbH Berlin

Since summer 2004 the Integrated Ocean Drilling Program (IODP) has completed its first two Mission Specific Platform (MSP) expeditions, the Arctic Coring Expedition (ACEX) and the Tahiti Sea-Level Expedition. Both were funded by the European Consortium for Ocean Research Drilling (ECORD). The British Geological Survey in conjunction with the University of Bremen and the European Petrophysics Consortium were the ECORD Science Operator (ESO).

IODP MSP expeditions operate in working environments similar to the lake drilling projects conducted by the International Continental Scientific Drilling Program (ICDP) and thus have very similar data management requirements. Both organizations require data capture and management systems that are mobile, flexible and that can be deployed quickly on small- to medium-sized drilling platforms for the initial collection of data, and which can also be deployed onshore in laboratories where the bulk of the scientific work is conducted. ESO, therefore, decided to use an adapted version of the ICDP Drilling Information System (DIS) for this task - the OffshoreDIS (Conze et al., 2004). The underlying OffshoreDIS data model is compatible with IODP(JANUS), the Bremen Core Repository, WDC-MARE/PANGAEA and the LacCore in Minneapolis.

An MSP expedition has typical stages during which specific types of data are produced:

Onboard data such as

a. technical data, e.g. drilling data
b. curatorial data: sample-core-section administration
c. scientific data, e.g. core photos, core scanner, palaeontological data

Repository data such as

a. curatorial data: sample-core-section administration
b. scientific data: core photos, core scanner, geochemistry, palaeontological data

Post-cruise data such as

scientific data produced after the cruise using core material even from previous expeditions of IODP, ODP, DSDP or ICDP.

The OffshoreDIS data management system will be of long-term benefit to both IODP and ICDP and it will be used in forthcoming MSP offshore projects, ICDP lake drilling projects and joint IODP-ICDP projects, such as the New Jersey Coastal Plain Drilling Project in summer 2006.

The overall IODP data management is still under construction. All 'Implementing Organizations' (IOs) use their own database system (JANUS, J-CORES, WDC-MARE/PANGAEA). In future, these data repositories will be combined into a general data portal for Scientific Earth Drilling Services SEDIS (Miville and Soeding, 2006) to provide a user-friendly access to IODP and ICDP data (Figure 1).

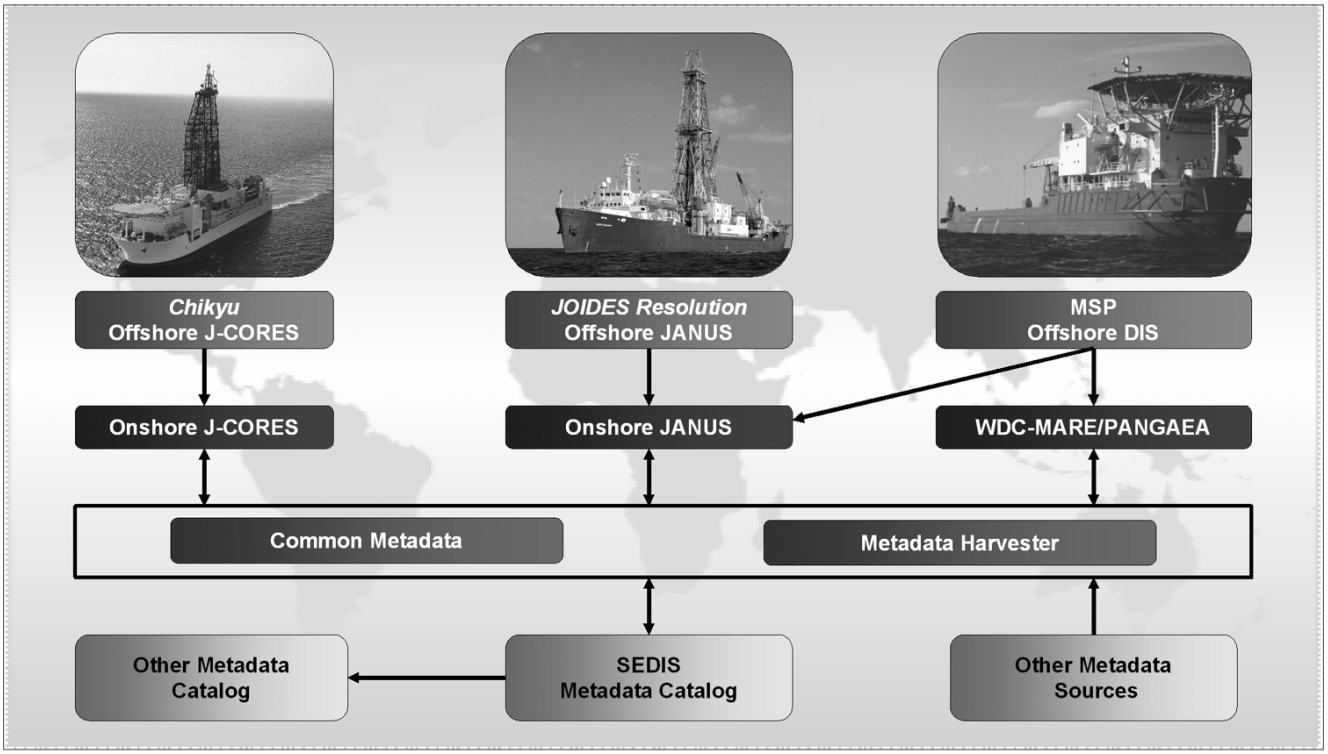

Figure 1: Schematic view of IODP data management. Data are collected by the IODP Implementing Organizations and integrated into a common portal.

WDC-MARE/PANGAEA handles the scientific data produced in the different stages of an IODP expedition. All scientific data from MSP expeditions, as well as post-cruise data from IODP in general, will be stored in the long-term archive. Publishing these scientific data to the worldwide earth science community is a major task for WDC-MARE/PANGAEA.

Several additional MSP data management components are in planning or being developed to meet future requirements. These include a stratigraphic correlation tool, taxonomic dictionaries and catalogues based on TaxonConcept (Huber et al., 2005), and a curation tool for sample registration and tracking.

References

Conze, R., Krysiak, F., Graham, C., Wallrabe-Adams, H.-J. (2004): Data Modeling, Development, Installation and Operation of the ACEX Offshore Drilling Information System for the Mission Specific Platform Expedition to the Lomonosov Ridge, Arctic Ocean. AGU 2004 Fall Meeting, Poster GC51D-1084, San Francisco.
Huber, R. and Klump, J., 2005. TaxonConcept, a new taxonomic information system. EGU General Assembly 2005, Geophysical Research Abstracts, 7: 02357.
Miville, B., Soeding, E. (2006): Data Management in IODP, Scientific Drilling, 2: 48-49

IODP

Orbital forced cyclicity in the depositional environment in the Cape Basin? An integrated study of borehole and seismic data

Estella Weigelt*, Gabriele Uenzelmann-Neben*
*Alfred Wegener Institute for Polar and Marine Research, Postfach 120161, D-27515 Bremerhaven. Contact: eweigelt@awi-bremerhaven.de

The southern hemisphere's response to significant changes in global climate is still poorly understood. A clue can be offered by the study of sedimentary sequences along the continental margin off southwest Africa. The depositional structures were shaped by an interaction of climate, oceanic currents and sea level fluctuations. The region lies under the influence of the Benguela Current Upwelling System (BCUS), which is one of the major upwelling systems worldwide. Due to its high sedimentation rate this area is favourable to study climate influences on sedimentation in a fine scale.

We present a seismostratigraphic model for the Neogene and Quarternary sedimentary layers in the Cape Basin based on a combination of reflection seismic lines with drill site records of the ODP Leg 175 sites. The drill site data were converted from depth domain to two-way traveltime domain by sonic logs calculated from P-wave velocities of the site data. This procedure enables dating and areal tracing of reflectors mirroring changes in deposition system concerning the composition of the sediments as well as changes in currents and deposition style.

For the middle and northern Cape Basin our study reveals an apparently regular sequence of continuous high amplitude reflectors characterizing the upper seismic units. They are well pronounced for about the last 3.5 Ma. The computed spectra of depth and age over the strong amplitude reflectors indeed indicate a certain periodicity. Periods of 95 to 120 cycles/ky dominate especially the undisturbed sequences close to Sites 1082, 1083 and 1084. As a reason for the regularity of reflectors we suggest glacial to interglacial cycles as they present climate thresholds at which sediment composition drastically changes. These changes also influence density and P-wave velocity of the deposits and, consequently, find their expression in impedance contrast and thus in the seismic reflection pattern. Considering a certain inaccuracy of depth and hence of age determination for the seismic reflectors, we suggest these cycles to coincide with obliquity cycles of the earth's orbit.

In the southern Cape Basin however, we cannot observe such a distinct cyclicity of reflectors throughout the last 15 Ma. Here, the frequency and sequence of reflectors is much lower and shows only a weak maximum around the period of 400 ky. In this region a much lower sedimentation rate probably prevents the resolution of a fine scale reflector sequence. Additionally, the deposition sequence seemed to be disturbed by mass movements as indicated in numerous slump scarps recorded on the seismic lines.

IODP

New high-resolution chronology from the first complete late Paleocene - early Eocene marine records from Walvis Ridge: duration of Chron 24r and new constraints on the timing of early Eocene global warming events

Thomas Westerhold[1], Ursula Röhl[1], Gerold Wefer[1], Jacques Laskar[2], Isabella Raffi[3], Julie Bowles[4], Lucas J. Lourens[5] and James C. Zachos[6]
[1]Marum - Zentrum für Marine Umweltwissenschaften, Universität Bremen, Leobener Strasse, Bremen, 28359, tho@uni-bremen.de; [2]Astronomie et Systèmes Dynamiques, IMCCE-CNRS UMR8028, 77 Av. Denfert-Rochereau, Paris, 75014, France; [3]Facoltà di Scienze, Dipartimento di Geotecnologie per l'Ambiente e il Territorio, Università "G. d'Annunzio" di Chieti-Pescara, Campus Universitario, Via dei Vestini 31, Chieti Scalo, 66013, Italy; [4]Scripps Institution of Oceanography, University of California, San Diego, 9500 Gilman Drive, MC0220, La Jolla, CA 92093, USA; [5]Faculty of Geosciences, Department of Earth Sciences, Utrecht University, Budapestlaan 4, Utrecht 3584 CD, Netherlands
6 Earth Sciences, University of California, Santa Cruz, Santa Cruz, CA 95064, USA

Progress in characterizing Paleogene oceanography and climate history, particularly the abrupt transient events, has been hampered for a relatively long time by the lack of high quality, high resolution sequences. This dead end situation ceased with the new records available from ODP Legs 198, 199, 207 and 208. Especially the sites from Legs 198 (Shatsky Rise, Westerhold and Röhl, 2005) and 208 (Walvis Ridge) are providing the first complete spliced records ("composite sections") for the early Paleogene from drilling multiple holes, as the first depth transects for the early Paleogene for both the Pacific and Atlantic Ocean. Within our current project these sites have been utilized to construct a high resolution floating time scale spanning the magnetic polarity chrons C24r to C30n (53.5 - 66 Ma). Detailed correlation between the sedimentary records revealed that the five sections drilled at the Walvis Ridge represents the first complete late Paleocene and early Eocene deep-sea record with moderate to relatively high sedimentation rates (1 to 3 cm/kyr).

Here, we present the unique ~ 4.3 million year long interval recovered from Walvis Ridge that spans the late Paleocene to early Eocene (magnetochrons C24r, C25n, and upper C25r) containing the Paleocene-Eocene thermal maximum (PETM; Zachos et al., 2005) and recently identified new early Eocene global warming events (ELMO layer; Lourens et al., 2005; "X" event; Röhl et al., 2005). We have developed a detailed chronology by using records of elemental concentrations obtained by an X-ray fluorescence (XRF) Core scanner and non-destructive core logging data (magnetic susceptibility, color data). To define a complete time series of the investigated interval new revised composite depth records have been constructed for ODP Leg 208 Sites 1263, 1267, and ODP Leg 171 Site 1051. Extensive spectral analysis and computation of evolutive spectra using wavelet analysis (Figure 1) of multiple proxies in the depth domain suggests that the dominant early Paleogene sedimentary cycles are related to Milankovitch orbital forcing. All sites reveal almost perfect precession cycles modulated by the short (100-kyr) and long (405-kyr) eccentricity cycle. Direct counting of precession cycles in the iron concentrations as well as the redness over greenness ratio (a*) of the color data at multiple sites results in revised estimates for the duration of magnetochrons C24r and C25n. We consider the developed relative time scale based on cycle counting spanning 4.26 Ma to be accurate to the level of one precession cycle. We have also determined the exact relative position of the critical PETM and Elmo layer intervals within Chron C24r, which is of major importance for identifying these events in other marine- and continental sections. The newly defined position of the PETM (at C24r.64) is very robust as it is in agreement with estimates from continental sections (e.g., Wing et al., 2000; Bighorn Basin).

In order to obtain absolute age estimates for the PETM, the Elmo layer and the magneto-chron boundaries, the geological data have been compared to the current available astronomical solutions for orbital eccentricity (Laskar et al., 2004; Varadi et al., 2003). For the first time it is now possible to provide robust estimates for the absolute ages of not just the magnetochrons C24r and C25n, but even more for the early Eocene warming events (Figure 2) using the amplitude modulation of the precession cycle in combination with cycle counting. We are convinced that because of the stability of the long eccentricity cycle our absolute estimates are accurate. The new absolute age of 55.525 Ma for the onset of the PETM is consistent with recalibrated radiometric estimates. Comparison of the amplitude modulation of the precession cycle in the geological data with current astronomical computations of eccentricity suggests that the Paleocene-Eocene Thermal Maximum (PETM) and the Elmo layer are related to 100-kyr maxima, but do not show any association to 405-kyr eccentricity maxima.

[Figures 1 and 2 next page]

References:
Laskar, J., Robutel, P., Joutel, F., Gastineau, M., Correia, A. and Levrard, B., 2004. A long-term numerical solution for the insolation quantities of the Earth. Astronomy and Astrophysics, 428: 261-285.
Lourens, L.J., Sluijs, A., Kroon, D., Zachos, J.C., Thomas, E., Röhl, U., Bowles, J. and Raffi, I., 2005. Astronomical pacing of late Palaeocene to early Eocene global warming events. Nature, 435(7045): 1083-1087.
Röhl, U., Westerhold, T., Monechi, S., Thomas, E., Zachos, J.C. and Donner, B., 2005. The Third and Final Early Eocene Thermal Maximum: Characteristics, Timing and Mechanisms of the "X" Event, Geological Society of America Abstracts with Programs, Vol. 37, No. 7, p. 264.
Varadi, F., Runnegar, B. and Ghil, M., 2003. Successive Refinements in Long-Term Integrations of Planetary Orbits. Astrophysical Journal, 592: 620-630.
Wing, S.L., Bao, H. and Koch, P.L., 2000. An early Eocene cool period? Evidence for continental cooling during the warmest part of the Cenozoic. In: B.T. Huber, K.G. MacLeod and S.L. Wing (Editors), Warm Climates in Earth History. Cambridge University Press, Cambridge, pp. 197-237.
Westerhold, T. and Röhl, U., 2005. Data report: Revised composite depth records for Shatsky Rise Sites 1209, 1210, and 1211. In: T.J. Bralower, I. Premoli Silva and M.J. Malone (Editors), Proc. ODP, Sci. Results, 198 [Online]. Available from World Wide Web: http://www-odp.tamu.edu/publications/198_SR/122/122.htm.
Zachos, J.C., Röhl, U., Schellenberg, S.A., Sluijs, A., Hodell, D.A., Kelly, D.C., Thomas, E., Nicolo, M., Raffi, I., Lourens, L.J., McCarren, H. and Kroon, D., 2005. Rapid Acidification of the Ocean During the Paleocene-Eocene Thermal Maximum. Science, 308(5728): 1611-1615.

ICDP

On the geochemistry of gases occurring at an active plate-bounding fault system: the SAFOD example (San Andreas Fault Observatory at Depth)

T. Wiersberg and J. Erzinger, GeoForschungsZentrum Potsdam, Germany (wiers@gfz-potsdam.de)

Introduction

To achieve a better understanding on the processes at active plate-bounding fault systems at the location of their origin, the SAFOD wells were drilled in 2002 and 2004/2005 within the framework of ICDP. A site close to Parkfield town (California) was selected for drilling because of the simultaneous occurrence of creep and repeating small-magnitude earthquakes at drillable depths. SAFOD consists of two wells: the pilot hole (PH) and the main hole (MH), both drilled in only a few meters distance. In contrast to the straight PH, which penetrates through 768 m of quartery and tertiary sediments into cretaceous granites down to 2168 m final depth, the MH is deviated towards the SAF and returns into sedimentary strata below 1930 m, where it remains down to the bottom of the hole (3987 m). Recently observed casing deformation implies that the SAF is active at 3310 m depth.

The knowledge about the role and origin of fluids and gases associated with the San Andreas Fault zone (SAF) is relatively poor. Besides the open question how fluids are linked with fault zone processes in general, also the spatial distribution of fluids at depth and in the contribution in particular of mantle-derived fluids to the total fluid inventory of the SAF are outstanding topics. To gain information on fluids and gases at depth, we performed real-time mud gas monitoring during drilling of both SAFOD wells. Gas extracted from returning drill mud was piped into a

Figures 1 and 2 of Westerhold et al.]

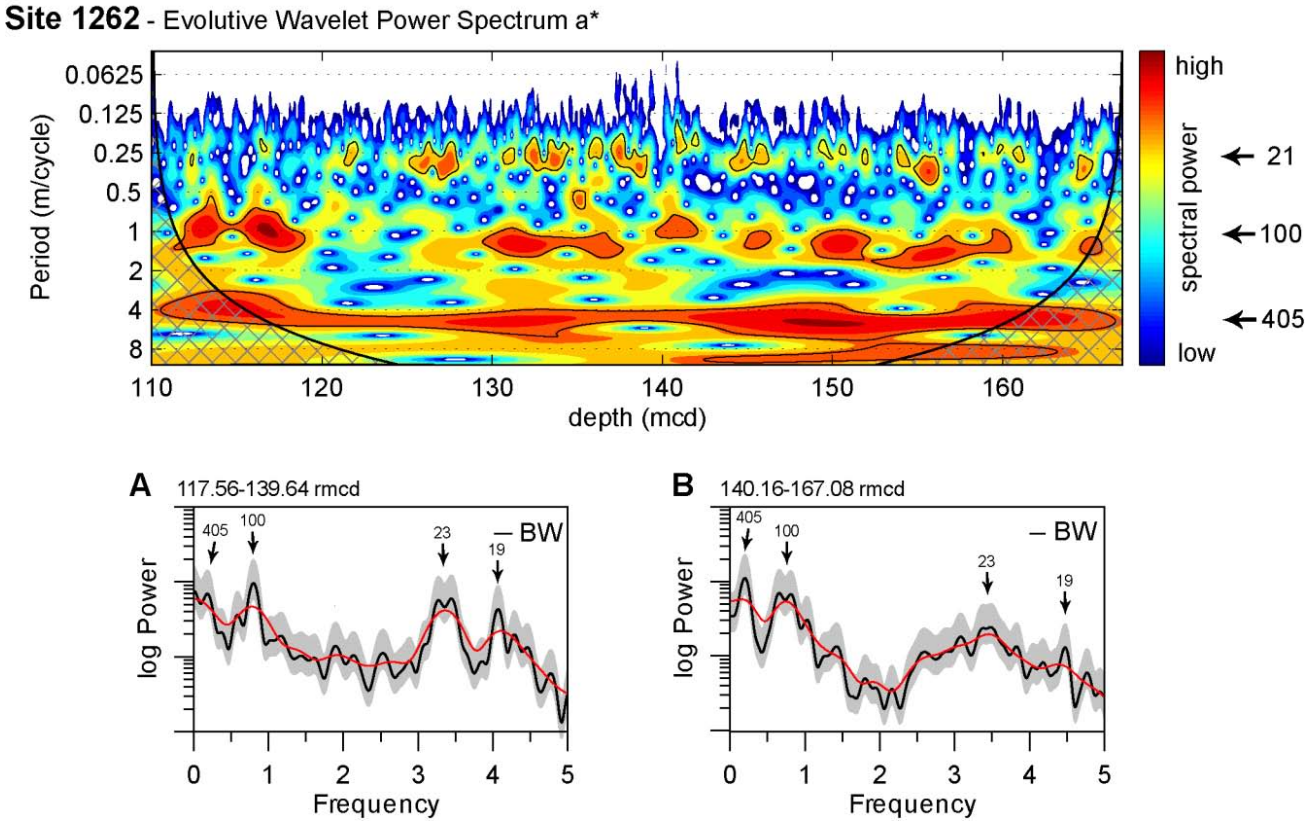

Figure 1. Evolutive wavelet analysis of the a* value for Site Site 1262 in the depth domain. The shaded contours are normalized linear variances with blue representing low spectral power, and red representing high spectral power. The black contour lines enclose regions of greater than 95% confidence. Cross-hatched regions on either end indicate the cone of influence where edge effects become important. Note the distinct bands (marked by arrows) that run across the spectra which indicate the dominance of Milankovitch related periods (precession with a central frequency of 21-kyr, and eccentricity with frequencies at 100- and 405-kyr). The plotted power spectra represent the periods prior to the PETM (B) and between the PETM and Elmo layer (A). The Blackman-Tukey power spectra (bold black line) have been calculated by the AnalySeries program using 80% confidence interval (gray area), bold red line is the estimated background noise. Bandwidth (BW) and confidence limits are based on a Bartlett-window with a number of lags that equal 30% of the length of the data series. The spectra reveal strong spectral peaks at precession and eccentricity related periodicities according to bio- and magnetostratigraphy.

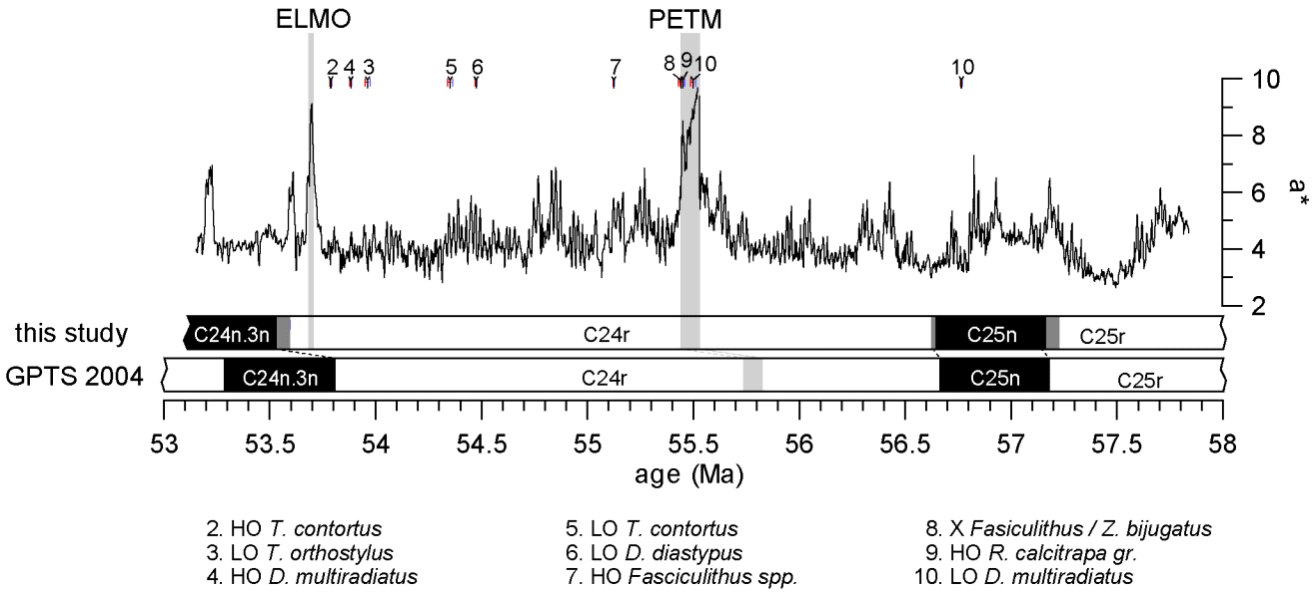

Figure 2. Absolute time scale of Site 1262 a* data with magnetochron C24r and C25n, calcareous biostratigraphy, Elmo layer, and the PETM compared to the Geomagnetic Time Scale 2004. The arrows with error-bars indicate the position of calcareous nannofossils datums.

nearby laboratory trailer and analyzed on-line. When significant amounts of non-atmospheric gases were detected, off-line gas samples were collected from the gas line for further isotope studies.

Results from mud gas monitoring

Mud gas data from the upper 1900m of the MH are in good agreement with PH data (Erzinger et al., 2002) and will not be discussed further. Here, we present results from the lower part of MH-I (1900-3051m) and MH-II (3051-3980m). During drilling of this predominantly sedimentary sections, the most abundant non-atmospheric gases in drill mud were hydrogen (up to 6 vol%), methane (up to 10 vol%), and carbon dioxide (up to 4 vol%). The concentration of helium remained low (>10ppmv), whereas radon activity reached values of up to 5000 Bq/m^3.

Two major sections could be identified where these gases were enriched in mud gas: from 2700-2900 m and below 3550 m down to the bottom of the hole at 3987 m depth (Fig.1). A positive correlation between the numbers of beddings and fractures in this sections, identified by geophysical logging, and the radon activity implies that fluids enter the hole through open fissures. Furthermore, the radon activity indicates that the fluids are not stained, but active circulating.

In both sections, radon also correlates positively with H_2, CO_2, and in part also CH4. However, the relative proportions of these gases are different in both sections. The upper is relatively enriched in ^{222}Rn and H_2, the lower in CO_2 and CH_4.

Based on their distinct chemical composition, we conclude that both sections represent individual hydrologic systems. Evidence for mixing is only little. The gas concentrations found in the drill mud between 2900 m and 3550 m depths are low, in particular in 222Rn. Only two sections, from 3150 - 3200 m and at 3340 m, show some higher gas concentrations. The spike like gas kick at 3340 m, very close to the active part of SAF (3310 m), is almost exclusively composed by hydrocarbons. From 3150 - 3200 m, drilling through carbonate-rich strata caused additionally a somewhat higher CO_2 content. Lithological data supports the interpretation of gas accumulation trapped in permeable sandstones embedded in less permeable strata.

Also striking is the high amount of hydrogen found in both gas-rich intervals. We can widely exclude a significant contribution of artificial hydrogen (drilling artefacts) or mantle hydrogen. From soil gas studies, it is known that fault zones sometimes show enhanced concentration of hydrogen (King, 1986). As a possible source of hydrogen, the interaction of water with freshly ground rock, caused by fault zone movement, is discussed. An alternative explanation would be serpentinization of basaltic rocks, however, at Parkfield, serpentine outcrops are known only from NE of the SAF within the North American Plate, however, the higher hydrogen concentrations were found on the Pacific Plate, making this source less likely. Isotopic studies on hydrogen and laboratory experiments to test hydrogen synthesis by rock-water interaction are ongoing.

Noble gas data

Mantle-derived fluids, indicated by a helium isotopic ratio clearly different form crustal values, are known from shallow wells and hot springs in the vicinity of the SAF (Kennedy et al., 1997). It is poorly understood to what extend this feature is linked with the SAF itself. Kennedy et al. found ^{3}He/^{4}He ratios of 1.6 R_a (R_a=atmospheric ratio of ^{3}He/^{4}He= 1.39*10^{-5}) in only 1.4 km distance to the SAF (Varian-Phillips well). The highest ^{3}He/^{4}He ratios of approx. 4 R_a were found at Mercy Hot Springs in ~40km distance to the SAF. The authors conclude that the input of mantle-derived helium from earlier magmatism to the total helium inventory of the SAF is negligible. Lost of mantle-derived helium and ingrown of radiogenic ^{4}He be decay of U and Th after emplacement of volcanic rocks (30-8 Ma ago) would have extinct a possible mantle helium signature in these rocks. Indeed, no correlation between the age of volcanic activities and the helium isotopic composition on distinct locations was found. Therefore, Kennedy et. al. explained the occurrence of mantle derived He with overpressured mantle fluids passing the ductile-brittle barrier, which separates the upper form the lower crust. The question to what extend deep-seated fluids can pass the ductile-brittle barrier is of fundamental importance to understand how overpressured fluids may influence seismic processes which take place along major plate-bounding fault systems.

We have performed noble gas isotope investigations on 14 mud gas samples taken during drilling of SAFOD MH. Much care has been taken for the air correction of the measured helium ratios, as the circulating drill mud is loaded with air; therefore the gas extracted from drill mud principally contains a strong atmospheric contribution. We have carried out the air correction assuming that the measured ^{2}0Ne is atmospheric, which can be demonstrated by a neon isotopic composition indistinguishable from air.

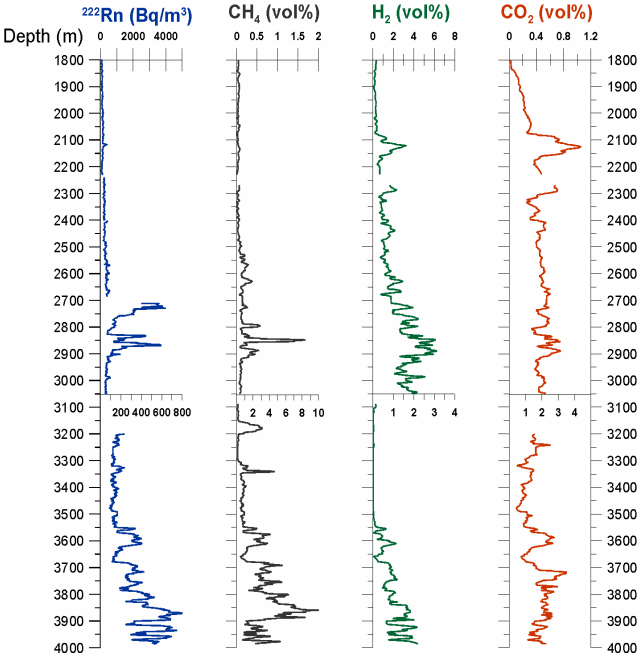

Fig. 1 Mud gas profiles from the SAFOD-MH phase 1 (down to 3051 m) and phase 2 (3987 m) for the most prominent non-atmospheric gases

All air-corrected ^{3}He/^{4}He ratios are lower than the atmospheric ratio, but higher than the mean crustal values of 0.1 R_a; therefore helium is a mixture of crustal helium with a small portion of mantle-derived helium. The atmospheric contribution on the helium is in a range between 6-89%. Down to a depth of 3051 m, air-corrected ^{3}He/^{4}He ratios of >0.45 R_a show that the contribution of mantle-derived helium is small (approx. 5%) on the Pacific Plate, which composes the SW of the SAF. The ^{3}He/^{4}He ratios become significantly higher at depths below 3781 m on the North American Plate, were ^{3}He/^{4}He ratios of 0.9 R_a were found, revealing a mantle contribution of 10-12% to the total helium budget. Two samples collected at 3196 m and 3433 m indicate some mixing between both reservoirs (R_a ~0.6), but both samples contain only a very small portion of non-atmospheric helium. Based on our observations, we conclude that the contribution of mantle-derived fluids to the total fluid budget at the SAF is small. Higher ^{3}He/^{4}He ratios found in nearby wells imply that the fluid migration from depth through the SAF is to some extend hampered. The distinct helium isotopic compositions down to 3051m and below 3781m depths, with only little evidence for mixing between both hydrologic systems, demonstrate that the SAF in some way acts as a barrier for fluid migration.

First isotopic studies on $\delta^1$3C of methane indicate mixing of microbial methane with only small amounts of methane generated

by thermal degradation of organic matter within the upper ~2500 m. $CH_4/(C_2H_6+C_3H_8)$ significantly drops from >100 to <30 towards the bottom of the main hole and methane becomes isotopically heavier, both typical for thermogenic hydrocarbons.

References

Erzinger J., Wiersberg T., and Dahms E. (2002): Real-time mud gas logging during drilling of the SAFOD Pilot Hole in Parkfield, CA, Geophys. Res. Lett., 31, L15S18

Kennedy B. M., Kharaka Y. K. Evans W. C. Ellwood A. DePaolo D. J. Thordsen J. Ambats G. and Mariner R. H. (1997): Mantle Fluids in the San Andreas Fault System, California, Science (278), 1278-1281

King (1986): Gas Geochemistry Applied to Earthquake Prediction: An Overview, J. Geophys. Res., 91, 12,269-12,281

ICDP

Lithological heterogeneity of the Onaping Formation and its importance for understanding post-impact deformation of the Sudbury Impact Structure, Canada

Andrea Wittek[1], Ulrich Riller[2], Lutz Hecht[1,2]

[1]Freie Universität Berlin, Institut für Geologische Wissenschaften, Malteser Strasse 74-100, 12249 Berlin, e-mail: andrea.wittek@museum.hu-berlin.de; [2]Humboldt-Universität Berlin, Institut für Mineralogie, Invalidenstrasse 43, 10115 Berlin.

The suevitic Onaping Formation overlies the layered Main Mass of the 1.85 Ga Sudbury Igneous Complex (SIC) of the Sudbury Impact Structure, Ontario. The Formation consists of four Members, namely from top to bottom, the Black, the Green, the Gray and the Basal. Post-impact NW-SE shortening during the Penokean Orogeny (ca. 1.9-1.75 Ga) affected the Onaping Formation and led to the lobate shape of the SIC in plan view. In order to investigate the possible fold origin of the NE-lobe of the SIC, a field-based structural analysis of the Onaping Formation was conducted in the Frenchman Lake area. The analysis is based on structural measurements at 580 stations and encompasses the orientation of mineral shape fabrics as well as their intensity. In addition to these quantities, lithological variation and metamorphic overprint of the Onaping Formation was examined. Special attention was paid thereby to the Green Member since previous workers stated that it forms a continuous unit at the base of the Black Member.

Individual Members of the Onaping Formation differ in mineral composition, size and abundance of clasts as well as in color and texture of the matrix, the latter one of which ranges from cryptocrystalline to coarse-grained as well as in the content of felsic minerals. The grain size of the matrix as well as size and content of clasts increase from the top of the Onaping Formation towards its base. The Green Member is well apparent by the presence of angular chlorite aggregates. Therefore, these aggregates became known as "chloritic shards" and possibly represent original fragments of melt particles. In the Frenchman Lake area, the Green Member forms a 70 - 100 m thick, discontinuous band, whereby the strike of its contacts at surface varies highly. By contrast, intra-formational lithological contacts of the lower units of the Onaping Formation are rather straight.

Microscopic inspection of samples from the Black, Green and Gray Members shows that mineral shape fabrics are chiefly defined by chlorite and epidote. This points to post-impact deformation under lower greenschist-facies metamorphic conditions. Deformation of the Onaping Formation varies greatly with position. This is indicated by the orientation and intensity of planar mineral shape fabrics. Fabric intensity was visually estimated and is based on the shape-preferred alignment of matrix minerals and clasts. It varies as a function of the mineralogical composition and grain size of the matrix, clast content and distance to the NE-lobe. More specifically, fabric intensity increases towards the top of the Onaping Formation suggesting that mechanical strength during deformation of the Formation increased toward its lower contact. This is corroborated by the variation in strike of intra-formational lithological contacts, which are straight at the base but highly irregular towards the top of the Formation, and may well account for the discontinuous nature of the Green Member.

An increase in shape fabric intensity is also apparent towards the east. Similarly, the strike of planar shape fabrics becomes more uniform in this direction, i.e., NE-SW, which is axial-planar to the acute bisectrix of the NE-lobe. This may indicate that the effect of folding of the SIC on the fabric development in the Onaping Formation decreases towards the west. The planar shape fabrics also display a progressive change in their overall strike from NE-SW in the NE-lobe to ENE-WSW towards the west of the lobe. This change in strike can be explained by the curvature of the fold axis of the NE-lobe. Despite the strong heterogeneity of deformation in the Frenchman lake area, the orientation in, and gradients in intensity of, planar shape fabrics in the Onaping Formation are consistent with a fold origin of the NE-lobe, which formed under lower greenschist-metamorphic conditions.

ICDP

Isotope (O-Sr-Nd-Pb) and fluid inclusion distributions in the CCSD main hole

Yilin Xiao[1], Jochen Hoefs[1], Rolf L. Romer[2], Alfons van den Kerkhof[1] and Zeming Zhang[3]

[1]Geowissenschaftliches Zentrum der Universität Göttingen, Goldschmittstrasse 1, D-37077 Göttingen, Germany (yxiao@gwdg.de); [2]GeoForschungsZentrum Potsdam, Telegrafenberg, D-14473 Potsdam, Germany; [3]Institute of Geology, CAGS, Baiwanzhuang Road 26, 100037 Beijing, China

1. Introduction

The main-hole of the Chinese Continental Scientific Drilling Project (CCSD) in Donghai of the Dabie-Sulu UHP metamorphic belt in East China has reached its final depth of 5118 m in March 2005. As shown in Fig. 1, orthogneiss, paragneiss, eclogite, amphibolite (mostly retrograded from eclogite), and ultramafic rocks are the main rock types; schist and quartzite were occasionally found as thin interlayers within paragneiss and eclogite. All rock types down to 5118m have been subjected to UHP metamorphism, as documented by the preservation of coesite inclusions in zircon (personal communication of Liu F-L).

Combining petrological observations, fluid inclusion data, and isotope (O-Sr-Nd-Pb) investigations on selected drillcores from the CCSD main hole, we aim to: (i) verify the depths of the meteoric water/rock interactions and oxygen isotope characteristics a 5000 m vertical profile of a UHP slab, (ii) obtain information about possible changes of fluid composition with depth, and (iii) provide constraints on chemical interactions between the mantle wedge and subducted continental crust.

2. Vertical (0-5100m) oxygen isotope distributions and its tectonic implications

In general, the investigated rocks can be divided into two groups: 18O-depleted rocks (as low as $\delta^{18}O = -7.4‰$ for garnet) indicate interaction with cold climate meteoric waters, whereas [1]8O-normal rocks (with bulk $\delta^{18}O > +5.6‰$) have preserved the O-isotopic compositions of their protoliths (Fig. 2). Transitions from rocks with depleted $\delta^{18}O$ values to those with normal oxygen isotopic compositions are gradual, with eclogites and gneisses in close contact having very similar oxygen isotope ratios. As the meteoric water/rock interaction occurred before the UHP event (e.g., Zheng et al. 1998; Rumble and Yui 1998), these features indicate that the UHP rocks are not dismembered tectonic mélanges, but share a common pre-subduction history. Furthermore, oxygen isotope depletions have been observed down to about 3300 m; rocks below this depth have normal O-isotope compositions, regardless of lithology. This feature suggests that the ancient meteoric water/rock interaction has reached depths of about 3300 m.

3. Correlation between oxygen isotope and fluid inclusions

Five types of fluid inclusions were identified in the drillcores: (i) texturally earliest aqueous inclusions occurring either in quartz blebs in garnet or in the allanite core of zoned epidote porphyroblasts, (ii) Ca-rich or NaCl-dominated high-salinity inclusions in garnet, omphacite and kyanite, (iii) low to intermediate salinity inclusions occuring randomly in quartz, (iv)

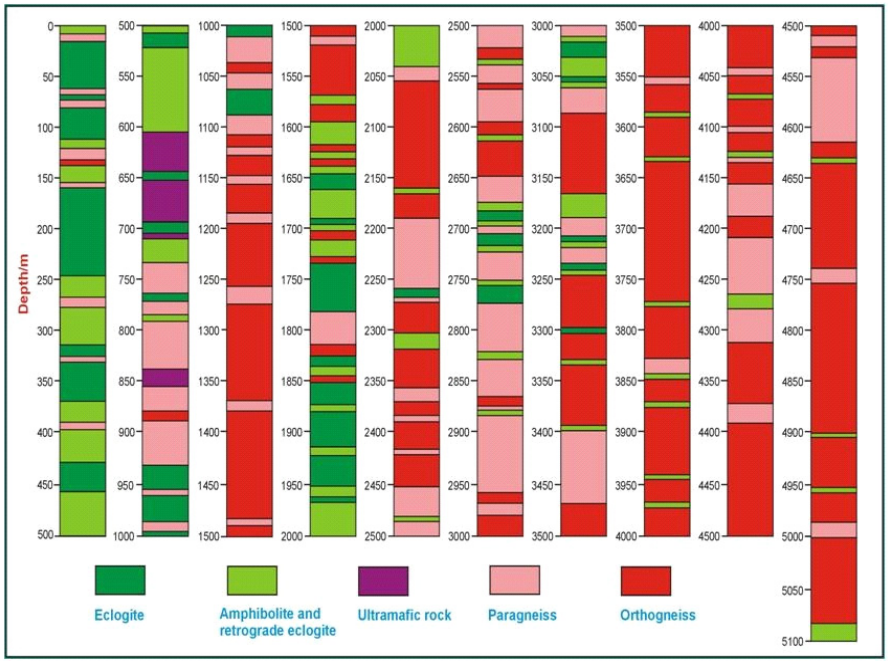

Fig. 1 Lithological profile of the CCSD main hole (0-5118m). At depths above 2000 m eclogite is the principal lithological type, whereas below 2000m it only appears rarely. Gneiss is mainly observed from 1100 to 1600 and below 2000m (the figure is in color; Xu et al., unpublished data).

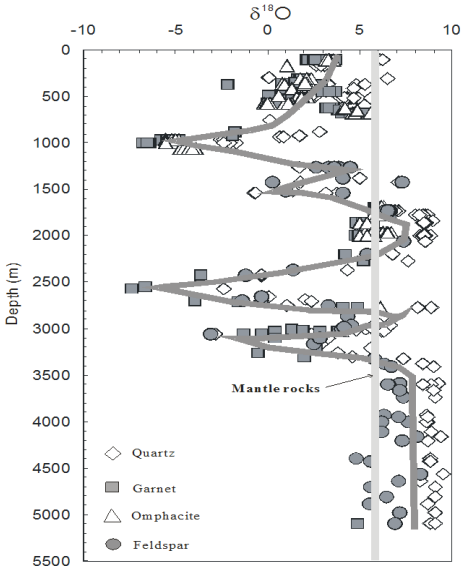

Fig. 2 Oxygen isotope distribution of the UHP rocks from 0-5100 m of the CCSD main hole. 18O depletions were observed at depths of 0-1600m, 2300-2700, and 3000-3300m.

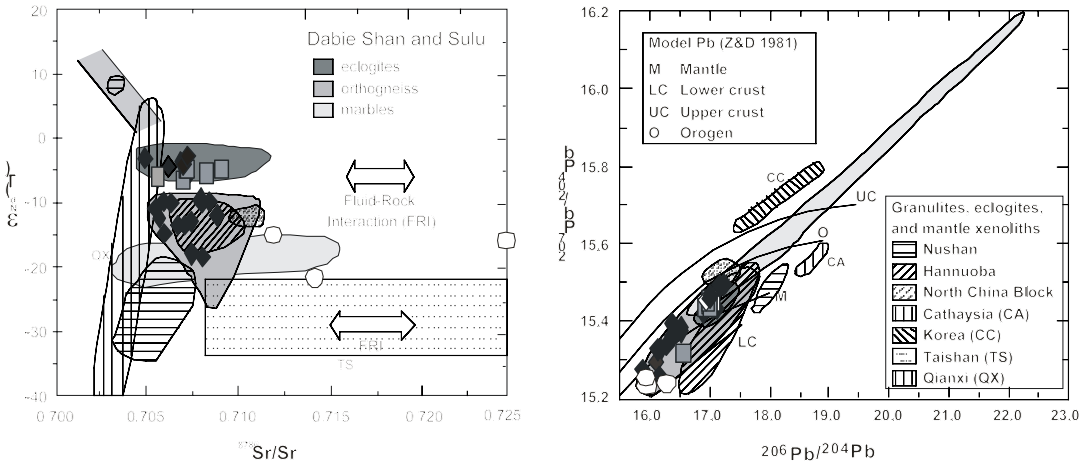

Fig. 3. Sr-Nd-Pb isotope systemticas rocks from the drill hole, regionally occurring UHP comples and mantle xenoliths (modified after Wawrzenitz et al., in press). Eclogite, paragneiss and orthogneiss from CCSD are labelled with solid diamond, half-solid square and open circle, respectively.

high density CO2 inclusions found in quartz and, (v) secondary almost pure water inclusions in healed fractures.

High-salinity aqueous fluid inclusions are prevalent in ^{18}O-depleted CCSD rocks, whereas rocks with $\delta^{18}O$ values >5.6 per mil are dominated by high-density CO2 inclusions. Therefore, high-salinity fluid inclusions are related to the process that established the low $\delta^{18}O$ signature rather than to lithology. In general, fluids in both groups evolved from high water activity (represented by low to medium salinity fluid inclusions) to low water activity (demonstrated by high-salinity brines and/or high density CO2 inclusions) from prograde- to peak-metamorphism. After the peak of metamorphism the fluid composition changed from high salinity to almost pure water. All rocks have had very low water-activity during peak metamorphism. These features are similar to the fluid evolution in the Dabie area (Xiao et al. 2000, 2001, 2002).

4. Sr-Nd-Pb isotope compositions of the UHP rocks (0-4000m)

The Sr-Nd-Pb isotopic compositions of samples from 0-4000 m of the CCSD main hole are shown in Fig. 3. The $\varepsilon_{Nd}(T)$ and $^{87}Sr/^{86}Sr$ (T) values indicate the involvement of the Archaean crust. Eclogite and orthogneiss differ in Nd isotopic composition, the latter showing less evolved Nd that in part falls in the range of the marbles. The retarded Pb growth in combination with relatively high $^{207}Pb/^{204}Pb$ values reflects not only Archaean crust, but also Archaean depletion of U and Th relative to Pb during high-grade metamorphism. A negative correlation in $^{87}Sr/^{86}Sr$ vs. $^{206}Pb/^{204}Pb$ diagram and a weak positive correlation of $^{143}Nd/^{144}Nd$ vs. $^{206}Pb/^{204}Pb$, $^{207}Pb/^{204}Pb$ vs. $^{206}Pb/^{204}Pb$, and $^{208}Pb/^{204}Pb$ vs. $^{206}Pb/^{204}Pb$ among eclogites, Mesozoic volcanics, Cenozoic basalts from the North China craton and the depleted MORB mantle under eastern China suggest significant interaction between UHP metamorphic rocks (formerly subducted continental crust) and the eastern China mantle.

References

Rumble D and Yui TF (1998) Geochim Cosmoschim Acta, 62:3307-3321.
Wawrzenitz N et al. Lithos (in press).
Xiao YL et al (2000) Contrib Mineral Petrol, 139:1-16.
Xiao YL et al. (2001) J Metamorph Geol, 19:3-19.
Xiao YL et al. (2002) J Petrol, 43:1505-1527.
Zheng YF et al (1998) Earth Planet Sci Lett, 155:113-129.

ICDP

Pre-site survey for a new ICDP site in southern Patagonia (Argentina)

Bernd Zolitschka[1], Christian Ohlendorf[1], Flavio Anselmetti[2], Daniel Ariztegui[3], Marc De Batist[4], Catalina Gebhardt[5], Torsten Haberzettl[1], Frank Niessen[5], Michael Fey[1] and the SALSA team

[1]GEOPOLAR, Institute of Geography, University of Bremen, Germany; [2]Geological Institute, ETH-Zurich, Switzerland; [3]Institute Forel and Dept. of Geology & Paleontology, University of Geneva, Switzerland; [4]Renard Center of Marine Geology, Ghent University, Belgium; [5]Alfred-Wegener-Institute for Marine and Polar Research, Bremerhaven, Germany

Seismic investigations were carried out as part of an intense pre-site survey for the future deep drilling location Laguna Potrok Aike (southern Patagonia, Argentina) within the framework of ICDP. Overall goals were to determine thickness, geometry and distribution of sediments in this 770 ka maar lake. Several different seismic investigations were carried out during four field campaigns by leading European research teams. Obtained results allow to identify sediment types, associated depositional processes and past lake level fluctuations, all of which are critical for the determination of the ideal coring sites for the ICDP deep drilling project PASADO (Potrok Aike Sediment Archive Drilling Project).

In 2003 a high-resolution 3.5 kHz survey imaged the shallower subsurface in great detail and provided crucial information to interpret a 19 m long piston core which was recovered following this seismic campaign. In the central basin the acoustic signal penetrated down to 13 m and in windows to max. 20 m below the lake floor (Fig. 1). Sediments are characterized as a well-layered succession locally interrupted by mass flow deposits (Fig. 2). Such events occasionally occur on the lower slopes as the result of slope instabilities. The shallow and gently-dipping shoulder surrounding the lake down to a water depth of ~30 m is separated from the deep basin by very steep slopes and represents a sedimentary system, that is independent of the succession in the center of the lake (Fig. 1). A prominent unconformity consistently cropping out at ~35 m water depth marks the maximum depth of a Holocene lake level low stand. At this unconformity steeply dipping slope sediments below are overlain by gently dipping sediments deposited during a later period of higher lake levels (Fig. 1). The transgression occurred stepwise as indicated by a series of paleoshorelines visible at the surface of the erosional unconformity on high resolution 3.5 kHz seismic images.

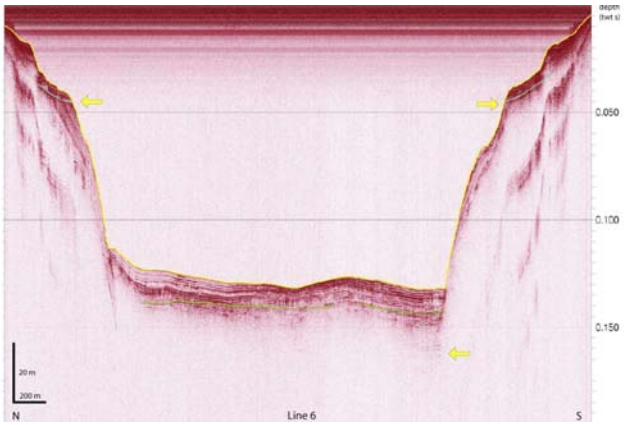

Fig. 1: 3.5 kHz seismic N-S profile of Laguna Potrok Aike showing pelagic sediments in the center with one window of deeper penetration (lower arrow) and erosional unconformities at the lake shoulder in 30 m water depth (upper arrows).

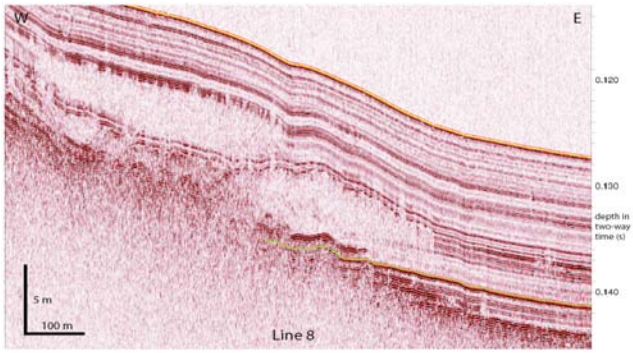

Fig. 2: 3.5 kHz seismic image of the western margin of the basin showing a well-layered sedimentary record with intercalated stacked mass flow deposits.

A stronger double airgun source was applied in early 2004 because sediment thickness exceeds seismic penetration of the 3.5 kHz seismic system. Surprisingly, the stronger and lower-frequency double airgun signal did not penetrate the entire lake area to a greater subsurface depth and penetration down to ~80 m was only achieved in some windows. Therefore, a third survey with a stronger sparker system was accomplished in December 2004. Again, penetration was locally restricted but documented in some areas well-layered sediments down to 105 m depth (Fig. 3) demonstrating that the lake bottom holds an extensive sedimentary record. The deeper reflections observed in both, airgun and sparker data bend slightly upward towards the rim of the lake, indicating a bowl-shaped sedimentary architecture that gradually becomes filled-up (Fig. 1). No bedrock signature was obtained. Deepest reflections have gradually lower amplitudes and less lateral coherency preventing a complete evaluation of the geometry of the

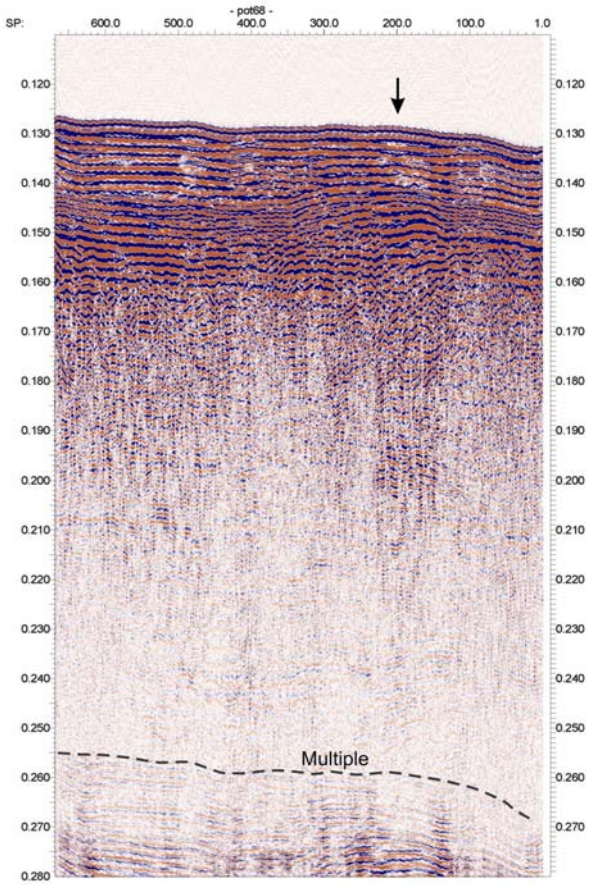

Fig. 3: W-E sparker seismic profile obtained by "horizontal stacking". Arrow indicates a window of deeper seismic penetration (cf. Fig. 1). Units on y-axis are given as two-way-travel time in ms.

sedimentary infill. Most sediments appear to be of pelagic origin documenting the huge potential of these sediments as a long archive of climatic and environmental history.

A fourth seismic survey was carried out in March 2005 using a G-Gun with a volume of 40 cubic inches. In order to allow deep acoustic penetration and detection of the sediment bedrock/ interface this acoustic source was combined for data acquisition with a multi-channel streamer, three lake-based sonobuoys and two Reftek™ land stations. Multi-channel data exhibit excellent signal-to-noise ratios over ~450 m depth below lake surface or 600 ms two-way-travel time (twt), but the data show overprints by multiples making interpretation of strata below the first multiple (~200 m) difficult until fully processed profiles are available (Fig. 4). Nevertheless, strong reflectors visible on each end of the seismic profiles indicate a steep slope down to a depth of 300 to 400 m (Fig. 4). This interface may represent the diatreme/bedrock interface.

Sonobuoy data exhibit refractions below 700 ms twt. A first analysis allows the distinction of four different velocity layers ranging from 1630 to 3090 m s-1 (Fig. 5). The lowest velocity is indicative for soft lacustrine sediments of low densities, the highest for diatreme breccias and/or sandstones (e.g. Miocene Sta. Cruz Formation) forming the bedrock and catchment area of Laguna Potrok Aike. A preliminary depth estimation of the different layers in the lake center suggests that the transition from soft lake sediments to more consolidated underlying deposits is located at approximately 250 m below the lake water surface. No sub-bottom velocities were detected that are indicative for a volcanic basement. Possibly the expected volcanic vent is too small to be detected by refraction seismics, the profiles did not cross such a feature or the vent is deeply buried by thick diatreme breccias.

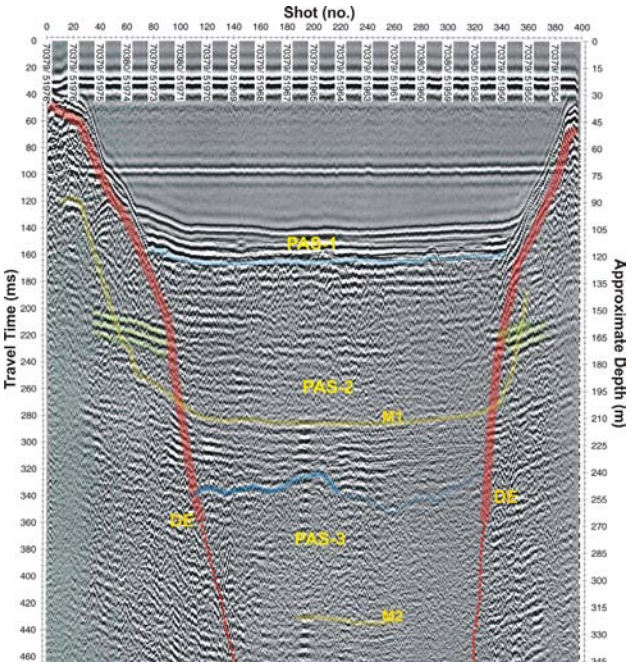

Fig. 4: Single-channel reflection seismic N-S profile. Processed data suggest a seismic stratigraphy of three layers: PAS-1 is well stratified, PAS-2 is also stratified but more diffuse. Weak and diffuse hummocky reflectors characterize PAS-3. PAS-1 and PAS-2 are interpreted as soft lacustrine sediment fill. PAS-3 has higher velocities of >2000 m s-1 and may consist of lapilli tuff. M1 and M2 are multiples partly masking the record. DE marks our interpretation of the approximate location of the diatreme/bedrock interface.

[Figure 5 next page]

IODP

Long-term evolution of the mid-Pleistocene bottom current regime in the Subpolar Northeast Atlantic

C. Zühlsdorff[1], R. Henrich[1], and J.-B. W. Stuut[2]
[1]University of Bremen, Faculty of Geosciences, P.O. Box 330 440, 28334 Bremen; [2]Research Center Ocean Margins, University of Bremen, P.O. Box 330 440, 28334 Bremen

The Arctic and subarctic regions are some of the most important locations to global climate and ocean systems, since much of the world's deep waters are formed in the high latitude oceans (Jansen and Raymo, 1996). This deep water production and the process of overturning represent a key element of the global thermohaline circulation. During the mid-Pleistocene a fundamental climate transition occurred between 1.2 and 0.6 Ma, which is also known as Mid-Pleistocene Revolution (MPR). During the MPR a change in earth's climate was observed from the 41-kyr obliquity signal to the 100-kyr eccentricity cycle (Berger and Jansen). Subsequent to the MPR, increases in glacial-interglacial contrasts were recorded globally and North Atlantic Deep Water (NADW) production decreased during the glacials (Raymo, 1997). This study on sediments from ODP site 984 from Björn Drift will elaborate Pleistocene paleocurrent reconstructions in response to deep and intermediate water formation close to one of the main locations of NADW production with regard to recent progress in unraveling ice-rafted debris of silt size from bottom current transported fine sediments. Detailed grain-size distributions of the terrigenous fine sand and silt fraction provide the base for the end-member modeling (Weltje, 1997), a mathematical-statistical approach to unmix sediments of distinct size fractions but different in their origin. As the study of Prins et al. (2002) indicates, a differentiation of silt-sized sediments supplied by icebergs or sea ice is needed to get a better grip on the interpretation of grain-size distributions of high-latitude ocean sediments as well as for a better insight into the physical flow regime of the global thermohaline circulation during this time.

Berger, W.H. and Jansen, E., 1994. Mid-Pleistocene climate shift: The Nansen connection. In: O.M. Johannessen, R.D. Muench and J.E. Overland (Editors), The Polar Oceans and Their Role in Shaping the Global Environment: The Nansen Centennial Volume, AGU Geophys. Monog. AGU Washington, pp. 295-312.
Jansen, E. and Raymo, M.E., 1996. Leg 162: New frontiers on past climates. In: E. Jansen, M.E. Raymo, P. Blum et al. (Editors), Proceedings of the Ocean Drilling Program, Initial Report. College Station, TX, pp. 5-21.
Prins, M.A. et al., 2002. Ocean circulation and iceberg discharge in the glacial North Atlantic: Inferences from unmixing of sediment size distribution. Geology, 30(6): 555-558.
Raymo, M.E., 1997. The timing of major climate terminations. Paleoceanography, 12: 577-585.
Weltje, G.J., 1997. End-member modeling of compositional data: numerical-statistical algorithms for solving the explicit mixing problem. Journal of Mathematical Geology, 29: 503-549.

[Figure 5 of Zolitschka et al.]

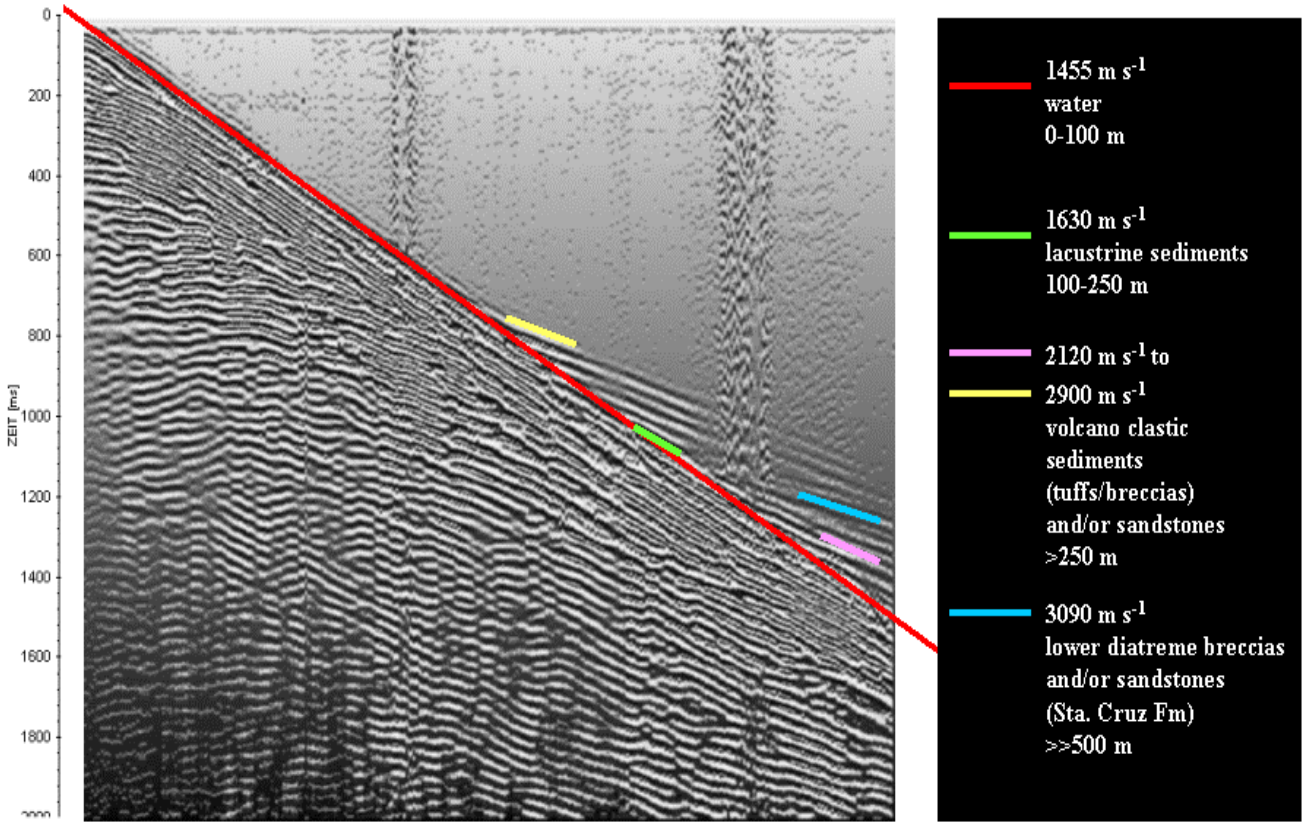

Fig. 5: N-S refraction seismic profile 10L. Preliminary interpretation of data indicates that the thickness of lacustrine sediments is around 150 m (velocity range from 1630 to 2120 m s^{-1}).

Für die Mitarbeit und Hilfe bei der Durchführung der Tagung möchte ich mich im Namen aller Tagungsteilnehmer ganz herzlich bedanken bei den Mitarbeiterinnen und Mitarbeitern des Instituts für Geographie und Geologie der Universität Greifswald:

Juliane Bornstedt
Dr. Grit Büttner
Matthias Falke
PD Dr. Heiko Hüneke
Hannelore Kuhr
Dagmar Lau
Renate Martens
Erika Möller
Heike Sengpiehl
Markus Zingelmann

Umgebungsplan

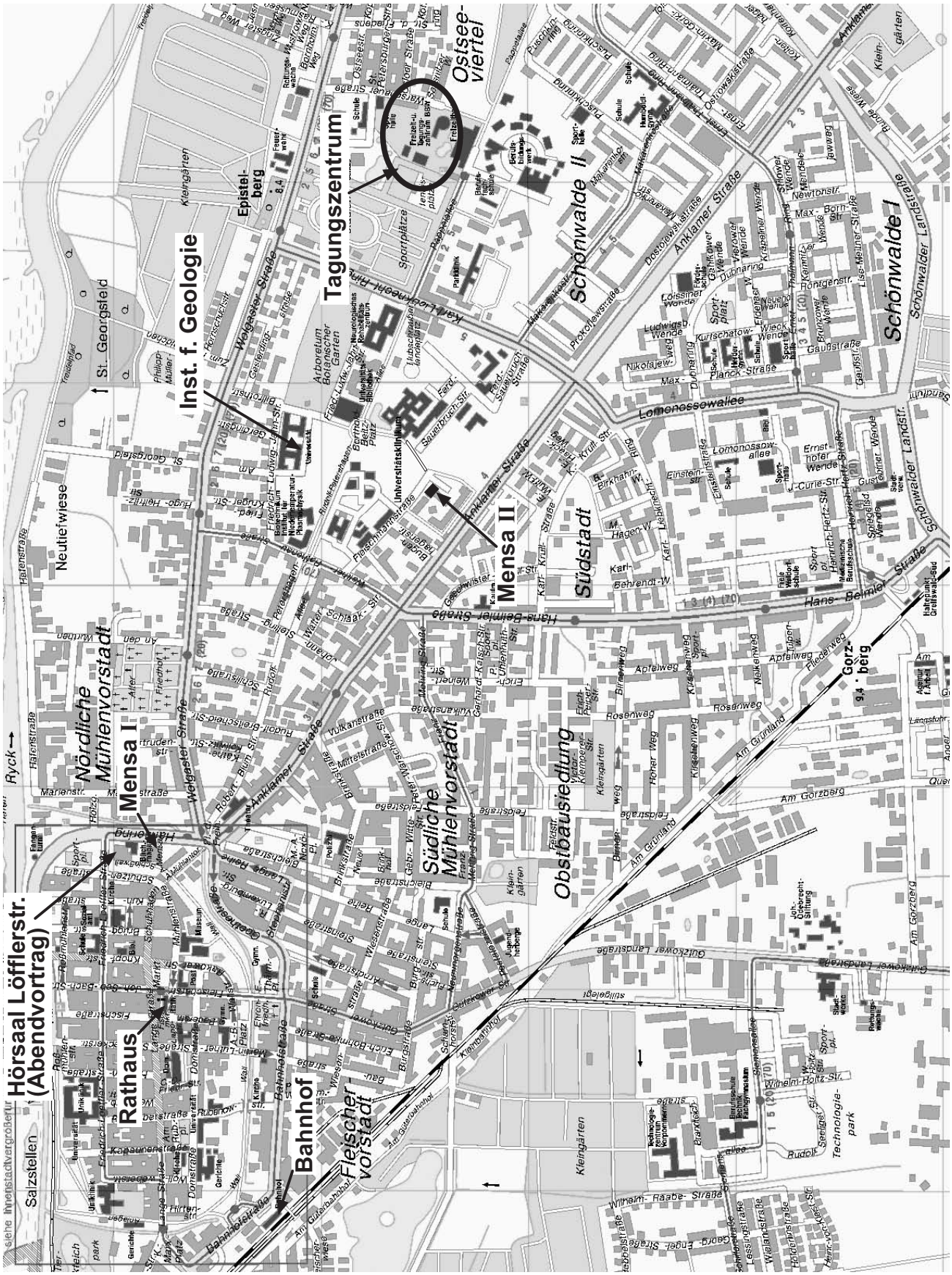








DSDP
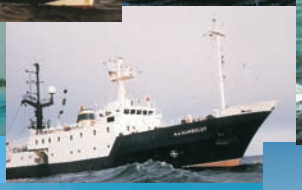




ODP

IODP

ICDP







KTB